AN INTEGRATED APPROACH TO WATER-ENERGY NEXUS WITH MULTIPLE

ENERGY SOURCES

A Dissertation

by

FADHIL YOUSUF MOHAMMED AL-ABOOSI

Submitted to the Office of Graduate and Professional Studies of
Texas A&M University
in partial fulfillment of the requirements for the degree of

DOCTOR OF PHILOSOPHY

Chair of Committee,	Mahmoud M. El-Halwagi
Co-Chair of Committee,	Hisham Nasr-El-Din
Committee Members,	Sergiy Butenko
	Nimir Elbashir
Interdisciplinary Chair,	Timothy Jacobs

August 2019

Major Subject: Interdisciplinary Engineering

ABSTRACT

The sustainable development of the entire world is confronting considerable challenges due to the tremendous expansion in energy demand that synchronizes with fresh water scarcity, vast depletion of conventional energy sources and climate change. Consequently, the necessity has emerged for creating suitable management strategies for existing water resources (e.g., wastewater treatment) and for integrating traditional energy sources with renewables (e.g., solar energy, wind energy, biofuels, etc.). The objective of this study is to develop a novel design framework of the water-energy nexus system, which optimized according to economic and environmental metrics using certain parameters (leading to deterministic optimization) and uncertain parameters (leading to stochastic optimization). The system comprises multiple energy sources, cogeneration process, and desalination technologies.

Solar energy is incorporated to provide thermal power directly to a multi-effect distillation plant (MED) exclusively (to be more feasible economically), or to the entire system through a steam generator. Thus, MED is driven by direct solar energy, indirect solar energy (thermal energy storage), and surplus heat from the cogeneration process. Additionally, electric power production is intended to meet a reverse osmosis plant (RO) demand and the local electric grid (if it is connected to the system). The deterministic optimization problem is formulated as a multi-period Mixed Integer Non-Linear Programming (MINLP) to discretize operation period to track the diurnal fluctuations of solar energy. However, the stochastic optimization problem is formulated as a multi-scenario MINLP problem that is a deterministic equivalent of a two-stage stochastic

programming model for handling uncertainty in operational parameters (normal direct irradiance, fossil fuel price) through a finite set of scenarios. A case study is solved for water treatment and energy management for Eagle Ford Basin in Texas to obtain the maximum annual profit of the entire system.

The long-term evaluation for the techno-economic performance of solar energy conversion systems is highly dependent on the availability of solar radiation data and their accuracy. This study offers hierarchical calculation methodologies to estimate solar irradiance values for a specific location under different sky conditions. A case study is solved to predict hourly direct normal irradiance for San Antonio city in Texas.

DEDICATION

To GHUFRAN, *my soul mate, my inspiration, my dear wife*

To ABDULLAH, *my source of happiness in life, my dear son and Aggie!*

ACKNOWLEDGEMENTS

CONTRIBUTORS AND FUNDING SOURCES

NOMENCLATURE

a, b, c, d, e, f	Empirical coefficients
a_o, a_1, a_2, a_3	Correlation constants
a_1, a_2, a_3, a_4, a_5	Transmission functions
a_{aa}, b_{aa}, c_{aa}	Constants
a_w	Water vapor absorptance
a, b, and c	Coefficients for the LS-3 collector
A	Permeability
$A_{S,m}$	Membrane area per module
A,B,C,D	Empirical coefficients
AFC^{MED}	Annualized fixed capital cost of the multi-effect desalination
AFC^{RO}	Annualized fixed capital cost of the reverse osmosis
AFC^{SC}	Annualized fixed capital cost of the solar collector
AFC^{cogen}	Annualized fixed capital cost of the cogeneration system
A^{SC}	Effective surface area of the solar collector
A_{SF}	Solar field aperture area
AFC_{PR}	Annualized fixed capital cost of an industrial process
AFC_{EQ}	Annualized fixed capital cost of equipment
AFC_S	Annualized fixed capital cost of supplements
AOC_{PR}	Annualized operating cost of an industrial process

ANI_{Cogen}	Annualized income of the cogeneration process
ANI_{TW}	Annualized income of the treated water
ANI_{WW}	Annualized value of avoided cost of discharging wastewater
ANI_{PR}	Annualized income of processing facilities (midstream) production
A_{httfe}	Heat transfer area for tubes of HTFFE for n_{th} effect
A, B	Site climate-related constants
AFC	Total annual fixed cost
AOC	Total annual operating cost
A and B	Parameters that depend on the type of the turbine
bbl	Barrel
c^{Waste}	Value of avoided cost of discharging wastewater
$c_{t,m}^{Fossil}$	Value of fossil fuel
C_{DS}	Disposal cost per volume unit
C_F	Fuel cost per thermal power unit
C_{FW}	Fresh water cost per volume unit
C_{OM}	Operation and maintenance cost per thermal power unit
C_{PST}	Primary and secondary treatment cost per volume unit
C_{SF}	Solar field cost per area unit
C_{SG}	Steam generator system cost per thermal power unit

C_{TES}	Thermal storage system cost per thermal power unit
C_{TR}	Transportation cost per volume unit
Cp_{ms}	Specific heat of the molten salt
Cp_{oil}	Specific heat of oil
C_F	Salt fraction in feed flowrate
C_D	Salt fraction in distillate flowrate
C_{FB}	Salt fraction in brine flowrate
C_F	Solute concentration
C_S	Average solute concentration in shell side
C_{CO}	Cost of a column
C_{TR}	Cost of a tray
C_{HE}	Cost of a heat exchanger
d_o	Outer diameter of the receiver pipe
$D_{t,m}^{Tutbine}$	Design variable of the turbine
DNI	Direct normal irradiance
$\frac{D_{2M}}{K\delta}$	Salt flux constant
e_{MED}	Electric energy requirements of MED
e_{RO}	Electric energy requirements of RO
E	Time equation
E_T	Turbine shaft power output

$E_{t,m}^{Total}$	Electric energy provided by the cogeneration turbine
ft^3	Cubic feet
f	Focal length of the collectors
FCI_B	Fixed capital cost of a boiler
FCI_{PST}	Fixed capital cost of the primary and secondary treatment
FCI_{SF}	Total fixed capital cost of the solar field
FCI_{SG}	Fixed capital cost estimation of the steam generator system
FCI_T	Fixed capital cost of the turbine
FCI_{TES}	Fixed capital cost of the thermal storage system
FCI_{Total}	Total fixed capital cost
F_f	Soiling factor (mirror cleanliness)
FPW	Flowback and produced water
$F_{t,m}^{Fossil}$	Volumetric flow rate of fossil fuel
$F_{t,m}^{MED}$	Volumetric flow rate of desalinated water from MED
$F_{t,m}^{RO}$	Volumetric flow rate of desalinated water from RO
F_F	Volumetric flow rate of feed
F_D	Volumetric flow rate of permeate
F_B	Volumetric flow rate of reject
GOR	Gained output ratio
h_{act}^{out}	Actual outlet enthalpy of the turbine
h^{in}	Inlet enthalpy of the steam

h_{is}^{out}	Outlet isentropic enthalpy
H_{SC}	Solar constant
HCE	Sum of heat collection element
$\overline{H_d}$	Monthly average daily diffuse irradiance
$\overline{H}$	Monthly average daily global radiation on a horizontal surface
$\overline{H_o}$	Monthly average daily extraterrestrial solar irradiance on a horizontal surface
$\overline{H_G}$	Monthly average daily global irradiance on a horizontal surface
H	Site elevation
h	Differential head
HTFFE	horizontal-tube falling film evaporator
I_{DNI}	Direct normal irradiance
$\overline{I_G}$	Monthly average hourly global irradiance on a horizontal surface
$\overline{I_d}$	Monthly average hourly diffuse irradiance
$\overline{I}_{DNI,H}$	Monthly average hourly direct solar irradiance on a horizontal surface
$\overline{I}_{DNI}$	Monthly average hourly direct solar irradiance

$I_{G_{cs}}$	Hourly global solar radiation on a horizontal surface under cloudless sky
$I_{G_{cc}}$	Hourly global solar radiation on a horizontal surface under cloud cover condition
I_d	Hourly diffuse radiation on a horizontal surface
$I_{DNI,KC}$	Direct normal irradiance (DNI) under different sky conditions
I_{oN}	Extraterrestrial radiation measured on the plane normal to the radiation
I_{cal}	Calculated value
I_{meas}	Measured value
$I_{meas,avg}$	Average of measured data
I_o	Solar constant
J_{water}	Water flux
J_{solute}	Solute (salt) flux
$K(\Theta)$	Incidence angle modifier
$\overline{K_T}$	Monthly mean clearness index
k_f	Annualized factor for investment
k_γ	Annual operation time
L_{SCA}	Length of a single collector assembly
L	Latitude

L_{ao}	Aerosol optical depth
L_{st}, L_{loc}	Standard meridian for local time zone and longitude
$L_{spacing}$	Length of spacing between troughs
L_f	Fiber length
L_S	Seal length
$\dot{m}$	Inlet turbine steam flowrate
m_r	Air mass at standard pressure
$m_{r,ABW}$	A specific air mass
m_{air}	Air mass at actual pressure
m^{max}	Maximum mass flowrate of the turbine
m_{ms}	Mass flow rate of molten salt
m_{oil}	Mass flowrate of oil
m_e	Air mass corrected for elevation
$m_{air,KUM}$	A specific air mass
m_F	Total mass flowrate
m_D	Mass flowrate of distillate
m_B	Mass flowrate of brine
MED	Multi-effect distillation plant
MINLP	Mixed integer nonlinear program
MM	Million
n	Number of observations

N_P	Factor to account for the operation pressure of the boiler
N_j	Number of the day
N_T	Factor accounting for the superheat temperature of the boiler
N	Cloud cover number
N	Service life of the property in years
N	Number of MED effects
N_{PS}	Number of processing steps
N_{EQ}	Number of major equipment
NSRDB	National Solar Radiation Data Base
OC_{OM}	Operation and maintenance cost
O_{EL}	Optical end loss
OC_F	Cost of fuel
$O_{t,m}^{Turbine}$	Operation variable of the turbine
$OPEX_{t,m}^{MED}$	Annualized operational expenditure of MED
$OPEX_{t,m}^{RO}$	Annualized operational expenditure of RO
$OPEX_{t,m}^{SC}$	Annualized operational expenditure of the solar collector
$OPEX_{t,m}^{SC-storage}$	Annualized operational expenditure of the thermal storage system
$OPEX_{t,m}^{cogen}$	Annualized operational expenditure of the cogeneration system

P_g	Gauge pressure of the boiler
PTC	Parabolic trough collector
P	Actual pressure
p_o	Standard pressure
P_{opof}	Osmotic pressure of feed
P_F	Pressure of feed
P_D	Pressure of permeate
P_B	Pressure of reject
q_{MED}	Thermal energy requirements of MED
Q_{Boiler}	Thermal power output of the boiler rate
Q_{LFP}	Thermal power that loss from the headers (pipes)
Q_{LFV}	Thermal power that loss from the expansion tank (vessel)
Q_{TES}	Net thermal power inside the tank
Q_{in}	Inlet thermal power
Q_B	Amount of thermal power that produced by the boiler
Q_{acc}	Accumulated thermal power in the tank from preceding iterations
$Q_{collector \rightarrow ambient}$	Total thermal power that loss from a collector to ambient
$Q_{collector \rightarrow fluid}$	Thermal power that transferred from a collector to a fluid
$Q_{collector \rightarrow reciever}$	Thermal power that absorbed by the receiver tube of a collector Loop

Q_{htffe}	Thermal power emitted by condensing distilled water into the tubes of the horizontal-tube falling film evaporator
q	Flow capacity
Q_{out}	Outlet thermal power
$Q_{solar\ field \rightarrow final\ demand}$	Useful thermal power that produced by the solar field
$Q_{sun \rightarrow collector}$	Solar thermal power that produced by the solar field
Q_{loss}	Thermal power loss
$Q_{t,m}^{Direct,SC}$	Direct thermal power from the solar thermal collector
$Q_{t,m}^{Fossil}$	Direct thermal power from the combustion of fossil fuels
$Q_{t,m}^{In\_Stored-SC}$	Inlet thermal power of the thermal storage system
$Q_{t,m}^{Out\_Stored\_SC}$	Indirect thermal from solar energy through the thermal storage system
$Q_{t,m}^{SC}$	Thermal power captured by the solar collector
$Q_{t,m}^{Stored-Loss}$	Loss thermal power of the thermal storage system
$Q_{t,m}^{Stored-SC}$	Thermal power stored in the thermal storage system
$Q_{t,m}^{Total}$	Total thermal power needs for water treatment
$Q_{t,m}^{Turbine}$	Thermal power from steam leaving the cogeneration turbine
$Q_{t-1,m}^{Stored-SC}$	Thermal power stored from previous iterations
r_t	Ratio of monthly average hourly global irradiance to monthly average daily global irradiance

r_d	Ratio of monthly average hourly diffuse irradiance to monthly average daily diffuse irradiance
r_i	Inside radius of fibers
r_o	Outside radius of fibers
R	Relative humidity (%)
R_{SL}	Row shadow loss
RO	Reverse osmosis plant
ROI	Return on investment
$\overline{S}$	Monthly average daily sunshine hours
$\overline{S_o}$	Maximum possible monthly average daily length
SC	Number of storage capacity hours
ST	Solar time
SDT	Standard time
T_{CT}	Cold tank temperature
T_{dew}	Dew point temperature
T	Average maximum temperature
T_o	Temperature at zero altitude
T_{amb}	Ambient temperature
T_{LTF}	Linke turbidity factor
T_{HT}	Hot tank temperature
T_{SH}	Superheat temperature

T_{amb}	Ambient air temperature
T_{in}	Temperature at the inlet of the turbine
T_{ms}	Temperature of the molten salt
T_{rec}	Mean receiver pipe temperature
T_{sat}^{in}	Saturation temperature at the inlet of a turbine
$T_{vapor,avg}$	Average temperature of the vapor
U_{rec}	Overall heat transfer coefficient of the receiver pipe
U_1	Pressure-corrected relative optical-path length of precipitable water
U_3	Ozone's relative optical-path length
U_{htffe}	Overall heat transfer coefficient
W_c	Width of the collector aperture
W_w	Volumetric flow rate of discharging wastewater
W	Watt
$W^{\grave{}}$	Precipitable water-vapor thickness under the actual condition
X_o	Total amount of ozone in a slanted path
X_w	Total amount of precipitable water in a slanted path
x_F	Salt fraction in total flow rate
x_D	Salt fraction in distillate flow rate
x_B	Salt fraction in bine flow rate

Subscript and superscript symbols

ac	Actual
acc	Accumulated
amb	Ambient
B	Boiler
c	Collector aperture
Cogen	Cogeneration process
CT	Cold tank
DS	Disposal
EL	End loss
f	Factor
F	Fuel
FW	Freshwater
g	Gauge
HT	Hot tank
is	Isentropic
LFP	Loss from pipes
LFV	Loss from vessel
m	Time period
MED	Multi-effect distillation plant
ms	Molten salt
m_D	Total distillate water collected from MED effects

OM	Operation and maintenance
P	Pressure
PST	Primary and secondary treatment
rec	Receiver
RO	Reverse Osmosis plant
sat	Saturation
SC	Solar collector
SCA	Single collector assembly
SF	Solar field
SG	Steam generator
SH	Superheat
SL	Shadow loss
t	Time period
T	Turbine
TES	Thermal energy storage
TR	Transportation
w	Wastewater

Greek symbols

η_{boiler}	Efficiency of the boiler
η_{is}	Isentropic efficiency of the steam turbine
a_Y	Annual operation time

$\Omega_{t,m}^{Turbine}$	Vector set of the turbine
$\nu_{t,m}^{MED}$	Value of produced water from MED
$\nu_{t,m}^{RO}$	Value of produced water from RO
$\forall m$	For every month (operational period)
$\forall t$	For every hour (sub- period)
$\forall s$	For every scenario
Δh_{is}	Isentropic enthalpy change
η_{opt}	Peak optical efficiency of a collector
θ	Solar incidence angle
θz	Solar zenith angle
γ	Intercept factor
δ	Declination
ΔT	Difference between inlet and outlet of the oil
ρ	Reflectivity
τ	Glass transmissivity
ω	Hour angle
α	Absorptivity of the receiver pipe
θ_z	Zenith angle
τ_{aa}	Atmospheric attenuation
θ_δ	Declination angle
θ_h	Solar hour angle

τ_{bulk}	Bulk atmospheric transmittance
τ_{rt}	Air transmittance
τ_{ot}	Ozone transmittance
τ_{gt}	Gas transmittance
τ_{wt}	Water transmittance
τ_{at}	Aerosol transmittance
β_1, β_2	Angstrom exponent and Angstrom turbidity coefficient respectively
τ_{as}	Aerosol scattering transmittance
τ_w	Precipitable water transmittance
τ_{md}	Direct transmittance of all molecular effects except water vapor for Atwater
τ_o	Ozone transmittance
α_w	Water vapor absorption
θ_{hs}	Sunset hour angle
$\Delta H_{c,avg}$	Latent heat of condensation
β^{MED}, β^{RO}	Recovery fraction
μ	Viscosity
v^{RNG}	Cost of raw natural gas
v^L	Cost of labor
v^{RO}	Value of produced water from RO

v^{MED}	Value of produced water from MED
v^{Fuel}	Value of produced Fuel
$v^{Chemicals}$	Value of produced Chemicals

TABLE OF CONTENTS

LIST OF FIGURES

LIST OF TABLES

xxx

CHAPTER I

INTRODUCTION

1.1 Background

The globally vast demand for energy and water is one of the most significant challenges for sustainable development in different regions of the world that synchronizes with the considerable scarcity of fresh water, fast depletion of conventional energy sources and climate change. Accordingly, renewables, which are still lack for more subsidies and carbon tax credit activation, have emerged as a promising replacement for fossil fuels in the long-term. In addition, the proper management strategies for water resources like recycling/ reusing wastewater by utilizing desalination technologies are other tactics to diminish a deficiency in fresh water and energy supply. The growing demand for water and energy cannot be treated separately according to the reciprocal connection between water and energy, which is called the water-energy nexus.

The water-energy nexus term bolsters the concept of maintaining regional and global sustainability through optimal exploiting of natural resources and considering attractive industrial processes design that requires less capital investment and minimal water and energy usage during the operational period. The early design stages and operational pattern for a water-energy nexus system, which includes different industrial processes, can be optimized by using economic, environmental and safety metrics. In the same context, the sustainable performance of existing systems (e.g., power plants, refineries, chemical, pulp and paper, etc.), either they are utilized to produce various energy forms by consumption a significant amount of water, or they are used for treating

saline water and wastewater by consuming a massive amount of energy, can be advanced by retrofitting an existing system, system expansion, and grassroots design [1].

Process integration provides a unique framework accompanying with efficient techniques set and empowering tools for sustainable design. These techniques and tools are described by [2, 3]. Furthermore, these techniques have been improved to integrate units, streams, resources, and objectives for optimizing a whole process because if units of a process are optimized individually, an entire process is not optimized. Consequently, the optimal systematic design and optimal mix of energy for an industrial process and among various industrial processes can be achieved through process integration. Finally, process integration is a holistic approach to process operation, design, and retrofitting that affirms on the process unity [2].

The optimal sustainable design of industrial processes, which is considered among the largest water and energy consumption sectors, is a challenging task to sustain natural resources by recycling and reusing, mitigate pollution as well as enhance quality and yield of production to increase profitability. The rapid depletion of fossil fuels (81.6%, nearly of the global total energy supply) and the modest growing of renewable energy sources (13.3%, nearly of the global total energy supply) have contributed to introduce the unconventional energy sources as a competitive replacement to the traditional energy resources. Shale gas has emerged one of the significant the unconventional energy resources and can meet an important portion of the global demand of energy [4]. According to the Energy Information Administration (EIA), the advancement in shale gas

production will be from 23% of total U.S gas production in 2010 to 49% in 2035 [5]. Texas is considered at the top of shale gas producers in the U.S.

Hydraulic fracturing and horizontal drilling are the essential technologies to extract natural gas from shale rock. Water plays a significant role in shale gas production through mixing millions of gallons of water with sand, chemicals, corrosion inhibitors, surfactants, flow improvers, friction reducers, etc. to produce fracturing fluid. Under the high pressure, the fracturing fluid is injected into the wellbore to make cracks within the rock layers to increase the production [6, 7].

Because of the high-water consumption that used for the fracturing process (e.g., in the eagle ford, annual water use was 18 MMm^3 for 1040 wells) [8]. Life cycle water management of a shale well is complicated and costly, the major challenges for life cycle water for a shale gas well are high cost of acquisition for fresh water, transportation of the fresh and waste water over long distances, treatment, and disposal. Recycling and reuse processes are successfully alternative strategies for management of flow-back and produced water of a shale gas well because they can alleviate pressure on fresh water resources that utilized in fracturing process, and to lessen the amount of flow-back and produced water that must be transported, treated, and disposed [9].

In addition to the obvious influence of the oil and gas industry (which involves upstream, midstream and downstream industries) on the water-energy balance, other factors including populated explosion, urbanized growth, and industrialized expansion, climate change and governmental regulations are still affecting the global economic sustainability by threatening the water and energy resources, specifically, in the regions

that are suffering from water-energy stress. Therefore, there is a necessity to develop systematic approaches for identifying and optimizing the water-energy nexus systems for producing fresh water and electric power.

1.2 Objectives

This work presented within the scope for developing a novel systematic approach to design, operation, integration, and optimization of the water-energy nexus system which integrates solar energy and fossil fuels for producing electricity and desalinated water. The proposed system consists of a concentrated solar power field, a thermal storage unit and cogeneration process that are coupled with a reverse osmosis plant (RO) and a multiple-effect distillation (MED). For adjusting dynamic fluctuations of solar energy, a fossil fuel boiler and thermal energy storage are utilized to maintain the system operates at steady-state. The system is analyzed and optimized according to technical, economic, and environmental metrics to minimize the annual profit of the entire system. The optimization problem of a first systematic approach will be formulated under certain parameters as a deterministic optimization. The multi-period approach can be applied to discretize operation period to track the diurnal fluctuations of solar energy. while, in a second systematic approach, an industrial process (midstream industry) is incorporated in the system and solar energy can be added as a thermal power source to the system in a various scenario from that will be presented in the first approach. The optimization problem of a second approach will be formulated under uncertainty as a stochastic optimization. According to the difficulty of obtaining high-quality solar irradiance data and the high cost of measuring instruments and their calibration, this study will offer hierarchical

calculation methodologies to estimate solar irradiance values under different sky conditions that can be utilized to assess the techno-economic performance for solar energy conversion system, which is used in the system.

1.3 Structure of the Dissertation

This work is organized into six chapters. Chapter I presents a simple introduction including the background and objective of this research. Chapter II introduces a broad literature review to properly cover the topics related to this work. Chapter III presents an integrated approach to water-energy nexus in shale gas production through covering a problem statement, a proposed approach for solution strategies that based on a deterministic optimization, a theoretical description of modelling and optimization formulations and results obtained from solving a case study. Chapter IV presents an integrated approach is developed under uncertainty based on a stochastic optimization perspective for the water-energy system that contributes to treating wastewater in shale gas site. It includes a problem statement, a proposed approach, a detailed description for modelling and optimization equations and obtained results from solving a case study which is selected to demonstrate the ability of a solution approach. Chapter V offers hierarchical calculation methodologies to estimate solar irradiance values under different sky conditions that strengthen the capability of integrated approaches of a solution by evaluating the techno-economic performance for concentrated solar power plant. Chapter VI summaries the most significant concepts that are addressed in this work.

CHAPTER II

LITERATURE REVIEW

The main purpose of this chapter is to introduce a general overview for several topics that included in this work. To properly cover a broad area of the proposed system components of this research, the literature review is divided into five major sections and several subsections: concentrated solar power field, thermal energy storage, desalination plants and cogeneration process comprises (desalination plants, cogeneration process, conventional desalination, solar desalination), water management of shale gas and oil industry includes (water consumption for hydraulic fracturing in the U.S., water consumption for hydraulic fracturing in Texas, water treatment), and finally, process integration and optimization.

2.1 Concentrated Solar Power (CSP)

Solar energy is the most abundant energy resource on earth. The amount of solar energy falling on the earth's surface at one hour equals to the consumed energy from the entire human activities during one year [10]. Concentrated solar power systems are designed to harness solar radiation to generate thermal power that is utilized for electricity production and as a thermal source for various industrial applications.

CSP systems can be utilized to concentrate a direct solar radiation, while the non-directional radiation types (diffuse and reflected radiation) cannot be used in these systems. The enhancement of the solar collector performance for CSP systems is based on the solar tracking methods that used to focus a direct solar radiation on the focal target as well as to minimize a value of an incident angle [11, 12].

Concentrated solar thermal plants are among the most spreadable renewable energy systems in the world that can supersede traditional fossil-fueled power plants. However, these power plants are still not competitive economically unless subsidized [13]. Parabolic trough plants have become the most advanced technology in the industrial market [14].

A detail performance model for parabolic trough plant (PTC) with and without thermal energy storage (TES) has been developed in the following literature: [4, 15-27]. Some researchers have extended their work to include a performance model and an economic model together for PTC plant [13, 28-33]. Other researchers evaluate the thermal-economic performance of concentrated solar systems under various conditions, especially, in arid areas [34-39].

National Renewable Energy Laboratory researchers [40] have presented the current and future assessment of the cost and performance basis extensively for PTC plants based on SunLab and S&L experience. Price [41] studied the trade-off between performance, economic, and cost parameters for PTC power plant through a computer model. Kalogirou [42] introduced a historical survey for several different types of solar thermal collectors that are in common use such as flat-plate, evacuated tube, compound parabolic, Fresnel lens, parabolic trough, etc. On the other hand, the optical thermodynamic, and thermal analysis is provided for collectors and their applications that showed significant benefits.

2.2 Thermal Energy Storage (TES)

In order to provide a steady thermal power on demand from solar thermal power plants, a thermal energy storage system can be integrated to these power plants. Therefore, the security of thermal power supply is increased with the support of a storage system due to the unpredictability and intermittency of solar energy. The benefits of thermal energy storage in CSP plants are the capacity to keep providing thermal power after the sunset or in cloudy weather and to provide dispatchable thermal power [43].The existence of a storage system can be useful to store a surplus thermal energy in different types of TES systems that allow utilizing this thermal energy later when there is a deficit in thermal power [44]. Thermal energy storage systems play the essential role to improve CSP plants dispatchability. A review of different thermal energy storage design concepts (e.g., size, efficiency, and cost) that are used or may be used for CSP plants as well as the selection of storage materials has been presented by [43, 45-47]. The properties of various materials that utilized in thermal energy storage systems and the dynamic performance of these systems were discussed in [48].

A two-tank storage system is the most developed among thermal energy storage systems, but it is still comparatively expensive comparing with a single tank. Also, there is a problem with nitrate salts (molten salts), which is used as storage medium in this system, due to high freezing point and fluctuated price [43]. A performance and economic analysis of a two-tank molten salt storage based on the operation experience for the SEGS plants were evaluated by [49]. García-Barberena et al. [50] developed and simulated a fully transient storage tank model.

8

A thermocline thermal energy storage is a modified concept for a two-tank storage system to save cost. This a modified concept is based on fluid bouncy forces to separate the hot and cold fluid into two isothermal regions inside a single tank along the vertical axis. A new model was developed by [51] to offer a simulation of molten salt thermocline tank operation at low cost for CSP plants, Vilella and Yesilyurt [52] evaluated the techno-economic performance of a thermocline tank for solar tower power plant. An assessment of operation approaches for CSP plants with a thermocline tank has been achieved by developing a simulation model using the TRNSYS [53].Vilella and Yesilyurt [52] demonstrated that the thermocline storage system can replace the two-tanks storage system efficiently in Andosol solar plant-Spain because of its low cost. The performance comparison of CSP plants with two types of thermal storage systems (Two-tank, thermocline) was carried out by simulation models for various values of energy storage capacity. This study showed that a two-tank storage system has higher performance and higher cost than a thermocline energy storage [54].

2.3 Desalination Plants and Cogeneration Process

2.3.1 Desalination Plants

Desalination technologies have been developed to improve the quality of water and to provide fresh water for different life requirements. Seawater represents about 97.5% of the total water abundance on earth. The remaining percentage (2.5%) is distributed between surface water and underground, 80% of this water is glaciers. Consequently, the amount of water in rivers, lakes, and aquifers is 0.5% of the total amount of water on earth [55].

Desalination water technologies are categorized into commercial plants on a large-scale and the empirical plant under research and development. The process of separating the salts from the water in desalination plants requires consuming considerable amount of energy, which can be electrical power as in RO or thermal power as in MED. The amount of energy consumption in thermal desalination plants (e.g., Multi-Effect Desalination (MED) and Multi-Stage Flash (MSF)) is greater than the energy consumption in desalination technologies (e.g., Reverse Osmosis) that are driven by electric power.

The water production cost of desalination technologies is a combination of energy cost, capital investment, and operation and maintenance cost. Since the energy cost represents 50% of the desalinated water cost, renewable energy sources can utilize to satisfy energy (thermal, electric) requirement for desalination plants to diminish fossil fuels consumption [56]. The using pretreatment systems are significant to protect desalination plants (e.g., MED, RO) from fouling, a comprehensive review was presented for two types of pretreatment systems by [57].

2.3.2 Cogeneration Process

The advantages of a cogeneration process arise from improving energy efficiency of the whole plant, reducing the amount of fuel consumption, and mitigation of environmental impact. In addition to electrical power production, the surplus thermal power of the cogeneration process can be used to provide an enough heat to various industrial sectors (e.g., chemical, refineries, desalination, pulp and paper, etc.). A various types of fossil fuel (e.g., natural gas, petroleum, shale gas) are used (along with renewable energy sources) for cogeneration purposes. The flared gas (a byproduct) can be exploited

in cogeneration process to sustain fossil fuel resources by reducing their consumption, Eljack et al. [58] developed an optimization approach for the design of cogeneration systems using flared gases are collected from various industrial plants to provide power, heat, and reduce environmental impact.

2.3.3 Conventional Desalination (Fossil Fuel)

Sanchez et al. [59] presented a feasibility analysis for a modified plant that uses the waste heat for a stack gas and the steam turbine condensate (combined cycle) as a heat source for MED process. Nápoles-Rivera et al. [60] offered an optimization formulation for a macroscopic water network that incorporates desalination plants into power plants. The surplus heat of power plants can be provided to desalination plants and an electric power production is sold to minimize the cost of treated water production. The thermal performance of a new system that consists of an organic Rankine cycle, an ejector, and MED plant was analyzed using the model and sensitivity analysis. This proposed system may be utilized to treat seawater or flowback water produced during the hydraulic fracturing process [61].

The technical characteristics, amount of consumed energy, capability of renewable energy to operate the desalination plants, environmental impacts have been reviewed and analyzed. Additionally, the current and future costs of treated water that produced from traditional and alternative energy desalination plants have been discussed [56]. Ghobeity et al. [62] carried out a review of thermal desalination and cogeneration plants as well as reverse osmosis. In this review, the design and economic performance have been considered for hybrid desalination plants for existing systems. Finally, various studies of

the optimization of hybrid desalination plants have been reviewed including objective functions, optimal hardware configurations, and optimization methods. An overall survey and assessment of different desalination technologies (MED, MSF, RO) have been presented, it included producing water cost, energy consumption, and technology improvements. Also, an additional analysis has been given for cogeneration, desalination, future water situation and its policy [63].

2.3.4 Solar Desalination (Solar Energy)

The integration of renewable energy sources with desalination technologies is a significant concept toward enhancing sustainability of desalination technologies [55, 64]. Desalination technologies can be sustained by integrating them with renewable energy sources. In this context, a review of various desalination technologies that integrated with solar energy was carried out, including several novel methods of desalination (e.g., freezing and adsorption desalination), furthermore, a simple description of using solar energy to provide a direct thermal power to MED plant was given [65].

A thermo-economic analysis of the coupled production of water and electricity for solar thermal plant that is integrated with MED and RO plants has been investigated. Regeneration and reheating were used to enhance the thermal efficiency of the power block. The combined system shows low levelized water cost [66]. A technical- economic performance of desalination plants integrating with renewable energy sources has been discussed. Consumed power and distilled water cost of each plant were compared [67]. The different configurations for the combination of parabolic trough collector plant with

MED and RO technologies have been simulated to evaluate a thermodynamic and economic performance [68-79].

The following works used the concept of a mixed integer nonlinear programming (MINLP) and optimization, In [80], a mathematical model of cogeneration system that includes a power plant, multistage flash (MSF), and reverse osmosis has been proposed to minimize total annual cost and the genetic algorithm was used to solve the model. The multi-objective model of optimal design and operation for a system that consists of parabolic trough solar collectors, a Rankine cycle, thermal energy storage, and reverse osmosis was developed. The minimization of cost and environmental impact for the system were evaluated while considering a certain water demand [81].

2.4 Water Management of Shale Gas and Oil Industry

The massive amount of water consumption during hydraulic fracturing of shale gas production is the most challenging problems. This problem may cause constraining shale gas production, especially in semiarid areas that suffer from the scarcity of water. The annual average water consumption per well for hydraulic fracturing in different regions of the U.S. is between 1000 m^3 and $30,000 \text{ m}^3$. During the past decades, Texas has been precedence on shale gas production in the entire U.S., therefore, Texas has ranked one of the highest consumers of water utilized in the fracturing process with 457.42 MMm^3 for 40,521 wells [82].

2.4.1 Water Consumption for Hydraulic Fracturing in the U.S.

Chen and Carter [82] presented an overall review of water usage for the hydraulic fracturing processes in 14 states across the U.S. between 2008 to 2014. This study reported that recycled wastewater to prepare hydraulic fracturing fluids were utilized in 6221 wells of 80,047 wells (represent 10% of the whole wells that were working at the time of preparing this literature). Additionally, some states were reported that the recycling process of wastewater could not be implemented due to the low flow rate of flowback and produced water (FPW) and the high cost of the water treatment processes. From evaluating data between 2012 to 2014, the annual volumetric flow of water used in shale gas was 116 billion liters per year and 66 billion liters per year of unconventional oil. The integration of operational data from 6 to 10 years shows that the total amount of flowback and produced water gathering from shale gas/oil wells was 803 billion liters [83]. Warner et al. [84] and Albright et al. [85] discussed the effects of preparing, exploration, and hydraulic fracturing process of shale gas wells on the water availability (quantity and quality) in the U.S.

2.4.2 Water Consumption for Hydraulic Fracturing in Texas

The net amount of water used in shale gas production was quantified by collecting data from three major shale gas plays (Eagle Ford, Haynesville, and Barnett) in Texas. In addition to study the capability of replacing fresh water with brackish water, the total accumulative amount of water use in shale gas production during the next 50 years [8]. Rahm [86] demonstrated the regulations that organize the work in hydraulic fracturing of shale gas sites focusing on Texas. Clark et al. [87] studied the life cycle of production for

shale gas and conventional natural gas emphasizing on the water consumption. This study estimated the amount of water consumption for shale gas and conventional natural gas in the various steps of production, the amount of flowback and produced water and the amount of shale gas production using as fuel in electricity and transportation. Thus, shale gas industry consumes water more than conventional natural gas during the life cycle. Reedy et al.[88] performed a comparison for the amount of water that consumed in the fracturing process of conventional oil and shale gas/oil production. This study found out that the U.S. has utilized a massive amount of water in hydraulic fracturing due to expanding in the shale gas production through using fracturing process.

2.4.3 Water Treatment

To enhance the efficiency and sustainability of shale gas process, the pretreatment processes are important to remove an assortment of pollutants that accompanied flowback and produced water (FPW) of hydraulic fracturing before conveyance to the desalination plants. The global optimization of the MINLP-based model was applied to many feedwater configurations and certain composition constraints to minimize the cost [89]. Bruning et al. [90] used a risk quotient approach to recognize organic pollutants in flowback and produced water of hydraulic fracturing and their impacts on the ecosystems of water resources. Furthermore, the flowback and produced water treatment technologies were proposed to remove contaminated compounds. Estrada and Bhamidimarri [91] offered a review of features, and environmental impacts of flowback and produced water of hydraulic fracturing. This literature found that reuse and deep injection well are

widespread techniques in the U.S., additional treatments (e.g., MED, RO) are required to achieve the discharge requirements.

Arias Chavez et al. emphasize on the economic feasibility of using desalination technologies (MED, MVC, RO) for reusing produced water (high salinity) of shale gas site [92]. This work found that these technologies are feasible technically and economically. The expanding in using these technologies is based on reducing capital and operating costs.

Ponce-Ortega et al. [93] developed a mathematical programming model for the combination of water networks in the shale gas site considering the quality and quantity of water, the uncertainty of used and flowback water, the optimal size of treatment units, thermal storage system, and disposals, the objective function of water networks has been solved to minimize the total annual cost. Gao and You [6] formulated the problem of water networks in the shale gas site as a mixed integer linear fractional programming (MILFP) problem to maximize the profit per unit of freshwater consumption. Grossmann et al. [94] developed the two-stage mixed integer linear programming (MINLP) model under uncertainty to address the problem of water availability for shale gas formations. The optimization of water usage life cycle of well-pads is to minimize the cost of treatment, storage, transportation, and disposal for the profit of gas production, as well as to determine the optimal hydraulic fracturing schedule commensurate with transportation of water and its reuse and treatment.

The techno-economic analysis of Integrated Precipitative Supercritical (IPSC) process, which was developed at Ohio University, was carried out by using Aspen process

software and Microsoft Excel. From this analysis, the average cost of flowback and produced water was $6.33 per barrel, while from sensitivity analysis, a cost range was $2.93-$16.03 per barrel [95].

3.5 Process Integration and Optimization

There is a robust linkage between process integration and optimization as El-Halwagi states "Optimization is a very effective and powerful tool that aids in the systematic solution of process integration problems" [96] . El-Halwagi [97] discussed the development of algorithmic methods that used to formulate the synthesis of chemical processes as an optimization problem, and he pointed out that the mixed-integer programming is the suitable tool for these methods. The essential steps to formulate an optimization model were given in [3].

The key idea for efficiency enhancement along with cost reduction of an industrial process is to develop energy integration techniques. The prime opportunity to achieve the typical integration of energy within a specific industrial process lies in integrating cogeneration process with thermal and electrical power requirements of an industrial process as well as multiple energy sources.

Many researchers have developed the techno-economic analysis for the dual-purpose system (cogeneration process and desalination technologies), which is used to supply fresh water and electricity. In these articles [80, 98-107] a mathematical model of the dual- system was described as a MINLP problem, as multi-objective genetic algorithm problem, or other proposed problem, and an optimization problem was performed to minimize the total annual cost for the entire system. El-Nashar [108] presented the optimal

17

design of a system including cogeneration process and desalination technologies for producing treated water and electric power along with considering the reliability of equipment. Al-Thubaiti et al. [109] developed an algorithmic approach to determine the optimal design and operating parameters for the cogeneration process.

The recent works in the field of the typical management (integration, optimization) of energy can be reviewed through the following publications, particularly, energy integration techniques that have been developed to meet the requirements of the methodical design and optimization of cogeneration process [110-112], trigeneration process (power, heating, cooling) [113], heat exchange networks [114]. In this context, the aforementioned topics are covered by the following recommended books [96, 115-117].

This work is aimed to develop a novel systematic approach to design, operation, integration, and optimization of a water-energy system for producing electricity and desalinated water (by treating shale-gas wastewater) through integrating renewables (solar energy) and fossil fuels (natural gas). The system is analyzed and subsequently optimized, (either by using deterministic optimization or by using stochastic optimization), by using economic and environmental metrics. To evaluate concentrated solar collectors' performance which is included in the system, two hierarchical calculation methodologies are proposed to obtain solar irradiance data.

CHAPTER III

AN INTEGRATED APPROACH TO WATER-ENERGY NEXUS IN SHALE-GAS

PRODUCTION[*]

3.1 Introduction

Recently, major discoveries of shale gas reserves have led to substantial growth in production. For instance, the US production of shale gas has increased from 2 trillion ft^3 in 2007 to 17 trillion ft^3 in 2016 with estimated cumulative production of more than 400 trillion ft^3 over the next two decades [118]. Consequently, there are tremendous monetization opportunities to convert shale gas into value-added chemicals and fuels such as methanol, olefins, aromatics, and liquid transportation fuels [119-125]. A major challenge to a more sustainable growth of shale gas production is the need to address natural resource, environmental, and safety issues [126, 127]. Specifically, the excessive usage of fresh water and discharge of wastewater constitute major problems. Hydraulic fracturing and horizontal drilling are the essential technologies to extract natural gas from shale rock. Water plays a significant role in shale gas production through mixing millions of gallons of water with sand, chemicals, corrosion inhibitors, surfactants, flow improvers, friction reducers, and other constituents to produce fracturing fluid. Under the high pressure, the fracturing fluid is injected into the wellbore to make cracks within the rock layers to increase the production [6, 7]. Large quantities of water are used in the fracturing and related process [94]. The typical annual water consumption per well for hydraulic

---

fracturing ranges between 1,000 and 30,000 m^3 leading to substantial amounts of water usage. For instance, the annual water usage in shale gas production is estimated to be about 120 MM m^3. In the Eagle Ford Shale Play, the annual water use is 18 MM m^3 for 1040 wells [8]. Wastewater associated with shale gas production is discharged in two forms: flowback water (which is released over several weeks following production) and produced water (which is the long-term wastewater) [94, 128]. Treatment of shale gas wastewater followed by recycle and reuse can provide major economic and environmental benefits [6-9, 94, 128]. Regrettably, a small fraction of the shale-gas wastewater is recycled. A recent study [93] reported that in 2014, less than 10% of the roughly 80,000 wells in the US used recycled water after proper treatment. Lira-Barragán et al. [93] developed a mathematical programming model for the combination of water networks in the shale gas site by taking into consideration the requirement of water, the uncertainty of used and flowback water, and the optimal size of treatment units, storage systems, and disposals. Gao and You [6] addressed the shale-gas water problem as a mixed integer linear fractional programming (MILFP) problem to maximize the profit per unit of freshwater consumption. Yang et al. [94] developed a two-stage mixed integer linear programming (MINLP) model has been proposed for shale gas formations with the uncertainty of water availability. Several approaches may be used for treatment and management of shale gas wastewater [7-9, 82, 92-94, 128]. These approaches include conventional technologies such as multi-effect distillation and reverse osmosis. Additionally, emerging technologies such as membrane distillation may be used to exploit excess heat from flared gases, compression stations, and other on-site sources and to provide a modular system with high

20

levels of salt rejection [58, 60, 107, 128-132]. Additionally, renewable energy (such as solar) may be utilized to enhance the sustainability of the system. Therefore, it is important to consider the water management problem for shale gas production via a water-energy nexus framework.

This work is aimed at developing a new systematic approach to design, operation, integration, and optimization of a dual-purpose system which integrates solar energy and fossil fuels for producing electricity and desalinated water while treating shale-gas wastewater. In addition to fossil fuels, a concentrated solar power field, a thermal storage system, conventional steam generators, and cogeneration process are coupled with two water treatment plants: reverse osmosis (RO) and multiple-effect distillation (MED). A multi-period mixed integer nonlinear program (MINLP) formulation is developed to account for the diurnal fluctuations of solar energy. The solution of the mixed integer nonlinear program (MINLP) determines the optimal mix of solar energy, thermal storage, and fossil fuel and the details of wastewater treatment and water recycle.

3.2 Problem Statement

Consider a shale-gas production site with the following known information:

- Flowrate and characteristics of produced and flared shale gas.
- Demand for fresh water (flowrate and quality).
- Flowrate and characteristics of flowback and produced wastewater.

The site is not connected to an external power grid.

It is desired to systematically design an integrated system which:

21

- Treats the wastewater for on-site recycle/reuse.

- Uses solar energy and fossil fuels to provide the needed electric and thermal power needs.

- Satisfies technical, economic, and environmental requirements.

Given are:

- Flowrate and composition of shale gas (sold and flared).

- Flowrate and purity need for fresh water.

- Total volumetric flow of wastewater (flow-back and produced water) of shale gas play.

- Flowrate of flared gases that may be used in the cogeneration process.

- Electric energy requirement for RO and MED, (kWh_e/m^3).

- Thermal energy requirement for MED, (kWh_t/m^3).

To solve the problem, the following questions should be addressed:

- What the maximum annual profit of the whole system for producing desalinated water, electricity for the various percentage contribution of RO and MED in the total desalinated water production?

- What the minimum total annual cost of the entire system?

- What is the economic feasibility of the system?

- What is the optimal mix of solar energy, thermal storage, and fossil fuel for MED plant and the entire system?

- What is the optimal design and integration of the system?

- What are the optimal values of the design and operating variables of the system (e.g., minimum area of a solar collector, maximum capacity of a thermal storage system, etc.)?

- What is the feasible range of the percentage contribution of RO and MED in the total desalinated water production?

The Superstructure integrates primary components of solar energy and fossil fuels for producing electricity and desalinated water, as shown in Figure 1:

- To achieve a steady supply of thermal power to the whole system, solar energy (as direct solar thermal power), fossil fuel (shale gas, flared gas), and a thermal energy storage (as indirect solar thermal power) are used.

- Solar energy is used as a source of heat to provide thermal power directly to MED plant exclusively (to be more economically feasible), while the surplus thermal power is stored.

- A two-stage turbine is used to enhance the cogeneration process efficiency.

Figure 1: Proposed Superstructure Representation. Reprinted with
permission from [156]
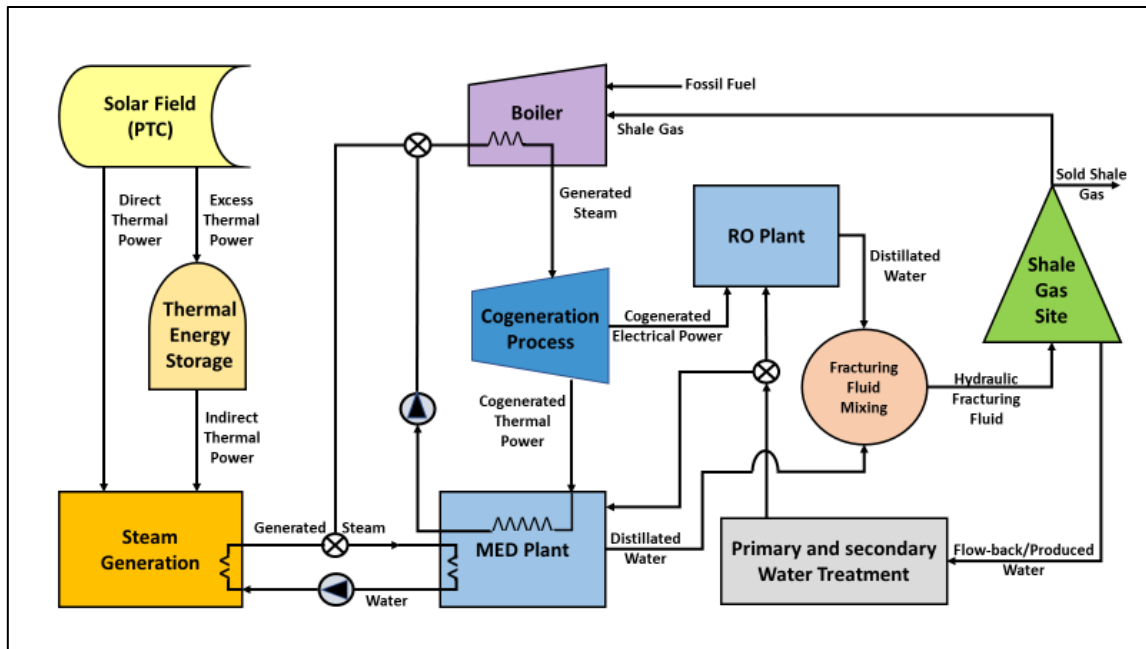
3.3 Approach

A hierarchical design is proposed to efficiently address the water-energy nexus
problem. Figure 2 demonstrates the main steps of the approach. The first step is to gather
the required data for the system then to select and formulate the appropriate models that
describe the major system components. Once the preceding steps are achieved, the
computational optimization is applied to the integrated system to maximize annual profit
of the system that produces a specific level of desalinated water and electricity. In treating
wastewater, focus is given to the management of flowback and produced shale gas
wastewater. To decompose the optimization problem, the percentage contribution of RO
and MED to treating wastewater is iteratively discretized. It is worth noting that the
proposed discretization approach offers significant reduction in the complexity of solving

24

the optimization problem. For each discretization, the thermal and electric loads are calculated. Therefore, the two energy systems can be designed separately then integrated and optimization. Such decomposition leads to computational efficiency. Similar approaches have been proposed earlier in literature for other applications [131, 133, 134]. The total annualized cost for each discretized iteration is calculated and finally the minimum-cost solution is selected.
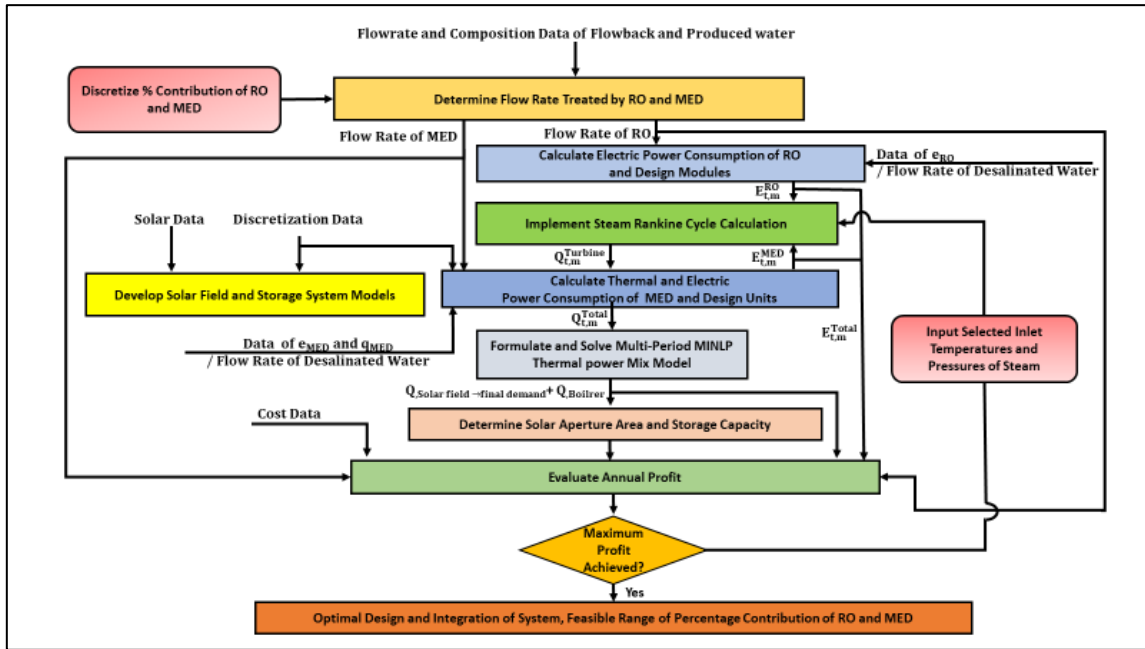
Figure 2: Proposed Approach. Reprinted with permission from [156]

3.4 Modeling the Building Blocks

The performance models for MED and RO have been taken from literature [96, 135-138]. For the solar system, a parabolic trough collector was selected. The modeling of the solar system was based on literature models and data [13, 25, 27, 33] as described

25

in this section. The solar thermal power (per unit length of a collector) that produced by the solar field when the direct normal irradiance (DNI) strikes collector aperture plane is given by the following expression:

$$Q_{sun \to collector}(W/m) = DNI.\cos \Theta . W_c \qquad (1)$$

where DNI (W/m^2) is the direct normal irradiance, Θ is the solar incidence angle, W_C (m) is the width of the collector aperture.

For North-South orientation, the incidence angle is calculated as follows:

$$\cos \Theta = \sqrt{\cos^2\theta_z + \cos^2\delta.\sin^2 \omega} \qquad (2)$$

where θ_z is the solar zenith angle, δ is the declination, ω is the hour angle.

To calculate the thermal power (per unit length of a collector) that absorbed by the receiver tube of a collector loop, the influences of the optical losses can be taken into consideration by inserting four parameters to Eq. is given by the following expression:

$$Q_{collector \to reciever}(W/m) = DNI.\cos \Theta . W_c . \eta_{opt}. K(\Theta). F_f. R_{SL}. O_{EL} \qquad (3)$$

Where η_{opt} is the peak optical efficiency of a collector, $K(\Theta)$ is the incidence angle modifier, F_f is the soiling factor (mirror cleanliness), R_{SL} is the row shadow loss, O_{EL} is the optical end loss.

The peak optical efficiency of a collector when the incidence angle on the aperture plane is 0° is:

$$\eta_{opt} = \rho.\gamma.\tau .\alpha \big|_{\Theta=0^o} \qquad (4)$$

where ρ is the reflectivity, γ is the intercept factor, τ is the glass transmissivity, α is the absorptivity of the receiver pipe.

The incidence angle modifier for a LS-3 collector is given by:

$$K(\theta) = 1 - 2.23073 \times 10^{-4}.\theta - 1.1 \times 10^{-4}.\theta^2 + 3.18596 \times 10^{-6}.\theta^3$$
$$-4.85509 \times 10^{-8}.\theta^4 \qquad 0^0 \leq \theta \leq 80^0$$
$$K(\theta) = 0 \qquad\qquad\qquad\qquad\qquad \theta > 80^o \qquad\qquad (5)$$

The row shadow factor is:

$$R_{SL} = \min\left[\max\left(0.0, \frac{L_{spacing}}{W_c} \cdot \frac{\cos\theta_z}{\cos\theta}\right); 1.0\right] \qquad (6)$$

where $L_{spacing}$ (m) is length of spacing between troughs.

The optical end loss is:

$$O_{EL} = 1 - \frac{f.\tan\theta}{L_{SCA}} \qquad\qquad (7)$$

where f is focal length of the collectors (m), L_{SCA} is length of a single collector assembly (m).

The total thermal power (per unit length of a collector) that loss from a collector represents the combination of the radiative heat loss from the receiver pipe to ambient ($Q_{reciever \to ambient}$) and convective and conductive heat losses from the receiver pipe to its outer glass pipe ($Q_{receiver \to glass}$), and is calculated by the following expression:

$$Q_{collector \to ambient} (W/m) = U_{rec} . \pi . d_o . (T_{rec} - T_{amb}) \qquad (8)$$

where U_{rec} (W/m$^2_{rec}$.K) is the overall heat transfer coefficient of a receiver pipe, d_0 (m) is the outer diameter of a receiver pipe, T_{rec} (K) is the mean receiver pipe temperature, T_{amb}(K) is the ambient air temperature.

The overall heat transfer coefficient of a collector is found experimentally depending on the receiver pipe temperature, and it can be given in the second-order polynomial equation:

$$U_{rec} = a + b\,(T_{rec} - T_{amb}) + c\,(T_{rec} - T_{amb})^2 \tag{9}$$

where a, b, and c coefficients have been calculated experimentally for the LS-3 collector have been reported in literature [27].

The thermal power (per unit length of a collector) that transferred from a collector to a fluid is given in the following expression [26]:

$$Q_{collector \rightarrow fluid}(W/m) = Q_{,collector \rightarrow receiver} - Q_{,collector \rightarrow ambient} \tag{10}$$

The thermal power (per unit length of a collector) that loss from the headers (pipes) is given in the following expression [24]:

$$Q_{LFP}(W/m) = 0.0583\,.W.\,(T_{rec} - T_{amb}) \tag{11}$$

The thermal power (per unit length of a collector) that loss from the expansion tank (vessel) is given in the following expression [24]:

$$Q_{LFV}(W/m) = 0.0497\,.W.\,(T_{rec} - T_{amb}) \tag{12}$$

The useful thermal power (per unit length of a collector) that produced by the solar field is given by the following expression, which represents the sum of Equations 10-12:

$Q_{\text{solar field}\rightarrow\text{final demand}}(W/m)$

$$= Q_{\text{collector}\rightarrow\text{receiver}} - Q_{\text{collector}\rightarrow\text{ambient}} - Q_{,\text{LFP}}$$

$$- Q_{\text{LFV}} \tag{13}$$

The inlet thermal power of the thermal storage is given in the following expression:

$$Q_{\text{in}} = m_{\text{ms}} . C_{P,\text{ms}} . (T_{\text{HT}} - T_{\text{CT}}) = \eta_{\text{EX}} . m_{\text{oil}} . C_{P,\text{oil}} . (\Delta T) \tag{14}$$

The expression of the discharge process (outlet thermal power) is given by:

$$Q_{\text{out}} = m_{\text{oil}} . C_{P,\text{oil}} . (\Delta T) = \eta_{\text{EX}} . m_{\text{ms}} . C_{P,\text{ms}} . (T_{\text{HT}} - T_{\text{CT}}) \tag{15}$$

where m_{ms} is the molten salt flow rate (Kg/s), ($C_{P,\text{ms}} = 1443 + 0.172\, T_{\text{ms}}$) is the specific heat of the molten salt (J/kg.$^\circ$C), T_{ms} is the temperature ($^\circ$ C) of the molten salt, T_{HT} is the hot tank temperature ($^\circ$C), T_{CT} is the cold tank temperature ($^\circ$C), η_{EX} is the efficiency of the heat exchanger, m_{oil} is the oil mass flowrate (Kg/s), ΔT is the difference between inlet and outlet of the oil.

The net thermal power inside the tank (w) can be calculated by the following expression:

$$Q_{\text{TES}} = Q_{\text{acc}} + Q_{\text{in}} - Q_{\text{out}} - Q_{\text{loss}} \tag{16}$$

where Q_{acc} is the accumulated thermal power in the tank from preceding iterations, Q_{loss} is the thermal power loss (kW/m^2) of the cold and heat tanks and it is given in the following empirical equation [46]:

$$Q_{\text{loss}} = 0.00017. T_{\text{ms}} + 0.012 \tag{17}$$

where T_{ms} is the temperature ($^\circ$ C) of the molten salt in the hot and in the cold tanks.

The optimal values of the Rankine cycle parameters of cogeneration process can be satisfied by formulated the entire cycle as an optimization problem. Thus, there is a necessity to obtain suitable correlations of thermodynamic properties that can be used in optimization formulations. In thermodynamic calculations of the Rankine cycle, mathematical equations are used to replace the steam tables because they could incorporate easily into optimization formulations. However, available correlations for steam tables are complicated (e.g., nonlinear, nonconvex function), and it is hard to insert them in optimization task. Consequently, a new set of thermodynamic correlations have been developed in literature [109] to estimate properties of steam and they can be incorporated easily into optimization formulation and cogeneration design. The isentropic efficiency of the steam turbine can be obtained from the turbine hardware model, which developed by Mavromatis and Kokossis [139], to show the efficiency variation with the load, the turbine size, and operating conditions, as in the following correlation:

$$\eta_{is} = \frac{6}{5 \cdot B}\left(1 - \frac{3.41443 \cdot 10^6 \cdot A}{\Delta h_{is} \cdot m^{max}}\right)\left(1 - \frac{m^{max}}{6 \cdot \dot{m}}\right) \tag{18}$$

where $\dot{m}$ is the inlet turbine steam flowrate (Ib/hr), and m^{max} is the maximum mass flowrate of a turbine(Ib/hr) , A and B are parameters that depend on the inlet saturation temperature (°F) and the type of turbine as in the following correlations:

$$A = a_o + a_1 \cdot T_{sat} \tag{19}$$

$$B = a_2 + a_3 \cdot T_{sat} \tag{20}$$

where a_o, a_1, a_2, a_3 the correlation constants and can be found in literature [112].

3.5 Optimization Formulation

Because of the diurnal nature of solar energy, a multi-period approach is adopted. The annual operation is discretized in a number of operational periods (e.g., monthly). The index m refers to the operational period. For each operational period, an average meteorological day is used to represent the solar intensity data. In turn, the meteorological day is discretized into a number of sub-periods (e.g., 24 hours) where the index t is used to designate a sub-period. Two water-treatment technologies are used: multi-effect distillation (MED) and reverse osmosis (RO). MED consumes mostly thermal energy and some electric energy which are respectively given by the specific requirements: q_{MED} (kWh_t/m^3) and e_{MED} (kWh_e/m^3). RO requires electric energy which is represented by the following specific energy consumption term: $e_{RO}(kWh_e/m^3)$.

For each sub-period t, the thermal power needs for water treatment is obtained directly from the combustion of fossil fuels ($Q_{t,m}^{Fossil}$), directly from a solar thermal collector ($Q_{t,m}^{Direct,SC}$), indirectly from solar energy through thermal storage ($Q_{t,m}^{Out\_Stored\_SC}$), and from steam leaving the cogeneration turbine ($Q_{t,m}^{Turbine}$). Hence,

$$Q_{t,m}^{Total} = Q_{t,m}^{Fossil} + Q_{t,m}^{Direct,SC} + Q_{t,m}^{Out\_Stored\_SC} + Q_{t,m}^{Turbine} \qquad \forall t, \forall m \qquad (21)$$

where

$$Q_{t,m}^{Total} = F_{t,m}^{MED} q_{MED} \qquad \forall t, \forall m \qquad (22)$$

The electric power provided by the cogeneration turbine is given by:

31

$$E_{t,m}^{Total} = F_{t,m}^{RO} \, e_{RO} + F_{t,m}^{MED} \, e_{MED} \qquad \forall t, \, \forall m \qquad (23)$$

The thermal power captured by the solar collector ($Q_{t,m}^{SC}$) is directly used

($Q_{t,m}^{Direct, \, SC}$) or is stored ($Q_{t,m}^{In\_Stored-SC}$) for subsequent usage, i.e.

$$Q_{t,m}^{SC} = Q_{t,m}^{Direct, \, SC} + Q_{t,m}^{In\_Stored-SC} \qquad \forall t, \, \forall m \qquad (24)$$

Over a sub-period, t, the thermal power balance for the thermal storage unit is given by:

$$Q_{t,m}^{Stored-SC} = Q_{t-1,m}^{Stored-SC} + Q_{t,m}^{In\_Stored-SC} - Q_{t,m}^{Out\_Stored-SC} - Q_{t,m}^{Stored-Loss} \qquad \forall t, \forall m \quad (25)$$

Such collected energy is a function of the solar-radiation intensity (Solar_Radiation$_{t,m}$) and the effective surface area of the solar collector (A^{SC}).

Although each period requires a certain area of the solar collector, the design value (which is also used for capital cost estimation) is the largest of all needed areas, i.e.:

$$A_{t,m}^{SC} \leq A_{Design}^{SC} \qquad \forall t, \forall m \qquad (26)$$

The cogeneration turbine is modelled through a performance function (e.g., isentropic expansion with an efficiency) that combines inlet and outlet steam conditions and relates the produced power to heat.

$$\Omega_{t,m}^{Turbine} (D_{t,m}^{Tutbine}, O_{t,m}^{Turbine}, Steam_{t,m}^{In}, Steam_{t,m}^{Out}, Power_{t,m}^{Out}) = 0 \qquad \forall t, \, \forall m \qquad (27)$$

The objective function seeks to maximize the profit for the water-energy nexus system:

Maximize Annual Profit = Annual value of treated water + Annual value of avoided cost of discharging wastewater – Cost of fossil fuels - Total annualized cost of solar collection system – Total annualized cost of solar storage system – Total annualized cost of cogeneration system - Total annualized cost of MED system – Total annualized cost of RO system

Maximum Annual profit =

$$\sum_m \sum_t (v_{t,m}^{RO} \ F_{t,m}^{RO} + v_{t,m}^{MED} \ F_{t,m}^{MED}) + c^{Waste} \ W_w - \sum_m \sum_t (c_{t,m}^{Fossil} \ F_{t,m}^{Fossil}) - \ AFC^{SC} -$$

$$\sum_m \sum_t OPEX_{t,m}^{SC} - \ AFC^{SC-Storage} - \sum_m \sum_t OPEX_{t,m}^{SC-Storage} - \ AFC^{Cogen} -$$

$$\sum_m \sum_t OPEX_{t,m}^{Cogen} - \ AFC^{MED} - \sum_m \sum_t OPEX_{t,m}^{MED} - \ AFC^{RO} - \sum_m \sum_t OPEX_{t,m}^{RO}$$

(28)

It is worth noting that the economic objective function can be altered to include sustainability and safety metrics by using the sustainability and safety weighted return on investment metrics [140, 141].

3.6 Case Study

To demonstrate the viability of the proposed approach for solution strategies, a case study will be solved that based on the Eagle Ford shale play, which is located south Texas. A dual-purpose system which integrates solar energy and fossil fuels for producing electricity and fresh water has been considered. The optimal design, operation, and integration of the system will be found through this case study that requires particular input data for each unit of the entire system. As mentioned earlier, this system includes concentrated solar power field, a thermal storage system, conventional steam generators,

and a cogeneration process into two water treatment plants, a reverse osmosis plant (RO) and a multiple-effect distillation plant (MED).

3.7 Flowback/Produced Water of Shale Gas Play

In order to supply a specific amount of flow-back and produced water (FPW) from a shale play to a desalination plant, the calculation of an FPW flow average for many years is an appropriate option to avoid the uncertainty in the amount of FPW. Specifically, if we know that wastewater of shale play is typically subjected to heavily regulated and should store in containers so that these containers can be utilized to get a constant flow approximately. Additionally, a large number of wells in a shale play can contribute to making the flow rate of FPW approximately constant because when the FPW production of one well starts declining, another well will start its production and compensate a drop of production in other wells.

The value of flowback and produced water returned from shale gas formations to the surface in the Eagle Ford Basin is estimated to be 151.22×10^6 m^3 [49] for 10 plays since the early 2000s until 2015. Table 2 summarizes the costs of RO and MED. Additional data can be obtained from the literature [142-144]. The techno-economic data for RO and MED are reported in Table1.

Table 1: Techno-economic data for RO and MED [96, 145]

Technology	Thermal energy consumption (kWht/m³ Desalinated water)	Electric energy consumption (kWhe/m³ Desalinated water)	Annualized fixed cost (AFC) ($/year)	Operating cost ($/m³ seawater)	Water recovery (m³ desalinated water/m³ feed seawater)	Value of desalinated water ($/m³ desalinated water)	Outlet Salt Content (ppm)
RO	-	4	$2.0 . 10^6 + 1,166 .$ (flowrate of seawater, m³/day)$^{0.8}$	0.18	0.55	0.88	200
MED	65	2	$13.0 . 10^6 + 2,227 .$ (flowrate of seawater, m³/day)$^{0.7}$	0.24	0.65	0.82	80

3.8 Solar Energy

The solar data are summarized in Appendix A. Table 2 summarizes the main cost data for the solar collectors.

Table 2: The direct capital cost of parabolic trough collector items [40, 41]

Item	Receivers	mirrors	Concentrator Structure	Concentrator Erection	Drive	Piping
Cost $/m^2$	43	40	47	14	13	10
Item	Electronic &control	Header piping	Civil works	Spares, HTF, Freight	Contingency	Structures &Improvement
Cost $/m^2$	14	7	18	17	11	7

The total fixed capital cost of the solar field ($) is the sum of heat collection element (HCE), mirror, support structure, drive, piping, civil work, structures, and improvements, as follows:

$$\text{FCI}_{\text{SF}} = C_{\text{SF}} \cdot A_{\text{SF}} \tag{29}$$

where C_{SF} is the solar field cost per area unit ($\$\,241/\text{m}^2$), A_{SF} is the solar field aperture area (m^2).

The thermal storage system is assumed an indirect two-tank type which is used the binary solar salt (sodium and potassium nitrate) as a storage material with the following fixed capital cost estimation ($):

$$\text{FCI}_{\text{TES}} = C_{\text{TES}} \cdot \text{SC} \cdot Q_{\text{solar field} \rightarrow \text{final demand}} \tag{30}$$

where C_{TES} is the thermal storage system cost per thermal energy unit ($27.18/kWh), SC is the number of storage capacity hours (hr), $Q_{\text{solar field} \rightarrow \text{final demand}}$ is the useful thermal power that produced by solar field (kW).

The fixed capital cost estimation of a steam generator system ($) is calculated as:

$$\text{FCI}_{\text{SG}} = C_{\text{SG}} \cdot Q_{\text{solar field} \rightarrow \text{final demand}} \tag{31}$$

where C_{SG} is the steam generator system cost per thermal power unit ($/kW_t$).

The fixed capital cost of a boiler ($), which is assumed a water-tube boiler fueled with gas or oil, is estimated as follows [109]:

$$FCI_B = 3 \cdot N_p \cdot N_T \cdot Q_{Boiler}^{0.77} \tag{32}$$

where Q_{Boiler} is the amount of thermal power (BTU/hr) transferred to the steam and equal to (Q_{Boiler}/η_{boiler}), η_{boiler} is the efficiency of a boiler, N_P is a factor to account for the operation pressure and it is given by: $N_P = 7 \cdot 10^{-4} \cdot P_g + 0.6$; P_g is the gauge pressure (pisg) of a boiler, N_T is a factor accounting for the superheat temperature and is given by:

$N_T = 1.5 \cdot 10^{-6} \cdot T_{SH}^2 + 1.13 \cdot 10^{-3} \cdot T_{SH} + 1$; T_{SH} is the superheat temperature (°F), $T_{SH} = T^{in} - T_{sat}^{in}$; T^{in} is the temperature at the inlet of a turbine, T_{sat}^{in} is the saturation temperature at the inlet of a turbine.

The fixed capital cost of a turbine ($), which is assumed a non-condensing turbine, is estimated as follows [109]:

$$FCI_T = 475 \cdot E_T \tag{33}$$

where E_T is the turbine shaft power output (BTU/hr); $E_{,T} = m \cdot (h^{in} - h_{act}^{out})$.

3.9 Flared Gas

The shale gas production from Eagle Ford wells can be used as a fuel for cogeneration process. Furthermore, the flared gas can be used also as a fuel source for cogeneration process that it will contribute to saving a considerable amount of shale gas along with diminishing CO_2 emissions accompanying to the flared gas. In Eagle Ford fields, 4.4 billion cubic feet of gas was flared in 2013 that represented around 13% of the gas in the formation [146].

3.10 Total Cost

The annual fixed cost (AFC) ($/year) of the system is determined as follows:

$$AFC=[(FCI_{SF} + FCI_{TES} + FCI_{SG} + FCI_B + FCI_T + FCI_{PST})/N] + AFC_{RO} + AFC_{MED} \quad (34)$$

The operation and maintenance cost ($/hr) of solar field, cogeneration process, thermal storage system, administration, and operations is estimated as follows, based on data are given by [40, 41]:

$$OC_{OM} = C_{OM} \cdot (Q_{solar\ field \rightarrow final\ demand} + Q_{Boiler}) \quad (35)$$

where C_{OM} is the operation and maintenance cost per thermal power unit ($0.0203/kWh$).

The type and amount of the selected fuel are necessary to estimate the cost of fuel ($/hr) and it is formulated as follows:

$$OC_F = C_F \cdot Q_B \cdot 3413 \cdot 10^{-6} \quad (36)$$

where C_F is the fuel cost ($/MMBTU), Q_B is the amount of thermal power (BTU/hr) that equals to (Q_{Boiler}/η_{boiler}), η_{boiler} is the efficiency of a boiler.

The annual operating cost (AOC) ($/year) is determined as follows:

$$AOC = a_Y \cdot (OC_{OM} + OC_F) \quad (37)$$

where a_Y is the annual operation time (hr/year).

The annual income ($/year) is the sum of the total desalinated water production value and the saving value of a reduction in the cost of transportation, fresh water acquisition, and disposal:

Annual income $= a_Y \cdot \{(0.88 \cdot \text{flowrate of desalinted water from RO, m}^3/\text{hr} +$

$0.82 \cdot \text{flowrate of desalinted water from MED, m}^3/\text{hr}) + [(C_{FW} + C_{DS} +$

$C_{TR}) \cdot \text{total flowrate of disalinated water from (RO, MED)}]/0.11924 \}$ \quad (38)

where C_{FW} is the fresh water cost per volume unit(0.24\$/bbl), C_{DS} is the disposal cost per volume unit(0.05\$/bbl), C_{TR} is the transportation cost per volume unit(0.89\$/bbl).

The net profit represents the sum of the total desalinated water production value and the saving value of a reduction in the cost of transportation, fresh water acquisition, and disposal. The treatment process of flowback and produced water in a shale gas site that can be contributed effectively to save a money for each barrel of flowback and produced water which should be trucked and disposed. Table 3 shows the cost of transportation, fresh water acquisition, primary /secondary treatment, and disposal depending on the characteristics of a water treatment plant with capacity an 2,380 barrel/day in Eagle Ford basin [147].

Table 3: Cost of transportation, fresh water, treatment, and disposal of FPW [147]

Fresh water (\$/barrel)	0.24
Disposal (Deep well + Landfill) (\$/barrel)	0.05
Primary & secondary treatment (\$/barrel)	0.34
Transportation (\$/barrel)	0.8

3.11 Results and Discussion

A detailed performance model of the parabolic trough was applied to the case study to determine the useful thermal power (per unit length of a collector) that produced by the solar field. The calculations of the solar field have been carried out depending on the monthly average of hourly direct solar irradiance, hourly ambient temperature, and hourly incidence angle. Moreover, the characteristics of the LS-3 collector were adopted and all types of thermal losses (convection, conduction, radiation) are considered for the entire

the solar field. The hourly variations in the useful thermal power for 12 months were obtained, as shown in Figure 3.
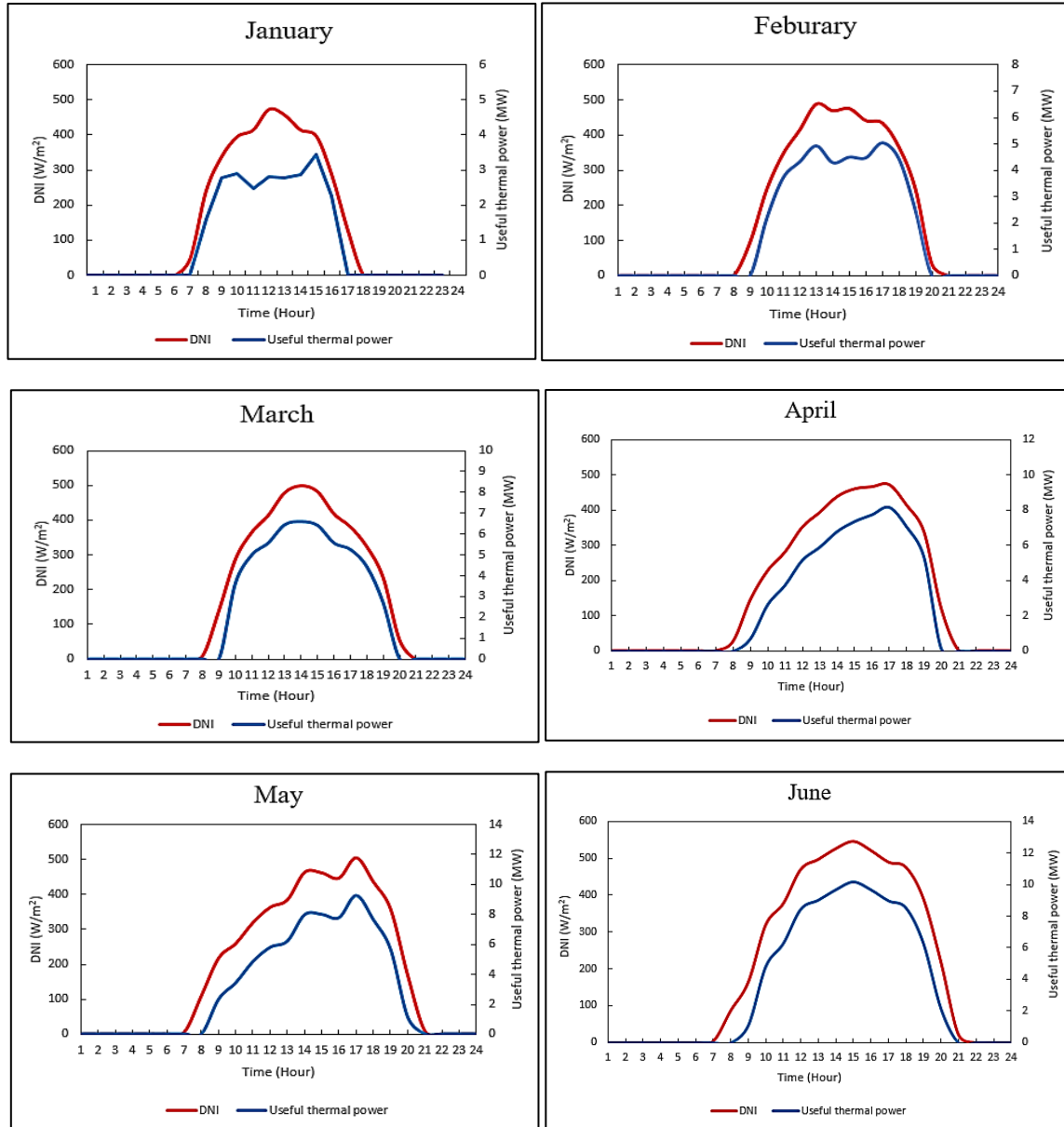
Figure 3: Monthly average of hourly DNI and useful thermal power. Reprinted with permission from [156]
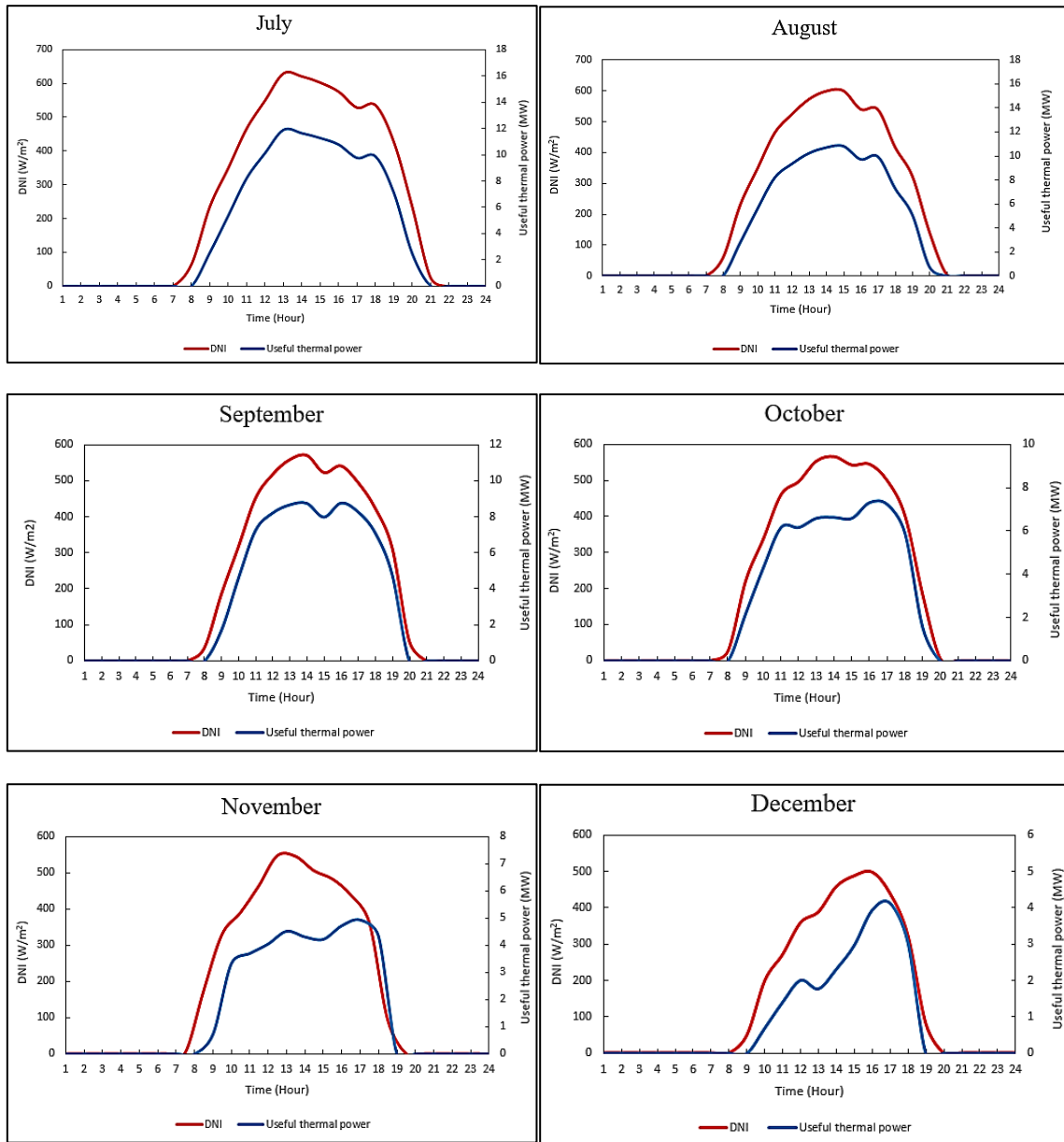
Figure 3: Continued. Reprinted with permission from [156]

The obtained results showed that the gained thermal power in the month January, February, November, and December is less than the rest eight months of the year due to low DNI and the high cosine effect. However, the four months, which have the lowest

value of useful thermal power still has the significant potential to provide a thermal power to the system. The selecting solar irradiance around ($500 \ \text{W/m}^2$) at design point to calculate the total area of collectors can give a great chance for these four months to contribute efficiently to supply a sufficient thermal power, despite a low value of average direct normal irradiance in the region that selected as a case study. In the same direction, the eight months, which have a higher DNI can be exploited to provide direct thermal power to MED and a surplus thermal power to a thermal storage system. Indeed, the optimal area of collectors and storage system capacity are based on the minimum total annual cost of the entire system that can be obtained through an optimization solution.

The monthly distribution of the optimal thermal power mix for MED plant and the entire system has been determined for the different percentage contribution of RO and MED in the total desalinated water production. The optimal thermal power mix for MED plant includes the direct thermal power of solar field, the indirect thermal power of thermal storage system, the surplus thermal power of cogeneration system, and the direct thermal from the combustion of fossil fuels. The monthly distribution varies over the year due to the availability of DNI and the variability of an incident angle, as shown in Figures 4-6.
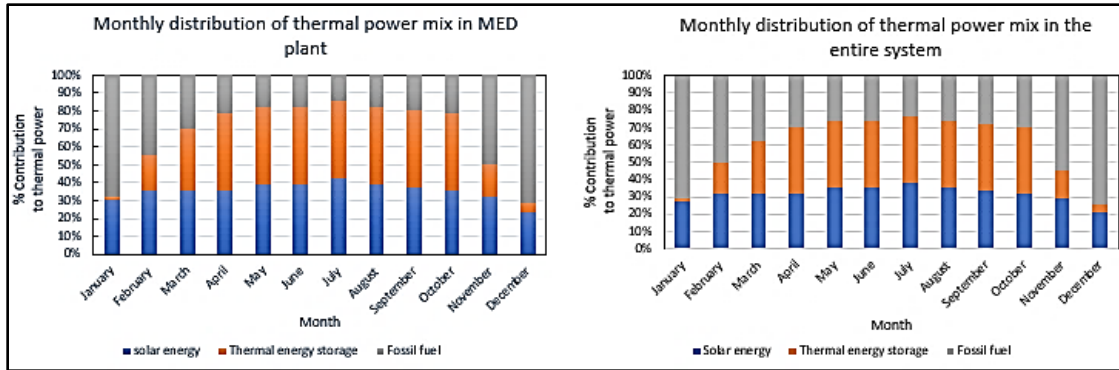
Figure 4: Optimal thermal power mix for MED plant and the entire system with (30% RO 70% MED). Reprinted with permission from [156]
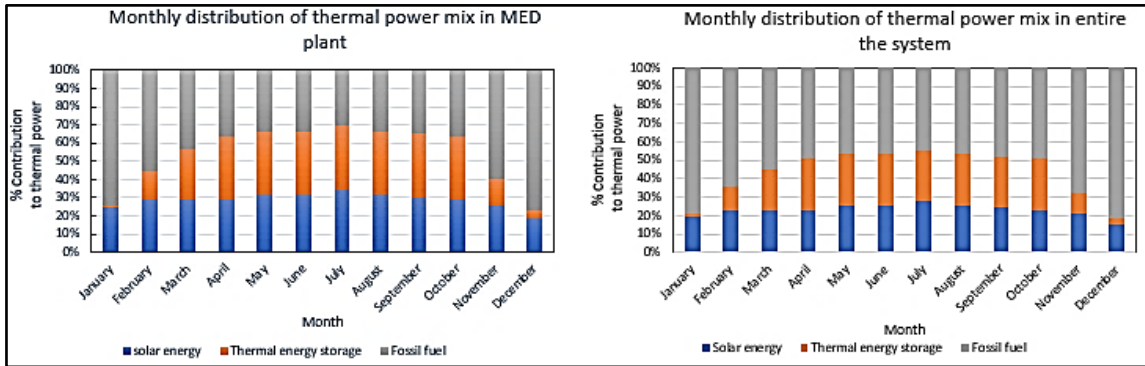
Figure 5: Optimal thermal power mix for MED plant and the entire system with (60% *RO* 40% *MED*). Reprinted with permission from [156]
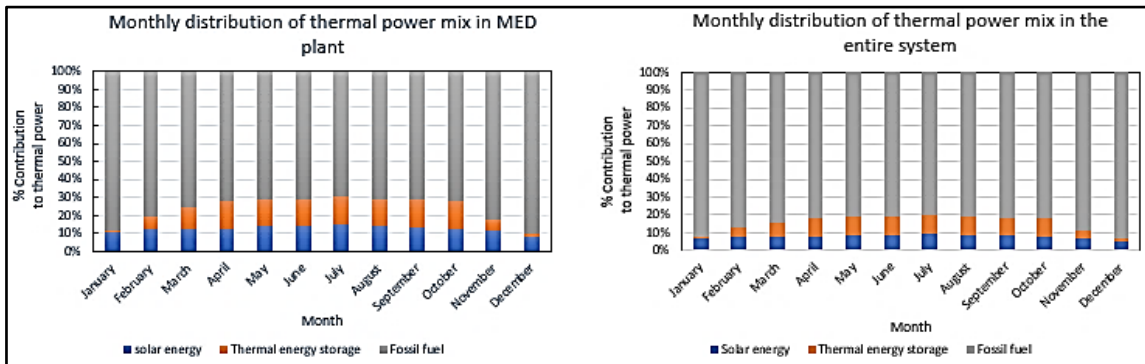
Figure 6: Optimal thermal power mix for MED plant and the entire system with (80% *RO* 20% *MED*). Reprinted with permission from [156]

The solution of the case study introduces two scenarios to the optimal operation for MED in accordance with the availability of solar energy regardless of the percentage contribution of MED, the first scenario is for the months of January, February, November, and December and shows that it favors the harness of direct solar thermal power during the hours of the diurnal and utilize fossil fuel in the early hours of the day and in the evening. However, stored solar thermal power can be contributed from 1 to 2 hours only because of lacking solar energy in these months, as illustrated in Figure 7, adapted from [148].

The second scenario is for the months of April, March, May, June, July, August, September and October and shows sharply diminishing fossil fuel use up to 2 h only. Typically, direct solar thermal power is exploited in the middle of the day, while stored solar thermal power is dispatched in the early hours and in the evening, as shown in Figure 8, adapted from [148]. In future work, the previous two scenarios can be applied to the entire system in the case of integrating solar energy into cogeneration process.
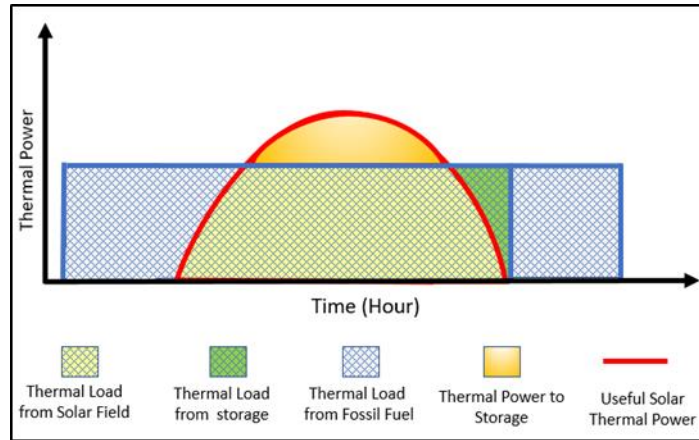
Figure 7: Optimal operation for MED during January, February, November, and December. Reprinted with permission from [156]
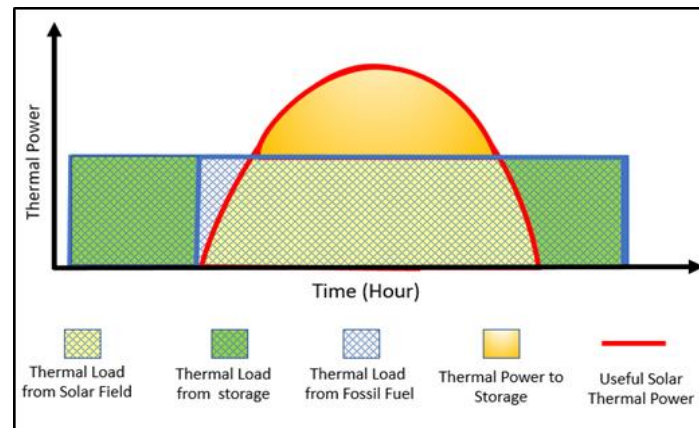
Figure 8: Optimal operation for MED during April, March, May, June, July, August, September, and October. Reprinted with permission from [156]

It is observed that the total annual cost of the system as mentioned in the previous section can be reduced by increasing the percentage contribution of RO over MED, but it requires consuming much amount of fossil fuel. More consumption of fossil fuel causes serious environmental impacts due to emitting a massive amount of CO_2. From the case study, the sustaining of fossil fuel resources and diminishing the emissions of greenhouse

45

gas requires enhancing the percentage contribution of MED in the system that based on solar energy as a provider for a high percentage of thermal power. Figure 9 offers an obvious comparison between the economic and environmental aspects of the system through the different percentage contribution of RO and MED in the total desalinated water production. Reconciliation of economic and environmental objective can be achieved using a sustainability weighted return on investment calculation [96, 141].
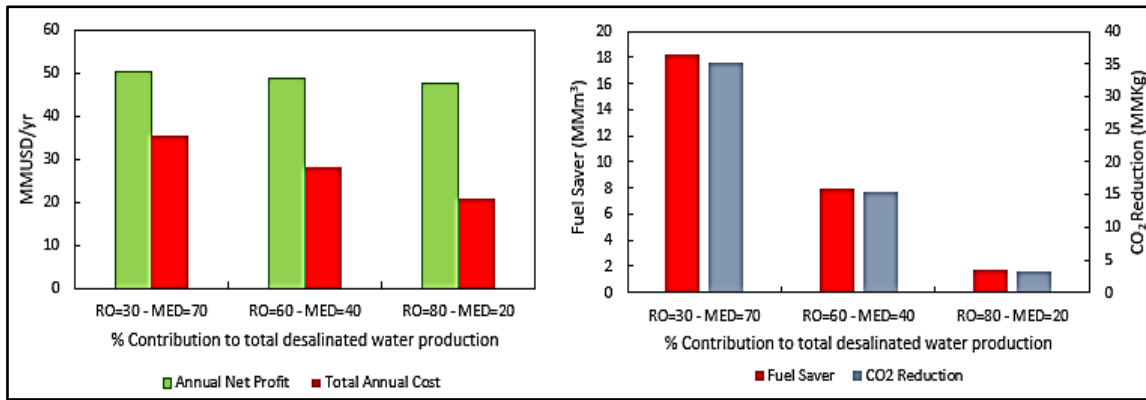
***Figure 9*:** Comparison between the economic and environmental aspects. Reprinted with permission from [156]

The case study shows that in Eagle Ford fields, 4.4 billion cubic feet of gas was flared in 2013 that represented around 13% of the gas in the formation [146]. Therefore, this significant amount of flared gas can be exploited as a major source of energy for the system or sharing shale gas in a specific percentage as a minor source of energy, the results of the different percentage contribution of flared gas are shown in Table 4.

Table 4: Technical and economic results for the system. Reprinted with permission from [156]

Percentage of Contribution *(%)	Percentage of Contribution **(%)	Total annual cost (MM$/year)	Annual Net (After − Tax)profit (MM$/year)	ROI (%)	Payback period (year)
30 RO 70 MED	0.0	35.3	50.4	14.9	5.9
30 RO 70 MED	50	35.1	50.6	14.96	5.6
30 RO 70 MED	100	34.8	50.8	15	5.5
60 RO 40 MED	0.0	28.1	48.8	17.2	4.9
60 RO 40 MED	50	27.8	49	17	4.8
60 RO 40 MED	100	27.5	49.2	17.3	4.8
80 RO 20 MED	0.0	23.5	47.7	19.1	4.4
80 RO 20 MED	50	23.2	47.9	19.2	4.3
80 RO 20 MED	100	22.8	48.1	19.3	4.3

*The percentage contribution of RO and MED plants in the total desalinated water production; ** The percentage contribution of flared gas as source of energy.

3.12 Summary

A water-energy nexus framework has been used to address water management in shale gas production. The following key elements have been integrated: solar energy, fossil fuel, cogeneration process, MED and RO. A hierarchical approach and a multi-period MINLP have been developed and solved to find the optimal mix of solar energy, thermal storage and fossil fuel and the optimal usage of water treatment technologies. A case study for Eagle Ford Basin in Texas has been solved to show the applicability of the proposed approach. The system has been analyzed according to the technical, economic and environmental aspects. The multi-period method has been applied to discretize the

operational period to track the diurnal fluctuations of solar energy. The percentage utilization of water treatment technologies has been iteratively discretized. Once the solution of the mixed integer nonlinear program (MINLP) was applied to each discretization, the optimal mix of solar energy, thermal storage and fossil fuel, the optimal values of the design and operating variables of the system (e.g., minimum area of a solar collector, maximum capacity of the thermal storage system, etc.) have been determined. The results show the system's economic and environmental merits using a water-energy nexus framework and enabling effective water management strategies while incorporating renewable energy.

CHAPTER IV

AN INTEGRATED APPROACH BASED ON STOCHASTIC OPTIMIZATION FOR

WATER-ENERGY NEXUS WITH MULTIPLE ENERGY SOURCES UNDER

UNCERTAINTY

4.1 Introduction

The rapid expansion in energy and water consumption, particularly in oil and gas industries, has emerged as a substantial problem due to economic and environmental considerations. These industries can be classified into the upstream, midstream, and downstream sectors and each sector has various requirements of energy and water based on its physical site and certain functionality. The recent advancement in hydraulic fracturing technology and horizontal drilling has contributed to considerable growth in shale gas production. For instance, the US production of shale gas has increased from 2 trillion ft^3 in 2007 to 17 trillion ft^3 in 2016, and the recent estimation shows that the cumulative production would be more than 400 trillion ft^3 over the next two decades [118]. The importance of shale gas comes from being as one of the most essential resources for electric power generation [149], and other industrial applications by converting shale gas raw into value-added chemicals and fuels such as methanol, olefins, aromatics, and liquid transportation fuels [119-125]. The upstream sector of shale sites which includes preparation for construction, drilling and fracturing wells to bring shale oil and gas to the surface. The shale gas and oil production are associated with utilizing millions of gallons of freshwater for construction, drilling, hydraulic fracturing, and well closure operations. Indeed, most of the injected water remains underground except 10% to 40% of the used

49

water may return to the surface as flowback and produced water (FPW), which contains a high concentration of dissolved solids and contaminated materials [150]. The direct injection of FPW into underground disposal wells was the most common option for wastewater management during the past decades. However, the disposal option is not extremely recommended due to a high transportation cost and environmental risks that motivate most researchers to evaluate the potential of recycling/reusing for FPW [85, 151]. The midstream sector of shale sites is managed by processing plants (which provides processing service to the upstream producers) after gathering of raw shale oil and gas from various shale sites. Additionally, it plays significant role to connect the upstream production with the downstream markets over distribution networks, as shown in Figure 10. The produced gas is transported by pipelines from shale sites to processing plants. The raw shale gas is divided into wet gas and dry gas based on the amount of natural gas liquids (NGLs), which are produced as byproduct and they can be sold at a high price for the downstream sector. All activities for the above-mentioned sectors are significantly featured to energy consumption, freshwater acquisition, as well as wastewater production, as shown in Figure 11.
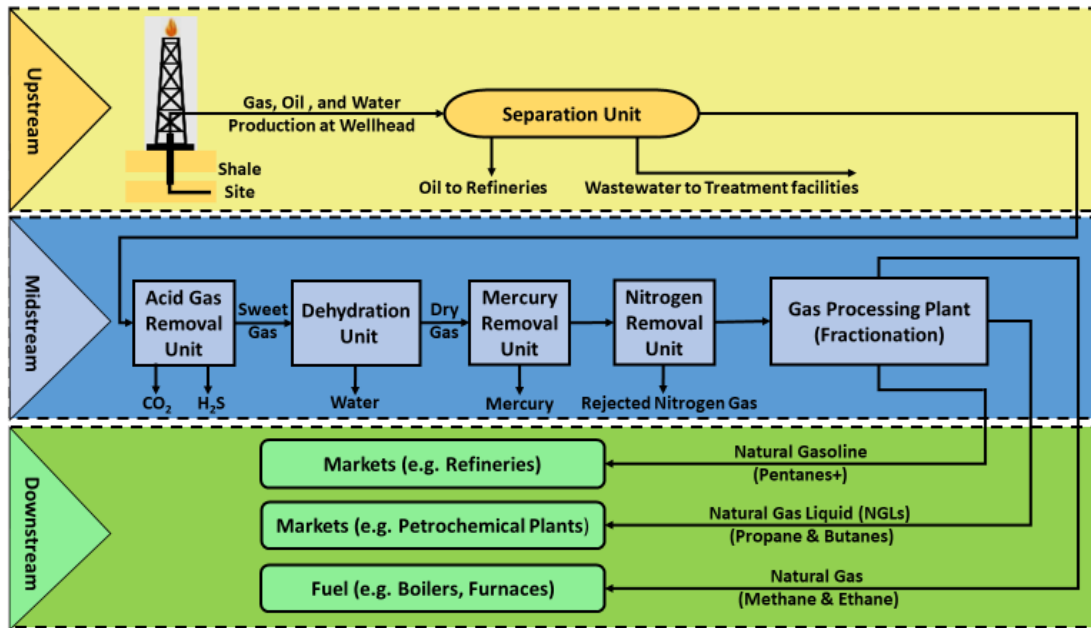
Figure 10: General flowsheet of shale gas processing

Approximately, 90% of water consumed in shale gas production is used in producing a fracturing fluid that is injected under high pressure to create cracks into the rock layers to enhance the production, while the remaining water percentage is consumed in the drilling process. The common water sources which is used in hydraulic fracturing may be surface water (rivers and lakes), groundwater, reused/recycled water. The most common freshwater sources throughout the year are: an interruptible water source (which is an uncertain water supply) and an uninterruptible water source (which is a guaranteed water supply). The interruptible water is pumped throughout a pipeline from a nearby water source (a small water body) to a shale site, while the uninterruptible water requires trucking transportation from a remote water source to a shale site. In some cases, these sources may be stored in a fresh water impoundment prior to its usage. Consequently, the

trade-off between the two freshwater sources is developed based on the availability and transportation cost of fresh water [94]. The operators in shale sites prefer transporting freshwater by pipelines from the nearest water source due to the high cost of trucking and its environmental impacts. In this context, the stimulation of a typical well requires about 4000–6500 one-way convoys of trucks [94]. Wastewater is discharged in two forms: flowback water, which is the short-term wastewater, and produced water, which is the long-term wastewater [94, 128, 152]. Additionally, the wastewater is typically subjected to rigorous regulation due to its content of contaminants materials, therefore it should be stored in containers to protect the surrounding environment prior to recycle/reuse it. Most current efforts are focusing on the potential of recycling/reusing flowback and produced water to avoid the crisis of fresh water scarcity. There are three competitive options to handle the wastewater problem accompanying shale sites production: mobile treatment unit (e.g., mobile desalination truck), centralized treatment plant (e.g., RO, MED, MSF), and underground injection in disposal wells [153]. Accordingly, there is a necessity to design a superstructure framework for managing the problem of water and energy for shale oil and gas industries via water-energy nexus framework.
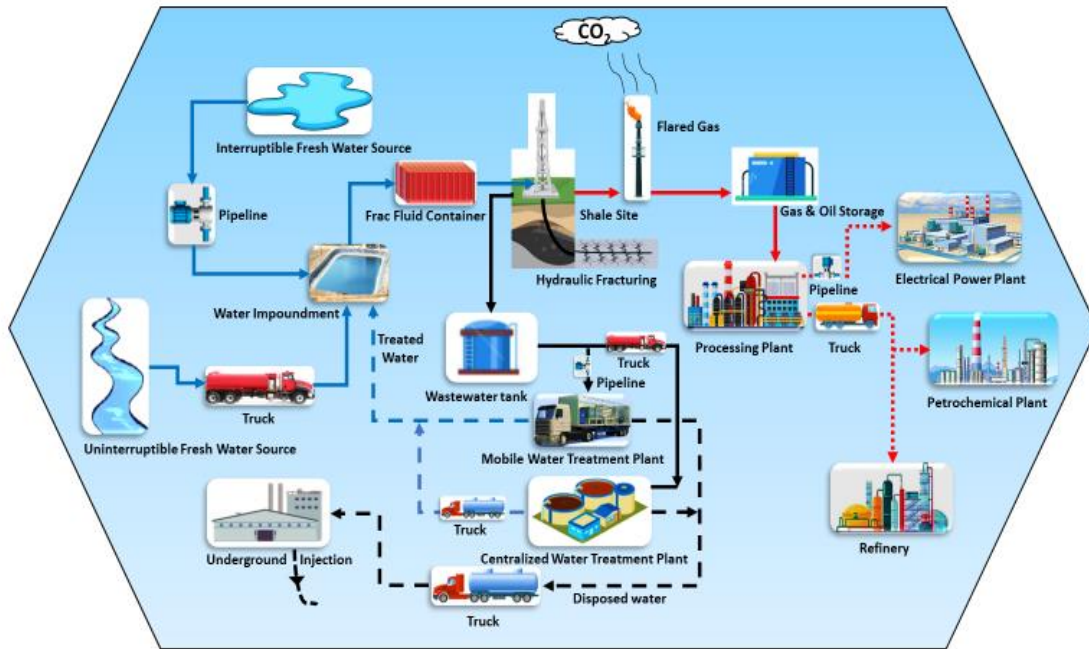
Figure 11: Water-energy nexus framework in shale gas and oil production

A superstructure refers to a system diagram that consists of all subsystem units and all relevant links for more sustainable designs. All system alternatives can be evaluated to select the optimal operation conditions for each subsystem unit by solving the superstructure optimization model [154]. Process integration techniques can be coupled with an optimization formulation to define the optimum configuration of the superstructure for the system. Integration of system units, streams, resources, and objectives is a critical design element in operating cost-effective and sustainable processes. Generally, process integration includes two significant integration concepts are heat integration and mass integration. Heat integration represents the effective exploiting of heat resources within the process (e.g., hot streams, cold streams) to reduce fossil fuels utilizing and greenhouse gas emissions, while mass integration is the effective utilization

of mass resources within the process (e.g., recycling and reusing of wastewater, reduction in fresh water usage) [3, 96, 155]. Many approaches used for treatment and management of shale sites wastewater rely on deterministic optimization models that neglect the different stochastic parameters. Alternatively, they use input parameters, which are known in advance by using the average values of uncertainty parameters [6, 7, 92, 94, 152, 156, 157]. Some of these approaches consider traditional technologies of desalination processes such as the reverse osmosis (RO) and the multi-effect distillation (MED). The deterministic approach of optimization has been used as a special case of the stochastic approach to solve a proposed model depending on one scenario for a specific forecast point [158]. Therefore, the optimal solution for each scenario is completely different from solutions of other scenarios.

Indeed, the design and operation of various industrial processes may be subjected to a number of uncertain parameters such as feedstock input, fuel price, production demand [159]. In order to get more realistic solutions to overcome the limitations of deterministic methods and to improve the system performance, uncertainty can be considered through the stochastic approach in the design of utility systems (e.g., heat and power demand, fuel price), water management networks (e.g., water source availability, water demand, flowback water), and shale sites production (e.g., flow rate, composition). To find the optimal and feasible solution for synthesizing a network operating over a range of uncertain parameter values, two major approaches can be used for achieving this objective. The first approach is based on flexibility by adjusting the control variables in the system when the uncertain parameters change, while the second approach is based on

stochastic programming by adjusting the recourse variables for each parameter realization to achieve optimality [160].

In stochastic optimization, a stochastic approach under uncertainty seeks to optimize the expected value of the objective function including the considered scenarios, instead of optimizing this function for a single scenario as in the deterministic approach. Scenarios are a set of all possible future alternatives with their probabilities of occurrence to sense the variation in the entire system. The probability distribution for random parameters of possible scenarios can be developed by reliable historical data [161, 162]. The stochastic programming techniques can be used to accommodate the uncertainty by considering multiple scenarios with their probabilities of occurrence to optimize the expected value of an objective function. According to the decision-making steps, the number of stages of the stochastic programming model is specified. A two-stage stochastic programming model is the most commonly used technique to associate uncertainty in the decision-making. The first stage or (here and now) decisions, which are made prior to the realization of uncertainty because they are related to the design aspects, also have control or (here and now) decision variables. Unlike, the second stage or (wait and see) decisions, which refers to the operating patterns, are made after the revealing of uncertainty, and have state or (wait and see) decision variables [163]. The two-stage stochastic programming model has been applied to various applications such as an industrial process design and operation, supply chain planning and distributed energy systems [160, 163-168]. In order to address the problems of process synthesis under uncertainty, the problem has been formulated as a two-stage stochastic model and continuous probability

distribution functions have been used to describe uncertain parameters to maximize the expected profit through a decomposition-based algorithm [169, 170]. Other investigators have proposed generalized benders decomposition and the outer approximation/equality relaxation algorithms to solve the process synthesis problems with partitioning the design variables into two types: structural and periodic [171], while A combined multiperiod stochastic optimization formulation has been proposed along with a decomposition-based algorithmic procedure for solving a process synthesis/planning problems [172].

Many strategies have been developed to satisfy thermal and electric power demands, which provided by utility systems, under fluctuated conditions. For example, the operation of a power plant is exposed to uncertainties, one reason is the high fluctuation of fuel prices, which have significant impact on the electricity prices. In this context, Chebeir et al. [165] developed a model to describe and optimize the shale gas supply chain network by using a two-stage stochastic programming model. The uncertainty in prices of natural gas and natural gas liquids (NGL) products is handled through using a scenario-based method. Steimel and Engell [173] dealt with the uncertainty in the operational parameters of chemical processes as a set of discrete scenarios. A two-stage formulation is used with considering the design parameters as the first-stage decisions to solve the optimization problem through stage decomposition. Shafiee and Topal [174] presented the evaluated study for the available fossil fuel prices models by comparing among them to select the most effective model for the long-term trend. Mirkhani and Saboohi [175] enhanced the limited capability of a deterministic energy supply model to handle with the uncertainty in the price of natural gas and to incorporate

renewable energy technologies in effective method. A binomial lattice is created based on the stochastic nature of the energy source and the energy system model is reformulated as a multi-stage stochastic problem. An overview how the uncertainty in fuel price over time can be modelled as a mathematical expression via a stochastic process is provided in these sources [176-178]. Iyer and Grossmann [179] suggested that uncertainties can be converted into multi-period deterministic values. Carpaneto et al. [180, 181] formulated uncertainties as multiple time frame approach for cogeneration planning. However, sun et al. [182] reported that using a certain period for random varying of the uncertainties might cause violation of some optimization constraints. Thus, they classified uncertain factors into two categories: time-based uncertain factors (which can be formulated as a multi-period model) and probability-based uncertain factors (which can use stochastic programming with recourse to formulate the model) to evaluate the effect of the uncertainties on the optimization objective. There are some of works have concerned in the water network synthesis under uncertainty and they have dealt with the optimal water reuse strategies in shale sites production. Some emerging technologies such as membrane distillation may be utilized to exploit surplus heat from cogeneration plant, flared gases, compression stations, and other on-site sources to provide a modular system which has high capability to reject salt [58, 107, 129].

The U.S. shale sites resources have boomed over recent few decades. Therefore, there is a necessity to additional facilities (e.g., transmission pipeline, storage fields, midstream processing facilities) to absorb the growing supplies of shale sites production [183]. The design of shale gas processing systems is a tremendous issue to handle

57

uncertainties in flow rate and compositions of received feedstock. Furthermore, the product specifications of shale gas processing systems might be violated without considering uncertainty in raw shale gas compositions. The shale gas production from various shale plays, or even from multiple shale wells of a given shale play [184], requires different processing necessities due to fluctuated production rate and compositions through the lifetime of a shale play or a shale well. In this context, Gong et al. [185] developed intensified process designs of shale gas processing systems by comparing among them to handle fluctuated flow rates and uncertain compositions of raw shale gas. An equipment capacity and process operating conditions of an intensified process design are determined based on the deterministic designs. However, the deterministic designs might generate off-specifications products, despite they could offer excellent integration strategies of a process superstructure [186].

Renewable energy resources (such as solar) could be utilized to improve the sustainability of the system. The solar energy may be used as a direct source of heat to industrial plants (e.g., desalination process) or as indirect heat source to the utility facilities (e.g., steam generator of steam Rankine cycle). To increase the reliability of incorporating solar energy into existing or proposed large-scale projects, the ahead prediction of solar radiation (per minute, hour, day, month, season, year) depending on the availability of solar radiation data and their accuracy is substantial for a long-term evaluation of the technical and economic performance of these projects. However, the intermittent nature of solar irradiance, which driven by the meteorological and geographic parameters such as maximum and minimum temperature, relative humidity, sunshine duration, cleanness

index, cloud cover, geographical site, etc., causes in high uncertainty in the final amount of energy production [187]. Moreover, to handle with the uncertainty in solar energy availability, a multi-period approach is adopted to discretize the operation time into a number of operational periods and operational sub-periods [21, 55, 61, 64-70, 73-75, 77-79, 81, 110, 112-114, 188].

This work presents a superstructure framework of a multi-purpose system to address the water-energy nexus problem of shale oil and gas industries. The system utilizes a hybrid of conventional energy (fossil fuels) and renewable energy (solar energy) as the external sources of thermal energy, which is supported by the thermal storage system to manipulate the diurnal fluctuation of solar energy, to produce electrical power, fresh water, fuels, and value-added chemicals while treating shale-gas wastewater. A new systematic approach is developed to the design, operation, integration and optimization of the system, which operates under uncertain operational conditions. The system consists of several subsystems are: cogeneration process (including non-condensing (back-pressure) steam turbine and water-tube boiler fueled with gas or oil), steam generator, solar collection process (parabolic trough collectors), thermal energy storage, multi-effects distillation plant, reverse osmosis plant, primary and secondary water treatment processes, and an industrial process. The optimization problem is formulated as a two stage multiperiod stochastic programming problem. Two uncertain operational parameters (normal direct irradiance, fossil fuel price) are considered in the model through a scenario-based approach, which represents a finite set of scenarios (or realizations) to describe the uncertain parameters and future outcomes with a certain probability for each of them.

Therefore, the problem is reformulated as a multi-scenario Mixed Integer Non-Linear Programming (MINLP) problem that is a deterministic equivalent of a two-stage stochastic programming model with recourse to account for the fluctuations of solar energy and fossil fuels price. The modelling equations of subsystems are included two sets of variables distributing on the first and second stages of optimization based on their performing before and after the realization of uncertain parameters. Heat integration is carried out among the hot and cold streams of an industrial process and subsystems of the entire system. The developed approach is aimed to address the following points:

- The optimal mix of solar energy, thermal storage energy, and fossil fuel for the entire system That meets the system requirements of electric and thermal power

- The minimum total annual cost of the entire system

- The maximum annual profit of the entire system

- The economic feasibility of the system

- The optimal design and operation of the system

- The impact of the system on environmental aspects

To address the abovementioned tasks, the incorporation of process integration technique, an optimization formulation which is based on the modelling equations, and randomness is the effective method to obtain a systematic approach for an optimal solution.

4.2 Problem Statement

Consider a typical multi-purpose system such as the schematic representation shown in Figure 12, which shows the key subsystems and streams involved in the system to systematically design an integrated system. The system may be installed at a shale-gas production site. The site connected to an external power grid. The system is considering the following options to satisfy technical, economic and environmental requirements.:

- An industrial process with several process hot and cold streams, these streams may exchange heat energy among them and with external heating and cooling utilities.

- An industrial process is considered to usage as a gas processing plant (fractionation) at the midstream sector which converts shale gas production of the upstream sector to fuels (to be used in a boiler) and chemicals (to be sent to the downstream sector).

- A parabolic trough collector is selected for the solar collection process.

- A two-tank storage system, which is used molten salts as a storage medium in this system, is selected.

- Steam which is produced in a steam generator may be provided directly to an industrial process or to a multi-effect distillation plant.

- Surplus steam (low-grade steam) from cogeneration process may be provided to a multi-effect distillation plant.

- An excess industrial process heat may be used to supply a cogeneration process or a multi-effect distillation through a steam generator. Also, a required heat of an industrial process may be supplied by a steam generator.

- Fossil fuel (shale gas, flared gas) and solar energy (as direct solar thermal power and as indirect solar thermal power from thermal energy storage) are used as external sources of heat (to be used in a boiler and a steam generator).

- The differences in shale gas flow rate and composition from different sources can be considered.

- Water is classified according to it's the Total Dissolved Content (TDS) concentration.

- Wastewater is typically subjected to rigorous regulations and should be stored on-site in tanks for future treatment or disposal, while fresh water is stored in impoundments.

- Treating the wastewater (flowback and produced water) for on-site recycling/reuse through three levels of treatments (primary, secondary, and tertiary). The tertiary level includes two water treatment plants: Reverse Osmosis (RO) and Multiple-Effect Distillation (MED).

- Brine stream from the tertiary level units is transported to inject into disposal wells.

- The uncertain parameters (i.e., Direct Normal Irradiance (DNI) and fossil fuels price) are considered and described through discrete approximation of probability distribution.

. The problem, which is addressed in this article, can be stated as follows:

Given are the following:

- The flowrate and characteristics of produced shale gas, flared shale gas, flowback and produced wastewater, and fresh water demand during stimulating a few shale-gas wells by hydraulic fracturing operations

- A set N_C of an industrial process cold streams (to be heated) and a set N_H of an industrial process hot streams (to be cooled). Given also are the heat capacity (flowrate $\times$ specific heat) of each process cold stream, $fc_{p,v}$, and of each process hot stream, $FC_{p,u}$; the inlet (supply) temperature of a cold stream, t_v^s; the inlet (supply) temperature of a hot stream, T_u^s; the outlet (target) temperature of a cold stream, t_v^t; the outlet (target) temperature of a hot stream, T_u^t, where $v = 1, 2, \ldots, N_C$, and $u = 1, 2, \ldots, N_H$.

- A selected temperature and pressure for inlet steam into a turbine.

- An external power grid demand.

- The solar data for a system site such as hourly dry bulb temperature, hourly wet bulb temperature, hourly direct normal solar irradiance, and hourly solar incidence angle.

- The forecast price of natural gas during a year
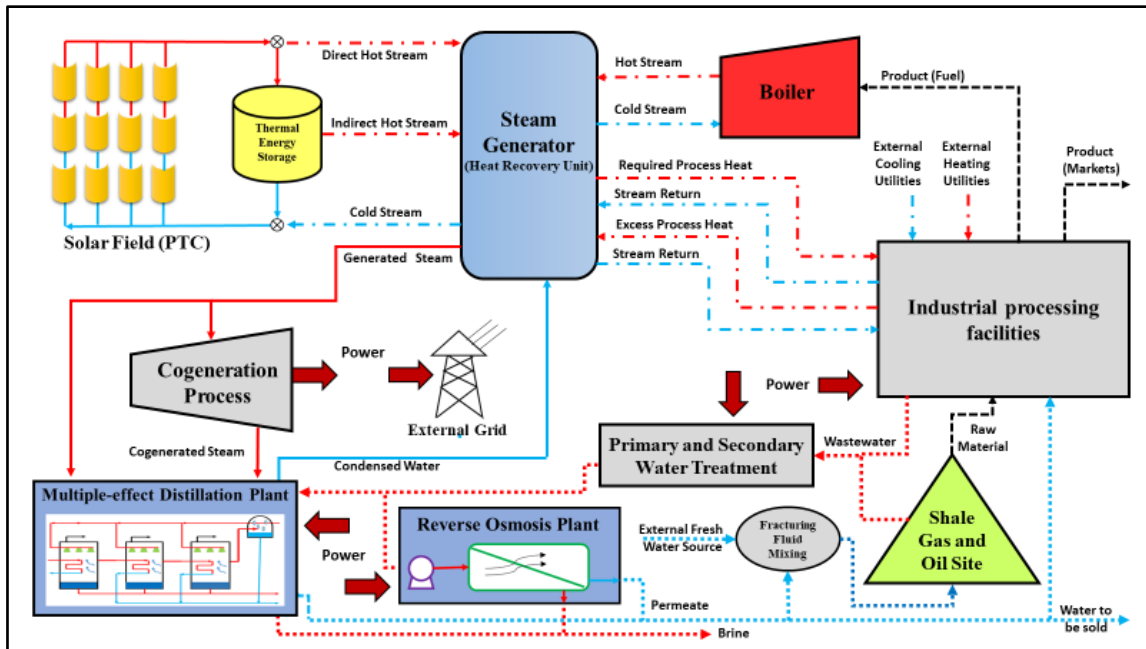
Figure 12: Proposed superstructure representation

- The direct capital cost of parabolic trough collector items (based on LS-3 collector type).

- The characteristics of a thermal storage system media.

- The techno-economic data for RO and MED

- The unit costs of fresh water acquisition, primary and secondary treatments of wastewater, disposal of wastewater, and transportation of wastewater.

- A percentage contribution of each water treatment plants in the total desalinated water production.

Available for service are the following:

- Solar energy is utilized as a source of heat. The useful thermal power of solar collectors fluctuates dynamically during the year. The size (design area) and

64

cost of the concentrated solar energy system are unknown and are to be specified through optimization formulation.

- A set N_{HU} of heating utilities ; $H_{UTILITY} = \{h|h = 1,2,\ldots,N_{HU}\}$; the temperature T_h^H and the cost C_h^H are known for each heating utility, and a set N_{CU} of cooling utilities; $C_{UTILITY} = \{c|c = 1,2,\ldots,N_{CU}\}$; the target temperature t_c^t and the supply temperature t_c^s are known for each cooling utility, while heating and cooling utilities flowrates are unknown.

- The cogeneration process exploits a steam turbine to generate power and the surplus steam that leaves the turbine as a heat source for several heating purposes. The optimal values of generated power and produced steam are to be determined.

4.3 Approach

The proposed approach is designed to identify the optimal configuration, design, and operation of the integrated system while trying to maximize the annual profit under uncertainty. The computational difficulties of optimization problem under uncertainty is a very challenging task. Thus, it requires finding proper techniques and alternative approaches that contribute significantly to reduce the complexity of a solution. Figure 13 demonstrates the structure of the hierarchical approach which is used in this study to find the optimal solution. Prior to formulating the stochastic optimization problem of the integrated system that produces a certain level of electricity, desalinated water, fuels, and value-added chemicals, there are several steps are necessary to be done. The starting step in the proposed approach is to obtain deterministic and uncertain data. The scenario-based

method is adopted to describe the uncertain parameters during all the time periods with an identified probability of occurrence based on a discrete approximation of continuous distributions, which allows reformulating a stochastic programming problem as a deterministic equivalent of a stochastic programming model with a finite number of scenarios to describe the uncertainty, for more detailed information is given in section 4.3.1. Next, the percentage contribution of RO and MED in treating wastewater is iteratively discretized, which leads to simplifying the solving of the optimization problem and raising computational efficiency. The RO and MED plants can be designed separately based on their known treatment tasks for each discretization step. Hence, thermal and power loads for plants are calculated. Similar approaches have been proposed earlier in the literature for other applications [131, 133, 134, 156]. Furthermore, various percentage of solar energy contribution in the total mix of thermal power that supplied to the system is chosen to add further simplifying to a computational approach and to assess the economic feasibility of incorporating solar energy to the system. Computer-aided simulation is used to estimate the heat duties of major equipment and streams temperature for an industrial process. Heat integration approach can be used to determine the deficit and surplus heat of an industrial process that can be coupled with the heat recovery unit (steam generator) of the system. Therefore, thermal pinch analysis technique [96] is used to integrate the hot and cold streams of an industrial process to calculate deficit and excess heat and the temperature at which it is available. Another important step is to select and formulate a set of models and constraints that characterize the subsystems involved in the entire system as in section 4.4. Once the foregoing steps are achieved and the total thermal

and electric loads are determined of the integrated system, the optimization problem is formulated as a multi-scenario Mixed Integer Non-Linear Programming (MINLP) problem that is a deterministic equivalent of a two-stage stochastic programming model with recourse to dealing with an uncertainty of solar energy and fossil fuels price for each period, more detailed information in section 4.3.2 and 4.5. The objective function is solved to minimize the sum of the capital costs (First stage) which are expended only once at the time of building the system and the operating costs (Second stage) which are expended during each scenario along with maximizing the system revenue. Upon identification the total annual profit and the thermal power mix of the system, the procedure is repeated for the various percentage contribution of RO and MED in treating wastewater. The obtained results are compared to select the maximum-profit solution and the optimal design and operation of the entire system.
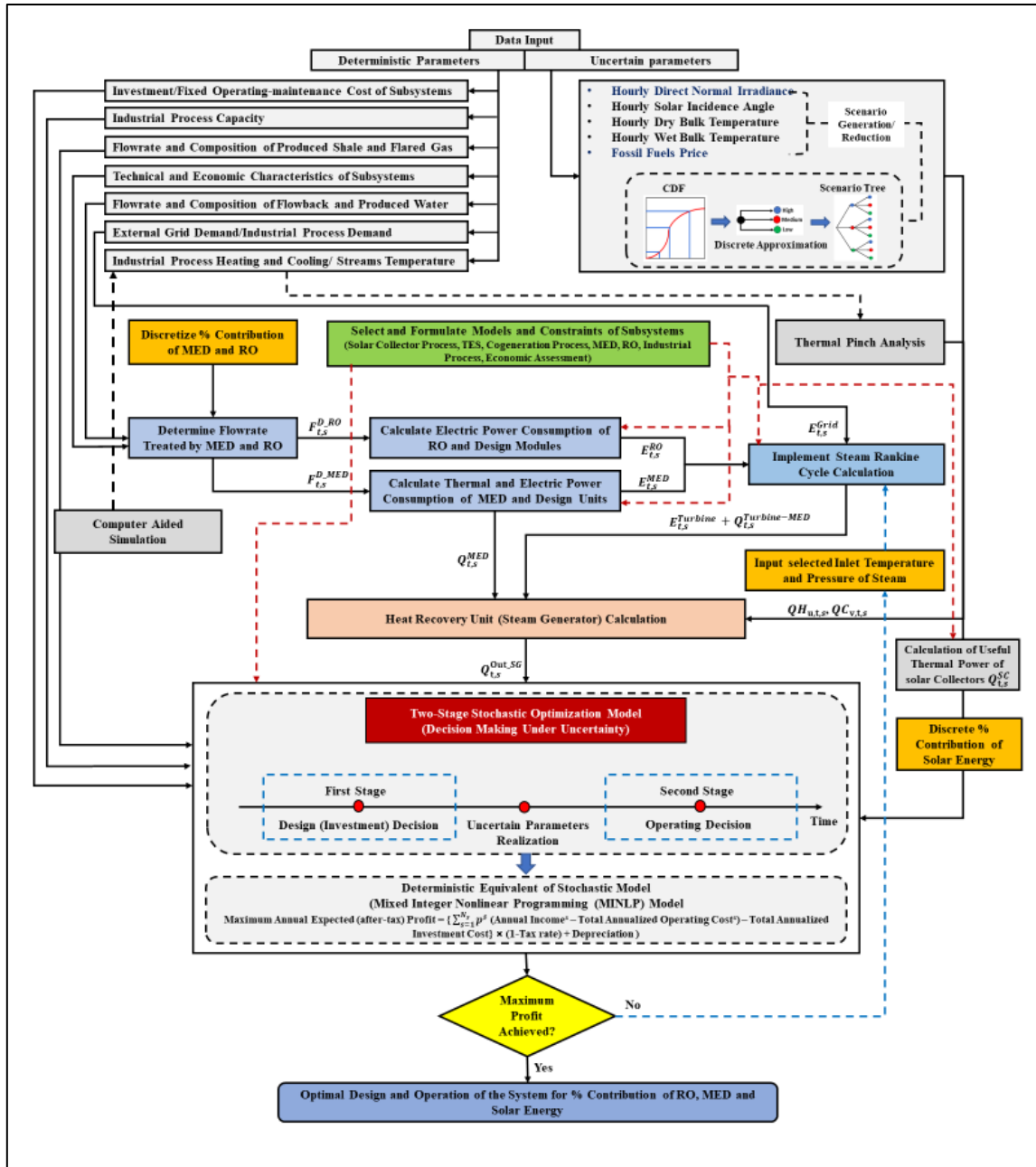
Figure 13: Proposed Approach

4.3.1 Generating Scenario Tree for Uncertain Parameters

The precise dealing with the required input data is very significant in enhancing computational efficiency of solving optimization problems. The input data are classified into deterministic and uncertain parameters. Deterministic input parameters are utilized in the model, specifically, the decision of selecting and designing the system units before the realization of uncertain parameters such as capital cost investment, fixed operation and maintenance cost, techno-economic characteristics, etc. Otherwise, it is generally intractable to optimize a stochastic problem by incorporating uncertain parameters as continuous random variables. Thus, these parameters can be represented as a multi-period scenario tree which grows with scenario tree nodes based on approximating continuous distributions into discrete distributions or Monte Carlo simulation random generated nodes (a random generation of information) from the common continuous distributions [189]. A scenario tree is represented by a set of nodes, $k \epsilon K$, and branches. Each scenario s is a path of flowing all possible information and realizing uncertain parameters. This path starts from the initial situation (which is called the root node) to a leaf node through the time horizon of a stochastic problem and it has a certain probability, $p^s = \Pi_{k \epsilon K} \, p_k^s$, which is the product of the occurrence probability (joint probability) of all nodes pertaining to the path. It is necessary to mention that the sum of the probability of all scenarios within a certain period in the time horizon is to be equal to one $\Sigma_s \, P_t^s = 1$. The main goal of scenario generation in the stochastic problem is to create a set of probabilistic scenarios, which describe precisely uncertain parameters space to make the best decisions for the first and second stages of a two-stage stochastic model.

In this work, the integrated system is subjected to significant uncertainties in solar-irradiation intensity (Direct normal irradiance) and fossil fuels (Natural gas) price, which take on finite values at different points of time, Particularly, from season to another season of a year, during system operation. Note that the natural gas demand peaks in the winter is higher than demand peaks in the summer due to the higher gas consumption in heating and power generation. The seasonal fluctuation of demand leads to significant price change. For illustrate, the U.S. gas market has two seasons: the surplus gas is stored by injecting into the ground in summer (April-October), while it is withdrawn in winter (November-March) to meet the increased demand [190]. Consequently, the exploiting of solar energy as energy source could contribute in increasing gas amount stored in summer due to the high intensity of solar irradiation, but this contribution is less important in winter because fluctuations in hourly direct normal irradiance are weak in summer but strong in winter. Accordingly, the uncertainty of solar energy and fossil fuels price can be represented by three scenario tree nodes (high, medium, low) with their appointed probabilities based on discrete approximations of continuous distributions to generate a finite number of N_s probabilistic scenarios included in a set $S = \{s|s = 1, ..., N_s\}$. The use a finite number of scenarios for uncertain parameters can lead to reduce complexity of a stochastic problem and computational costs by reformulating the two-stochastic stage model as a deterministic-equivalent model. In this work, the three-point Pearson-Tukey approximation technique for continuous probability distributions (e.g., normal, uniform, exponential) is used to substitute the entire continuous probability distribution by a few representative values (N discrete points) and their identified probabilities, which weights

the 0.05, 0.50, and 0.95 percentiles by 0.185,0.630, and 0.185 respectively, as shown in Figure 14. The three-point Pearson-Tukey (3-PT) approximation shows a great accuracy comparing with Monte Carlo simulation, comparisons have been made for the mean of a random variable and for conventional functions of one and two variables using a assort of known distributions, The using 3-PT would facilitate a problem solution because it requires the evaluation of only 3^n scenarios, where n is the number of random variables in the model. This technique that can match the first (2N-1) statistical moments statistical features (mean, variance, max, kurtosis and skewness) of the continuous distribution, where N is the number of discrete points [191-196]. The first task for modelling the operating system mathematically under uncertainty is to represent uncertain parameters using probabilistic scenarios, which is defined as scenario generation.
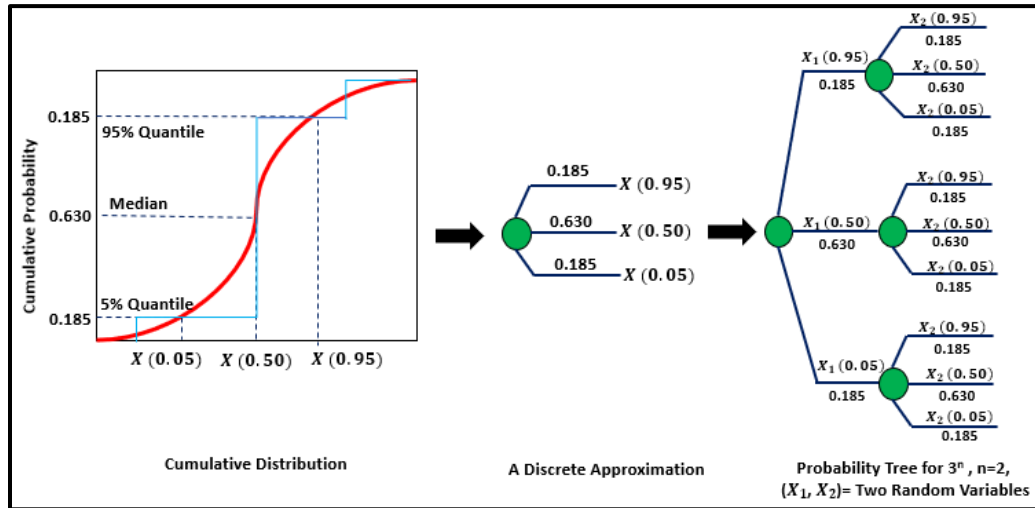
Figure 14: Three-Point Approximation Technique

In addition to use the number of uncertain parameters, as abovementioned, in estimating the number of scenarios, the number of stages or time periods proposed in the optimization problem are also used for the same purpose. Consequently, the number of scenarios can be calculated by the relationship $3^{n.t}$ or $3^{n.(T-1)}$, where n is the number of uncertain parameters in the model, t is the number of a specific period time, and T is the number of stages. It is worth noting that the length of each time stage can be planned according to modelling requirements (can be a period or multiple period time). In this work, a time horizon of the system operating represents one year, which can be divided into two or four time periods depending on the geographical site that determines a season length and the number of months associated with each season. To illustrate, if two uncertain parameters described by three nodes (high, medium, low) and four multiple periods represented by four seasons (e.g., spring, summer, fall, and winter) are considered, Hence, at the end of fourth period, 3^8 scenarios are generated. Similar approaches have been adopted in the literature of other applications [165, 167, 189]. The next step is to keep fewer scenarios possible to ensure that the problem of stochastic optimization can be solved with a reasonable computational effort. Scenario tree may grow exponentially with a significant increase in the number of time periods or stages. In such cases, several scenario reduction techniques such as forward selection, backward reduction, and K-means clustering algorithm can be adopted to decrease the scenario numbers that leads to minimize the computational time and cost of the optimization problems to be computationally tractable, these techniques used in various applications can be found in the literature [167, 197-201]. In the same context, some researchers observed that the

results with suitable accuracy can be obtained, when the number of scenarios is reduced to one quarter and the computational time is lowered four times [197]. Other investigators have the opposite opinion regarding the scenario reduction and it may cause a high error rate of an objective function value and jeopardize the accuracy of the modelling [202]. To reduce the number of scenarios, the model size, and computational requirements of this work, the three-point approximation technique is used to represent the uncertain parameters by a finite set of known values, in addition, to select typical seasons (time periods) that represent the full yearly horizon.

4.3.2 Two-Stage Stochastic Optimization Model

The optimal configuration of an integrated system requires considering all the design alternatives through the interconnection between system units operating under uncertain operating conditions. These uncertainties subject to several technical and commercial parameters, which may not be fully revealed at the early stages of the system design. It is obvious that the incorporation of uncertain aspects in the optimization problems causes the transformation of a deterministic problem (which can be solved by using standard methods of mathematical programming) to a stochastic problem (which requires special techniques and approaches to be solved). The incorporation of uncertain parameters makes the deterministic model is unsuitable to optimize the expected value of net profit in this work. A generally mathematical representation of the final structure and design under uncertainty can be presented as in the following form [170]:

73

$$P = \max_{y,d,z} f(y, d, z, x, \theta) \tag{39}$$

s. t.
$$h(y, d, z, x. \theta) = 0$$
$$g(y, d, z, x. \theta) \leq 0$$
$$d \epsilon D, z \epsilon Z, x \epsilon X, y \epsilon \{0, 1\}^m$$
$$\theta \epsilon \mathcal{R}^n$$

where P is the profit, f is a scalar objective function (an economic performance index) which must be optimized to find the maximum or minimum value, y is the vector of binary 0-1 variables for existing units, d is the vector of design variables (e.g. physical size of installed units), z and x represent the vectors of control and state variables (operating conditions) and θ is the vector of uncertain parameters. The set of equality constraints (h) are process equations (energy and mass balances), while the set of inequalities (g) be compatible with the design specifications and logical constraints, which also represents the linking constraints (hard constraints) that use to unify the choices of design decisions of the first- stage across all operational periods of the second- stage scenarios, otherwise, these constraints link the design variables with the variables of each scenario [160, 171].

A two-stochastic programming model with recourse is the most commonly used technique to deal with decision making under uncertainty in mathematical programming. Particularly, when this technique is used for solving problems of a large superstructure of an integrated system or extensive portion of a process plant by breaking these problems down into smaller independent components because each operational scenario may represent a large-scale optimization problem. In the same context, the mathematical programming problem accommodates very large decisions in the first stage and any number of subproblems in the second stage [171]. A general formulation of this model

can be found in [203], which can be used to maximize or minimize the expected value of an objective function for all scenarios considered under an uncertain future. The general formula of Equation 39 can be formulated in the two-stage stochastic programming framework. Consequently, the two-stage stochastic programming model is adopted to formulate the superstructure of the system. Hence, the superstructure variables can be classified as either design or operational variables. In the first stage, the essential units of the system with the design variables of each unit (e.g., solar collection area, thermal storage volume, evaporator area of MED, membrane area of RO, etc.) should be chosen, but the selected units may not be necessarily compatible with operational conditions of all possible time periods or scenarios. Once the design variables are decided, the operational aspects can be optimized over the time horizon for all scenarios according to the decisions made in the first stage. Therefore, a duplicate method is substantial to discretize the horizon time period iteratively in which the design variables are replaced along with adjusting the operating conditions until obtaining an optimal design, which is feasible over a certain range of operating conditions, by minimizing expected (investment and operating) costs and maximizing expected (profit) through the two stages.

The general formula of Equation 39 can be formulated in the two-stage stochastic programming framework. It is worth noting that it is not necessary to be the consistent relationship between stages and time periods. Therefore, in specific cases, all time periods can be lumped into the second stage of a stochastic programming model [204]. Therefore, it can be assumed that all time periods are accommodated in the second stage for the problem of this work, as shown in Figure 15. To avoid the challenges and complexity in

modelling and find the optimal solution for the system, a finite number of scenarios can be postulated to describe the randomness by representing finite values of the uncertain parameters in multiple scenarios. Hence, the operational pattern of the system can be adjusted for each scenario over all periods in the time horizon with maintaining the same system configuration and fixed capacity of the subsystems that determined in the first stage. Based on that, the objective function of the total expected profit, which accommodates the cost of the selected design and the expected optimal profit (revenue of sales and operating costs), can be optimized by allowing the transformation of the two-stage stochastic programming model into a multi-scenario mixed integer non-linear programming (MINLP) model that is a deterministic equivalent model as follows [170]:

$$P = \max_{y,d} \{ E_\theta\{f_s(y, d, \theta_s)\} - f^0(d) - cy \tag{40}$$

where

$$f_s(y, d, \theta_s) = \max_{z_s} \sum_{s=1}^{N_s} p_s f_s(y, d, z_s, x_s, \theta_s)$$

$$\text{s. t.}$$
$$\left. \begin{array}{l} h_s(y, d, z_s, x_s, \theta_s) = 0 \\ g_s(y, d, z_s, x_s, \theta_s) \leq 0 \end{array} \right\} s \in N_s$$
$$d\epsilon D, z_s \epsilon Z, x_s \epsilon X, y \in \{0, 1\}^m$$
$$\theta_s \in J(\theta_s)$$
$$\theta \in \mathcal{R}(d)$$

where P is the total expected profit of the system, f_s is a profit function, which represents the total expected revenue and operating cost of the system over all the scenarios, $f^0(d)$ is the capital cost function of the design, cy represents a fixed charge cost, E_θ is the expectancy operator, p_s represents the probability assigned to the occurrence of the N_s scenarios, and $J(\theta_s)$ is a probabilistic density function.

Prior to uncertainty realization, the first stage decisions (here and now) could be implemented immediately on the design aspects (i.e. selection and capacity of the subsystems) of the integrated system to specify an optimal vector of the design variables d while seeking for determining an optimal vector of control variables z (operational flexibility and feasibility) in the second stage (wait and see) for every uncertain realization θ, which are lying with the associated feasible region $\mathcal{R}$. Note that $\mathcal{R}$ represents the feasible region of the design d, $\theta \in \mathcal{R}(\theta)$, and $R(d) = \{\theta | \forall \theta \epsilon R \ \exists z : f(d, z, \theta) \leq 0\}$ [169]. The problem of feasibility can be addressed by considering further penalty functions or through transforming to the deterministic equivalent multiperiod problem by postulating a finite number of discrete points of uncertain parameters θ [172], as mentioned in section 4.3.1. Once the first decisions are made to estimate the capital cost of the design, the design variables cannot be changed over the time horizon of the second stage when the system is being operated. While the second stage decisions could be delayed until the appearance of uncertainty to carry out it on the operating pattern to evaluate the operating cost expenditure, which is highly dependent on the selecting of design variables of the first stage. It should be noted that the operational variables are scenario dependent to consider uncertain parameters which are significant in taking recourse action in the second stage.
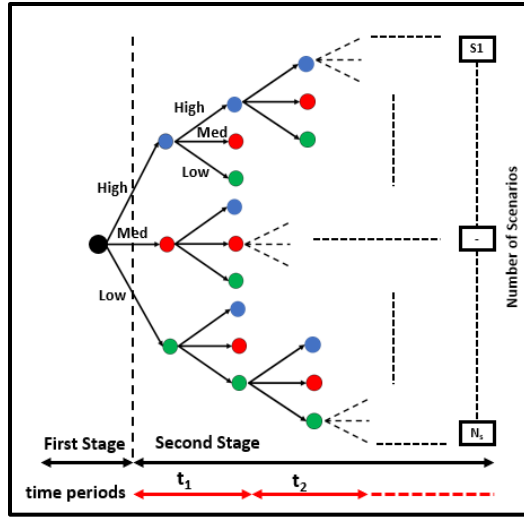
Figure 15: Schematic of scenario tree for uncertain events

4.4 Modeling Formulation

The formulation and selecting of suitable models are considered the significant steps to properly describe the main building blocks of the system, which was presented in Figure 12. The detailed equations are used for the models as follows:

4.4.1 Solar Collection Process

A parabolic trough collector was selected to represent the solar collection process which is incorporated in the system as the direct or indirect source of thermal power for the entire system. The modeling of the solar collection process was developed basing on literature models and data [13, 25, 27, 33, 156], as described in the following table:

Table 5: General modeling equations for solar collection process

Equation		Description	
$Q_{sun \to collector} = DNI. \cos\theta. W_c$	(41)	Thermal power (W/m) which can be produced by the solar collection process when the direct normal irradiance (DNI) hits the collector aperture	[13]
$\cos\theta = \sqrt{\cos^2\theta_z + \cos^2\delta. \sin^2\omega}$	(42)	Incidence angle for the north-south orientation	[13]
$Q_{collector \to reciever} = DNI. \cos\theta. W_c. \eta_{opt}. K(\theta). F_f. R_{SL}. O_{EL}$	(43)	Thermal power (W/m) which can be absorbed by a receiver tube of a collection system loop	[156]
$\eta_{opt} = \rho. \gamma. \tau. \alpha$	(44)	Peak optical efficiency of a collector when the incidence angle on the aperture plane is 0°	[27]
$K(\theta) = 1 - 2.23073 \times 10^{-4}. \theta - 1.1 \times 10^{-4}.\theta^2 + 3.18596 \times 10^{-6}. \theta^3 - 4.85509 \times 10^{-8}. \theta^4 ,$ $\qquad\qquad\qquad 0^0 \leq \theta \leq 80^0$ $K(\theta) = 0 \qquad\qquad\qquad \theta > 80°$	(45)	Incidence angle modifier for a LS-3 collector	[27]
$R_{SL} = \min\left[\max\left(0.0, \frac{L_{spacing}}{W_c}. \frac{\cos\theta_z}{\cos\theta}\right); 1.0\right]$	(46)	Row shadow factor	[33]
$O_{EL} = 1 - \frac{f. \tan\theta}{L_{SCA}}$	(47)	Optical end loss	[33]
$Q_{collector \to ambient} = U_{rec}. \pi. d_o. (T_{rec} - T_{amb})$	(48)	Total thermal power (W/m) which may be lost from a collector represents the combination of the radiative heat loss from the receiver pipe to the ambient environment $Q_{reciever \to ambient}$ and convective and conductive heat losses from the receiver pipe to its outer glass pipe $Q_{receiver \to glass}$.	[27]
$U_{rec} = a + b (T_{rec} - T_{amb}) + c (T_{rec} - T_{amb})^2$	(49)	Overall heat transfer coefficient of a collector is found experimentally depending on a receiver pipe temperature	[27]
$Q_{collector \to fluid} = Q_{collector \to receiver} - Q_{collector \to ambient}$	(50)	Thermal power (W/m) which can be transferred from a collector to a fluid	[156]

Table 5: Continued

Equation		Description	
$Q_{LFP} = 0.0583 . W_c . (T_{rec} - T_{amb})$	(51)	Thermal power (W/m) which may be lost from the headers (pipes)	[13]
$Q_{LFV} = 0.0497 . W_c . (T_{rec} - T_{amb})$	(52)	Thermal power (W/m) which may be lost from the expansion tank (vessel)	[13]
$Q_{PTC \to final\ demand} = Q_{collector \to receiver} - Q_{collector \to ambient} - Q_{LFP} - Q_{LFV}$	(53)	Net useful thermal power (W/m) which can be produced by the solar collection process	[156]

4.4.2 Thermal Energy Storage

Thermal storage is utilized to assist in supplying a steady thermal power to the system by manipulating the dynamic variability of solar energy. An indirect thermal storage system is selected that consists of two separated tanks. A binary molten salt (sodium and potassium nitrate) is used as the storage media. To describe the performance of the thermal storage system, the following equations can be used as in Table 6:

Table 6*: General modeling equations for thermal energy storage*

Equation		Description	
$Q_{in} = m_{ms} . C_{Pms} . (T_{HT} - T_{CT})$ $= \eta_{EX} . m_{oil} . C_{P,oil} . (\Delta T)$	(54)	Inlet thermal power (W) of the thermal storage (charge process)	[156]
$Q_{out} = m_{oil} . C_{Poil} . (\Delta T)$ $= \eta_{EX} . m_{ms} . C_{Pms} . (T_{HT} - T_{CT})$	(55)	Outlet thermal power (W) of the thermal storage (discharge process)	[156]
$C_{Pms} = 1443 + 0.172\ T_{ms}$	(56)	Specific heat of the molten salt	[49]
$Q_{TES} = Q_{acc} + Q_{in} - Q_{out} - Q_{loss}$	(57)	Net thermal power (W) inside the tank	[156]
$Q_{loss} = 0.00017 . T_{ms} + 0.012$	(60)	thermal power loss (kW/m^2) of the cold and heat tanks	[49]

4.4.3 Cogeneration Process

The co-production of power and low-grade steam for the entire system can be achieved by cogeneration process, which is based on a Rankine cycle. This process consists of a boiler (or a steam generator that used in this work to utilize various energy sources), a steam turbine, and a condenser which is replaced with a multiple-effect distillation plant to exploit the surplus heat production. The modeling of the Rankine cycle requires appropriate correlations for the thermodynamic properties to use in the optimization formulations. The complicated nature of available correlations of steam tables (e.g., nonlinear, nonconvex function) and the complexity of incorporating these correlations into an optimization task to find the optimal values of a Rankine cycle were significant motivation to develop a new set of thermodynamic correlations that could be inserted easily into the optimization formulation for a cogeneration design. In this study, a set of correlations, which has been developed in the literature [109], was adopted to estimate the properties of steam. These correlations and fundamental equations are shown in Table 7.

Table 7: General modeling correlations and equations of steam Rankine Cycle (SRC)

Equation		Description	
$T_{sat} = 112.72 \cdot P_{sat}^{0.2289}$	(61)	Saturated temperature as a function of pressure (can be used at the outlet of a condenser or at the inlet of a boiler) Error = ±0.64%	[109]

Table 7: Continued

Equation		Description	
$h_{sat}^f = 0.2674 . T_{sat}^{1.2127}$	(62)	Saturated liquid enthalpy (can be used at the outlet of a condenser or at the inlet of a boiler) $P \leq 2500$ psi Error $= \pm 3\%$	[109]
$s^v = (-0.5549 . \ln(T_{sat}) + 3.7876) . T^{0.1001 . \exp(0.0017 . T_{sat})}$	(63)	Entropy of steam (can be used at the inlet of a turbine) $P \leq 2,500$ psi $T \leq 1,500$ °F Error $= \pm 3.5\%$	[109]
$h^v = 0.2029 . T_{sat} . (s^v)^{3.647} + 817.35$	(64)	Enthalpy of steam (can be used at the inlet of a turbine or at the outlet of a turbine) $14.7 \leq P \leq 2,000$ psi Error $= \pm 0.6\%$	[109]
$\Delta h_{is} = h^v - h_{is}^v$	(65)	Isentropic enthalpy difference	[109]
$h_{act}^v = h^v - \eta_{is} . \Delta h_{is}$	(66)	Actual enthalpy at the outlet of a turbine	[109]
$m = \dfrac{Q_{process}}{h_{act}^v - h_{sat}^f}$	(67)	Mass flow rate in term of the required heat of the process (condenser)	[109]
$T = \dfrac{h_{act}^v - B(s)}{A(s)}$ $A(s) = -0.7918 . (s^v)^3 + 3.4575 . (s^v)^2 + 4.5513 . s^v + 2.1267$ $B(s) = 710.22 . (s^v)^3 + 3910.6 . (s^v)^2 + 7117.3 . s^v - 3253.5$	(68)	Outlet temperature of a turbine	[109]
$Q_{Boiler} = m (h^v - h_{sat}^f)$ $Q_{Boiler} = Q_{Fuel} . \eta_{Fuel}$	(69)	Thermal power output of a boiler	[109]
$m_F = \dfrac{Q_{Boiler}}{H_{v,F} . \eta_{boiler}}$	(70)	Mass flow rate of fuel is provided to a boiler	[109]
$E_{Turbine} = m (h^v - h_{act}^v)$	(71)	Turbine shaft power output	[109]

While the turbine hardware model, which was developed in the literature [139], can be used to obtain the isentropic efficiency for the steam turbine. The hardware model shows the variation of efficiency with operating conditions, a load, and a turbine size, as in the following correlations in Table 8:

*Table 8***:** Turbine hardware model

Equation		Description	
$$\eta_{is} = \frac{6}{5\,B}\left(1 - \frac{3.41443 \times 10^6 \times A}{\Delta h_{is} \times m^{max}}\right)\left(1 - \frac{m^{max}}{6 \times m}\right)$$ $$A = a_o + a_1 . T_{sat}$$ $$B = a_2 + a_3 . T_{sat}$$	(72)	Isentropic efficiency for a turbine a_o, a_1, a_2, a_3 are turbine regression coefficient [112]	[139]
$$\eta_{is} = \frac{1}{B}\left(1 - \frac{3.41443 \times 10^6 \times A}{\Delta h_{is} \times m^{max}}\right)$$	(73)	Isentropic efficiency for a turbine when m = m^{max} at design condition	[139]

4.4.4 Desalination Process

To make the proposed system contributes effectively in managing water resources on-site, the hybrid combination of two desalination plants (included MED and RO) has been considered to supply the fresh water to the entire system by recycling/ reusing the wastewater. Indeed, the multiple-effect distillation (MED) plant is used to improve the efficiency of the system by exploiting the surplus low-grade heat of the cogeneration process and an industrial process, while the reverse osmosis (RO) plant is used to add a significant feature to the system (to be more flexibility) by covering the largest area of treated water demand due to the ability of installing the RO plant in another geographical location. The performance modeling of desalination plants has been described through detailed equations of energy and mass balance. The average condition (AC) model, which is the simplified version of the shortcut method for the modeling MED plant (based on Forward-Feed MED Systems without Flashing Effects), has been taken from [96]. The main equations of the AC model are given in Table 9.

Table 9: General modeling equations and correlations of MED plant

Equation		Description	
$Q_{Total} = Q_{htffe} \cdot N$ $Q_{Total} = \Delta H_{c,avg} \cdot m_D$	(74)	Total thermal power loads (W) of all evaporators (assumed an equal thermal load of all evaporators)	[96]
$\Delta H_{c,avg} = 2.7532 \cdot T_{vapor,avg} + 3278.8$	(75)	Latent heat of condensation	[96]
$T_{vapor,avg} = \dfrac{T_{vapor,0} + T_{vapor,N}}{2}$	(76)	Average temperature of the vapor	[96]
$Q_{htffe} = U_{htffe} \cdot A_{htffe} \cdot \Delta T_{vapor}$	(77)	Thermal power (W) emitted by condensing distilled water into the tubes of the horizontal-tube falling film evaporator (htffe)	[96]
$U_{htffe} = 0.8552 + 4.7 \times 10^{-3} \times T_{vapor,avg}$	(78)	Overall heat transfer coefficient	[96]
$\Delta T_{vapor,avg} = \dfrac{T_{vapor,0} - T_{vapor,N}}{N}$	(79)	An average temperature driving force of evaporators by assuming an equal vapor temperature drop for each MED evaporator	[96]
$m_F = m_D + m_B$	(80)	Overall balance for MED plant	[96]
$m_F \cdot x_F = m_D \cdot x_D + m_B \cdot x_B$	(81)	Overall salt balance for MED plant	[96]
$\dfrac{m_D}{m_F} = 1 - \dfrac{x_F}{x_B}$	(82)	Recovery ratio at $x_D = 0$	[96]
$m_D = \beta^{MED} \cdot m_F$	(83)	Flow rate of distillate in term of recovery fraction	[96]
$m_B = (1 - \beta^{MED}) \cdot m_F$	(84)	Flow rate of brine in term of recovery fraction	[96]
$GOR = N \times 9.8^N = \dfrac{m_D}{m_s}$	(85)	Gained output ratio (Performance metric of MED)	[96]

The complete equations of the performance model for a hollow-fiber reverse osmosis module have been taken from the literature [96], in the same context, more detailed information can be found in the literature [135-138], as in the following table.

Table 10: General modeling equations and correlations for RO Plant

Equation		Description	
$F_F = F_D + F_B$	(86)	Overall balance of the module	[96]
$F_F . C_F = F_D . C_D + F_B . C_B$	(87)	Overall solute (salt) balance of the module	[96]
$m_D = \beta^{RO} . m_F$	(88)	Flow rate of distillate in term of recovery fraction	[96]
$m_B = (1 - \beta^{RO}) . m_F$	(89)	Flow rate of brine in term of recovery fraction	[96]
$F_{F,Total} = F_F . n$	(90)	Total flow rate when (n) modules are in parallel	[96]
$J_{water} = A \left(\Delta P - \dfrac{P_{opof}}{C_F} C_S \right) \Upsilon_{RO}$	(91)	Water flux	[96]
$\Upsilon_{RO} = \dfrac{\eta}{1 + \dfrac{16 . A . \mu . L_f . L_S . \eta_{RO}}{1.0133 \times 10^5 . r_i^4}}$ $\eta_{RO} = \dfrac{\tan \theta_{RO}}{\theta_{RO}}$ $\theta_{RO} = (\dfrac{16 . A . \mu . r_o}{1.0133 \times 10^5 . r_i^2})^{\frac{1}{2}} . \dfrac{L_f}{r_i}$	(92)	Module properties	[96]
$\Delta P \approx \dfrac{P_F + P_B}{2} - P_D = P_F - \left(\dfrac{\text{shell side pressure drop per module}}{2} + P_D \right)$	(93)	Pressure drop across the membrane	[96]
$C_S \approx \dfrac{C_F + C_B}{2}$	(94)	Average solute (salt) concentration	[96]
$J_{solute} = \left(\dfrac{D_{2M}}{K\delta} \right) . C_S$	(95)	Solute (salt) flux	[96]
$F_D = A_{S,m} . J_{solute}$	(96)	Volumetric flow rate of the distillate per module	[96]
$C_D \approx \dfrac{J_{solute}}{J_{water}}$	(97)	Solute (salt) concentration in the distillate	[96]
$A_{S,m} . A . \dfrac{P_{opof}}{2 C_F} . \Upsilon_{RO} . C_B^2 + \left[F_F - A_{S,m} . A \left(\Delta P - \dfrac{P_{opof}}{2} \right) . \Upsilon_{RO} \right] C_B - F_F . C_F = 0$	(98)	To determine the value of brine (rejection) concentration	[96]

Additionally, the balance equations for the hybrid combination of two desalination plants are given as follows:

Table 11*: Overall balance equations for the desalination process*

Equation		Description
$F_{F,Total} \cdot C_{F,Total} = F_{F,MED} \cdot C_{F,MED} + F_{F,RO} \cdot C_{F,RO}$	(99)	Overall salt balance on feed streams
$F_{D,Total} \cdot C_{D,Total} = F_{D,MED} \cdot C_{D,MED} + F_{D,RO} \cdot C_{D,RO}$	(100)	Overall salt balance on distillate streams
$F_{B,Total} \cdot C_{B,Total} = F_{B,MED} \cdot C_{B,MED} + F_{B,RO} \cdot C_{B,RO}$	(101)	Overall salt balance on brine streams

4.4.5 Economical Assessment

The selection of optimal design and operational patterns for the system and its subsystems is based on economic, environmental, and safety metrics. The economic optimality can be achieved by maximizing the profit of the system through minimizing the total annualized cost (TAC), which is calculated by annualizing the capital expenditure (CAPEX) and operating expenditure (OPEX), as in the following relationship [96]:

Annual net (after-tax) profit = (Annual income – Total annualized cost) × (1-Tax rate) + Depreciation

The evaluation of the economic feasibility for the system in this study requires considering the cost of equipment and fuel that contribute in the production of desired commodities (water and energy). However, the mutual water-energy nexus would not allow to minimize the cost of water and power together. Thus, a reduction in the

production cost for one commodity (as the cost of water production) would cause increasing in the cost of the other (as the cost of power production) due to the availability of resources. Accordingly, this work endeavors to balance between water and power production via maximizing the overall system profit.

The total cost estimation of the system depends on determining the main components cost as shown in Table 12. In the cogeneration process, the cost of the boiler and the turbine are the most significant capital cost of the process and it is determined as in Equation 102, whereas the pump cost is insignificant for the different operation conditions. The cost of the boiler, which is assumed to be a water-tube boiler worked by gas and oil, is based on the amount of thermal power transferred to the steam, superheated temperature, and operational pressure [109], as given in Equation 103. The cost of the turbine, which is considered as a non-condensing turbine, is related to the shaft power output of the turbine [109], as given in Equation 104. The fuel cost is the most substantial factor in estimating the operation cost during power production from the cogeneration process by contributing over 90% of the total power generation cost [109, 112] and it is modeled as in Equations 105 and 106. Additionally, the maintenance cost of the cogeneration process (particularly the boiler) represents about 30% of the fuel cost [205, 206].

The cost of concentrated solar power plants can be classified into three featured categories: capital cost (investment cost), operation and maintenance cost, and financing cost (mostly incorporated in capital cost) [40, 207]. The most cost of a concentrated solar power plant goes to the capital cost due to using parabolic trough power plant that does

87

not require fuel consumption to maintain high operating temperature as in solar tower power plant [208]. The capital cost as well as the operation and maintenance cost for parabolic trough collectors have been taken from the literature [156], as in Equations 107 and 108. The estimation of the thermal energy storage cost can be described as in Equations 109 and 110 [156]. The economic analysis for the two desalination plants which are adopted in this work is a crucial to determine the total annual cost (TAC) for the system.

It is noteworthy that the comprehensive economic model of RO plant has been introduced through detailed equations as described in [209], while the inclusive economic model for MED plant has been developed and described amply in [210]. Alternatively, the annualized fixed cost and operating cost for MED and RO plants can be calculated by the equations 111-114, which have been developed for a specific outlet salt content [142]. In order to estimate the fixed capital cost of an incorporated industrial process in the system, all expenses of major equipment costs, equipment purchased delivered, installation of equipment, pipes installations, building and its services, construction expenses, etc. are considered. Whereas the operating cost is calculated by encompassing all expenditure of direct cost of raw materials, utility cost, and operators cost [211].

To demonstrate the economic feasibility of the system, the net annualized profit needs to be increased by maximizing the annualized income. The annual income can be obtained from annual values of produced electricity, treated water, avoided cost of discharging wastewater (fresh water acquisition, transportation, and disposal), and

88

chemicals and fuels from processing facilities (midstream productions), as shown relationships (117-20).

Table 12: Summary of equations and correlations for economic evaluation

Equation		Description	
$AFC_{Cogen} = (AFC_{Boiler} + AFC_{Turbine}) \cdot k_f$	(102)	Annualized fixed capital cost of the cogeneration process	
$AFC_{Boiler} = 3 \cdot k_f \cdot N_P \cdot N_T \cdot Q_{Boiler}^{0.77}$	(103)	Annualized fixed capital cost of the boiler	[109]
$AFC_{Turbine} = 475 \cdot k_f \cdot E_{Turbine}^{0.45}$	(104)	Annualized fixed capital cost of the turbine	[109]
$AOC_{Cogen} = 1.3 \cdot F_P \cdot C_{Fuel} \cdot k_\gamma$	(105)	Annualized operating cost of the cogeneration process	[109]
$C_{Fuel} = a_{Fuel} \cdot Q_f \cdot 10^{-6} \cdot k_\gamma = k_f \cdot (Q_{Boiler}/\eta_f) \cdot 10^{-6} \cdot k_\gamma$	(106)	Fuel cost based on the selected type and amount of fuel	[112]
$AFC_{PTC} = C_{PTC} \cdot A_{PTC} \cdot k_f$	(107)	Annualized fixed capital cost of the parabolic trough collectors	[156]
$AOC_{PTC} = OC_{PTC} \cdot Q_{PTC \rightarrow final\ demand} \cdot k_\gamma$	(108)	Annualized operating cost of the parabolic trough collectors	[156]
$AFC_{TES} = C_{TES} \cdot SCH \cdot Q_{TES} \cdot k_f$	(109)	Annualized fixed cost of the thermal energy storage	[156]
$AOC_{TES} = OC_{TES} \cdot Q_{TES} \cdot k_\gamma$	(110)	Annualized operating cost of the thermal energy storage	[156]
$AFC_{MED} = 13.0 \times 10^6 + 2227 \cdot \left(F_{F,MED}, \frac{m^3}{day} \right)^{0.7}$	(111)	Annualized fixed capital cost of MED plant	[142]
$AFC_{RO} = 2.0 \times 10^6 + 1166 \cdot \left(F_{F,RO}, \frac{m^3}{day} \right)^{0.8}$	(112)	Annualized fixed capital cost of RO plant	[142]
$AOC_{MED} = 0.24 \cdot \left(F_{F,MED}, \frac{m^3}{hr} \right) \cdot k_\gamma$	(113)	Annualized operating cost of MED plant	[142]
$AOC_{RO} = 0.18 \cdot (F_{F,RO}, \frac{m^3}{hr}) \cdot k_\gamma$	(114)	Annualized operating cost of RO plant	[142]

Table 12: Continued

Equation		Description	
$\text{AFC}_{\text{PR}} = \left(\text{AFC}_{\text{EQ}} + \text{AFC}_{\text{S}}\right).\,k_f$ $\text{AFC}_{\text{EQ}} = C_{\text{CO}}.\,N_{\text{CO}} + C_{\text{TR}}.\,N_{\text{TR}} + C_{\text{HE}}.\,N_{\text{HE}}$	(115)	Annualized fixed capital cost of an industrial process	
$\text{AOC}_{\text{PR}} = (v^{\text{RNG}}.\,F_{\text{RNG}} + N_P\,.\,\eta_P\,.\,E_S \\ \qquad\qquad + v^L\,.\,N_L).\,k_\gamma$ $E_S = \dfrac{E_T}{\eta_P} = \dfrac{q.\,\rho.\,g.\,h}{3.6\times 10^6}$ $N_L = (6.29 + 31.7\,.\,N_{\text{PS}}^2 + 0.23\,.\,N_{\text{EQ}})^{0.5}$	(116)	Annualized operating cost of an industrial process	[211] [211]
$\text{ANI}_{\text{Cogen}} = \dfrac{a_e\,.\,E_{\text{Turbine}}\,.\,\eta_g}{3.413}\,.\,k_\gamma$	(117)	Annualized income of the cogeneration process (electric power generation)	[109]
$\text{ANI}_{\text{TW}} = \left(v^{\text{RO}}\,.\,F_{D,\text{RO}} \\ \qquad\qquad + v^{\text{MED}}\,.\,F_{D,\text{MED}}\right).\,k_\gamma$	(118)	Annualized income of the treated water	[156]
$\text{ANI}_{\text{WW}} = C_{\text{WW}}\,.\,F_{B,\text{Total}}\,.\,k_\gamma = (C_{\text{FW}} + C_{\text{TR}} + C_{\text{DS}})\,.\,F_{B,\text{Total}}\,.\,k_\gamma$	(119)	annualized value of avoided cost of discharging wastewater	[156]
$\text{ANI}_{\text{PR}} = \left(v^{\text{Fuel}}\,.\,F_{\text{FP}} \\ \qquad\qquad + v^{\text{Chemicals}}\,.\,F_{\text{CP}}\right).\,k_\gamma$	(120)	Annualized income of processing facilities (midstream) productions	

4.5 Optimization Formulation

The selection of a various collection of technologies that constitute the superstructure representation of the multi-purpose system may be required significant numbers of model and a hardly challenging for solution. To handle this challenging, the sets of the mathematical modeling can be defined as the generic optimization formulations. These generic formulations which include modeling equations and constraints of each subsystem can be presented generally as function of inlet and outlet stream, design, operation, and state variables. To handle the fluctuations (uncertainties) in solar energy availability and fuel price, a scenario-based approach for uncertain

parameters with their probabilities of occurrence is used to consider the effect of uncertain parameters on the system design and operation. A two-stage stochastic programming model is adopted as the operation scheduling in the economic objective function, which presented later in the formulation, to compensate uncertainties.

4.5.1 Solar Collection Process

The useful thermal power captured by solar collectors is a function of the solar-irradiation intensity ($Solar\_Radiation_t$) and the effective surface area of the solar collector (A^{SC}). The existence of the solar collector system is determined through a binary variable y^{SC} (which is 1 if the collector system exists, and 0 if the collector system does not exist). Multi-period operation is adopted to deal with the diurnal changes of solar energy. The probability-based uncertain factors (e.g., solar energy data) might follow a certain probability distribution, which can be discrete or continuous. These probability-based uncertain parameters can be formulated as described in the section 4.3.1 to use in the second (operation) stage of the two-stage stochastic programming with recourse. The optimal effective area of the solar collectors, which represents one of the design variables in the first stage, is sized according to the maximum requirements of any period through the linking constraints to obtain the optimal solution. Therefore, the largest area (which is used for capital cost estimation one-time at the time of constructing the system) is selected from various solar collector areas because there is a certain area of the solar collector for each operational period t and scenario s, which is given as:

$$A_{t,s}^{SC} \leq A_{Design\_max}^{SC} \, y^{SC} \quad \forall t, \forall s \tag{121}$$

The total thermal power provided by the solar collectors ($Q_{t,s}^{SC}$) is directly fed to the steam

generator ($Q_{t,s}^{Direct\_SC}$) and to the thermal energy storage ($Q_{t,s}^{In\_TES}$) for subsequent usage as

follows:

$$Q_{t,s}^{SC} = Q_{t,s}^{Direct\_SC} + Q_{t,s}^{In\_TES} \quad \forall t, \forall s \tag{121}$$

$$Q_{t,s}^{SC} \leq Q_{t,s}^{Useful\_SC} \quad \forall t, \forall s \tag{122}$$

where $Q_{t,s}^{Useful\_SC}$ is the useful thermal power per the optimal effective area of the solar
collectors.

The performance and limitations of the solar collectors are described by the vector

set of modeling equations and constraints, which is given as:

$$\Omega_{t,s}^{SC}\left(CS_{t,s}^{In\_SC}, HS_{t,s}^{Out\_SC}, Q_{t,s}^{Useful\_SC}, D^{SC}, O_{t,s}^{SC}, S_{t,s}^{SC}\right) = 0 \quad \forall t, \forall s \tag{123}$$

$$\Omega_{t,s}^{SC}\left(CS_{t,s}^{In\_SC}, HS_{t,s}^{Out\_SC}, Q_{t,s}^{Useful\_SC}, D^{SC}, O_{t,s}^{SC}, S_{t,s}^{SC}\right) \leq 0 \quad \forall t, \forall s \tag{124}$$

where $CS_{t,s}^{In}, HS_{t,s}^{Out}$ are the inlet (cold) and outlet (hot) streams, $Q_{t,s}^{Useful\_SC}, D^{SC}, O_{t,s}^{SC}, S_{t,s}^{SC}$ are

variables of the total thermal power, design, operation, and state of the solar collection

process respectively.

4.5.2 Thermal Energy Storage

The thermal power balance equation for the thermal energy storage during each period t

and scenario s is equal to the thermal power stored at the end of previous period ($Q_{t,s}^{acc\_TES}$)

plus the stored thermal power obtained from the solar collectors ($Q_{t,s}^{In\_TES}$) minus the outlet

thermal power sent to the steam generator ($Q_{t,s}^{Out\_TES}$) and the thermal power losses from

the thermal energy storage ($Q_{t,s}^{Loss\_TES}$), which is given by:

$$Q_{t,s}^{TES} = Q_{t,s}^{acc\_TES} + Q_{t,s}^{In\_TES} - Q_{t,s}^{Out\_TES} - Q_{t,s}^{Loss\_TES} \quad \forall t, \forall s \tag{125}$$

The storage unit must have enough capacity to accommodate the surplus thermal power obtained from the solar collectors. Physically, this constraint represents the design variable $V_{Design\_max}^{Cap\_TES}$ that is the maximum capacity allowable in the thermal storage system and must be greater than the storage capacity in each period t and scenario s, which is given by:

$$V_{t,s}^{TES} \leq V_{Design\_max}^{Cap\_TES} \quad \forall t, \forall s \tag{126}$$

A specific volume of thermal energy storage (e.g., 6 hours of thermal storage) must be appointed to estimate the capital cost, which incurred one-time at the time of constructing the system, of the storage unit. The existence of the storage system is determined through a binary variable (which is 1 if the storage system exists, and 0 if the storage system does not exist). Consequently, the volume of thermal storage for each operational period t and scenario s would be subjected to a capacity constraint of selected storage volume and it can meet or exceed the stored thermal power as follows:

$$Q_{t,s}^{TES} \leq Q_{Design_{max}}^{Cap_{TES}} \, y^{TES} \quad \forall t, \forall s \tag{127}$$

The performance and limitations of the storage tanks are described by the vector set of modeling equations and constraints, which is given as:

$$\Omega_{t,s}^{TES} \left(HS_{t,s}^{In\_TES}, CS_{t,s}^{Out\_TES}, Q_{t,s}^{Out\_TES}, D^{TES}, O_{t,s}^{TES}, S_{t,s}^{TES} \right) = 0 \quad \forall t, \forall s \tag{128}$$

$$\Omega_{t,s}^{TES} \left(HS_{t,s}^{In\_TES}, CS_{t,s}^{Out\_TES}, Q_{t,s}^{Out\_TES}, D^{TES}, O_{t,s}^{TES}, S_{t,s}^{TES} \right) \leq 0 \quad \forall t, \forall s \tag{129}$$

where $HS_{t,s}^{In\_TES}$, $CS_{t,s}^{Out\_TES}$ are the inlet (hot) and outlet (cold) streams, $Q_{t,s}^{Out\_TES}$, D^{TES}, $O_{t,s}^{TES}$, $S_{t,s}^{TES}$ are variables of the thermal power supplied by the thermal energy storage, design, operation, and state of the thermal energy storage respectively.

4.5.3 Cogeneration Process

To satisfy the optimal values of the steam Rankine cycle (SRC) parameters, the thermodynamic cycle is formulated as an optimization problem. The thermal power balance for the energy sources that supplied to the steam generator in the SRC for each operational period t and scenario s is described as follows:

$$Q_{t,s}^{In\_SG} = Q_{t,s}^{Fossil} + Q_{t,s}^{Direct\_SC} + Q_{t,s}^{Out\_TES} + Q_{t,s}^{Out,PR} \quad \forall t, \forall s \tag{130}$$

Whereas the total thermal power provided to the entire system from the steam generator for each operational period t and scenario s is described as follows:

$$Q_{t,s}^{Out\_SG} = Q_{t,s}^{SG-Turbine} + Q_{t,s}^{SG-MED} + Q_{t,s}^{SG-PR} \quad \forall t, \forall s \tag{131}$$

where $Q_{t,s}^{In\_SG}$ is the total thermal power provided to the steam generator, $Q_{t,s}^{Fossil}$ is the thermal power is obtained directly from the combustion of fossil fuels in the boiler, $Q_{t,s}^{Direct\_SC}$ is the direct thermal power supplied by the solar collectors, $Q_{t,s}^{Out\_TES}$ is the thermal power supplied by the thermal energy storage, $Q_{t,s}^{Out\_PR}$ is the thermal power supplied by an industrial process, and $Q_{t,s}^{SG-Turbine}$, $Q_{t,s}^{SG-MED}$, $Q_{t,s}^{SG-PR}$ are the thermal power supplied by the steam generator to the turbine, multiple-effect distillation, and industrial process.

The performance and limitations of the cogeneration turbine unit are described by the vector set of modeling equations and constraints, which is given as:

94

$$\Omega_{t,s}^{Turbine} \left(Steam_{t,s}^{In}, Steam_{t,s}^{Out}, E_{t,s}^{Turbine}, D^{Turbine}, O_{t,s}^{Turbine}, S_{t,s}^{Turbine}\right) = 0 \quad \forall t, \forall s \quad (132)$$

$$\Omega_{t,s}^{Turbine} \left(Steam_{t,s}^{In}, Steam_{t,s}^{Out}, E_{t,s}^{Turbine}, D^{Turbine}, O_{t,s}^{Turbine}, S_{t,s}^{Turbine}\right) \leq 0 \quad \forall t, \forall s \quad (133)$$

where $Steam_{t,s}^{In}, Steam_{t,s}^{Out}$ are the inlet and outlet steam conditions, $E_{t,s}^{Turbine}, D^{Turbine}, O_{t,s}^{Turbine}, S_{t,s}^{Turbine}$ are variables of the produced electric power, design, operation, and state of the turbine respectively.

For each operational period t and scenario s, the electric power produced by the cogeneration turbine is equal to the total energy fed to the SRC from the steam generation multiplied by an efficiency factor. Thus, the surplus thermal power (the thermal power that cannot be converted into electric power) is sent to MED to produce desalinated water and enhance the system efficiency as follows:

$$E_{t,s}^{Turbine} = Q_{t,s}^{SG-Turbine} \cdot \eta^{SRC} \quad \forall t, \forall s \quad (134)$$

$$Q_{t,s}^{Turbine-MED} = Q_{t,s}^{SG-Turbine} - E_{t,s}^{Turbine} \quad \forall t, \forall s \quad (135)$$

Where $Q_{t,s}^{SG-Turbine}$ is the thermal power supplied to the cogeneration turbine from the steam generation, η^{SRC} is the thermal efficiency of converting the total energy fed to the SRC into electricity, and $Q_{t,s}^{Turbine-MED}$ represents the surplus thermal power of the cogeneration turbine.

Furthermore, the thermal power needs for water treatment in MED is obtained directly from various sources of thermal power for each operational period t and scenario s, as follows:

$$Q_{t,s}^{MED} = Q_{t,s}^{Turbine-MED} + Q_{t,s}^{SG-MED} \quad \forall t, \forall s \quad (136)$$

where $Q_{t,s}^{SG-MED}$ is the thermal power supplied directly to MED from the steam generator.

The maximum electric power that produced by the cogeneration process is restricted to the amount of electricity met the system requirements and the amount of electricity sold to a local power grid as follows:

$$E_{t,s}^{Turbine} \leq E_{Design}^{Max\_Turbine} \quad \forall t, \forall s \tag{137}$$

The electric power produced can be utilized to supply the power demand of MED, RO, and an external power grid, which is given as:

$$E_{t,s}^{Turbine} = E_{t,s}^{MED} + E_{t,s}^{RO} + E_{t,s}^{Grid} + E_{t,s}^{PR} \quad \forall t, \forall s \tag{138}$$

$$E_{t,s}^{MED} = F_{t,s}^{MED} \cdot e_{MED} \quad \forall t, \forall s \tag{139}$$

$$E_{t,s}^{RO} = F_{t,s}^{RO} \cdot e_{RO} \quad \forall t, \forall s \tag{140}$$

where $F_{t,s}^{MED}$, $F_{t,s}^{RO}$ are the volumetric flowrate of the treated water, e_{MED}, e_{RO} are the electric energy requirement per the volumetric flowrate of the treated water.

4.5.4 Desalination Process

The treatment process of wastewater, which embedded in the system, is the hybrid of MED and RO plants. In addition to the reasons mentioned in section 4.4.4 that were used to select these two desalination plants, the quality of feed-water (e.g., total dissolved solid content, TDS) is also significantly crucial factor in selecting a proper desalination technology. Therefore, to enhance the performance and reliability for the treatment process against the variability in salinity concentration of feed-water, RO can be utilized effectively in desalinating low and medium salinity water (i.e., 55,000 to 70,000 ppm of TDS) compared to MED that recommended for high-salinity water (i.e., TDS > 70.000

96

ppm) [212]. Other factors for the determining the percentage contribution of RO and MED in the total desalinated water are their ability to realize intended product quality (e.g., TDS separation), and meet system restrictions (e.g., brine concentration).

The performance and limitations of the MED and RO are described by the vector set of modeling equations and constraints, which is given as:

$$\Omega_{t,s}^{MED}\left(F_{t,s}^{D\_MED}, X_{t,s}^{D\_MED}, X_{t,s}^{B\_MED}, D^{MED}, O_{t,s}^{MED}, S_{t,s}^{MED}\right) = 0 \quad \forall t, \forall s \tag{141}$$

$$\Omega_{t,s}^{MED}\left(F_{t,s}^{D\_MED}, X_{t,s}^{D\_MED}, X_{t,s}^{B\_MED}, D^{MED}, O_{t,s}^{MED}, S_{t,s}^{MED}\right) \leq 0 \quad \forall t, \forall s \tag{142}$$

$$\Omega_{t,s}^{RO}\left(F_{t,s}^{D\_RO}, X_{t,s}^{D\_RO}, X_{s,t}^{B\_RO}, D^{RO}, O_{t,s}^{RO}, S_{t,s}^{RO}\right) = 0 \quad \forall t, \forall s \tag{143}$$

$$\Omega_{t,s}^{RO}\left(F_{t,s}^{D\_RO}, X_{t,s}^{D\_RO}, X_{t,s}^{B\_RO}, D^{RO}, O_{t,s}^{RO}, S_{t,s}^{RO}\right) \leq 0 \quad \forall t, \forall s \tag{144}$$

where $F_{t,s}^{D\_MED}, F_{t,s}^{D\_RO}$ are the desalinated flow rate (distillate capacity) of MED and RO,

$X_{t,s}^{D\_MED}, X_{t,s}^{B\_MED}, X_{t,s}^{D\_RO}, X_{t,s}^{B\_RO}$ are the salinity content in desalinated and brine streams

, $D_{t,s}^{MED}, O_{t,s}^{MED}, S_{t,s}^{MED}, D_{t,s}^{RO}, O_{t,s}^{RO}, S_{t,s}^{RO}$ are variables of the design, operation, and state of MED and RO respectively.

$$F_{t,s}^{F\_Total}. X_{t,s}^{F\_Total} = F_{t,s}^{F\_MED}. X_{t,s}^{F\_MED} + F_{t,s}^{F\_RO}. X_{t,s}^{F\_RO} \quad \forall t, \forall s \tag{145}$$

$$F_{t,s}^{D\_Total}. X_{t,s}^{D\_Total} = F_{t,s}^{D\_MED}. X_{t,s}^{D\_MED} + F_{t,s}^{D\_RO}. X_{t,s}^{D\_RO} \quad \forall t, \forall s \tag{146}$$

$$F_{t,s}^{B\_Total}. X_{t,s}^{B\_Total} = F_{t,s}^{B\_MED}. X_{t,s}^{B\_MED} + F_{t,s}^{B\_RO}. X_{t,s}^{B\_RO} \quad \forall t, \forall s \tag{147}$$

The respective constraints (which relate the state variables) of the salinity content in the total flow rate of desalinated water stream and brine water stream, which represent a maximum allowable salinity in these streams, are given by:

$$X_{t,s}^{D\_Total} \leq X_{Max}^{D\_Total} \quad \forall t, \forall s \tag{148}$$

$$X_{t,s}^{B\_Total} \leq X_{Max}^{B\_Total} \quad \forall t, \forall s \tag{149}$$

Other constraints for the desalination process include the design capacity (which relate the design variables) of the desalinated water production for MED and RO as follows:

$$F_{t,s}^{D\_MED} \leq F_{Max}^{D\_MED} \quad \forall t, \forall s \tag{150}$$

$$F_{t,s}^{D\_RO} \leq F_{Max}^{D\_RO} \quad \forall t, \forall s \tag{151}$$

Furthermore, the limitation on some design variables for specific portion in MED and RO (e.g., evaporator area, membrane area) can be represented by Equations 152 and 153 respectively, or the constraint may be extended over the entire RO and MED to include the maximum number of MED effects (i.e., evaporators) and the maximum number of RO modules, which is used for capital cost estimation incurring one-time at the time of constructing the system, as in Equations 154 and 155 respectively.

$$D_{Min}^{MED} \leq D_{t,s}^{MED} \leq D_{Max}^{MED} \quad \forall t, \forall s \tag{152}$$

$$D_{Min}^{RO} \leq D_{t,s}^{RO} \leq D_{Max}^{RO} \quad \forall t, \forall s \tag{153}$$

$$D_{t,s}^{MED} \leq D_{Max}^{MED} \quad \forall t, \forall s \tag{154}$$

$$D_{t,s}^{RO} \leq D_{Max}^{RO} \quad \forall t, \forall s \tag{155}$$

4.5.6 Industrial Process

To satisfy the requirements for heating and cooling, heat integration is carried out for an industrial process between its streams and units that need to be heated and its streams and units that need to be cooled. Thus, the heat is transferred from the heat from the process hot streams to the process cold streams through heat integration before utilizing external heating and cooling utilities [96]. Consequently, heat integration can be

fulfilled with N_H process hot streams, N_C process cold streams, N_{HU} heating utilities, and N_{CU} cooling utilities.

The formulation of the heat balances is developed over the temperature intervals. The heat load of the uth process hot stream, which losses sensible heat, can be removed through the zth interval as in Equation 156, while the heat can be added through the zth interval to the vth process cold stream, which gains sensible heat, as in Equation 157:

$$HH_{u,z,t,s} = F_{u,t,s} \cdot C_{p,u,t,s} \cdot (T_{z-1,t,z} - T_{z,t,s}) \quad \forall u, z, t, s \tag{156}$$

$$HC_{v,z,t,s} = F_{v,t,s} \cdot c_{p,v,t,s} \cdot (t_{z-1,t,s} - t_{z,t,s}) \quad \forall v, z, t, s \tag{157}$$

where $T_{z,t,s}$, $T_{z-1,t,s}$, $t_{z-1,t,s}$, and $t_{z,t,s}$ are the hot-scale and cold-scale temperatures at the top and the bottom lines defining the zth interval for each period t and scenario s. The sum of the heating loads and cooling utilities can be represented as follow:

$$HH_{z,t,s}^{Total} = \sum_u HH_{u,z,t,s} \quad \forall z, t, s \tag{158}$$

$$HC_{z,t,s}^{Total} = \sum_v HC_{u,z,t,s} \quad \forall z, t, s \tag{159}$$

The incorporating heating and cooling utilities into heat integration of an industrial process i necessary to satisfy the heating and cooling requirements. The heat load of the uth heating utility and the cooling capacities of the vth cooling utility for temperature interval z is given by:

$$HHU_{u,z,t,s} = FU_{u,t,s} \cdot C_{p,u,t,s} \cdot (T_{z-1,t,s} - T_{z,t,s})$$

$$\text{where } u = N_H + 1, N_H + 2, ., N_H + N_{HU} \tag{160}$$

$$HCU_{v,z,t,s} = fU_{v,t,s} \cdot C_{p,v,t,s} \cdot (t_{z-1,t,s} - t_{z,t,s})$$

where $v = N_C + 1, N_C + 2, \dots, N_C + N_{CU}$ (161)

where $FU_{s,t,u}$ is the flowrate of the uth heating utility and $fU_{s,t,v}$ is the flowrate of the vth cooling utility during each period t and scenario s.

The total of all the heating loads for the uth heating utilities and all cooling capacities for the vth cooling utilities are given by:

$$HHU_{s,t,z}^{Total} = \sum_u HHU_{s,t,u,z}$$ (162)

$$HCU_{s,t,z}^{Total} = \sum_v HCU_{s,t,v,z}$$ (163)

During each operational period t and scenario s, the total heating loads of the uth heating utilities and the cooling capacities of the vth cooling utilities may be evaluated by summing up the individual heat loads and the individual cooling loads over intervals:

$$QH_{u,t,s} = \sum_z HHU_{u,z,t,s}$$ (164)

$$QC_{v,t,s} = \sum_z HCU_{v,z,t,s}$$ (165)

4.5.7 Objective Function

The main purpose of the optimization problem is to maximize the annual expected profit as an economic metric of the integrated system for each period t and scenario s, which is expressed as follows:

The maximum annual expected (after-tax) profit = { $\sum_{s=1}^{N_S} p^s$ (Annual Income^s – Total Annualized Operating Cost^s) – Total Annualized Investment Cost} × (1-Tax rate) + Depreciation (166)

where,

Annual Income^s = Annual value of treated water + Annual value of avoided cost of discharging wastewater + Annual value of electricity supplied for an external grid + Annual value of an industrial process (midstream) productions

Total Annualized Operating Cost^s = Annualized operating cost of the cogeneration process + Annualized operating cost of the parabolic trough collectors + Annualized operating cost of the thermal energy storage + Annualized operating cost of MED plant + Annualized operating cost of RO plant + Annualized operating cost of an industrial process

Total Annualized Investment Cost = Annualized fixed capital cost of the cogeneration process + Annualized fixed capital cost of the parabolic trough collectors + Annualized fixed cost of the thermal energy storage + Annualized fixed capital cost of MED plant + Annualized fixed capital cost of RO plant + Annualized fixed capital cost of an industrial process

Consequently, the objective function of a multi-scenario mixed integer non-linear programming (MINLP) model, which is a deterministic equivalent model of a two-stage stochastic programming model with recourse, can be given as follows:

$$\max \text{TAP} = \{k_\gamma \sum_s p^s \sum_t (v^{RO} \cdot F_{t,s}^{D\_RO} + v^{MED} \cdot F_{t,s}^{D\_MED}) + (C^{WW} \cdot F_{t,s}^{B\_Total}) +$$

$$(\frac{1}{3.413} \cdot a_e \cdot E_{t,s}^{Turbine} \cdot \eta_g) + (v^{Fuel} \cdot F_{t,s}^{FP} + v^{Chemicals} \cdot F_{t,s}^{CP}) - (OPEX_{t,s}^{Cogen} + OPEX_{t,s}^{SC} +$$

$$OPEX_{t,s}^{TES} + OPEX_{t,s}^{MED} + OPEX_{t,s}^{RO} + OPEX_{t,s}^{PR}) - k_f (CAPEX^{Cogen} + CAPEX^{SC} +$$

$$CAPEX^{TES} - CAPEX^{MED} + CAPEX^{RO} + CAPEX^{PR})\} \times (1\text{-Tax rate}) + \text{Depreciation}$$

$$(167)$$

The proposed model of this work, which is a multi-scenario mixed integer nonlinear programming (MINLP) model, comprises nonlinear, non-convex equations and mixed integer variables. Therefore, advanced approaches and techniques may be required to globally optimize the integrated system to obtain the optimal system configuration. The objective function of the stochastic programming model is solved using the stochastic programming solver for two-stochastic programs with recourse of the software LINGO® [213].

4.6 Case Study

In order to demonstrate the applicability of the proposed approach and a formulated optimization model, an illustrative case study is solved by considering a multi-purpose system that addresses the water-energy nexus problem of shale oil and gas industries for Eagle Ford Basin in Texas, which extends over 23 counties and becomes one of the significant producers of shale oil and gas in addition to the large aquifer (Carrizo-Wilcox) of brackish water source, as shown in Figure 16 that is adapted from [214].
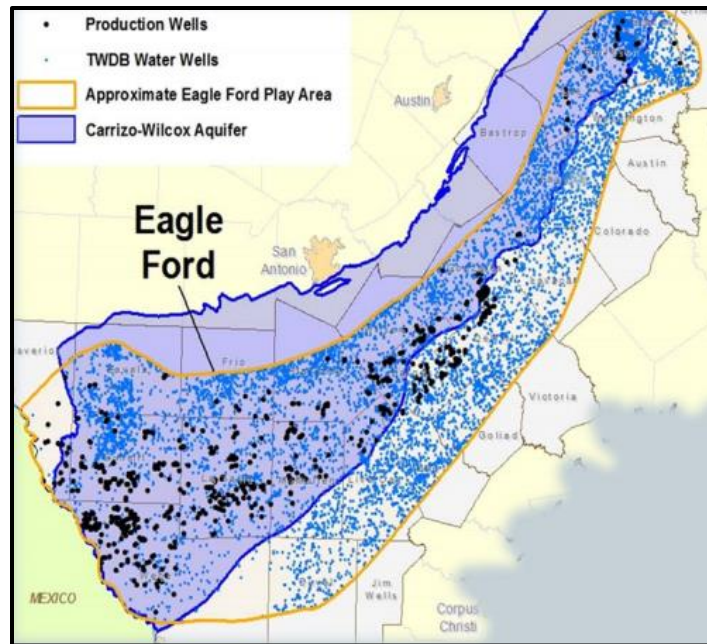
Figure 16: Eagle Ford Basin [214]

Based on data from 2012 and 2013, the water consumption of a typical well with a 5000 ft lateral length in the Eagle Ford is about 4.2 million gallons during hydraulic fracturing technology. A major company (Halliburton), which works in hydraulic fracturing, records that less than 14% of the water used in this process returns as flowback water [215] with the total dissolved solid content (TDS) of $15,000 - 55,000$ mg salt / L_{water} [76]. A large number of wells in a shale play and the heavy regulations of storing wastewater in containers can contribute to obtaining approximately a constant flow of flow-back and produced water (FPW) because there is always a compensation for declination in the amount production of FPW in a well from other wells and the capability of providing constant flow of wastewater to desalination plants from containers directly. Thus, to estimate the amount of FPW returned from a shale play to the surface that can be

considered as an input to desalination plants calculations in addition to avoid the uncertainty, the average of an FPW flow for 10 plays in the Eagle Ford Basin between the early 2000s to 2015 is estimated from the total FPW quantity (151.22 $\times 10^6$ m^3) during this period [85]. The following table provides techno-economic data for two desalination technologies [63, 143, 145] including RO and MED plants which are utilized to ensure removal salt and non-salt impurities and typical exploitation for energy sources.

Table 13: Summary of techno-economic data for RO and MED

Characteristics	RO	MED
Outlet Salt Content (ppm)	200	80
Water Recovery (m^3 Desalinated Water/m^3 Feed Seawater)	0.55	0.65
Value of Desalinated Water ($/m^3 Desalinated Water)	0.88	0.82
Thermal Energy Consumption (kWht/m^3 Desalinated Water)	-	65
Electric Energy Consumption (kWhe/m^3 Desalinated Water)	4	2

In addition, the treatment process (desalination plants) of flow-back and produced water in a shale gas site can participate in saving money effectively by reducing the cost of transportation, fresh water acquisition and disposal for each barrel of FPW. Accordingly, the characteristics of a water treatment plant with a capacity of 2380 barrels/day in Eagle Ford Basin [147], as shown in Table 14, are used to obtain the cost

data of primary/secondary treatment (PST), fresh water acquisition, transportation, and disposal.

Table 14: Cost of treatment, fresh water, transportation and disposal of FPW

Type	PST	Fresh Water	Transportation	Disposal
Cost ($/barrel)	0.34	0.24	0.89	0.05

The incorporation of solar energy in the system as an energy source represents a substantial challenge due to the availability of fossil fuels, especially, in the case of low prices in the world market. Site selection is the first step for constructing the system, hence, the estimation of solar intensity is necessary to demonstrate the ability to use solar energy in a selected site based on the available data of global solar irradiance, while the calculation of the useful thermal power which produced from concentrated solar plant (PTC) according to the direct solar irradiance data. The solar data for Eagle Ford Shale Play is extracted from the National Solar Radiation Data Base (NSRDB) are: hourly global solar irradiance, hourly direct solar irradiance, hourly solar incidence angle, hourly dry bulk temperature, hourly wet bulk temperature. The essential cost data of solar collectors (parabolic trough collectors) is summarized in Table 15 that can be used to calculate the fixed capital cost [40, 41].

Table 15: Capital cost of parabolic trough collector components

Component	Capital Cost ($/m²)	Component	Capital Cost ($/m²)
Receivers	43	Electronic and Control	14
Mirrors	40	Header Piping	7
Concentrator Structure	47	Civil Works	18
Concentrator Erection	14	Spares, HTF, , Freight	17
Drive	13	Contingency	11
Piping	10	Structure and Improvement	7

The shale gas production from the Eagle Ford plays can be utilized as fuel for the cogeneration process of the system or converted to valuable and expensive products in the world market through several processes of separation and fractionation which represent essential stages in natural gas processing plants. In this study, Conventional fractionation process is chosen as a key intermediate process to segregate the natural gas feed into a gas product (methane and ethane), liquefied petroleum gas (propane and butane) and stabilized natural gas liquid (pentane+), which can feed many industries such as cogeneration process, plastics, textiles, metal industry, motor fuel, etc. The proposed process consists of four columns are: De-ethanizer (methane and ethane are separated from the top of the column as vapor phase), De-butanizer (propane and butane are separated from the top of the column and the stabilized natural gas liquid goes to the bottom of the column, De-propanizer (propane and butane are separated to obtain pure propane product from the top of the column), Butane splitter (n-butane and iso-butene are segregated as specified products of the column). To determine the thermal power requirements (deficit and surplus) of the fractionation process through heat integration approach that they can be

coupled with the heat recovery unit (steam generator) of the system, the heat duties of reboilers and condensers for columns in addition to their streams temperature must be estimated based on feed stream condition and compositions, as shown in Table 16.

Table 16: Feed condition and composition of fractionation process [216]

Stream Name	First Feed (from well)	Second Feed (from dehydration unit)
Pressure (bar)	30	30
Temperature (ºC)	25	25
Mass Flow Rate (kg/hr)	25000	8000
Mole Fraction (Methane)	0.097	0.13
Mole Fraction (Ethane)	0.029	0.08
Mole Fraction (Propane)	0.035	0.1
Mole Fraction (i-Butane)	0.018	0.055
Mole Fraction (n-Butane)	0.028	0.113
Mole Fraction (i-Pentane)	0.026	0.104
Mole Fraction (n-Pentane)	0.025	0.091
Mole Fraction (n-Hexane)	0.064	0.122
Mole Fraction (n-Heptane)	0.09	0.11
Mole Fraction (n-Octane)	0.15	0.072
Mole Fraction (n-Nonane)	0.11	0.02
Mole Fraction (n-Decane)	0.09	0.003
Mole Fraction (n-C11)	0.079	0
Mole Fraction (n-C12)	0.071	0
Mole Fraction (n-C13)	0.031	0
Mole Fraction (n-C14)	0.023	0
Mole Fraction (n-C15)	0.018	0
Mole Fraction (n-C16)	0.014	0
H_2O	0.002	0

Furthermore, flared gas represents a significant source of CO_2 emissions that can be reduced by exploiting flared gas as a fuel for the cogeneration process. Particularly, in Eagle Ford basin, around 13% of the gas in the formation was flared which equivalents to 4.4 billion cubic feet of natural gas [146].

4.7 Results and Discussion

The first step of solar energy calculations has been carried to study the capability of incorporating solar energy as a source of thermal power in the system by estimating the potential of this type of energy in the selected site of a case study. The hourly global solar irradiance data measured in Eagle Ford area between 1991-2010 was used to calculate the monthly average hourly clearness index (k_t) values. The index is the ratio of the global solar irradiance on a horizontal surface (I) to the hourly extraterrestrial solar irradiance on a horizontal surface (I_o), as shown in equation 168, which is considered as a stochastic parameter because it is a function of a period of year, seasons, climatic conditions and geographic site [217].

$$k_t = \frac{I}{I_o} \tag{168}$$

Furthermore, the level of sky clearness can be classified according to the value of k_t as in Table 17 [218]:

Table 17: Classification of clearness index level

Sky Condition	k_t
Cloudy	< 0.3
Partly cloudy	$0.3 \leq k_t \leq 0.5$
Sunny	> 0.5

The results of calculating k_t between 1991-2010 have shown an acceptable coincide comparing to k_t values which were determined between 1952-1975 by Solar Energy Information Data Bank (SEIDB) [219], as shown in Figure 17.
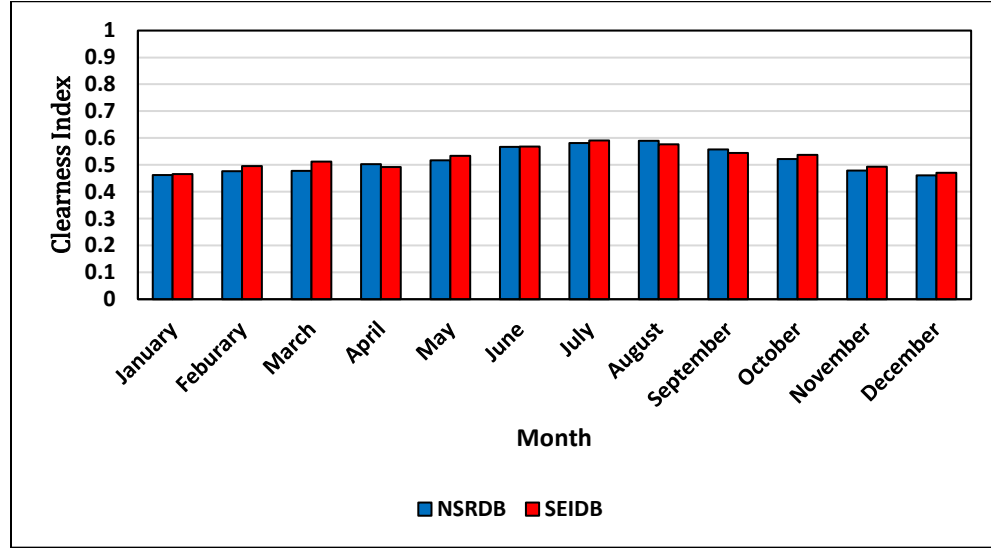
Figure 17: Monthly-average hourly clearness index

The analysis of the monthly-average hourly clearness index through the classification of the clearness index level shows that more than 80% of the days can be defined as either sunny or partly cloudy and less than 20% of the days are classified as cloudy. It has been also noted that the individual monthly sky conditions percentage of sunny daytime hours exceed 40% from April through September, while the percentage of cloudy daytime hours do not exceed about 20%. Consequently, the most significant component of solar radiation for concentrated solar collectors' performance is the direct normal irradiance (DNI), which is reduced dramatically with growing cloud cover. Concentrating solar collectors can operate efficiently under clear sky conditions of months

between June-October that have more than 50% of the sunny daytime hours with hourly k_t values exceed 0.5 and these collectors are less efficient for the rest months of the year with increasing the percentage of partially or completely cloudy daytime hours as in the following figure.
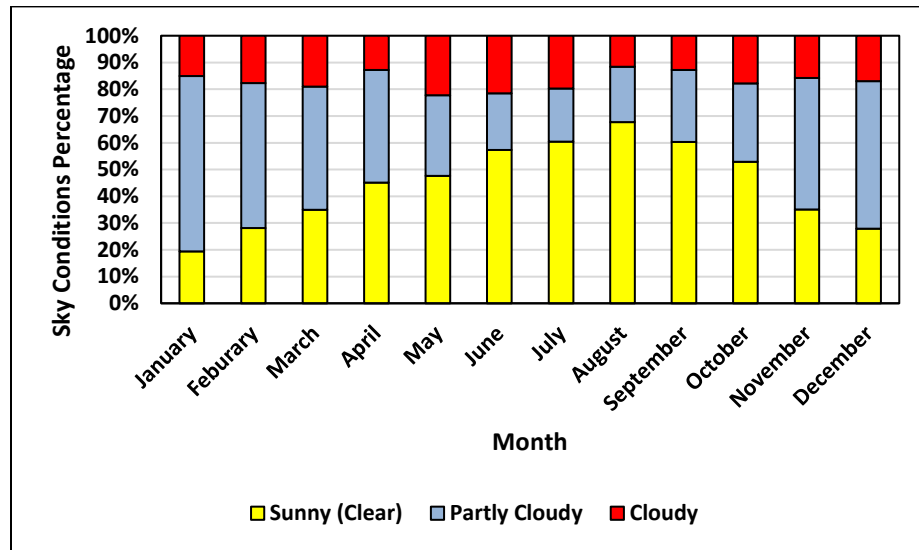
Figure 18: Monthly sky conditions during daytime hours

According to the comprehensive analyses of sections 4.3.1 and 4.7, the operational period of the system can be partitioned into two periods based upon solar radiation intensity: a relatively high-intensity between May-October and a low-intensity from November through April. Thus, the implementation of calculating the useful (net) solar thermal power that produced by the solar field requires using statistical analysis to find the probability distribution density (PDF) and the cumulative probability distribution (CDF) for obtained data of direct normal irradiance, solar incidence angle and dry bulb temperature, which represent uncertain parameters as in Figure 19.

These analyses can be used in the three-point approximation technique to generate a few representative values (discrete points) and their identified probabilities, which are given in Table 18. The discrete points have been introduced into a detailed performance model of the parabolic trough to provide the useful thermal power values of solar energy to the objective function of the stochastic model along with considering the characteristics of the LS-3 collector chosen and all types of thermal losses (convection, conduction, radiation) in the solar collection system. similar methodology in which has been used to generate representative points for solar energy. The data of natural gas price ($/MMBTU) was obtained from the Energy Information Administration (EIA) [132] for the period between 1997-2018. The data has been analyzed based on the time of year as shown in Figure 20.
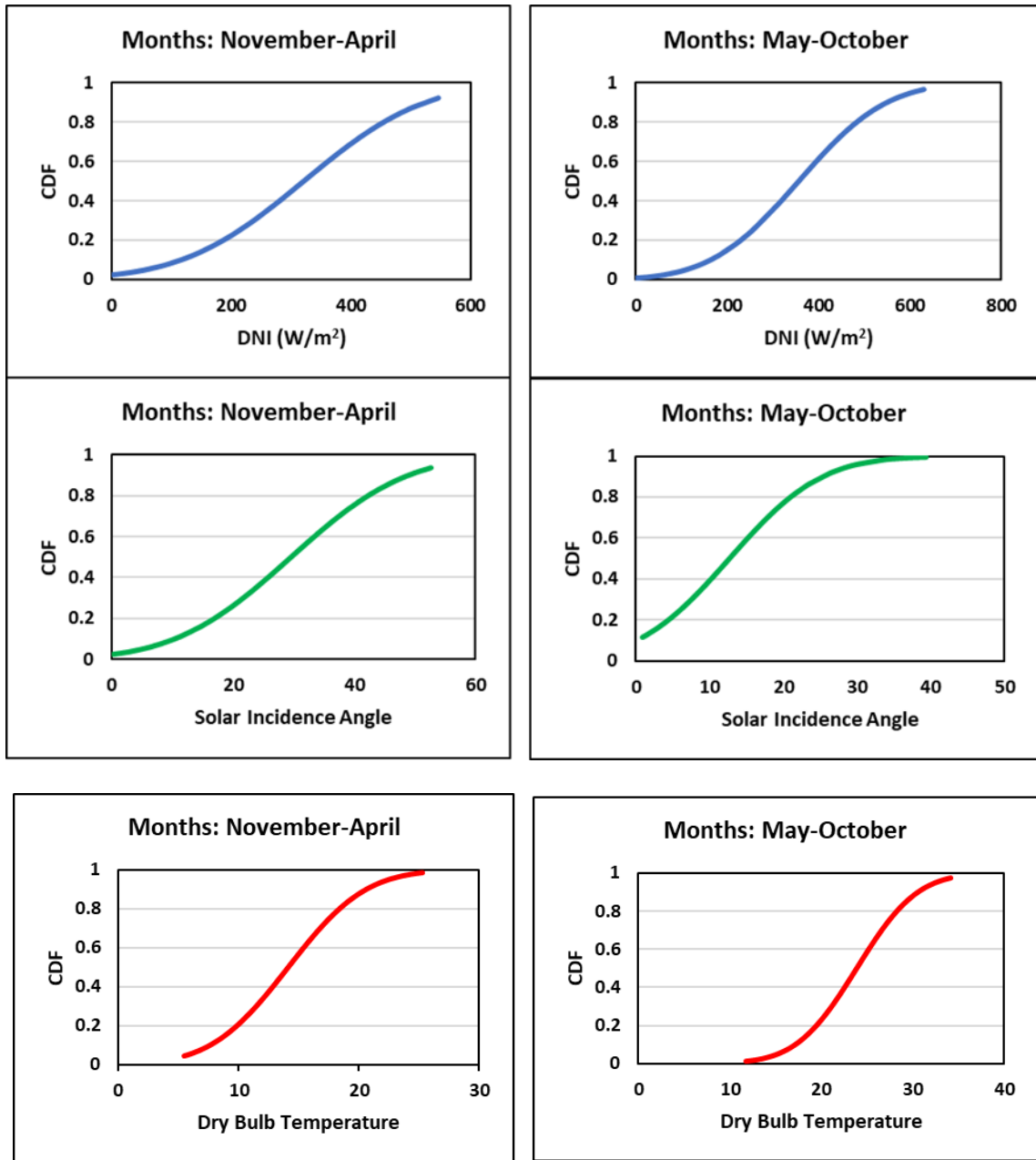
Figure 19: Cumulative distribution function of DNI (W/m^2), solar incidence angle ($^\circ$), and dry bulb temperature ($^\circ$C)
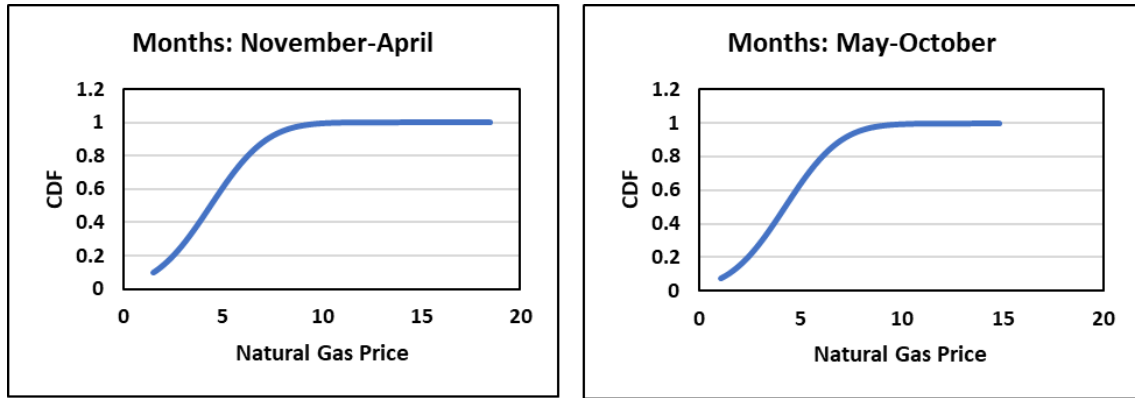
***Figure 20*:** Cumulative distribution function of Natural gas price (\$/MMBTU)

***Table 18*:** Continuous distributions and discrete approximations of uncertain parameters

Parameter	Continuous Distribution	Discrete Approximation
Direct normal irradiance (W/m^2) (Months: November-April)	$\theta \sim N(\mu, \sigma) \sim N(321.1, 159.3)$	Points: (59.3, 323.7, 555.2) Probabilities: (0.185, 0.630, 0.185)
Direct normal irradiance (W/m^2) (Months: May-October)	$\theta \sim N(\mu, \sigma) \sim N(356.0, 196.4)$	Points: (109.8, 356., 605.1) Probabilities: (0.185, 0.630, 0.185)
Solar incidence angle (Months: November-April)	$\theta \sim N(\mu, \sigma) \sim N(29.4, 15.1)$	Points: (4.4, 29.5, 53.1) Probabilities: (0.185, 0.630, 0.185)
Solar incidence angle (Months: May-October)	$\theta \sim N(\mu, \sigma) \sim N(12.6, 9.8)$	Points: (-2.2, 12.7, 29.7) Probabilities: (0.185, 0.630, 0.185)
Dry bulb temperature (Months: November-April)	$\theta \sim N(\mu, \sigma) \sim N(14.1, 5.0)$	Points: (5.7, 14, 22.4) Probabilities: (0.185, 0.630, 0.185)
Dry bulb temperature (Months: May-October)	$\theta \sim N(\mu, \sigma) \sim N(23.8, 5.1)$	Points: (15.4, 23.9, 32.3) Probabilities: (0.185, 0.630, 0.185)
Natural gas price (Months: November-April)	$\theta \sim N(\mu, \sigma) \sim N(4.3, 2.2)$	Points: (0.91, 4.3, 8.0) Probabilities: (0.185, 0.630, 0.185)
Natural gas price (Months: May-October)	$\theta \sim N(\mu, \sigma) \sim N(4.2, 2.1)$	Points: (0.5, 4.2, 7.7) Probabilities: (0.185, 0.630, 0.185)

The determination of minimum utility targets of the conventional fractionation process, which is shown in Figure 21, requires estimating heat duties for reboilers and condensers, in addition, to their stream's temperature.
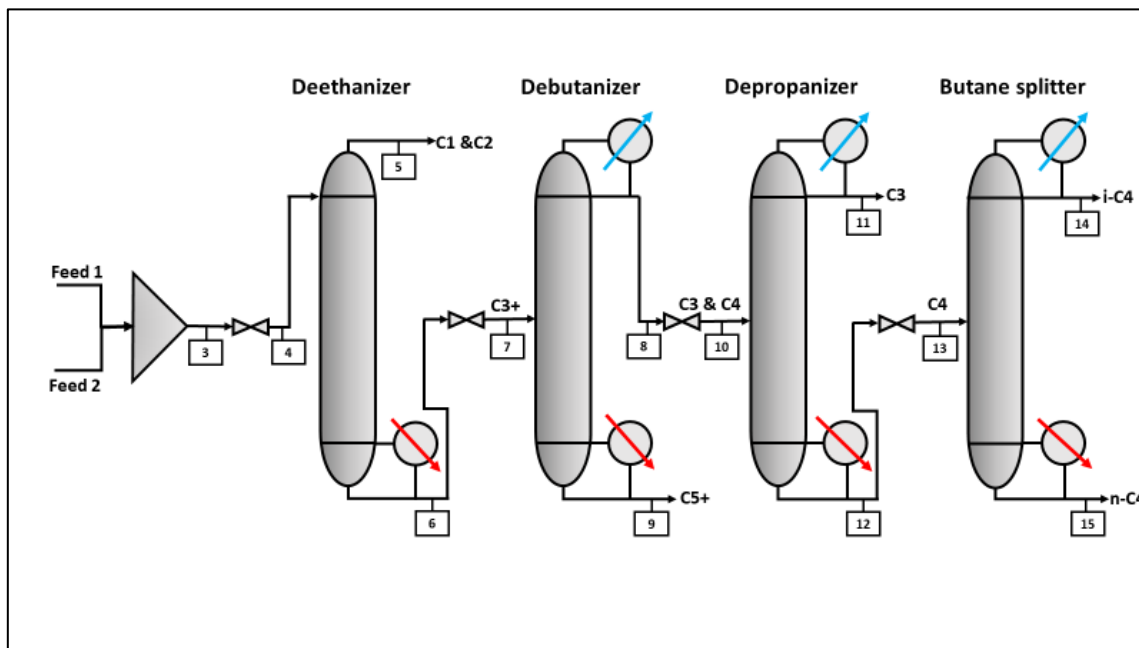
Figure 21: Conventional fractionation process

Therefore, the process was simulated using ASPEN Plus® for the feed stream condition and compositions, which is given in Table 16. The key results of the simulation such as the stream data, heat duty, stream temperature was summarized in Appendix B and Tables 19.

Table 19: Number of stages and heat exchangers data in each column

Description	Number of Trays	Reboiler Duty (kW)	Inlet Temperature of Reboiler (°C)	Outlet Temperature of Reboiler (°C)	Condenser Duty (kW)	Inlet Temperature of Condenser (°C)	Outlet Temperature of Condenser (°C)
Deethanizer	19	5587.1	189.7	246.6			
Debutanizer	19	735.5	228.2	244.3	-861.55	72.5	61.4
Depropanizer	19	247.99	75.3	77.6	-255.13	23.2	22.7
Butane Splitter	30	185.92	63.2	65.2	-190.74	30.5	29.1

Heat integration is carried out to identify the minimum utility targets through the thermal pinch analysis. The supply temperature, target temperature, and utility for each hot and cold stream of the process are provided in Table 20. The temperature interval diagram is set up, which is the first step in the pinch analysis, considering a minimum approach temperature is 5°K, as shown in Table 21 . Next, the cascade diagram calculations are carried out, as shown in Figure 22, to determine the minimum heating utility ($Q_{Heating}^{min}$) is 6570.07 kW and the minimum cooling utility ($Q_{cooling}^{min}$) is 1121.47 kW. Now, the grand composite curve (GCC) was developed for screening utilities to reduce the operating cost as shown in Figure 23. The minimum heating utility will be supplied by the steam exiting the steam generator.

Table 20: Stream data for the fractalization process

Stream (kW/ºK)	Flowrate X Specific Heat (ºK)	Supply Temperature (ºK)	Target Temperature (ºK)	Enthalpy Change (kW)
H1	78.32	346	335	-861.55
H2	255.13	297	296	-255.13
H3	95.37	304	302	-190.74
HU	?	525	522	?
C1	98.01	463	520	5587.1
C2	45.97	501	517	735.5
C3	82.66	348	351	247.99
C4	92.96	336	338	185.92
CU	?	291	292	?

Table 21: Temperature interval diagram for the fractionation process

Figure 22: Cascade diagram for the fractionation process
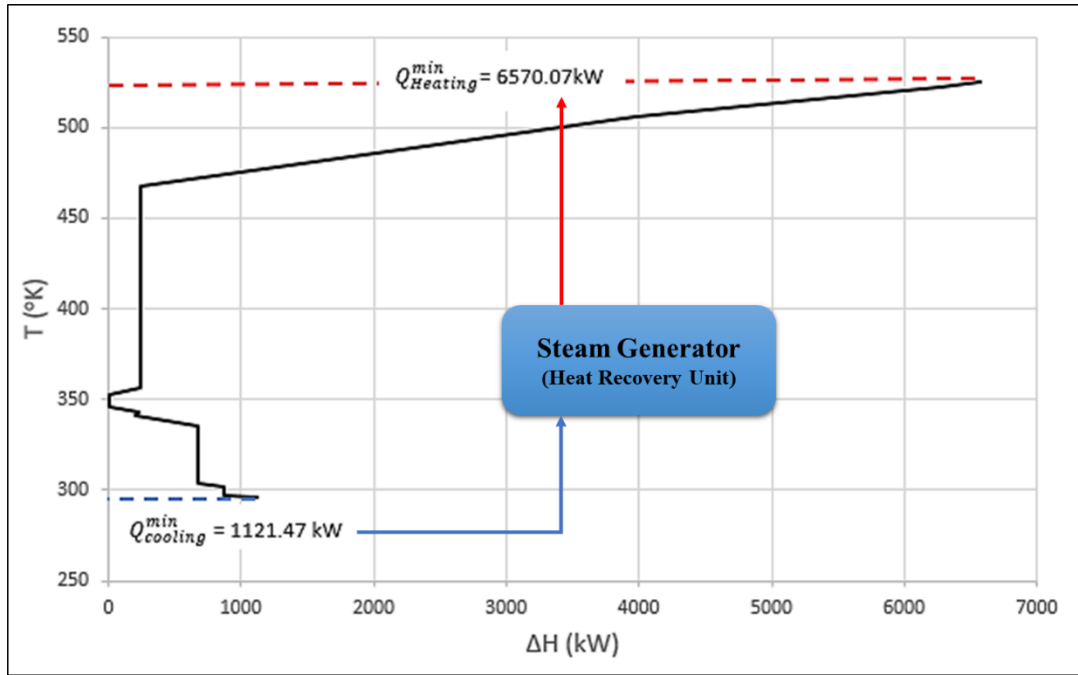
Figure 23: Grand composite curve for the fractionation process

The optimization formulations of the integrated system are solved for a case study by using the proposed approach, which is described in section 4.3, to obtain the optimal design and operation under uncertainty. The stochastic optimization problem is formulated as a multi-scenario Mixed Integer Non-Linear Programming (MINLP) problem that is a deterministic equivalent of a two-stage stochastic programming model with recourse and solved using the software LINGO® [213] and MS-Excel 2016 on Intel Core i7-6700 CPU with 16 GB RAM. The iterative discretization method has been presented to realize a significant reduction in the complexity solving of the optimization problem. Thus, in addition to discretize the percentage contribution of RO and MED in the total desalinated water production iteratively, the percentage contribution of solar energy in the total

thermal power mix of the system is also iteratively discretized that allows designing the RO and MED separately and to estimate the economic feasibility of integrating solar energy in the system. The objective function has been solved to obtain the expected value of the maximum annual net (after-tax) profit by postulating a finite number of scenarios to characterize the uncertain parameters of direct solar irradiance and natural gas price which take a finite set of known values with their assigned probabilities, as given in Table 18. The probability of each scenario in the final scenario tree equals the product of probabilities of all points that compose it. Consequently, 81 uncertain scenarios are generated by considering the available data of uncertain parameters during the seasonal periods of the year to find a solution for each case individually. A comprehensive study has been performed based on economic and sustainability metrics to demonstrate the potential of the proposed system in attaining the profitability and sustainability in the framework of water-energy nexus. responsible consumption for water and energy. The optimization results for all cases are summarized in Table 22 .

Table 22: Economic and sustainability metrics of the system

| (%RO,%MED)* | (% 25 Solar Energy, %75 Fossil Fuel)** | | | |
	TAC (MMUSD)	TAP (MMUSD)	ROI %	PBP (year)
30 RO, 70 MED	76.4	100	18.6	5.1
50 RO, 50 MED	73.6	99	18.4	4.4
70 RO, 30 MED	70.9	97.6	18.3	4.5
(%RO,%MED)*	(% 50 Solar Energy, %50 Fossil Fuel)**			
	TAC (MMUSD)	TAP (MMUSD)	ROI %	PBP (year)
30 RO, 70 MED	86.6	97.5	17	4.9
50 RO, 50 MED	75.2	97.9	17.1	4.8
70 RO, 30 MED	71.1	95.2	17.3	4.8
(%RO,%MED)*	(% 75 Solar Energy, %25 Fossil Fuel)**			
	TAC (MMUSD)	TAP (MMUSD)	ROI %	PBP (year)
30 RO, 70 MED	89.2	101	15.5	5.3
50 RO, 50 MED	84	100	16.1	4.9
70 RO, 30 MED	78.8	98.4	16.3	5.1

*The percentage contribution of RO and MED in the total desalinated water production

**The percentage contribution of solar energy and fossil fuel in the total thermal power mix of the system

Based on the above-mentioned results, it can be observed that the system has been offered a significant performance through using sustainability weighted return on investment (ROI) and payback period (PBP) calculations for the different percentage contributions of RO, MED, solar energy and fossil fuel. Additionally, the total annual cost (TAC) of the system can be reduced by increasing the percentage contribution of RO over MED and decreasing the percentage contribution of solar energy. This reduction in the total annual cost is based on two reasons: the high capital investment and operating

cost of MED, the competitive price of fossil fuels comparing to the relatively high cost of concentrated solar technologies, especially, in the short term. However, the incorporation of solar energy in the system is feasible economically and it will be more feasible in the long-term because of the exhaustion of fossil fuels resources and the diminishing in solar technologies cost.

A comparative study has been carried out between the obtained solutions of the stochastic model and those are obtained from the deterministic model with considering the specific percentage contribution of solar energy and fossil fuels (50% solar energy, 50% fossil fuels) and the various percentage of RO and MED contributions, as shown in Figure 24. This study indicates that the solving of the stochastic model offers a significant improvement on values of ROI and PBP comparing with the obtained values of the deterministic model, whereas the total annual costs of the system that obtained from solving the stochastic model are notably less than they obtained from the deterministic model.
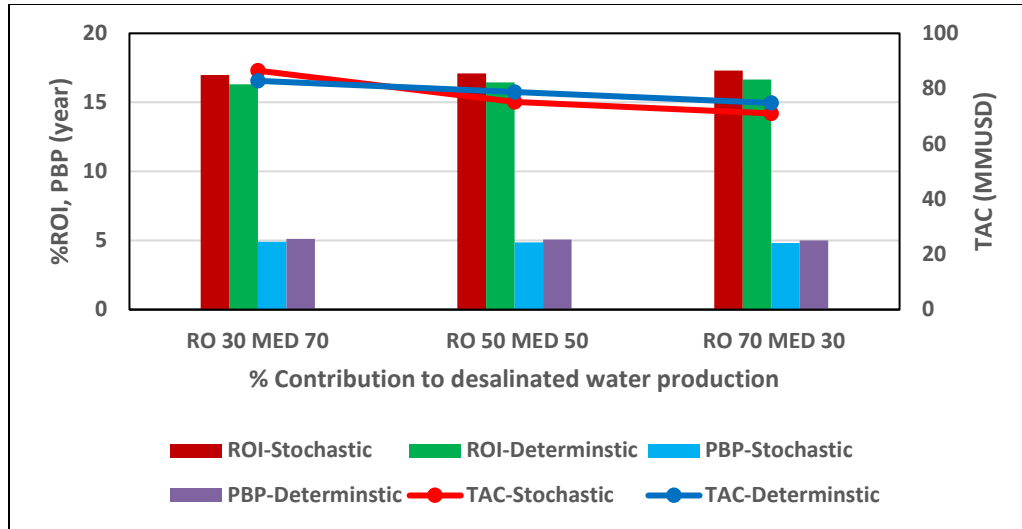
Figure 24: A comparative study between stochastic and deterministic models

It is worth noting that the optimal solution of the system under uncertainty comparatively deviated from the deterministic solution due to considering the uncertain parameters. The relative differences between the stochastic and deterministic cases stem from the capability of the system to meet its demand from thermal power during the operational period by adjustment the diurnal fluctuations of solar energy through utilizing fossil fuels and thermal energy storage system that make the system works in a nearly steady mode and inherits robustness against the uncertainty. However, there is still a necessity to handle the uncertain nature of the actual hourly, daily and seasonally data by developing the system design and operation under uncertainty that can address operational issues and provide the detailed design. These concepts are consistent with the objective of this work to start preliminary screening and then determine main targets that can be as a guide to the proper design and operation for the system.

In order to evaluate the impact of the system performance on the environmental aspects, a comprehensive comparison has been achieved for the amount CO_2 which can be reduced during the operational mode for the system, as described in Figure 25.

The comparison indicates obviously that the enhancement in the environmental performance of the system requires increasing the percentage of solar energy contribution and RO contribution because RO plant consumes less thermal power than MED plant and solar energy can be contributed to meet a demand of MED plant from the thermal power and lessen fossil fuel consumption, which causes sustaining fossil fuels resources and significantly diminishing in the emissions of greenhouse gases.
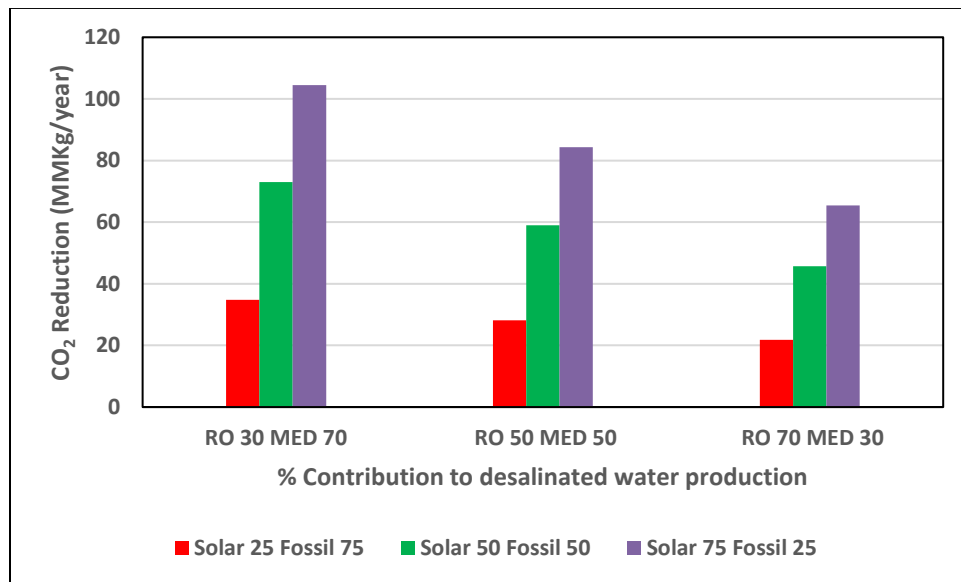
Figure 25: The estimation of reduction in an amount of CO_2 emission from the system

In the same context, flared gas can be converted from the source of greenhouse gas emissions in a shale site to one of the energy sources that may be contributing effectively

to improve the economic and environmental performance of the system. Consequently, reconciliation of economic and environmental objectives is crucial to attaining the optimal configuration of the system which operates under uncertainty conditions.

4.8 Summary

A new hierarchical procedure has been developed for formulating and optimizing an integrated system operating under uncertainty to address the problem of water-energy nexus in a shale oil and gas industry. The system utilizes a hybrid of fossil fuel and solar energy to enhance the sustainable design of the system that consists of the following key elements: concentrated solar collectors, thermal energy storage, cogeneration process, MED and RO. An industrial process (fractionation process) has been incorporated into the system to satisfy heating and cooling demands of the process. The optimization problem is formulated as a multi-scenario Mixed Integer Non-Linear Programming (MINLP) problem that is a deterministic equivalent of a two-stage stochastic programming model to characterize the uncertainty in the system by considering two uncertain operational parameters (normal direct irradiance, fossil fuel price). Solar energy is included as a source of thermal [power for the entire system through heat recovery system (steam generator). The heat integration technique has been carried out for hot and cold streams of the fractionation process to determine the surplus and deficit energy content in addition to the quality of hot and cold streams temperature. The operational period has been discretized based on two seasons of the year to create a finite number of scenarios for uncertain parameters. The percentage of incorporating water treatment technologies and solar energy into the system has been iteratively discretized. The results from solving a case

study for Eagle Ford Basin in Texas indicated the applicability of the integrated approach based on stochastic optimization to show the system's economic and environmental merits in solving the problem of water management in shale gas production using a water-energy nexus framework and incorporating renewables.

CHAPTER V

ESTIMATION OF SOLAR IRRADIANCE DATA FOR CONCENTRATING SOLAR

COLLECTORS USING HIERARCHICAL CALCULATION METHODOLOGIES

FOR DIFFERENT SKY CONDITIONS

5.1 Introduction

Renewable energy sources have taken increasingly significant attention these days. Particularly, solar energy that could contribute efficiently to attain the proper solution for the rapid growth problem in energy demand. The short-term solution can be through offering the sustainable system design via hybridizing solar energy with fossil fuel to sustain the existing energy resources, while the long-term solution can be the entirely replacing for the conventional energy sources to compensate the shortage in these resources. The depletion of fossil fuel resources (oil, natural gas, coal) approximately would be up to 2042, except coal which will be lasting after 2042 [220].

The primary assessment of the potential of solar energy at a specific site is essential for selecting and designing solar energy systems (e.g., photovoltaic systems and concentrating solar thermal power). However, the substantial impact of uncertainty of the solar irradiance forecast (especially, direct normal irradiance) on the solar power plants output and their profitability over time should be addressed. Moreover, much attention should been paid to the significance of acquiring hour-ahead or day-ahead forecasts of solar irradiance [221]. Accordingly, most recent studies have emphasized on attaining the best forecast accuracy based on high-quality solar irradiance data to reduce the effect of

the intermittency nature of solar energy on the uncertainty in the optimal design parameters and the errors in all modelling and measurements [222-224].

The solar radiation that travels through the sky until reaching the earth's surface can obtain various forms: direct (beam), diffuse, and reflected (scattered) radiation based on the distance traveled through the atmosphere, the cloudiness amount, the ozone layer intensity, the concentration of haze in the air (water vapor, dust particles, pollutants, etc.), and types of ground surface [225]. Indeed, the most relevant component of solar radiation for concentrated solar power technologies (including parabolic trough, central receiver, linear Fresnel reflector, and parabolic dish) is the direct normal irradiance (DNI). Thus, the performance of the previous technologies reduces dramatically with growing cloud cover. Whereas, photovoltaics can generate electric power from diffuse irradiation. Therefore, the long-term evaluation for the technical and economic performance of solar energy systems based on the availability of solar radiation data and their accuracy. To move successfully from the investment in small to large scale solar projects, accurate solar radiation data are essential because small uncertainty in the measured and estimated quantity of solar radiation may jeopardize the economic feasibility of proposed solar projects [187]. Solar radiation measuring instruments (e.g., pyranometer and pyrheliometer) are utilized to obtain reliable solar radiation data over various periods of time [225]. However, the measured data may not available or easily accessible due to the high cost of instruments which used in measuring stations and the technical difficulties to calibrate these instruments, especially in developing countries.

The lack of measured DNI data at the most solar project's sites is a challenging task for researchers and workers in the field of solar energy applications. Despite the availability of global horizontal irradiance (GHI) and diffuse (DHI) horizontal irradiance data that can be used to obtain DNI values, there is still a need to model the solar resource in most cases. Consequently, most researchers in this field have formulated various models, regression equations, and empirical correlations to predict solar radiation based on the division basis of the time period (e.g., hourly, daily, monthly) and on the meteorological and geographic parameters. These parameters are maximum and minimum temperature, relative humidity, sunshine duration, cleanness index, cloud cover, geographical site, etc. [187]. The estimated datasets from various models, regression equations, and empirical correlations require precise validation via comparing with high-quality measured datasets. For large-scale solar projects, the importance of the mutual relationship between a lower uncertainty in solar radiation data, minimal financial risks, and profitability has been discussed in [224].

The two categories of solar radiation models: parametric and decomposition are used to predict beam (direct), diffuse, and global components of irradiance based on the availability of other measured or calculated quantities. The Parametric (broadband) models have been formulated based on astronomical, atmospheric and geographic parameters to predict the solar irradiance precisely. Additionally, these models are the better choice than decomposition models when meteorological data are not obtainable [225-228]. First models have been formulated and tested to estimate the amount of clear-sky direct and diffuse solar radiation on horizontal surfaces under various climate

conditions [229-231]. The attenuation influence of a large range of atmospheric constituents on the DNI has been studied. This study demonstrated that the major attenuation was occurred by effecting of constituents, molecular scattering, and water vapor absorption respectively, while the ozone layer and CO_2 have a minor effect. The tested models have shown a reasonable agreement with small values of the zenith angle [232, 233]. The availability of the input parameters (aerosol optical depth or Link turbidity) and implementation simplicity were used as the selection criteria for a number of clear sky solar irradiance models and to evaluate their accuracy. The parameters, which are measured locally, were more recommended than climatic data sets to avoid underestimated values of the direct and global irradiance [234]. Several simple clear and cloudy sky models of solar global irradiance that do not need meteorological data as inputs have been evaluated. The models can be used to predict the global irradiance for the next few hours or might be for the next day. In addition, the clear sky model can be used for partially cloudy days and the estimated total cloud amount is crucial for the cloudy sky model [235]. Three types of analyses have been used to assess the validity, limitations, and performance of many clear sky solar irradiance models. These analyses were carried out based on studying the effect of atmospheric effects (e.g., water vapor absorption, aerosol extinction), statistical evaluation, and comparison with a large number of calculated and measured data [236]. The performance of broadband models has been evaluated to identify their accuracy to predict clear-sky direct normal irradiance (DNI) by comparing with high-quality measurements along with a large range of conditions that were selected carefully. Furthermore, the uncertainty in the predicted values of DNI

increase pointedly with air mass and they were more sensitive to errors in values of turbidity and precipitable water, which are the two substantial inputs of the parametric models [227, 237]. The evaluation procedure, which consists of forty-two stages, has been created to test fifty-four parametric models through the sensitivity analysis. These models can be used to compute global and diffuse irradiance on a horizontal surface. The input data for the models have been adopted from satellite measurements including ground meteorological data and atmospheric column integrated data [238]. The significant review for eighteen clear-sky models has been carried out to assess their performance by comparison between predicted values and measured values under various climate conditions. The high-quality input data were collected from five locations. The selected models can be applied to set up solar datasets, solar resource maps, and large-scale applications. All models were ranked based on their accuracy that determined by four statistical indicators. It has also been found that there is complexity in the prediction of DNI, the prediction of DHI is less accurate, and the number of the model input may not have that obvious influence on its performance and precise [239]. To select a suitable site to install the concentrating solar power plant, seventeen clear-sky models have been studied to verify which model can be used for predicting the more precise values of direct normal irradiance. The performance and accuracy of the models have been tested by comparing their predictions with measured irradiance of a specific site along with using the statistical accuracy indicators. In this study, the parametric models have been classified into two groups: simple models that are included less than three inputs (astronomical and geographical parameters) such as ASHRAE, Meinel, HLJ, etc., and complex models that

130

are based on various parameters (the air mass, the ozone layer, aerosols, precipitable water and Linke turbidity factor) such as Bird family models. It is worth noting that simpler models can offer more accurate DNI data than complex models, in other words, an increase in the number of model inputs (e.g., atmospheric parameters) may not necessarily enhance the accuracy and performance of a model [240].

Based on the above-mentioned, the clear-sky models (Parametric models) have been developed to estimate the clear sky irradiation (in the absence of clouds). Hence, they cannot be used to predicate direct normal irradiance (DNI) under cloudy conditions. Consequently, decomposition models are based on the phenomenon of fitting the historical experimental data through empirical correlations, which are typically utilized to calculate direct normal radiation and diffuse radiation on a horizontal surface from global solar radiation data [241]. It is axiomatic that the availability of solar radiation at the earth's surface is considerably influenced by cloudy sky condition. The direct normal irradiance is attenuated significantly with increasing cloud cover and its value may be reached to zero. In contrast, once the value of cloud cover attains intermediate range values, the diffuse solar irradiance (sky radiation) starts growing in the sky until mounting to a maximum value at high range values of cloud cover, or fading to zero at the overcast sky condition [242]. Because of that, the sky state study, based on the temporal and spatial distribution modelling of clouds, is crucial to estimate the availability of all radiation types at a specific site [243]. The various concepts of cloud detection and classification have been discussed, various techniques were developed for cloud classification based on

instruments (ground-based, satellite integrated) that used to determine the state of the sky [244-246].

Numerous types of cloud cover-based models have developed to estimate hourly and daily solar radiation using cloud cover data [221, 247-249]. The cloud-cover radiation model (CRM) is widely used to obtain hourly global solar irradiance forecast based on the cloud cover, which is measured in Oktas and ranging from zero Oktas (an entirely clear sky) through eight Oktas (an entirely overcast sky). The CRM was developed by Kasten and Czeplak using ten years of hourly cloud amount data [250]. Many researchers have tested the Kasten–Czeplak model (CRM) using the dataset of various sites around the world, and to improve the model's accuracy, the locally fitted coefficients for each of the selected locations were determined by regression analysis [243, 245, 247, 248, 251-254].

In order to obtain average hourly solar radiation values from long-term daily values, global solar radiation decomposition models can be used to transform daily solar radiation values into hourly solar radiation values [255]. The existing models can be divided into three categories based on parameters, physical significance, and constructing methods: the first group of models entails the time factor like solar time, day length, solar hour angle, etc. The most widely used models are the Whillier model [256], Liu & Jordan model [257], and Collares-Pereira & Rabl model [258, 259], the second group of models is developed in the Gaussian function form such as Jain model 1 [260], Jain model 2 [261], Shazly model [262], and Baig et al. model [263], Newell model [264] is the most known model of the third group of models, which is modified from the Collares-Pereira & Rabl model [226, 255, 265].

132

Other empirical models have been developed by correlating the clearness index, diffuse fraction, and meteorological parameters based on using the measured data of selected sites to estimate the global and diffuse solar irradiation. The meteorological parameters consist of sunshine period, cloud cover, minimum and maximum temperature, relative humidity, and geographical location.

The clearness index is a random parameter which can sense the meteorological stochastic effects (e.g. atmospheric aerosols, cloudiness, temperature, etc.) on the solar radiation for a time of the day, a season of the year, and a geographical site [266]. It should be noted that the clearness index is sensitive to the short-term effects (atmospheric influences which are described by statistics and the long-term effects (Earth's movement which is described by astronomy) [218]. In general, it represents the ratio of the global solar irradiance on a terrestrial horizontal surface (which is a stochastic quantity) to the global solar irradiance on an extraterrestrial horizontal surface (which is a deterministic quantity) for the same time and site [217, 225]. In this context, the concepts of long-term of solar radiation data (either daily or monthly average daily) and short-term of solar radiation data (either hourly or monthly average hourly) can be utilized to estimate the cleanness index [225]. As already stated, the clearness index and diffuse fraction are essential factors for evaluating the impacts of cloud on extraterrestrial radiation. Therefore, they both should be considered as random variables to construct probability functions (PDF and CDF) through studying the statistical distribution of their past occurrence to predict their future values within a precise range. Based on that, several investigators have used probability function, which depends on local conditions, in

modelling clearness index to predict terrestrial solar radiation and to classify the level of the sky clearness [218, 228, 257, 267-271].

The sunshine duration is another key indicator for specifying the different sky conditions along with the clearness index and cloud cover. It is the ratio of the actual (bright) hours of sunshine (which is a stochastic value) to the average daylight hours (which is a deterministic value). When the sky is completely cloudless, the bright sunshine hours will be equal to the average daylight hours and the ratio will be 1 and the majority of radiations that gained by the solar energy systems are direct normal irradiance (DNI). In contrast, on a completely or partially cloudy day, the bright sunshine hours may reach zero, thus diffuse radiation will dominate the working of solar energy systems during the time of spreading scattered thin clouds in the sky [254]. When the sunshine duration fraction is approximately 0.3 to 0.5, the highest diffuse radiation values typically is obtained [241]. However, the uncertainty influence of scattered clouds and their movement in the sky is still representing a great obstacle in estimating a nature and quantity of received radiations on the earth surface [272]. The estimation of sunshine duration data from cloud cover by developing an empirical correlation is quite useful to calculate global solar radiation on the horizontal surface [273]. In the same context, a simple theoretical model has been presented that represents the interrelation of sunshine duration and cloud cover fraction to predict cloud cover fraction that can be further used to calculate global solar radiation on the horizontal surface (GHI) under different sky conditions [272].

134

Thus, the Angstrom-Prescott correlation, which represents the simple, linear, and pioneering relationship between clearness index and relative sunshine, was established by Angstrom and then was modified by Prescott [274, 275]. Over the last decades, there were considerable endeavors for evaluating and interpreting the Angstrom-Prescott equation [276]. New formulations (either linear or non-linear) of the Angstrom-Prescott equation were proposed by many researchers using clearness index against sunshine fraction [226, 254, 265, 273, 277-285], ambient temperature [226, 265, 278, 283, 285, 286], relative humidity[226, 265, 285], precipitation [265, 278, 287, 288], cloud cover [265, 273, 277, 289], and multi-parameters [265, 276, 283, 285, 290].

It is obvious that the performance evaluation of solar energy systems (solar photovoltaics and solar thermal applications) and selecting their optimized design depends on the availability of solar radiation data and its components. The diffuse radiation is undoubtedly a significant component besides direct normal irradiance for assessing the solar radiation quality. Hence, numerous empirical correlations have been developed to predict diffuse radiation or monthly average daily diffuse solar radiation using clearness index, relative sunshine duration, and cloud cover data [228]. The first correlation developed by Liu and Jordan [257] to estimate hourly diffuse radiation on a horizontal surface from global solar radiation, and based on the same concept, many correlations have been modified by researchers using a large amount of data from different locations over a period of years [291-295]. Other models have been developed for calculating monthly average diffuse solar radiation by employing regression analysis to correlate diffuse fraction with clearness index and relative sunshine duration [257, 296-298]. To

135

enhance the accuracy of models for estimating diffuse solar radiation or monthly average daily diffuse solar radiation, several researchers have demonstrated the importance of adding more variables such as ambient temperature, relative humidity, cloud cover, etc. [299]. The prediction of hourly, daily, and monthly global solar radiation and its components on inclined surfaces were discussed in [266, 300, 301] because the maximum amount of incident solar radiation is received on inclined surfaces.

The aim of this study is to develop two hierarchical calculation methodologies for estimating hourly solar irradiance using various models, empirical correlations and regression equations. Specifically, hourly direct normal irradiance data which is utilized for designing solar concentrated collectors. The accuracy of the proposed approaches for estimating solar data is demonstrated by using various statistical indicators while comparing with measured solar data.

5.2 Theoretical Analysis

The design and operation of various solar energy technologies and their applications such as photovoltaic systems and concentrated solar thermal energy systems require obtaining high-quality solar irradiance data for a specific site at any time of a day and a year to make the long-term evaluation for the techno-economic performance for these technologies. Thus, various existing models, empirical correlations and regression equations, which have been discussed in detail in section 5.1, will be investigated along with developing some regression equations in this work to predict different solar radiation types based on the time period and the meteorological and geographic parameters.

136

5.2.1 Estimation of Hourly Direct Normal Irradiance

5.2.1.1 Parametric (Broadband) Models

A large number of parametric models have selected and then tested for accuracy fit by using statistical indicators. The existing models, which have been formulated based on astronomical, atmospheric and geographic parameters, are used to predict direct normal irradiance (DNI) under clear sky condition. The performance of 22 models have been assessed by comparing their results with the measured high-quality datasets through statistical indictors. These models are summarized in Table 23.

Table 23: Summary of selected parametric models

Equation		Description	
$I_{DNI,FR} = I_{oN} \tau_{bulk}^{m_e}$	(169)	Fu and Rich model	[302]
$I_{DNI,ASH} = A \exp[\dfrac{-B}{\cos\theta_z}]$ A, B from table [226, 266]	(170)	ASHRAE model	[226, 302]
$I_{DNI,HLJ} = I_{oN} \tau_{aa}$ $\tau_{aa} = a_{aa} + b_{aa} \exp[-\dfrac{c_{aa}}{\cos\theta_z}]$ a_{aa}, b_{aa}, c_{aa} are constants [231, 240]	(171)	HLJ model	[240]
$I_{DNI,KUM} = 0.56\,I_{oN}[\exp(-0.65\,m_{air}) +$ $\exp(-0.095\,m_{air,KUM})]$ $m_{air} = m_r p/p_o$ $m_r = \{[1229 + (614\,\cos\theta_z)^2]^{0.5} - 614\,\cos\theta_z\}$	(172)	Kumer model	[302]
$I_{DNI,HS1} = I_{oN} \exp(-m_{air}\,\sigma\,T_{LTF})$ $\sigma = 1/(6.62960 + 1.7513m_{air} - 0.1202m_{air}^2 + 0.0065m_{air}^3$ $\qquad\qquad - 0.00013m_{air}^4)$ $m_{air} = m_r p/p_o$ $m_r = 1/\cos\theta_z$ T_{LTF}: Linke turbidity factor [240]	(173)	Heliosat-1 model	[302]

Table 23: Continued

Equation		Description	
$I_{DNI,ESRA} = I_{oN} \exp(-m_{air}\ \sigma\ T_{LTF})$ $m_{air} = m_r p/p_o$ $m_r = 35/[(1224 \cos^2\theta_z) + 1]^{0.5}$	(174)	ESRA model	[302]
$I_{DNI,Bird} = 0.9662\ I_{oN}\ \tau_{total}$ $\tau_{total} = \tau_{rt}\ \tau_{ot}\ \tau_{gt}\ \tau_{wt}\ \tau_{at}$ $\tau_{rt} = \exp[-0.0903\ m_{air}^{0.84}(1 + m_{air} - m_{air}^{1.01})]$ $\tau_{ot} = 1 - [0.1611U_3(1 + 139.48U_3)^{-0.3035} - 0.002715U_3(1 + 0.044U_3 + 0.0003U_3^2)^{-1}]$ $\tau_{gt} = \exp(-0.0127m_{air}^{0.26})$ $\tau_{wt} = 1 - 2.4959U_1[1 + 79.034U_1)^{0.6828} + 6.385U_1]^{-1}$ $\tau_{at} = \exp[-L_{ao}^{0.873}(1 + L_{ao} - L_{ao}^{0.7808})m_{air}^{0.9108}]$ $m_{air} = m_r p/p_o$ $m_r = 35/[(1224 \cos^2\theta_z) + 1]^{0.5}$ $L_{ao} = f(\beta_1, \beta_2)$	(175)	Bird model	[230, 240]
$I_{DNI,Hoyt} = I_o \left(1 - \sum_{i=1}^{5} a_i\right) \tau_{as}\ \tau_r$ $m_{air} = m_r p/p_o$ $m_r = 35/[(1224 \cos^2\theta_z) + 1]^{0.5}$ $m_r = [\cos\theta_z + 0.15\ (93.885 - \theta_z)^{-1.253}]^{-1}$ $a_1, a_2, a_3, a_4, a_5 = f(U_1, U_3, m_r, m_a, \tau_{ot}, \tau_{as})$	(176)	Hoyt (Iqbal B) model	[228, 230]
$I_{DNI,MET} = 0.9751\ I_{oN}\ \tau_{total}$ All transmittances (τ_{total}) are similar to Bird model except aerosol transmittance, $\tau_{at} = \exp(-m_{air}\ L_{ao})$ $m_{air} = m_r p/p_o$ $m_r = 35/[(1224 \cos^2\theta_z) + 1]^{0.5}$	(177)	METSTAT model	[302]
$I_{DNI,CSR} = C_{CSR}\ I_{oN}\ \tau_{total}$ $C_{CSR} = [50 + |\cos(\frac{N_j}{325})|]/49.25$ All transmittances (τ_{total}) are similar to Bird model except aerosol transmittance, $\tau_{at} = \exp(-m_{air}\ L_{ao})$ $m_{air} = m_r p/p_o$ $m_r = 35/[(1224 \cos^2\theta_z) + 1]^{0.5}$	(178)	CSR model	[240]
$I_{DNI,IqbalC} = 0.9751\ I_{oN}\ \tau_{total}$ All transmittances (τ_{total}) are similar to Bird model	(179)	Iqbal model C	[228]

Table 23: Continued

Equation		Description	
$I_{DNI,MIqbalC} = 0.9751\ I_{oN}\ \tau_{total}$ $\tau_{at} = (0.12445\beta_1 - 0.0162)$ $\qquad\qquad + (1.003 - 0.125\beta_2)\exp[-m_{air}\ \beta_1(1.089\ \beta_2$ $\qquad\qquad + 0.5123)]$ $\tau_w = 1 - 2.4959U_1[1 + 79.034U_1)^{0.6828} + 6.385U_1]^{-1}$ $U_1 = W^{\grave{}}m_r$ $W^{\grave{}} = 0.1\exp(2.2572 + 0.05454\ T_{dew}) = \text{Won'sequation}$ $m_{air} = m_r p/p_o$ $m_r = 35/[(1224\ \cos^2\theta_z) + 1]^{0.5}$	(180)	Modified Iqbal model C	[240]
$I_{DNI,AWB} = I_o\ (\tau_{md} - a_w)\ \tau_{at}$ $\tau_{md} = 1.041 - 0.16\ [m_r\ (949 \times 10^{-6}p + 0.051)]^{0.5}$ $a_w = 0.077(U_1 m_{air})^{0.3}$ $U_1 = W\ m_r$ $W = W^{\grave{}}\ (\dfrac{p}{p_o})^{0.75}\ (T_o/T_{amb})^{0.5}$ $W^{\grave{}} = 0.1\exp(2.2572 + 0.05454\ T_{dew}) = \text{Won'sequation}$ $m_{air} = m_r p/p_o$ $m_r = 35/[(1224\ \cos^2\theta_z) + 1]^{0.5}$	(181)	Atwater and Ball model (The model can be used for clear and cloudy sky)	[230, 302]
$I_{DNI,DH} = I_o\ (\tau_o\ \tau_{rt} - \alpha_w)\ \tau_A$ $\tau_o = \{[\dfrac{(1 - 0.02118X_o)}{(1 + 0.042X_o + 0.000323X_o^2)}] - [(1.082X_o)/(1$ $\qquad\qquad + 138.6X_o)^{0.805}] - [(0.0658X_o)/(1$ $\qquad\qquad + (103.6X_o)^3]$ $\alpha_w = 2.9X_w/[(1 + 141.5X_w)^{0.635} + 5.925\ X_w]$ $\tau_A = (0.12445\alpha - 0.0162)$ $\qquad\qquad + (1.003 - 0.125\alpha)\ \exp[-\beta\ m_{air}(1.089\alpha$ $\qquad\qquad + 0.5123)]$ $X_o = U_3\ m_r$ $X_w = U_1\ m_r$ $m_{air} = m_r p/p_o$ $m_r = 35/[(1224\ \cos^2\theta_z) + 1]^{0.5}$	(182)	Davis and Hay model	[230]
$I_{DNI,DPP} = 950.2\ \{1 - \exp[-0.075\ (90^o - \theta_z)]\}$	(183)	Daneshyar-Paltridge-Proctor (DPP) model	[226]
$I_{DNI,Meinel} = I_{oN}\ 0.7^{m_{air}^{0.678}}$ $m_{air} = m_r p/p_o$ $m_r = 1/\cos\theta_z$	(184)	Meinel model	[226]
$I_{DNI,Laue} = I_{oN}\ [(1 - 0.14\ L)\ 0.7^{m_{air}^{0.678}} + 0.14\ L]$ $m_{air} = m_r p/p_o$ $m_r = 1/\cos\theta_z$	(185)	Laue model	[226]
$I_{DNI,Haw} = 1098\ \cos\theta_z\ \exp[-0.057/\cos\theta_z]$	(186)	Haurwitz model	[303]

Table 23: Continued

Equation		Description	
$I_{DNI,BD} = 0.70\ I_{oN}\cos\theta_z$	(187)	Berger and Duffie model	[303]
$I_{DNI,ABCG} = 951.39\ (\cos\theta_z)^{1.15}$	(188)	Adnot, Bourges, Campana and Gicquel model	[303]
$I_{DNI,KC} = 910\cos\theta_z - 30$	(189)	Kasten and Czeplak model	[303]
$I_{DNI,RS} = 1159.24\ \{(\cos\theta_z)^{1.179}\exp[-0.0019\ (90 - \theta_z)]\}$	(190)	Robledo and Soler model	[303]

Based on the above-mentioned description of parametric models, they can be classified: a simple group, and complex group. The simple models are developed by using the zenith angle in addition to a few atmospheric parameters such as temperature, pressure and relative humidity. Whereas, various input atmospheric parameters such as aerosols, ozone layer and perceptible water are included in models that account as a complex group. Table 24 is the summary of various astronomical and atmospheric parameters which were used to develop the models

Table 24: Summary of astronomical and atmospheric parameters

Equations		Parameters name	Parameters type	
$\cos\theta_z = \sin L\ \sin\theta_\delta + \cos L\ \cos\theta_\delta\ \cos\theta_h$	(191)	Solar zenith angle	Astronomical	[225]
$\theta_\delta = 23.45\sin[\dfrac{360}{365}(284 + N_j)]$	(192)	Declination angle	Astronomical	[225]
$\theta_h = 15^{\circ}(ST - 12)$	(193)	Solar angle	Astronomical	[225]

Table 24: Continued

Equations		Parameters name	Parameters type	
$ST = SDT + 4(L_{st} - L_{loc}) + E$ $E = 229.2(75 \times 10^{-6} + 186 \times 10^{-6} \sin B - 0.032207 \sin B - 0.014615 \sin 2B - 0.04089 \sin 2B)$ $B = (N_j - 1)\dfrac{360}{365}$	(194)	Solar time Time equation	Astronomical	[240]
$I_{oN} = I_o [1 + 0.033 \cos(\frac{360 N_j}{365})]$	(195)	Extraterrestrial radiation measured on the plane normal to the radiation	Astronomical	[225]
$m_e = \exp(-0.000118h - 1{,}638 \times 10^{-9}h^2) / \cos\theta_z$	(196)	Air mass corrected for elevation	Atmospheric	[240]
$m_r = \{[1229 + (614 \cos\theta_z)^2]^{0.5} - 614 \cos\theta_z\}$	(197)	A specific air mass	Atmospheric	[240]
$m_{air} = m_r p / p_o$	(198)	Air mass at actual pressure	Atmospheric	[302]
$m_r = 1/\cos\theta_z$	(199)	Air mass at standard pressure	Atmospheric	[302]
$m_{air,MIqbalC} = m_r \exp(-0.001184\ h)$	(200)	Actual air mass value depends on altitude and relative air mass at standard pressure	Atmospheric	[240]
$m_r = 35/[(1224 \cos^2\theta_z) + 1]^{0.5}$	(201)	Air mass at standard pressure	Atmospheric	[230]
$m_r = [\cos\theta_z + 0.15 (93.885 - \theta_z)^{-1.253}]^{-1}$	(202)	Air mass at standard pressure	Atmospheric	[240]

5.2.1.2 Cloud Cover Model (CRM)

In order to predict direct normal irradiance (DNI) under different sky conditions, the cloud-cover radiation model (CRM), which represents a regression-type model and described detailly in section 5.1, can be used. The performance of this model is evaluated

against the dataset extracted from a selected site. The first step toward determining DNI from the Kasten–Czeplak model (CRM) is to estimate the hourly global solar radiation on a horizontal surface under a cloudless sky. The obtained value is used along with cloud cover range (measured in Okats) to find the hourly global radiation on a horizontal surface under cloud cover condition. Several instruments (ground-based, satellite integrated) are utilized to determine the sky conditions Next, the hourly diffuse radiation is determined to obtain the value of hourly DNI, as described in the following formulas that are summarized in Table 25.

Table 25: Cloud-cover radiation model (CRM)

Equation		Description	
$I_{G_{cs}} = A \sin \theta_\alpha - B$ $\sin \theta_\alpha = \cos \theta_z = \sin L \sin \theta_\delta + \cos L \cos \theta_\delta \cos \theta_h$ $\theta_\delta = 23.45 \sin[\frac{360}{365}(284 + N_j)]$ $\sin \theta_h = \frac{\sin \theta_\alpha - \sin \theta_\delta \sin L}{\cos \theta_\delta \cos L}$ A, B: Empirical coefficients	(203)	Hourly global solar radiation on a horizontal surface under cloudless sky	[248]
$I_{G_{cc}} = I_{G_{cs}} [1 - C(\frac{N}{8})^D]$ N = cloud cover (Oktas); [0(clear sky) $\qquad\qquad - 8$ (completely overcast sky)] C, D: Empirical coefficients	(204)	Hourly global solar radiation on a horizontal surface under cloud cover condition	[247, 250]
$I_d = I_{G_{cc}} [0.3 - 0.7 (\frac{N}{8})^2]$	(205)	Hourly diffuse radiation on a horizontal surface	[248]
$I_{DNI,KC} = (I_{G_{cc}} - I_d)/ \cos \theta_z$	(206)	Direct normal irradiance (DNI) under different sky conditions	

5.2.1.3 A Hierarchical Calculation Methodology

Accordingly, the hourly direct normal irradiance under various sky conditions for different geographical locations can be estimated based on the previous equations, which may contribute to compensate for lack of the solar dataset for a certain site. It should be noted that the availability of DNI dataset is essential to the design and operation of concentrated solar power technologies including central receiver, linear Fresnel, dish sterling and parabolic trough collector. Particularly, if the expected contribution of these technologies in the total renewable energy production would be about 50.34% by 2030 [240]. The hierarchical methodology is summarized in Figure 26, which can be used to predict DNI values in this work through testing fit accuracy of the selected models using statistical indicators and high-quality measured datasets.
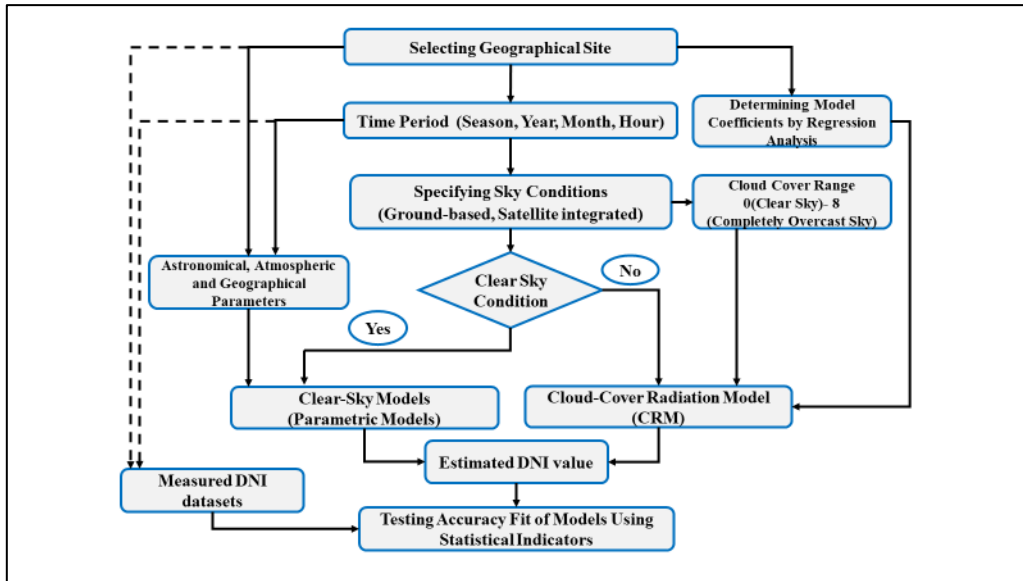
Figure 26*: A hierarchical methodology of predicting DNI*

5.2.2 Estimation of Monthly Average Hourly Direct Solar Irradiance from Daily Data

5.2.2.1 Daily Global Solar Radiation (Decomposition Models)

The decomposition models can be utilized to transform daily values (long-term data) of solar radiation into hourly values (short-term data). The two frequently used correlations for this purpose have been chosen. The Collares-Pereira and Rabl correlation represents the ratio of monthly average hourly global irradiance to monthly average daily global irradiance, whereas, the Liu and Jordan correlation represents the ratio of monthly average hourly diffuse irradiance to monthly average daily diffuse irradiance [225], as illustrated in Table 26.

Table 26: Two decomposition models

Equation		Description	
$r_t = \dfrac{\overline{I_G}}{\overline{H_G}}$ $= \dfrac{\pi}{24}\,(a + b\cos\theta_h)\left[\dfrac{\cos\theta_h - \cos\theta_{hs}}{\sin\theta_{hs} - \left(\dfrac{\pi\,\theta_{hs}}{180}\right)\cos\theta_{hs}}\right]$ $\theta_{hs} = \cos^{-1}[-\tan L \cdot \tan\theta_\delta]$ θ_h $= \pm 0.25\,(\text{number of minutes from local solar noon})$ $a = 0.4090 + 0.5016\sin(\theta_{hs} - 60)$ $b = 0.6609 - 0.4767\sin(\theta_{hs} - 60)$	(207)	Collares-Pereira and Rabl correlation (Ratio of monthly average hourly global irradiance to monthly average daily global irradiance)	[225]
$r_d = \dfrac{\overline{I_d}}{\overline{H_d}} = \dfrac{\pi}{24}\left[\dfrac{\cos\theta_h - \cos\theta_{hs}}{\sin\theta_{hs} - \left(\dfrac{\pi\,\theta_{hs}}{180}\right)\cos\theta_{hs}}\right]$	(208)	Liu and Jordan correlation (Ratio of monthly average hourly diffuse irradiance to monthly average daily diffuse irradiance)	[225]
$\overline{I}_{DNI,H} = \overline{I_G} - \overline{I_d}$	(209)	Monthly average hourly direct solar irradiance on a horizontal surface	
$\overline{I}_{DNI} = \overline{I}_{DNI,H}/\cos\theta_z$	(210)	Monthly average hourly direct solar irradiance	

5.2.2.2 Angstrom-Prescott Correlation

A number of formulations (linear and non-linear) of the Angstrom-Prescott correlation were selected for the estimation of the monthly average daily global solar radiation on a horizontal surface using clearness index against sunshine fraction, ambient temperature, relative humidity, precipitation, cloud cover, and multi-parameters. Four of regression equations have been utilized that developed by modifying the Angstrom--Prescott correlation as given in Table 27.

Table 27: Regression equations of Angstrom-Prescott model

Equation		Description	
$\dfrac{\overline{H_G}}{\overline{H_o}} = a + b\,\dfrac{\overline{S}}{\overline{S_o}}$	(211)	Linear model	[276]
$\dfrac{\overline{H_G}}{\overline{H_o}} = a + b\,\dfrac{\overline{S}}{\overline{S_o}} + c\,(\dfrac{\overline{S}}{\overline{S_o}})^2$	(212)	Quadratic model	[265]
$\dfrac{\overline{H_G}}{\overline{H_o}} = a + b\,\dfrac{\overline{S}}{\overline{S_o}} + c\,T + d\,R$	(213)	Multi-parameters model	[265]
$\dfrac{\overline{H_G}}{\overline{H_o}} = a + b\cos L + c\,H + d\,\dfrac{\overline{S}}{\overline{S_o}} + e\,T + f\,R$	(214)	Gopinathan's model	[290]
$\overline{K_T} = \dfrac{\overline{H}}{\overline{H_o}}$	(215)	Monthly mean clearness index	[225]
$H_o = \dfrac{24}{\pi}\,H_{sc}\,[1 + 0.033\cos(\dfrac{360N_j}{365})]\,[\cos L\,\cos\theta_\delta\,\sin\theta_{hs} + \dfrac{\pi}{180}\,\theta_{hs}\sin L\,\sin\theta_\delta$	(216)	Monthly average daily extraterrestrial solar irradiance on a horizontal surface	[225]
$S_o = 2\,\theta_{hs}/15$	(217)	Maximum possible monthly average daily length (hr)	[225]

5.2.2.3 Empirical Models

Decomposition models have been developed to estimate hourly global and diffuse irradiance that have an essential role in solar energy engineering applications. Such models are formulated based on the correlations between the diffuse fraction, cleanness index, and sunshine fraction. Four representative models have been selected which are expressed as the ratio of diffuse to global irradiance on a horizontal surface. These are described as in Table 28.

Table 28: Summary of empirical models

Equation		Description	
$\dfrac{\overline{H_d}}{\overline{H_G}} = 1.39 - 4.027\,(\dfrac{\overline{H_G}}{H_o}) + 5.5310\,(\dfrac{\overline{H_G}}{H_o})^2 \\ \qquad\qquad - 3.108\,(\dfrac{\overline{H_G}}{H_o})^3$	(218)	Liu and Jordan model	[298]
$\dfrac{\overline{H_d}}{\overline{H_G}} = 1.2547 - 1.2547\,(\dfrac{\overline{S}}{\overline{S_o}})$	(219)	Iqbal model	[298]
$\dfrac{\overline{H_d}}{\overline{H_G}} = 1.194 - 0.838\left(\dfrac{\overline{H_G}}{H_o}\right) - 0.0446\,(\dfrac{\overline{S}}{\overline{S_o}})$	(220)	Gopinathan model	[298]
$\dfrac{\overline{H_d}}{\overline{H_G}} = 0.775 + 0.00606\,(\theta_{hs} - 90) \\ \qquad - [0.505 \\ \qquad + 0.00455\,(\theta_{hs} \\ \qquad - 90)]\cos\,(115\left(\dfrac{\overline{H_G}}{H_o}\right) - 103)$	(221)	Collares-Pereira and Rabl	[225]

5.2.2.3 A Hierarchical Calculation Methodology

The implementation of calculating monthly average hourly direct solar irradiance from daily data requires using a hierarchical calculation methodology that consists of multiple sequences steps as described in Figure 27. The first step in a proposed approach

is to estimate geographical and astronomical parameters $(L, \theta_\delta, \theta_{hs}, T, R, H)$ based on a selected site and period of time through using equations 203,207. In order to estimate monthly average daily global irradiance on a horizontal surface ($\overline{H_G}$) from equations of Table 27 and monthly average daily diffuse ($\overline{H_d}$) on a horizontal surface from equations of Table 28, the estimated values of monthly average daily extraterrestrial irradiance H_o (from Equation 216) and maximum possible monthly average daily length S_o (from Equation 217) should be determined. Next, the obtained daily irradiance data can be transformed to the hourly irradiance data by utilizing Equation 207 to estimate the value of monthly average hourly global irradiance on a horizontal surface ($\overline{I_G}$), and Equation 208 to estimate monthly average hourly diffuse irradiance on a horizontal surface ($\overline{I_d}$). Once, the values of ($\overline{I_G}$) and ($\overline{I_d}$) are obtained, monthly average hourly direct solar irradiance ($\overline{I_{DNI}}$) can be estimated from Equations 209 and 210. Eventually, to demonstrate the capability of the proposed methodology and used equations, the statistical indicators can be utilized for comparing estimated irradiance values with measured irradiance datasets.
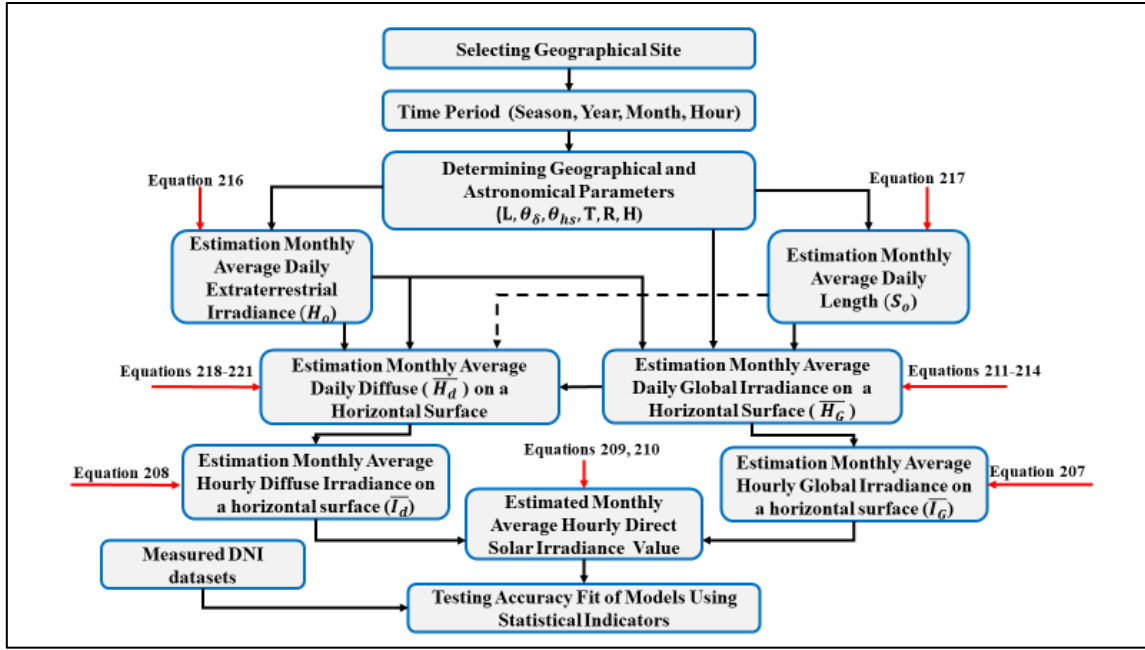
Figure 27*:* A hierarchical methodology of predicting monthly average hourly direct solar irradiance

5.3 Site Description and Data Collection

In order to demonstrate validation of proposed methodologies and selected models to estimate reliable and high-quality solar radiation data for different sites in Texas or other locations around the world, San Antonio city (29.42° N, 98.49° W) has been chosen as a case study as depicted in Figure 28. The solar data for San Antonio is obtained from the National Solar Radiation Data Base (NSRDB) between 1991-2010 are: hourly global solar irradiance, hourly direct solar irradiance, hourly diffuse solar irradiance, hourly solar incidence angle, hourly dry bulk temperature, hourly wet bulk temperature, and relative humidity.

Figure 28: The location map of a case study in Texas

5.4 Statistical Methods of Model Evaluation

The performance of proposed methodologies and selected models have been tested through comparison between their estimated data and measured data by using various statistical indicators. For this purpose, five statistical indicators have been applied including Mean Bias Error (MBE), Root Mean Square Error (RMSE), Absolute Percent Error (MAPE), Coefficient of Determination (R^2), t statistic method (t_{stat}), and the percentage error (e %), as given in Table 29.

Table 29: Statistical indicators

Equation		Description
$\text{MBE} = \dfrac{\sum_{i=1}^{n}(I_{cal} - I_{meas})}{n}$	(222)	Mean Bias Error
$\text{RMSE} = \sqrt{\dfrac{\sum_{i=1}^{n}(I_{cal} - I_{meas})^2}{n}}$	(223)	Root Mean Square Error
$\text{MPAPE} = \dfrac{100}{n} \sum_{i=1}^{n} \dfrac{(I_{cal} - I_{meas})}{I_{meas}}$	(224)	Absolute Percent Error
$R^2 = 1 - \dfrac{\sum_{i=1}^{n}(I_{cal} - I_{meas})^2}{\sum_{i=1}^{n}(I_{meas} - I_{meas,avg})^2}$	(225)	Coefficient of Determination
$t_{stat} = [\dfrac{(n-1)\text{MBE}^2}{\text{RMSE}^2 - \text{MBE}^2}]^{1/2}$	(226)	t statistic method
$e\% = \dfrac{I_{cal} - I_{meas}}{I_{meas}}$	(227)	percentage error

5.5 Results and Discussion

In this study, the monthly average daily global irradiance data on a horizontal surface, which were measured in San Antonio, Texas during the time period 1991-2010, has been analyzed to calculate the monthly average clearness index ($\overline{K_T}$). This index is the ratio between monthly average daily total radiation on a terrestrial horizontal surface ($\overline{H}$) and monthly average daily total radiation on an extraterrestrial horizontal surface ($\overline{H_o}$), as defined in Equation 215 . The comparison between the obtained values from calculating ($\overline{K_T}$) in the time interval 1991-2010 and the values of ($\overline{K_T}$) that provided by Solar Energy Information Data Bank (SEIDB) [219] in the time interval 1952-1975 has been carried out and its result has shown a responsible agreement, as shown in Figure 29. Similarly, the

monthly average hourly clearness index (k_t) values have been calculated and reported in Table 30, which is the ratio of the global solar irradiance on a horizontal surface (I) to the hourly extraterrestrial solar irradiance on a horizontal surface (I_o), as given in Equation 228.

$$k_t = \frac{I}{I_o} \tag{228}$$
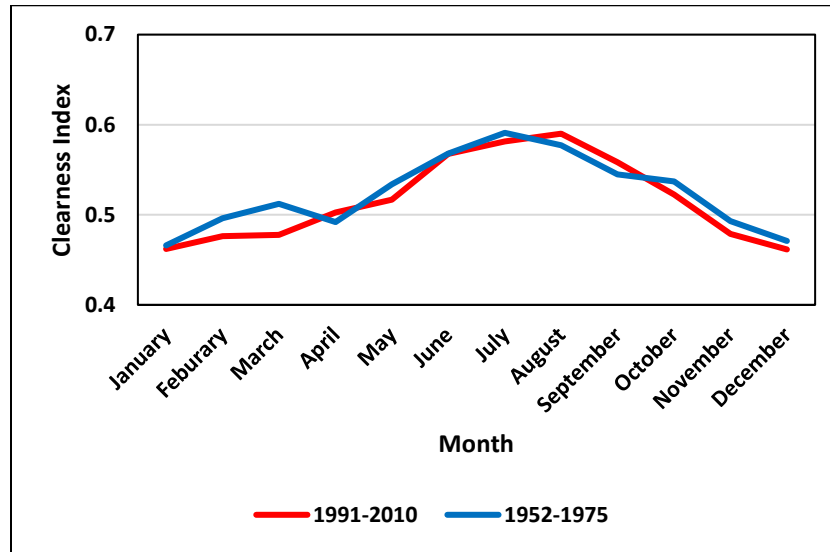
Figure 29:Monthly average clearness index

The daily clearness index can be utilized to partition days throughout the year according to the sky condition (Sunny, partly cloudy and cloudy) that dominates transmission of the extraterrestrial irradiance to the earth surface in the chosen site, as shown in Figure 30.
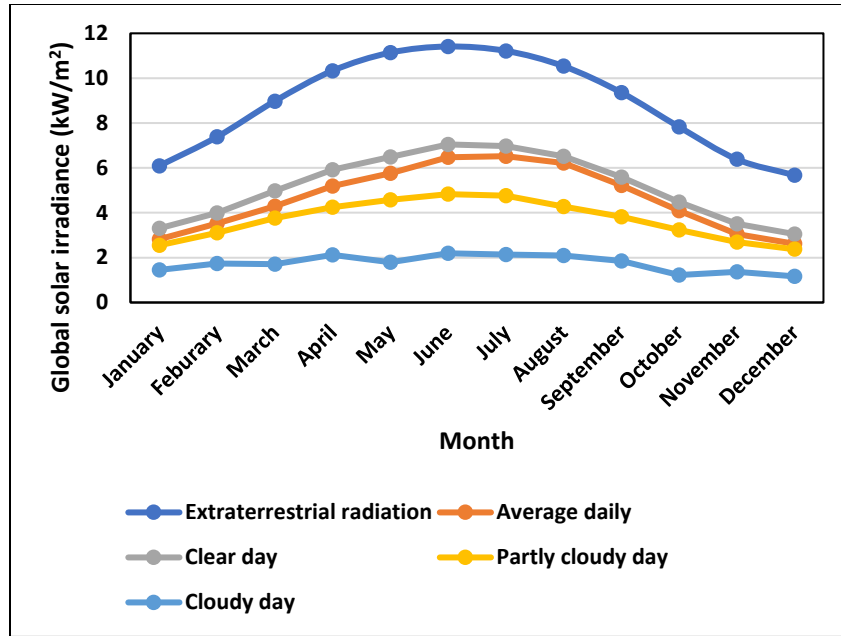
Figure 30 : Monthly average daily global radiation according to the sky condition

In addition, the solar irradiance may be subjected to the atmospheric attenuation (absorption, diffusion) during passing through the earth atmosphere due to air pollution, cloudy conditions, and other influencing parameters. Therefore, the hourly clearness index (k_t), which is considered as a stochastic parameter because it is a function of a period of year, seasons, climatic conditions and geographic site, can be used to predict the influence of these parameters by calculating the average daily sunshine (bright) hours based on the classification of clearness index level, as follows,

Cloudy   : $k_t < 0.3$

Partly cloudy   : $0.3 \leq k_t \leq 0.5$

Sunny   : $k_t > 0.5$

152

Table 30: Monthly average hourly and daily values for the clearness index

Month	Hour														Daily
	7	8	9	10	11	12	13	14	15	16	17	18	19	20	
January			0.23	0.34	0.40	0.45	0.48	0.50	0.50	0.49	0.47	0.42	0.32		0.462
February			0.24	0.34	0.41	0.45	0.48	0.51	0.52	0.52	0.50	0.46	0.37		0.476
March			0.03	0.23	0.34	0.40	0.46	0.50	0.52	0.54	0.55	0.55	0.50	0.42	0.478
April		0.16	0.29	0.37	0.44	0.49	0.53	0.55	0.58	0.58	0.57	0.54	0.46	0.33	0.502
May		0.02	0.21	0.31	0.40	0.46	0.50	0.54	0.57	0.59	0.60	0.60	0.58	0.51	0.517
June	0.05	0.24	0.33	0.45	0.51	0.57	0.61	0.65	0.65	0.65	0.64	0.62	0.56	0.44	0.568
July	0.01	0.23	0.34	0.46	0.54	0.59	0.61	0.65	0.65	0.65	0.65	0.61	0.56	0.44	0.582
August		0.20	0.36	0.49	0.57	0.61	0.63	0.64	0.66	0.64	0.64	0.61	0.53	0.39	0.590
September		0.14	0.33	0.45	0.51	0.57	0.59	0.62	0.62	0.62	0.61	0.56	0.46		0.558
October			0.27	0.39	0.47	0.52	0.56	0.58	0.59	0.60	0.57	0.50	0.37		0.522
November			0.21	0.34	0.42	0.48	0.51	0.54	0.54	0.54	0.50	0.43	0.30		0.479
December			0.13	0.31	0.40	0.45	0.49	0.51	0.52	0.51	0.49	0.42	0.29		0.462

The analysis of the monthly-average hourly clearness index through the classification of the clearness index level shows that more than 80% of the days can be defined as either sunny or partly cloudy and less than 20% of the days are classified as cloudy. It has been also noted that the individual monthly sky conditions percentage of sunny daytime hours exceed 40% from April through September, while the percentage of cloudy daytime hours do not exceed about 20%, as shown in Figure 31.
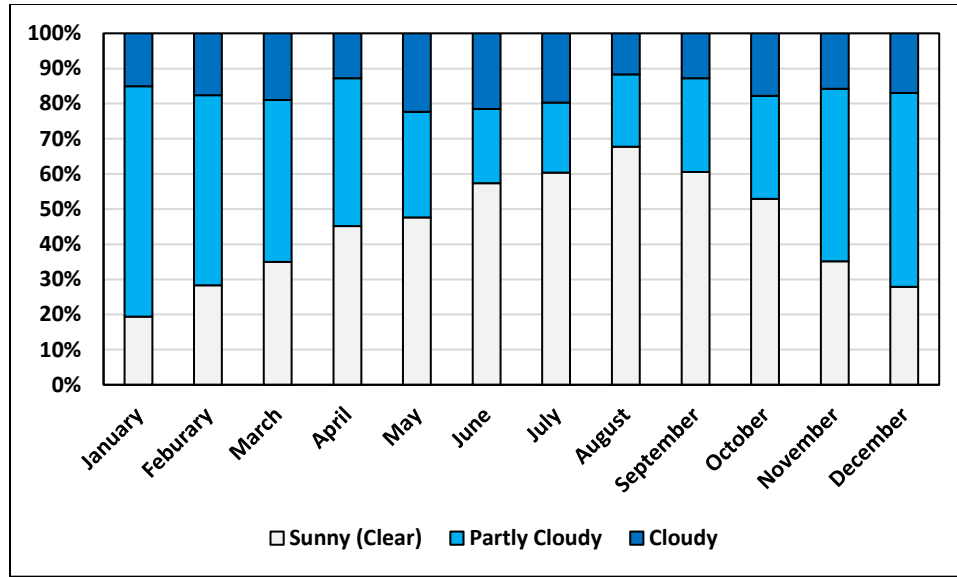
Figure 31: Monthly sky conditions of San Antione, Texas during daytime hours

It is apparent from the above-mentioned comprehensive analysis of the irradiance data and the clearness index, the selected region is characterized by a relatively high value of the monthly average percentage for sunny and partly cloudy days, which can be more than 80% throughout the year. Furthermore, the monthly average percentage of sunny daytime hours exceeds more than 50% in the interval time June-October along with a relatively high ($k_t > 0.5$). Consequently, the San Antonio region in Texas is unequivocally amenable to harnessing solar energy as the prime source of energy by utilizing concentrating and non-concentrating solar energy systems.

In addition to collecting the measured solar irradiance data for the implementation of the proposed methodologies and models, the average daily sunshine hour, average daily length of sunshine hours, ambient temperature and relative humidity are also essential for this purpose, as given in Table 31.

Table 31: Ambient temperature, relative humidity and daily sunshine ratio for San Antonio region

Month	T($^\circ$K)	RH%	$\dfrac{\bar{S}}{S_o}$
January	16	62	0.194
February	18.7	60	0.283
March	23.1	54	0.349
April	26.8	54	0.451
May	29.6	57	0.476
June	33.2	54	0.573
July	35	50	0.603
August	35.2	49	0.676
September	31.8	53	0.605
October	27.6	53	0.528
November	22.2	54	0.351
December	17.5	59	0.278

The performance of the selected parametric models (22 models) has been tested by comparing its estimations with measured data. The obtained results from implementing the clear-sky models on specific days for 12 months are visualized in Figures 32-43. it can be seen that the estimated values of hourly direct normal irradiance for most models are in favorable agreement with the measured values for all the months of the year. However, the accuracy and quality evaluation of models' performance require statistical tests for selecting the most precise models under the San Antonio climate conditions.
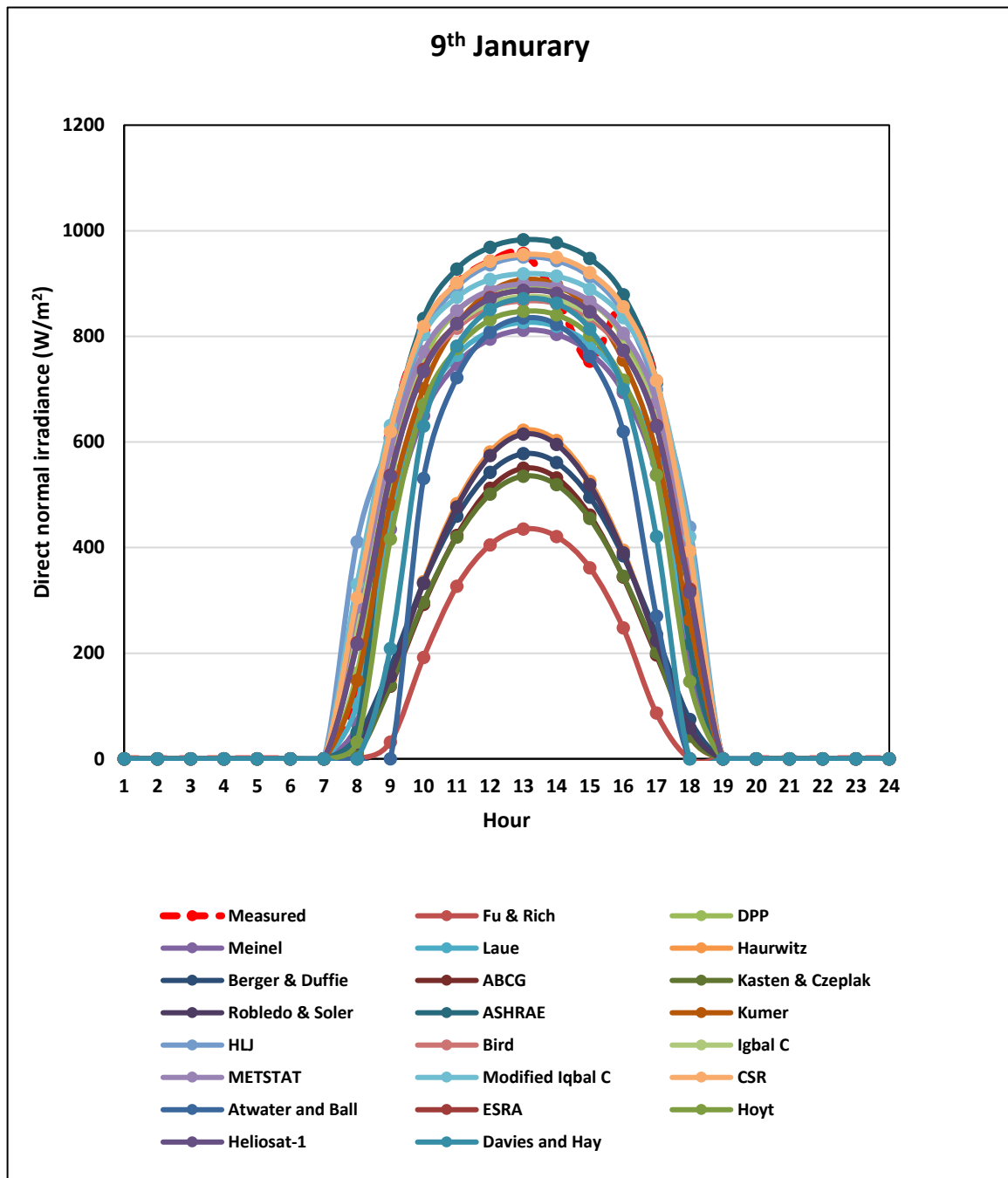
Figure 32: Measured and estimated DNI by 22 models for January
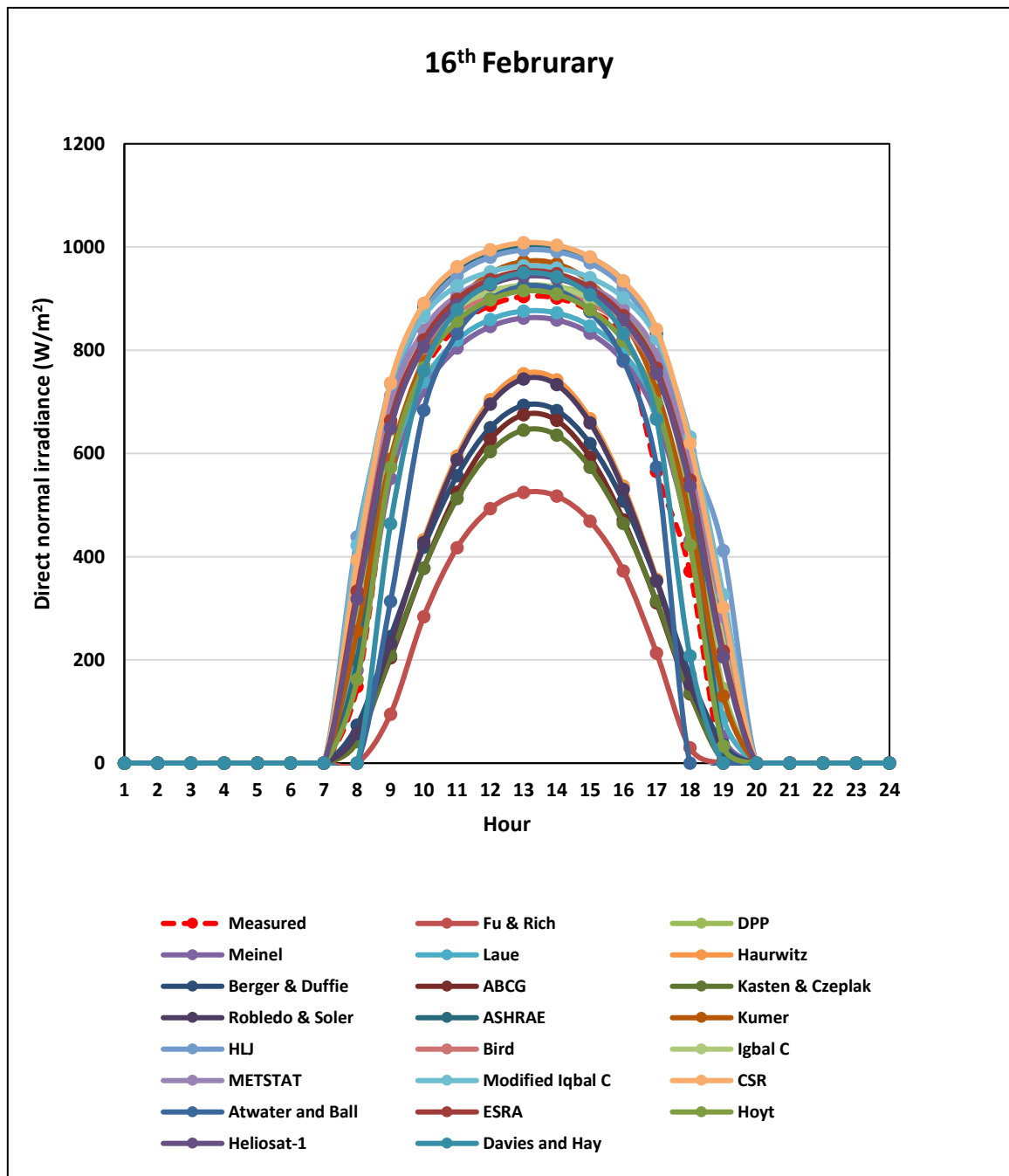
Figure 33*:* Measured and estimated DNI by 22 models for February
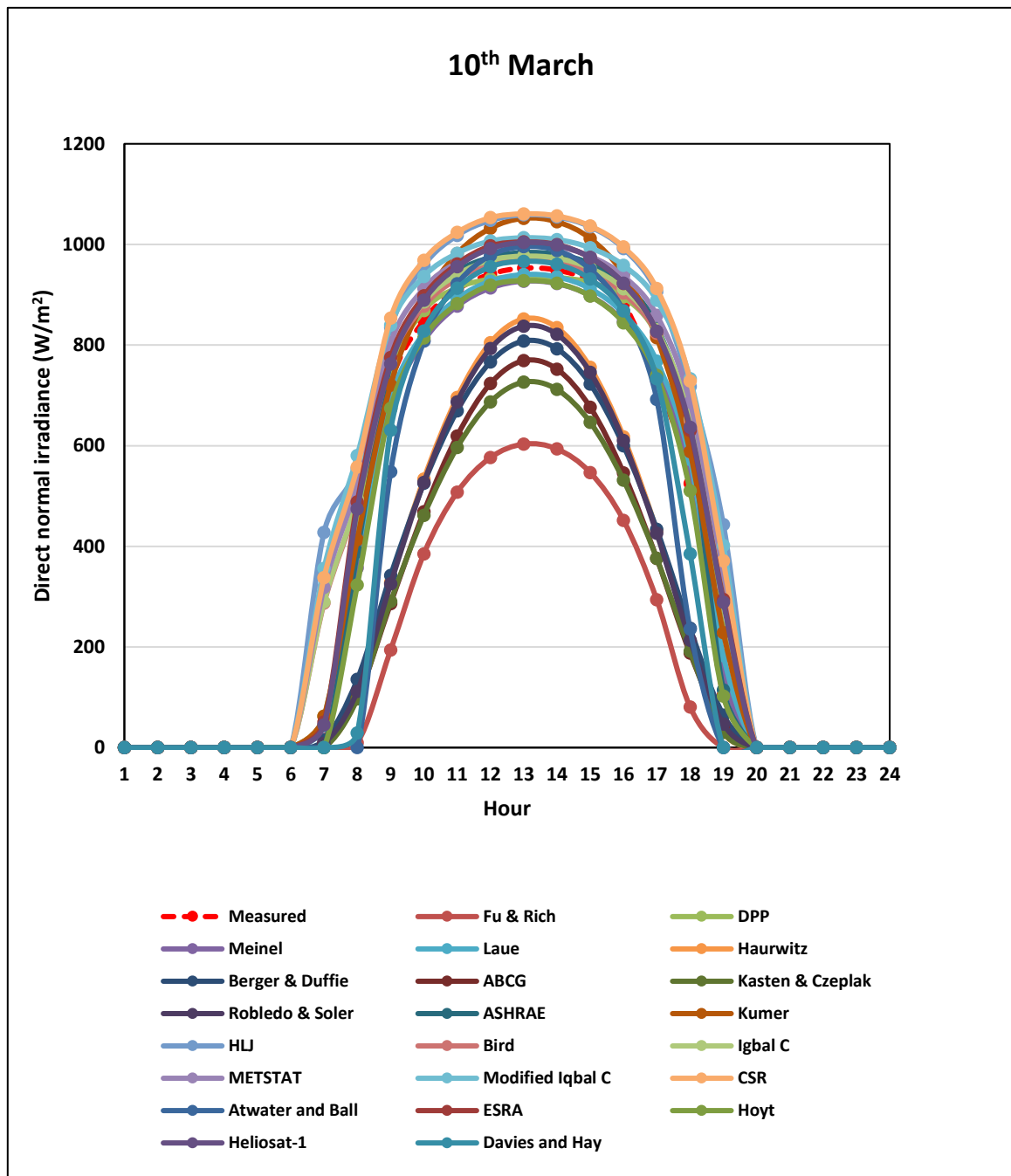
Figure 34*:* Measured and estimated DNI by 22 models for March
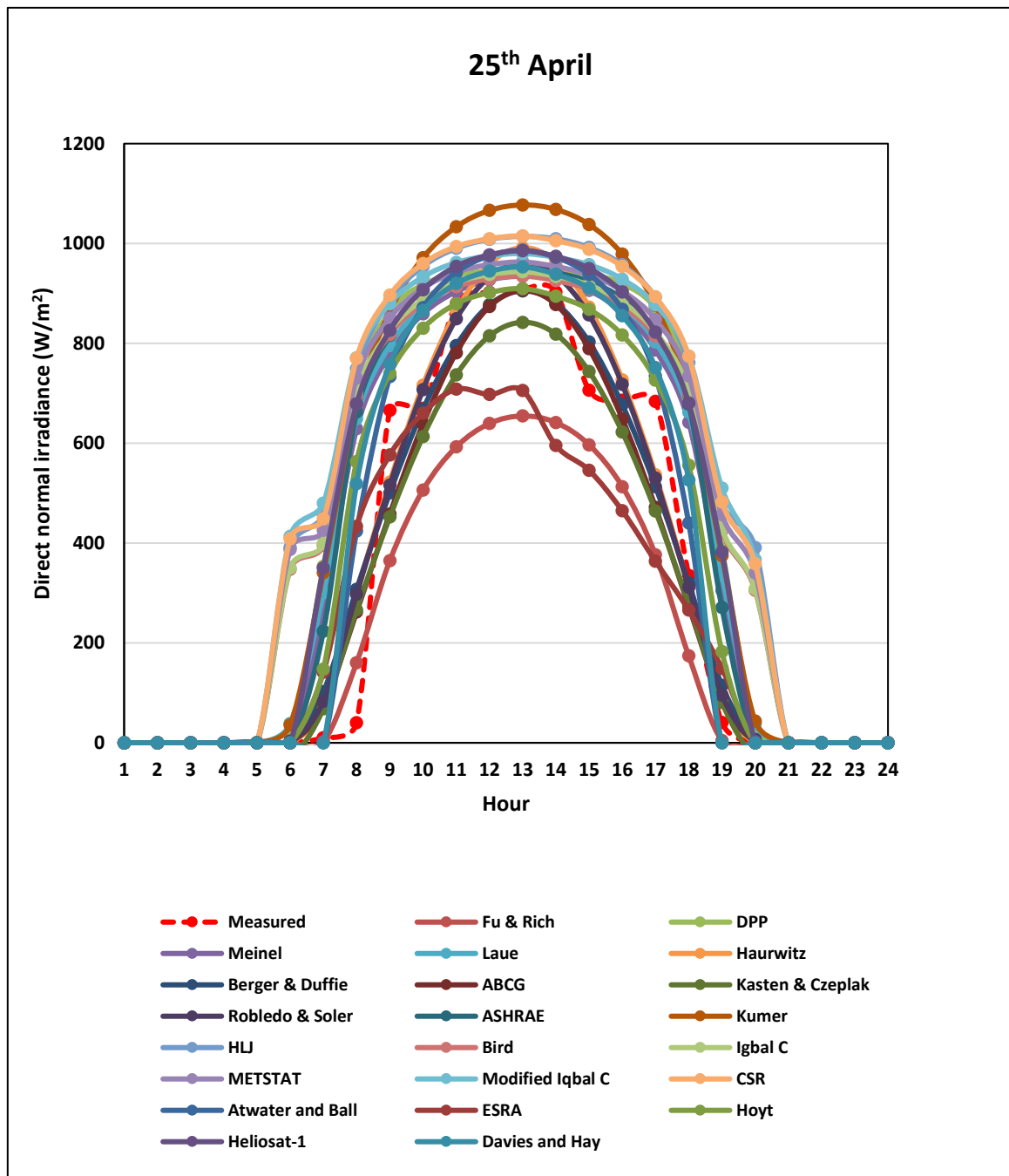
Figure 35: Measured and estimated DNI by 22 models for April
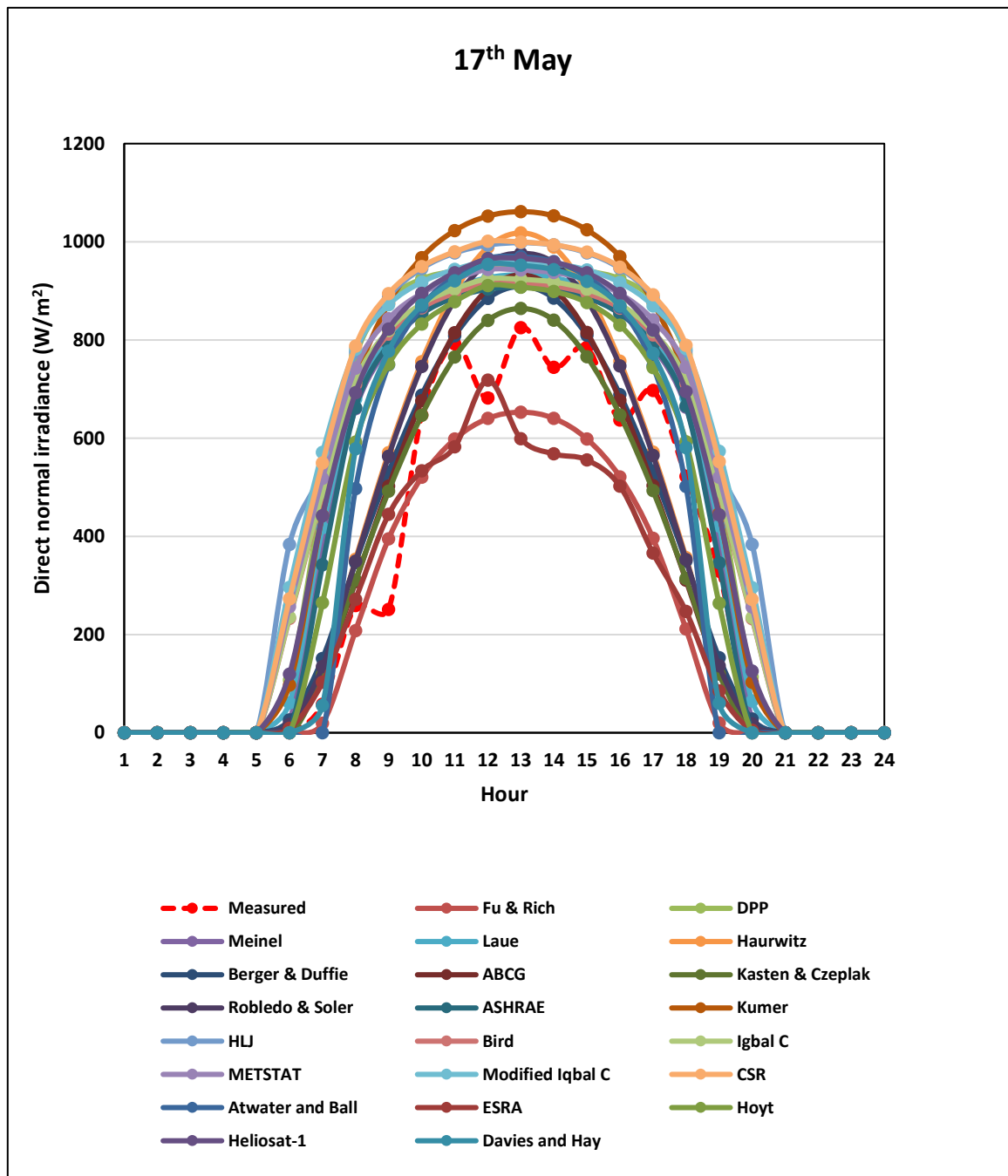
Figure 36: Measured and estimated DNI by 22 models for May
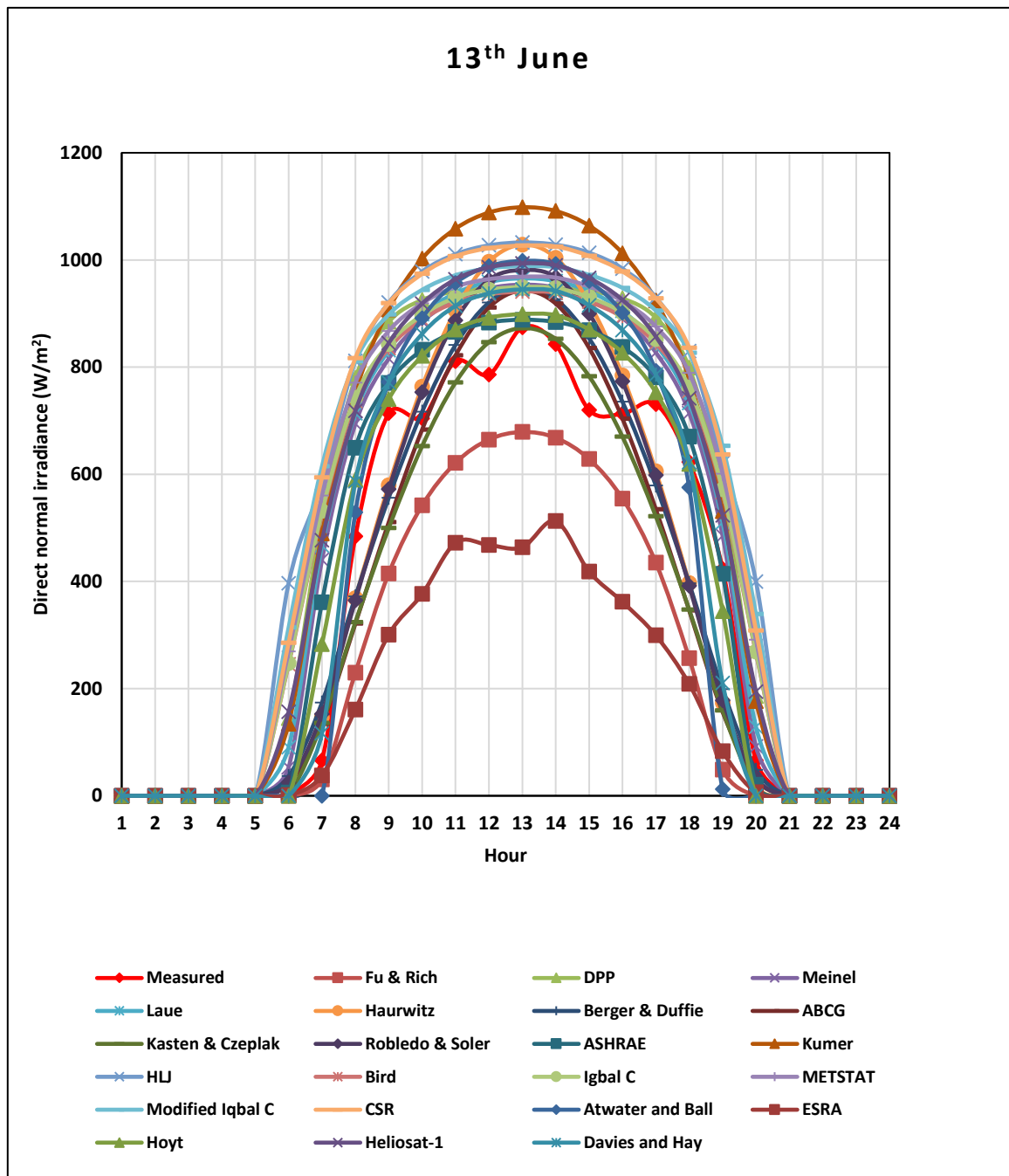
Figure 37: Measured and estimated DNI by 22 models for June
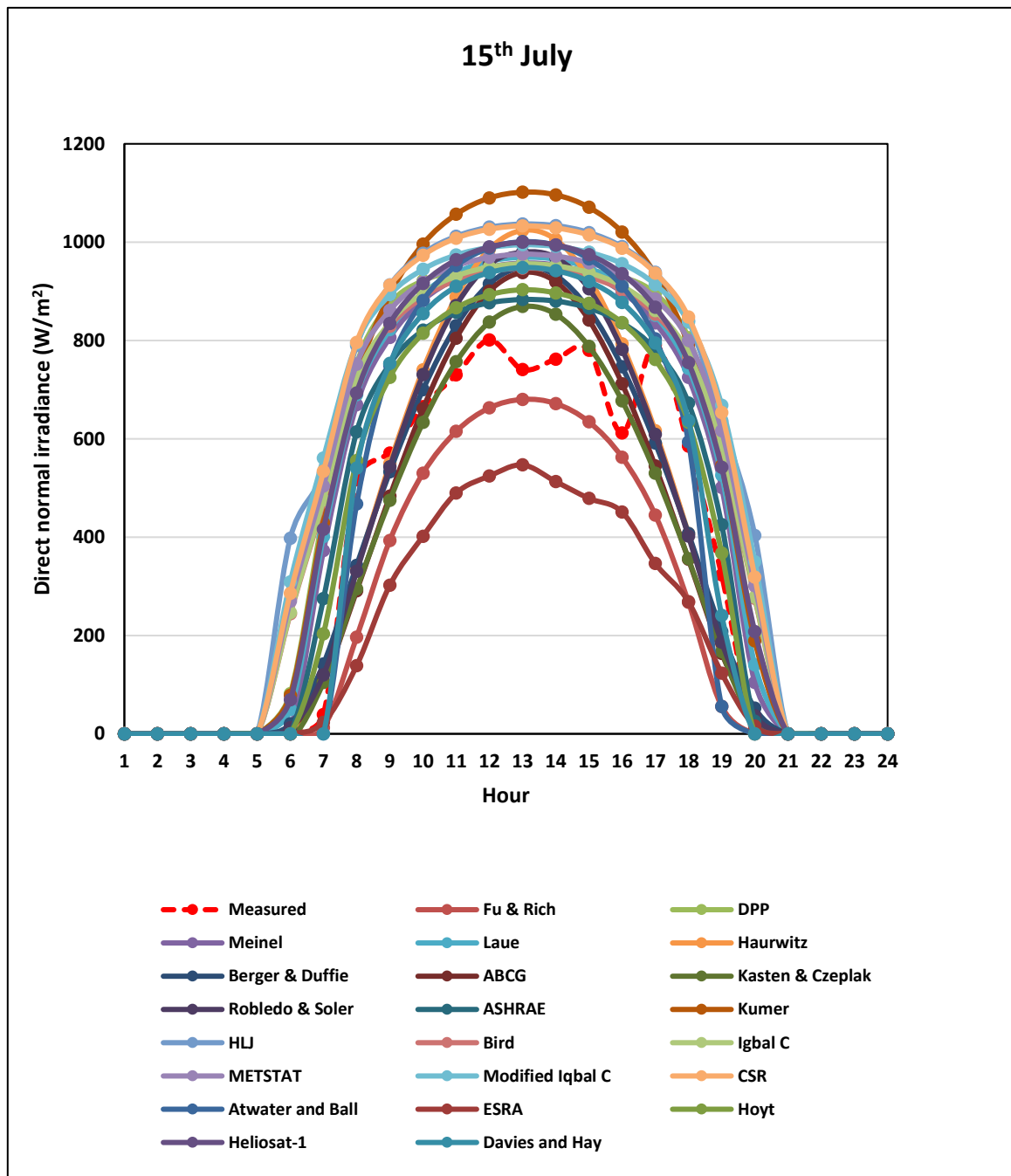
Figure 38*:* Measured and estimated DNI by 22 models for July
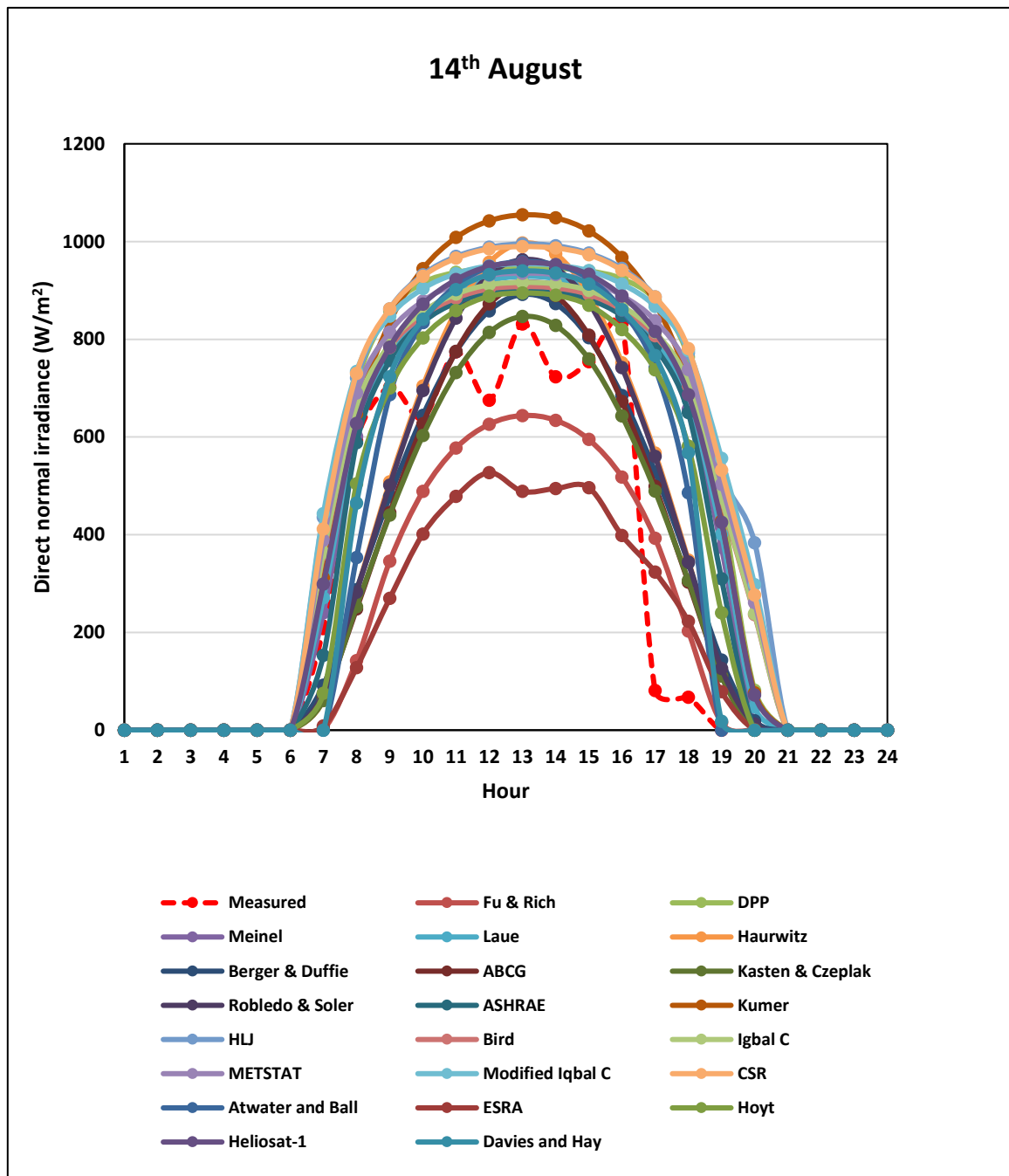
Figure 39*:* Measured and estimated DNI by 22 models for August
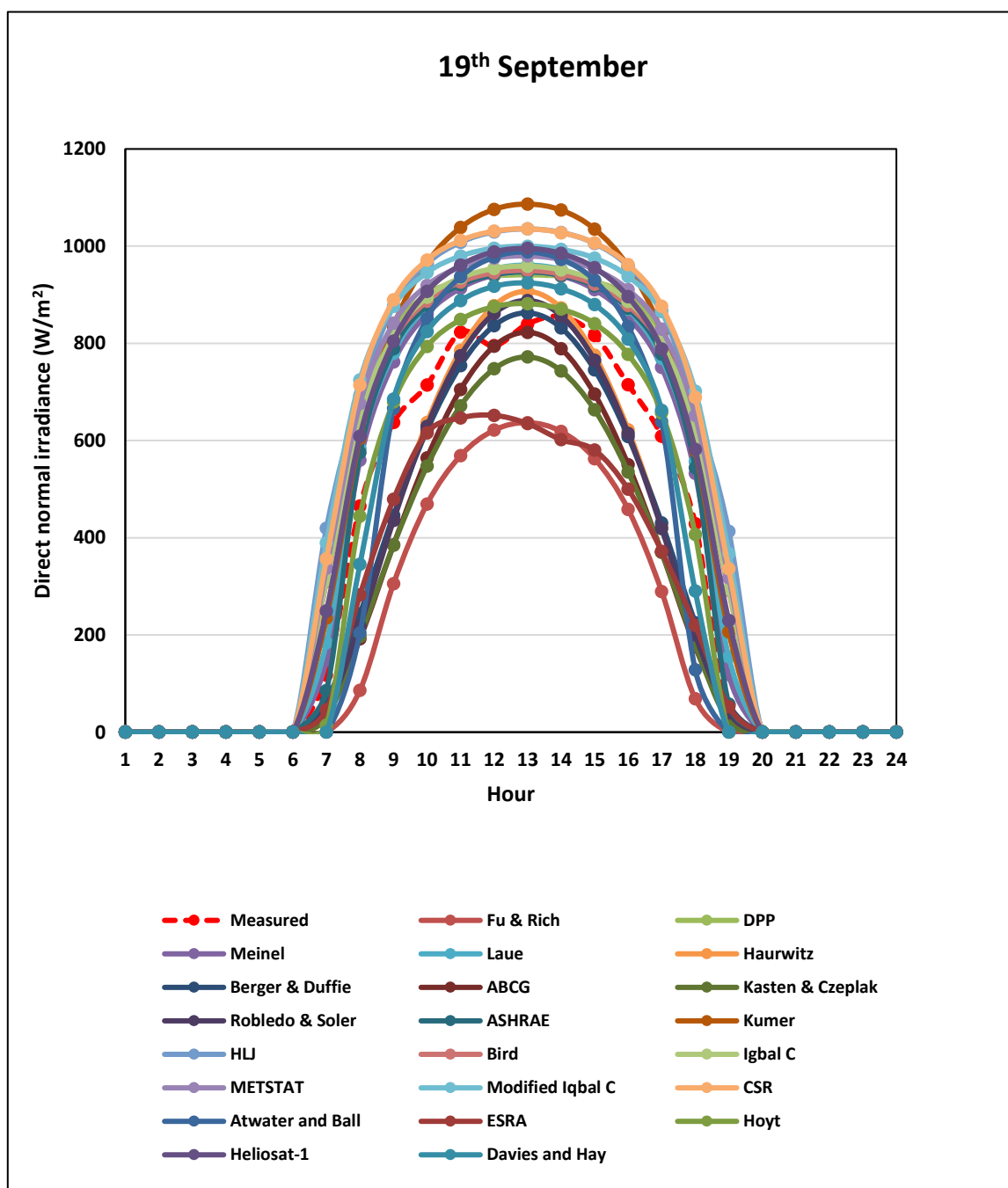
Figure 40*:* Measured and estimated DNI by 22 models for September
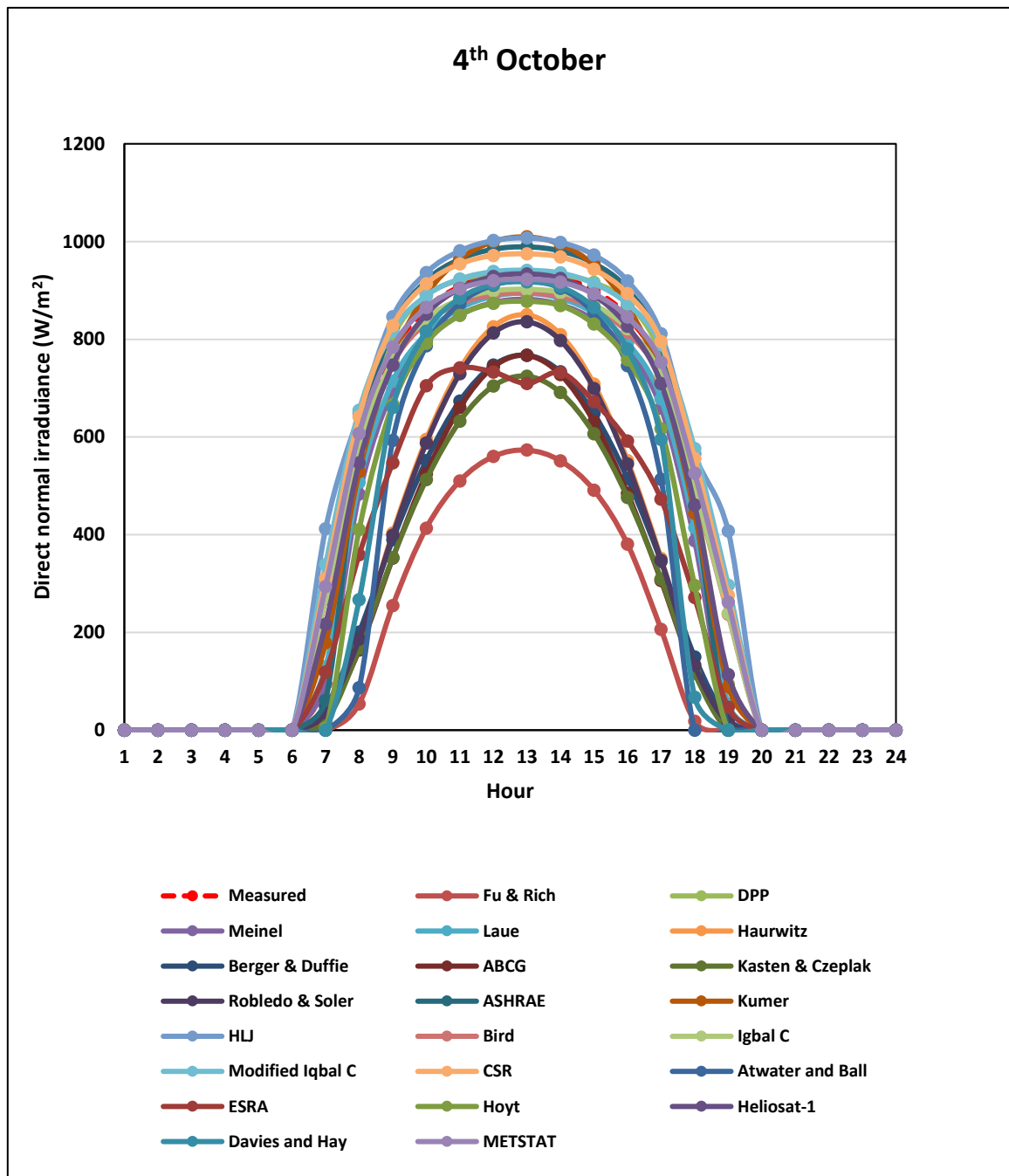
Figure 41*:* Measured and estimated DNI by 22 models for October
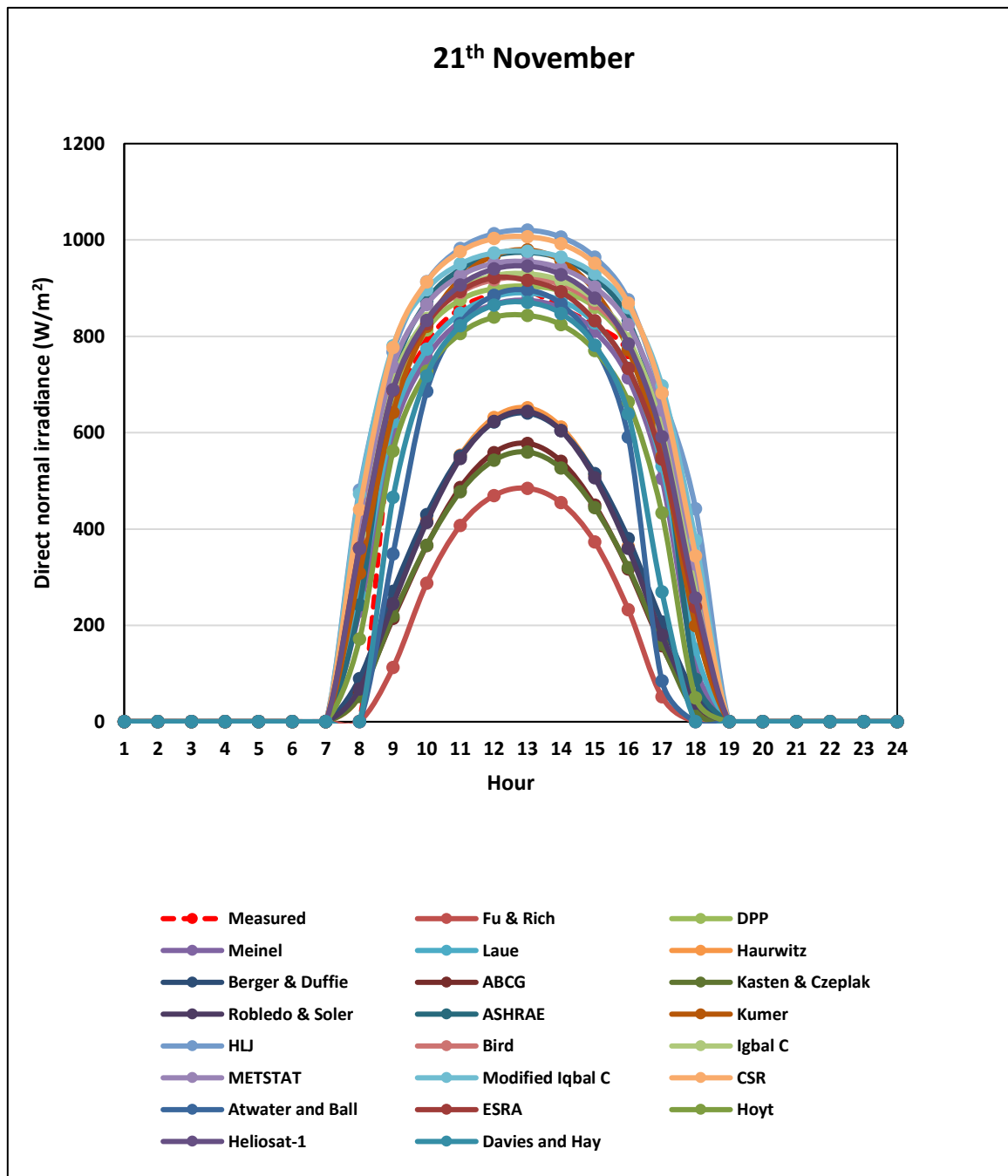
Figure 42*:* Measured and estimated DNI by 22 models for November
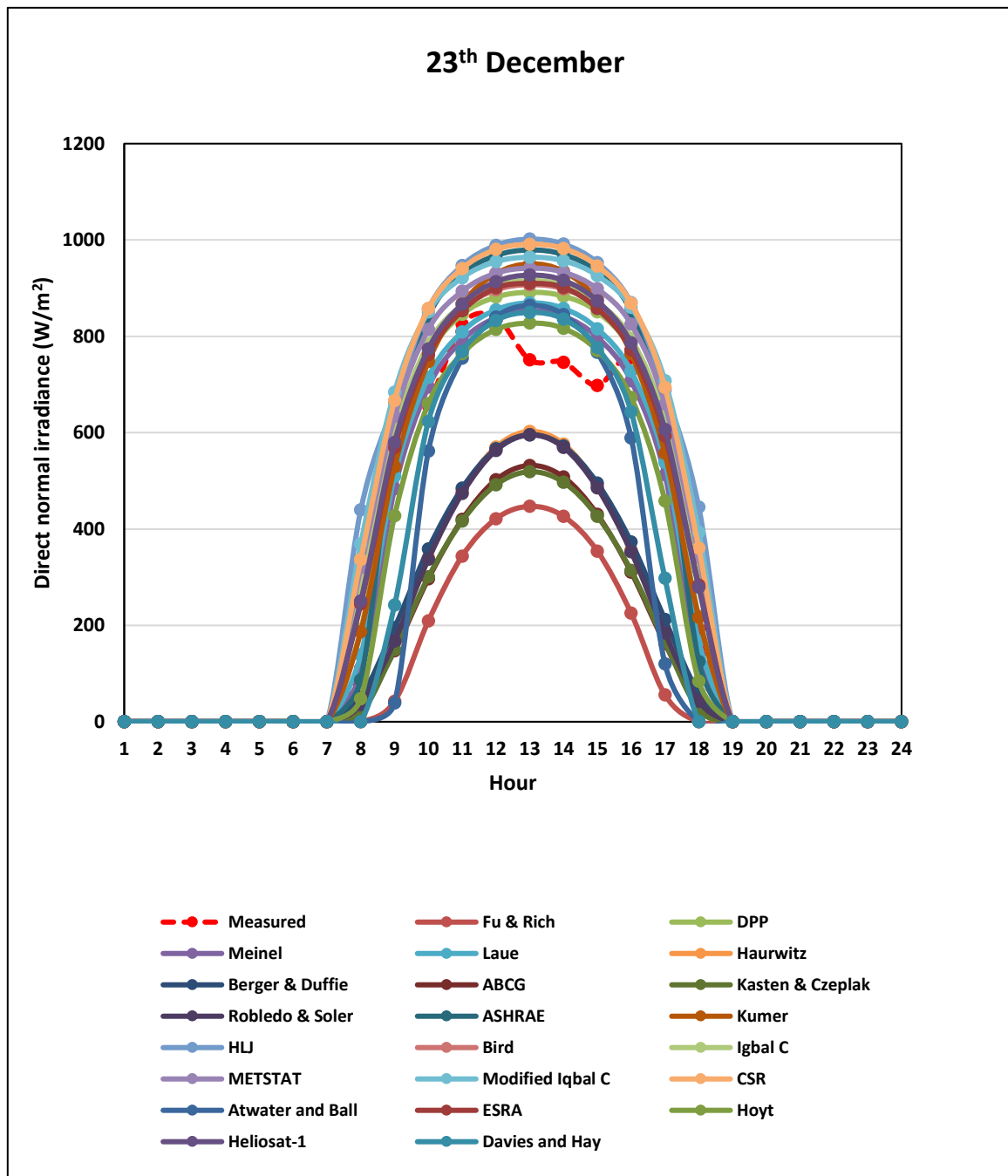
Figure 43*: Measured and estimated DNI by 22 models for December*

The results of testing the performance of 22 parametric models through using statistical indicators have been tabulated in Appendix C. In addition to more complicated models that consist of a large number of atmospheric parameters such as Davies-Hay, Hoyt (Iqbal B) models, some simpler models like Meinel and Laue have shown a good fit accuracy for all months during the year. Also, the models can be classified into two groups based on their performance during the months of summer and winter seasons. The first group, which includes simple models with a few parameters (less than three geographic and astronomical parameters) such as Meinel, Laue, Haurwitz, Berger-Duffie, ABCG, Kasten-Czeplak, Robledo- Sole, ASHRAE, Kumer and HLJ, can provide relatively accurate DNI values. While the second group, which comprises more sophisticated (complex) models such as Bird, Iqbal C, METSTAT, Modified Iqbal C, CSR, Atwater-Ball, ESRA, Hoyt (Iqbal B), Heliosat-1, Davies-Hay and Iqbal A models, have shown more accuracy in estimating DNI values during winter months (October-March) than summer months (April-September). Thus, precise values of DNI that are essential for selecting a proper location to install solar energy conversion systems and calculating the harvested amount of solar irradiance on the earth surface may be estimated using simpler parametric models.

The impact of cloud amount on the estimation of solar irradiance on a specific month (November is chosen as a study paradigm) under the climate conditions of San Antonio, Texas has been studied by using the cloud-cover radiation model (CRM). The cloud amount utilized in this model is evaluated in oktas, ranging from 0 to 8, and the regression coefficients of the model have been obtained from [252]. It can be observed the

168

significant influence of cloud amount on reducing the intensity of global solar irradiation as shown in Figure 44, specifically DNI, whereas the amount of diffuse irradiance increases in the atmosphere until reaching zero under an overcast sky.
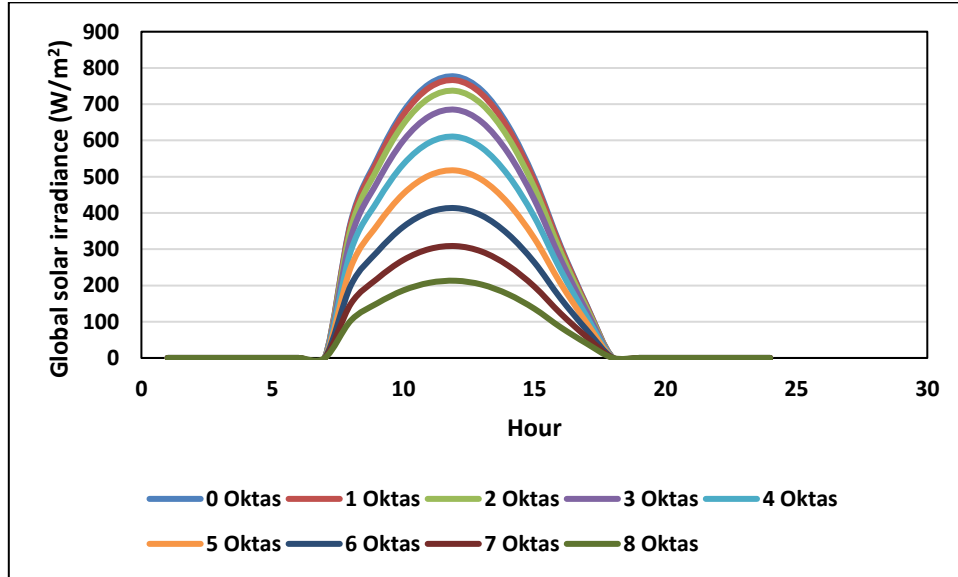
Figure 44: The impact of cloud cover on solar irradiance

To elucidate the capability of the hierarchical calculation methodology proposed in section 5.2.2.3 for estimating DNI precisely, four formulations of the Angstrom-Prescott correlation were developed through regression analysis to determine their coefficients as shown in Table 32. The correlations accuracy has been tested by comparing the estimated values of the monthly average daily global solar radiation on a horizontal surface with measured data (which represents monthly average daily solar radiation for thirty-year in San Antonio, Texas offering by [304], [305], the National Solar Radiation Data Base (NSRDB), and Solar Energy Information Data Bank (SEIDB) [219] using

statistical indicators, as given in Table 32. It is obvious from Figures 45-49 that the estimated values obtaining from correlations show a good agreement with measured data form different sources.

Table 32: Regression coefficients and statistical indictors of correlations

Equation	Description	MBE	RMSE	MAPE	e %	R2
$\frac{\overline{H_G}}{\overline{H_o}} = 0.3841 + 0.2946 \frac{\overline{S}}{\overline{S_o}}$	Linear model	-0.11	0.17	-3.4	3.7	0.98
$\frac{\overline{H_G}}{\overline{H_o}} = 0.4656 - 0.1235 \frac{\overline{S}}{\overline{S_o}} + 0.4767 \left(\frac{\overline{S}}{\overline{S_o}}\right)^2$	Quadratic model	-0.11	0.18	-3.3	4.2	0.98
$\frac{\overline{H_G}}{\overline{H_o}} = 0.235 + 0.179 \frac{\overline{S}}{\overline{S_o}} + 0.0036\, T + 0.0019\, R$	Multi-parameters model	-0.10	0.17	-3.4	3.8	0.98
$\frac{\overline{H_G}}{\overline{H_o}} = 0.801 - 0.378 \cos L + 0.0128\, H + 0.316 \frac{\overline{S}}{\overline{S_o}} - 1.214 \times 10^{-3}\, T - 1.049 \times 10^{-3} R$	Gopinathan's model	-0.02	0.14	-1.4	2.8	0.99
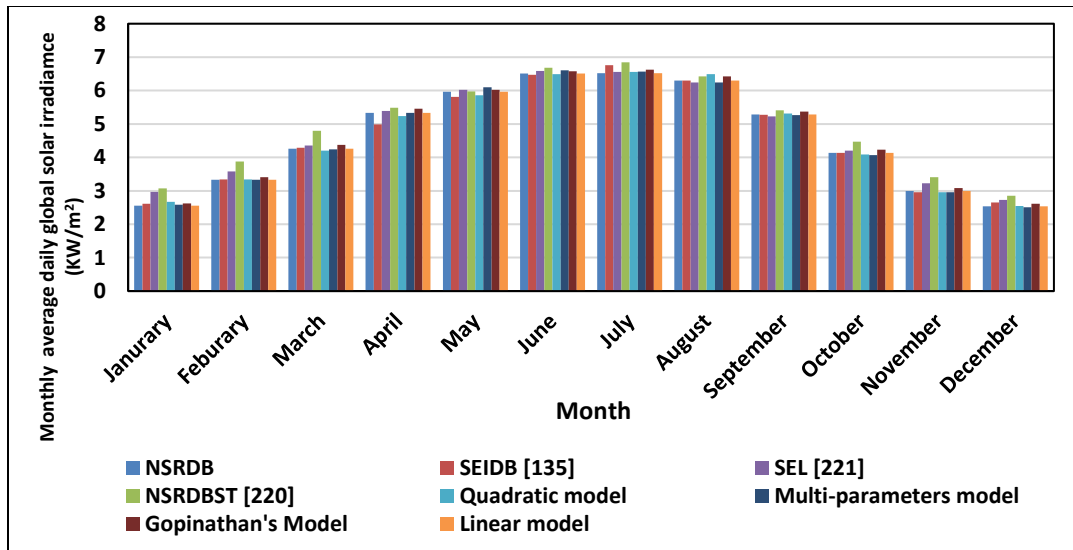
Figure 45*:* Comparison between estimated (by four models) and measured (from different sources) values of monthly average daily global solar irradiance for San Antonio, Texas
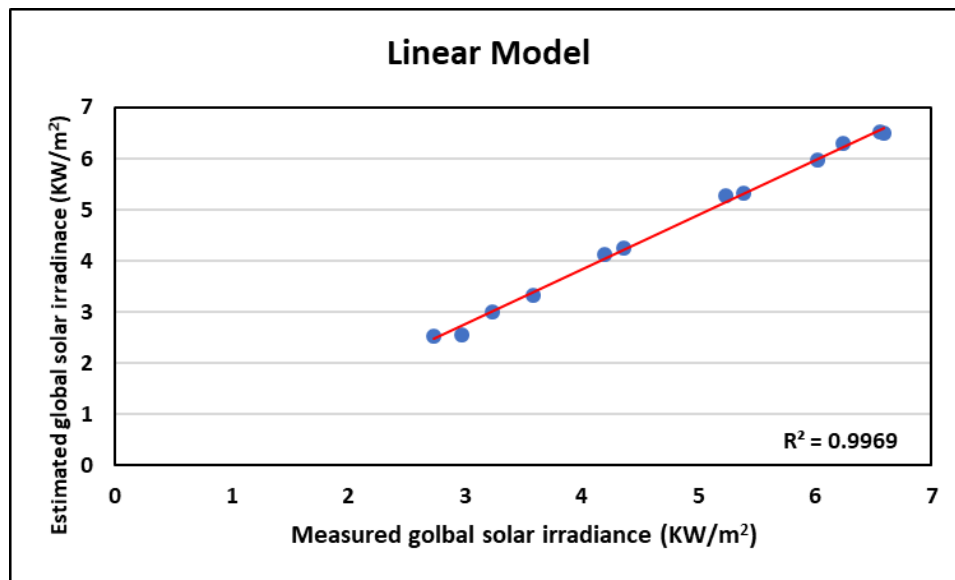
Figure 46*:* Estimated (by Linear model) and measured values of monthly average daily global solar irradiance for San Antonio, Texas

171
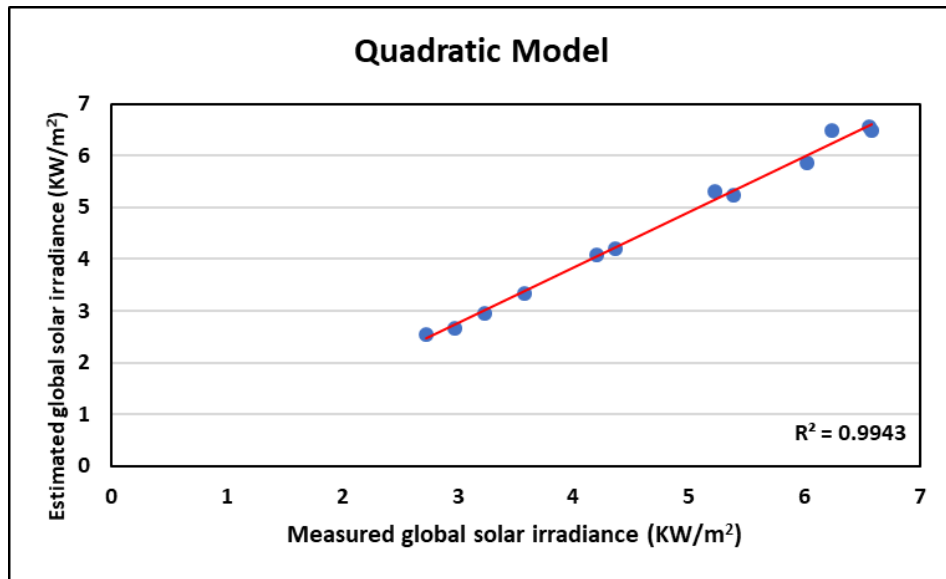
Figure 47: Estimated (by Quadratic model) and measured values of monthly average daily global solar irradiance for San Antonio, Texas
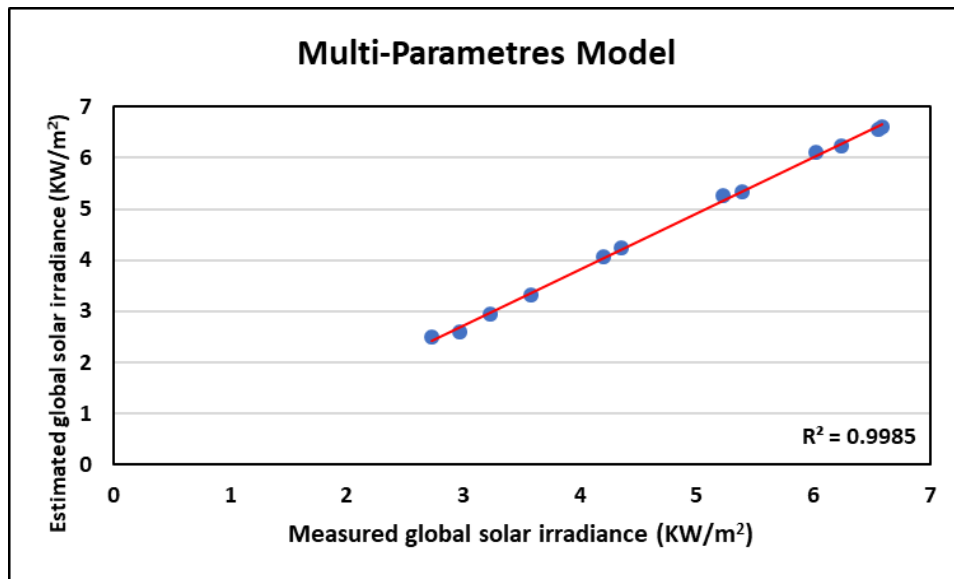
Figure 48: Estimated (by Multi-Parameters model) and measured values of monthly average daily global solar irradiance for San Antonio, Texas
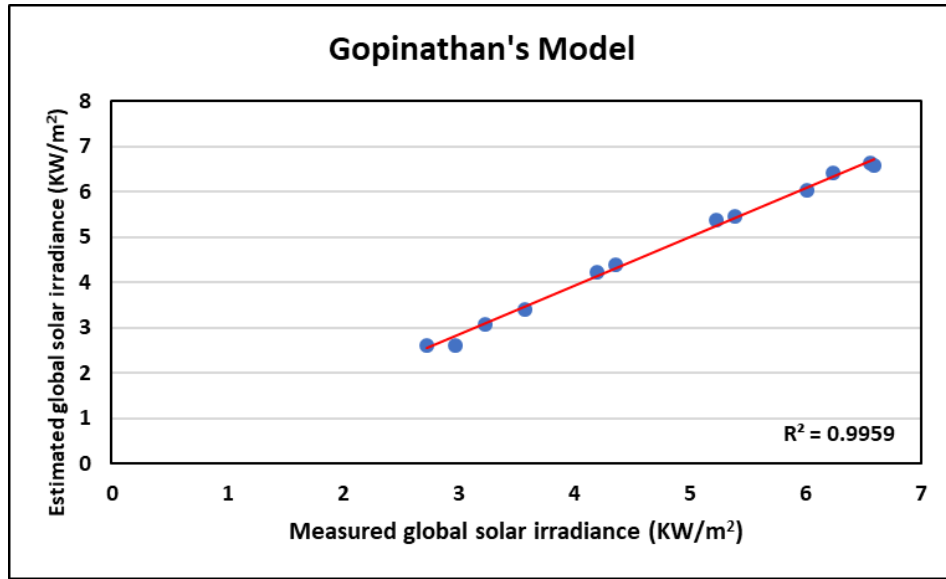
Figure 49*:* Estimated (by Gopinathan's model) and measured values of monthly average daily global solar irradiance for San Antonio, Texas

In addition to the significance of monthly average daily global solar irradiance in calculating monthly average hourly direct solar irradiance on a horizontal surface by using two decompositions models that transform daily solar irradiance data to hourly solar irradiance, monthly average daily diffuse solar irradiance values are essential for the same purpose. Therefore, the validation of four selected empirical models has been performed by comparing their estimated values of monthly average daily diffuse solar irradiance against the measured data. Clearly, the estimated values, which are obtained from three models including Collares-Pereira and Rabl, Liu and Jordan, Gopinathan models, are in good agreement with the measured data [304] except for Iqbal model that shows less consent with measured data, as shown in Figures 50-53.
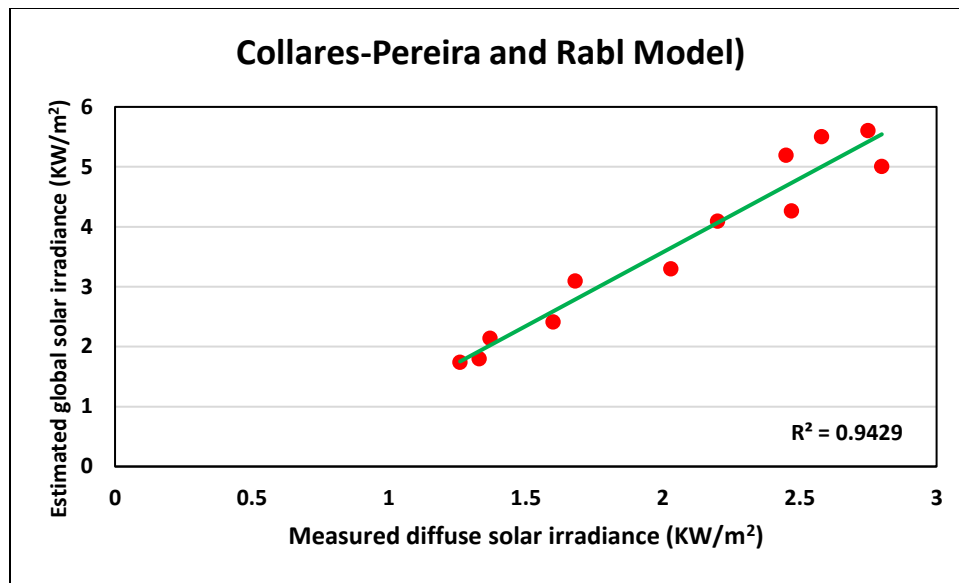
Figure 50*:* Estimated (by Collares-Pereira and Rabl model) and measured values of monthly average daily diffuse solar irradiance for San Antonio, Texas
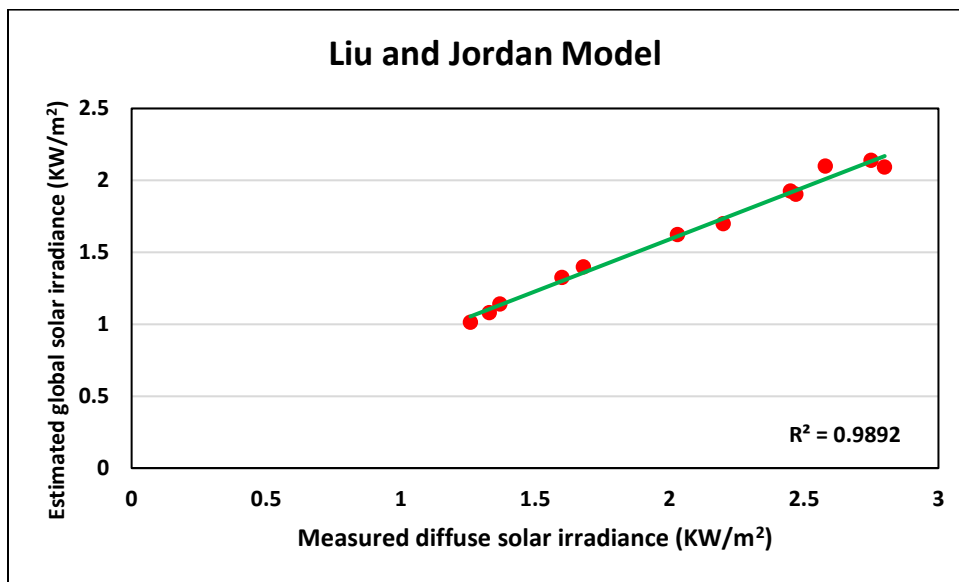
Figure 51*:* Estimated (by Liu and Jordan model) and measured values of monthly average daily diffuse solar irradiance for San Antonio, Texas
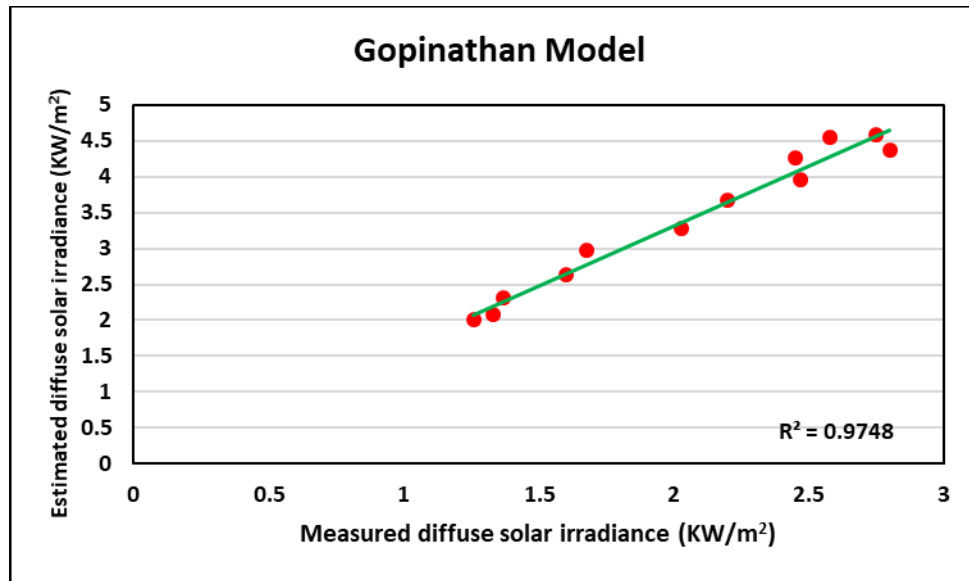
Figure 52*:* Estimated (by Gopinathan model) and measured values of monthly average daily diffuse solar irradiance for San Antonio, Texas
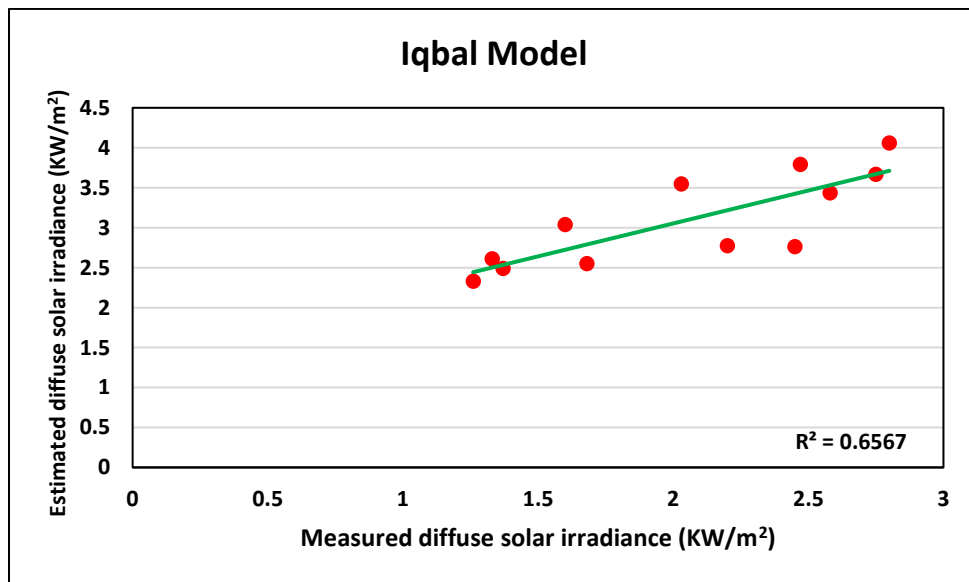
Figure 53*:* Estimated (by Iqbal model) and measured values of monthly average daily diffuse solar irradiance for San Antonio, Texas

Based on the previously estimated values of monthly average daily global (by linear model) and diffuse (Liu and Jordan model) solar irradiance and two decomposition models. the estimated values of monthly average hourly direct solar irradiance on a horizontal surface have been calculated to attain monthly average DNI values through utilizing zenith angle for this purpose. Scatter plot of the estimated values and measured data (is extracted from the National Solar Radiation Database (NSRDB) and [304]) is demonstrated in Figure 54, which exhibits a good agreement between these values.
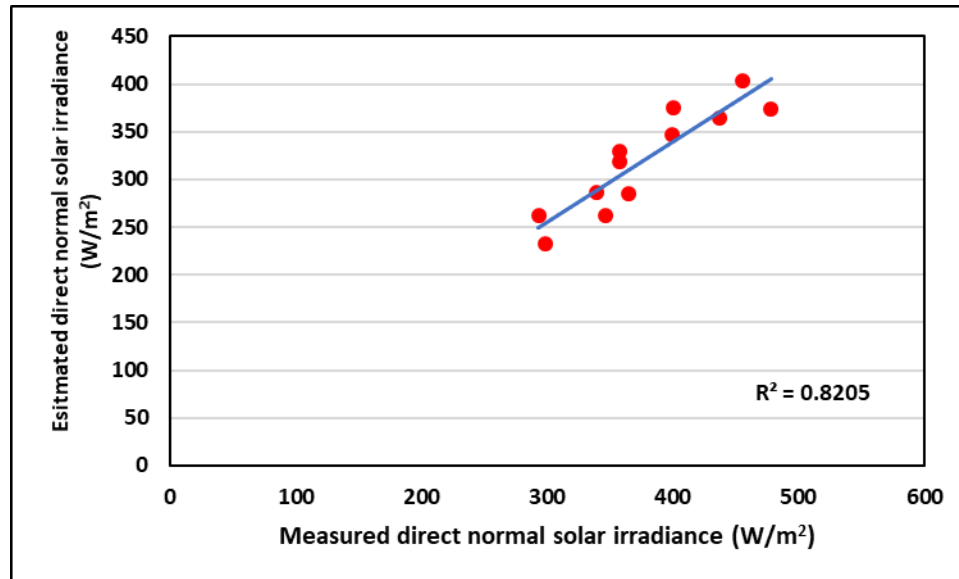
Figure 54: Estimated and measured values of monthly average hourly direct normal solar irradiance for San Antonio, Texas

5.6 Summary

In this study, two hierarchical calculation approaches have been developed by using various models, empirical correlations and regression equations to estimate hourly solar irradiance under different sky conditions. A case study for the San Antonio region

176

in Texas has been solved to demonstrate the accuracy of the proposed approaches for estimating hourly DNI and monthly average hourly DNI data, which is utilized for designing solar concentrated collectors. The estimated data has been shown a good accuracy comparing with measured solar data by using various statistical indicators. Additionally, the proposed approaches can be implemented for other worldwide locations around the world by creating new coefficients for empirical and regression correlations.

CHAPTER VI

CONCLUSIONS

The inextricable link between water and energy in various sectors of life, particularly, in the oil and gas industry, requires the proper management strategies to sustain their resources. Consequently, in this study, a water-energy nexus framework has been used to develop new hierarchical approaches to address water management in shale gas production while incorporating renewable energy to enhance sustainability.

In chapter III, a hierarchical approach has been applied for the integrated system, which has the following key elements: solar system collectors, thermal energy storage, cogeneration process, MED and RO. The optimization problem has been developed as a multi-period MINLP and solved deterministically according to economic and environmental metrics. The integrated system has been shown enabling in creating effective water and energy management strategies.

In chapter IV, another hierarchical approach has been applied for the previous integrated system with integrating the fractionation process. The optimization problem has been developed and solved as a two-stage stochastic programming model for handling uncertainty in operational parameters. The results show the capability of the system in addressing water-energy nexus problems based on the system's economic and environmental merits.

Additionally, in chapter V, hierarchical calculation methodologies have been proposed to obtain high-quality solar data that can be used to evaluate the long-term techno-economic performance for concentrated solar collectors.

178

REFERENCES

1. Raissi, K., *Total site integration*. 1994, The University of Manchester.

2. El-Halwagi, M.M., *Pollution prevention through process integration.* Clean Products and Processes, 1998. **1**(1): p. 5-19.

3. El-Halwagi, M.M., *Process Integration*. 2006: Elsevier Science.

4. Melikoglu, M., *Shale gas: Analysis of its role in the global energy market.* Renewable and Sustainable Energy Reviews, 2014. **37**(Supplement C): p. 460-468.

5. EIA, U.S. *Annual Energy Outlook 2012 with Projections to 2035*. 2012 October, 2017]; Available from: https://www.eia.gov/outlooks/aeo/pdf/0383(2012).pdf.

6. Gao, J. and F. You, *Optimal design and operations of supply chain networks for water management in shale gas production: MILFP model and algorithms for the water-energy nexus.* AIChE Journal, 2015. **61**(4): p. 1184-1208.

7. Carrero-Parreño, A., et al., *Optimal Pretreatment System of Flowback Water from Shale Gas Production.* Industrial & Engineering Chemistry Research, 2017. **56**(15): p. 4386-4398.

8. Nicot, J.-P. and B.R. Scanlon, *Water Use for Shale-Gas Production in Texas, U.S.* Environmental Science & Technology, 2012. **46**(6): p. 3580-3586.

9. Boschee, P., *Produced and Flowback Water Recycling and Reuse: Economics, Limitations, and Technology.* SPE-0214-0016-OGF, 2014. **3**(01).

10. Frankl, P., et al., *Technology roadmap: solar photovoltaic energy.* International Energy Association, 2010.

11. Günther, M., et al., *Parabolic trough technology*, in *Advanced CST teaching materials, enerMENA*. 2011.

12. Mousazadeh, H., et al., *A review of principle and sun-tracking methods for maximizing solar systems output.* Renewable and sustainable energy reviews, 2009. **13**(8): p. 1800-1818.

13. Mittelman, G. and M. Epstein, *A novel power block for CSP systems.* Solar Energy, 2010. **84**(10): p. 1761-1771.

14. Giostri, A., et al., *Comparison of different solar plants based on parabolic trough technology.* Solar Energy, 2012. **86**(5): p. 1208-1221.

15. García, I.L., J.L. Álvarez, and D. Blanco, *Performance model for parabolic trough solar thermal power plants with thermal storage: Comparison to operating plant data.* Solar Energy, 2011. **85**(10): p. 2443-2460.

16. Lippke, F., *Simulation of the part-load behavior of a 30 MWe SEGS plant*. 1995, Sandia National Labs., Albuquerque, NM (United States).

17. Patnode, A.M., *Simulation and performance evaluation of parabolic trough solar power plants*. 2006, University of Wisconsin--Madison.

18. Kumar, D. and S. Kumar, *Year-round performance assessment of a solar parabolic trough collector under climatic condition of Bhiwani, India: A case study.* Energy Conversion and Management, 2015. **106**: p. 224-234.

19. Aldali, Y. and K. Morad, *Thermal performance improvement of Derna electric power station (unit5) using solar energy.* Journal of Sustainable Development, 2014. **7**(1): p. 60.

20.   Padilla, R.V., *Simplified methodology for designing parabolic trough solar power plants*. 2011: University of South Florida.

21.   Al-Sulaiman, F.A., F. Hamdullahpur, and I. Dincer, *Performance assessment of a novel system using parabolic trough solar collectors for combined cooling, heating, and power production.* Renewable Energy, 2012. **48**: p. 161-172.

22.   Silva, J.P., *Modelling and Simulation of Parabolic Trough Power Plant.*

23.   Suresh, N., et al., *Methodology for sizing the solar field for parabolic trough technology with thermal storage and hybridization.* Solar Energy, 2014. **110**: p. 247-259.

24.   Quaschning, V., R. Kistner, and W. Ortmanns, *Influence of direct normal irradiance variation on the optimal parabolic trough field size: A problem solved with technical and economical simulations.* TRANSACTIONS-AMERICAN SOCIETY OF MECHANICAL ENGINEERS JOURNAL OF SOLAR ENERGY ENGINEERING, 2002. **124**(2): p. 160-164.

25.   Eck, M., et al., *Guidelines for CSP yield analysis–optical losses of line focusing systems; definitions, sensitivity analysis and modeling approaches.* Energy Procedia, 2014. **49**: p. 1318-1327.

26.   Lovegrove, K. and W. Stein, *Concentrating solar power technology: principles, developments and applications*. 2012: Elsevier.

27.   Goswami, D.Y. and F. Kreith, *Energy conversion*. 2007: CRC press.

181

28. Dersch, J., et al., *Trough integration into power plants—a study on the performance and economy of integrated solar combined cycle systems*. Vol. 29. 2004. 947-959.

29. Hagos, D.A., *Techno-Economic Assesment of Parabolic Trough Steam Generation for Hospital*. 2011.

30. Reddy, V.S., et al., *State-of-the-art of solar thermal power plants—A review.* Renewable and Sustainable Energy Reviews, 2013. **27**: p. 258-273.

31. Montes, M., et al., *Solar multiple optimization for a solar-only thermal power plant, using oil as heat transfer fluid in the parabolic trough collectors.* Solar Energy, 2009. **83**(12): p. 2165-2176.

32. Zhang, Y. and S.J. Smith, *Long-term modeling of solar energy: analysis of concentrating solar power (CSP) and PV technologies*. 2007, Pacific Northwest National Laboratory (PNNL), Richland, WA (US).

33. Channiwala, S. and A. Ekbote. *A generalized model to estimate field size for solar-only parabolic trough plant*. 2015. 3rd Southern African Solar Energy Conference, South Africa, 11-13 May, 2015.

34. Trabelsi, S.E., et al., *Techno-economic performance of concentrating solar power plants under the climatic conditions of the southern region of Tunisia.* Energy Conversion and Management, 2016. **119**: p. 203-214.

35. Mokheimer, E.M., et al., *Techno-economic performance analysis of parabolic trough collector in Dhahran, Saudi Arabia.* Energy Conversion and Management, 2014. **86**: p. 622-633.

36.   Makhbal, T., S. Sukchai, and P. Thanarak, *Techno-economic assessment of future perspectives of the concentrated solar power plant in Mongolia.* International Journal of Renewable Energy, 2012. **7**(2): p. 17-30.

37.   Antonanzas, J., et al., *Potential solar thermal integration in Spanish combined cycle gas turbines.* Renewable and Sustainable Energy Reviews, 2014. **37**: p. 36-46.

38.   Liqreina, A. and L. Qoaider, *Dry cooling of concentrating solar power (CSP) plants, an economic competitive option for the desert regions of the MENA region.* solar energy, 2014. **103**: p. 417-424.

39.   Abbas, M., et al., *Assessment of a solar parabolic trough power plant for electricity generation under Mediterranean and arid climate conditions in Algeria.* Energy Procedia, 2013. **42**: p. 93-102.

40.   Laboratory, N.R.E., *Assessment of parabolic trough and power tower solar technology cost and performance forecasts*. 2003: DIANE Publishing.

41.   Price, H. *A parabolic trough solar power plant simulation model*. in *ASME International Solar Energy Conference, Kohala Coast, HI, March*. 2003.

42.   Kalogirou, S.A., *Solar thermal collectors and applications.* Progress in energy and combustion science, 2004. **30**(3): p. 231-295.

43.   Sattler, J., et al., *Thermal Energy Storage*. 2015, Technical report, Deutsches Zentrum für Luft-und Raumfahrt-DLR.

44.   Wallentinsen, B.S., *Concentrated Solar Power Gas Turbine Hybrid with Thermal Storage*. 2016, NTNU.

45.   Kuravi, S., et al., *Thermal energy storage technologies and systems for concentrating solar power plants.* Progress in Energy and Combustion Science, 2013. **39**(4): p. 285-319.

46.   Herrmann, U. and D.W. Kearney, *Survey of thermal energy storage for parabolic trough power plants.* TRANSACTIONS-AMERICAN SOCIETY OF MECHANICAL ENGINEERS JOURNAL OF SOLAR ENERGY ENGINEERING, 2002. **124**(2): p. 145-152.

47.   Hale, M., *Survey of thermal storage for parabolic trough power plants.* NREL Report, No. NREL/SR-550-27925, 2000: p. 1-28.

48.   Alva, G., et al., *Thermal energy storage materials and systems for solar energy applications.* Renewable and Sustainable Energy Reviews, 2017. **68**: p. 693-706.

49.   Herrmann, U., B. Kelly, and H. Price, *Two-tank molten salt storage for parabolic trough solar power plants.* Energy, 2004. **29**(5-6): p. 883-893.

50.   Zaversky, F., et al., *Transient molten salt two-tank thermal storage modeling for CSP performance simulations.* Solar Energy, 2013. **93**: p. 294-311.

51.   Flueckiger, S.M., et al., *System-level simulation of a solar power tower plant with thermocline thermal energy storage.* Applied Energy, 2014. **113**: p. 86-96.

52.   Vilella, A.G. and S. Yesilyurt. *Analysis of heat storage with a thermocline tank for concentrated solar plants: Application to AndaSol I.* in *2015 IEEE International Conference on Industrial Technology (ICIT).* 2015. IEEE.

53.   Biencinto, M., et al., *Simulation and assessment of operation strategies for solar thermal power plants with a thermocline storage tank.* Solar Energy, 2014. **103**: p. 456-472.

54.   Cocco, D. and F. Serra, *Performance comparison of two-tank direct and thermocline thermal energy storage systems for 1 MWe class concentrating solar power plants.* Energy, 2015. **81**: p. 526-536.

55.   Cipollina, A., G. Micale, and L. Rizzuti, *Seawater desalination: conventional and renewable energy processes*. 2009: Springer Science & Business Media.

56.   Al-Karaghouli, A. and L.L. Kazmerski, *Energy consumption and water production cost of conventional and renewable-energy-powered desalination processes.* Renewable and Sustainable Energy Reviews, 2013. **24**: p. 343-356.

57.   Voutchkov, N., *Considerations for selection of seawater filtration pretreatment system.* Desalination, 2010. **261**(3): p. 354-364.

58.   Tovar-Facio, J., et al., *Optimal Design of Multiplant Cogeneration Systems with Uncertain Flaring and Venting.* ACS Sustainable Chemistry & Engineering, 2016. **5**(1): p. 675-688.

59.   Chacartegui, R., et al., *Feasibility analysis of a MED desalination plant in a combined cycle based cogeneration facility.* Applied thermal engineering, 2009. **29**(2): p. 412-417.

60.   González-Bravo, R., et al., *Involving integrated seawater desalination-power plants in the optimal design of water distribution networks.* Resources, Conservation and Recycling, 2015. **104**: p. 181-193.

61.   Li, C., et al., *A new combined power and desalination system driven by low grade heat for concentrated brine.* Energy, 2012. **46**(1): p. 582-595.

62.   Zak, G.M., et al., *A review of hybrid desalination systems for co-production of power and water: analyses, methods, and considerations.* Desalination and Water Treatment, 2013. **51**(28-30): p. 5381-5401.

63.   Mezher, T., et al., *Techno-economic assessment and environmental impacts of desalination technologies.* Desalination, 2011. **266**(1): p. 263-273.

64.   Compain, P., *Solar energy for water desalination.* Procedia Engineering, 2012. **46**: p. 220-227.

65.   Sharon, H. and K. Reddy, *A review of solar energy driven desalination technologies.* Renewable and Sustainable Energy Reviews, 2015. **41**: p. 1080-1118.

66.   Ortega-Delgado, B., L. García-Rodríguez, and D.-C. Alarcón-Padilla, *Thermoeconomic comparison of integrating seawater desalination processes in a concentrating solar power plant of 5 MW e.* Desalination, 2016. **392**: p. 102-117.

67.   Al-Qaraghuli, A. and L.L. Kazmerski. *Comparison of technical and economic performance of the main desalination processes with and without renewable energy coupling.* in *Proceedings of the American Solar Energy Society World Renewable Energy Forum.* 2012.

68.   Palenzuela, P., et al., *Simulation and evaluation of the coupling of desalination units to parabolic-trough solar power plants in the Mediterranean region.* Desalination, 2011. **281**: p. 379-387.

69.   Blanco, J., et al., *Preliminary thermoeconomic analysis of combined parabolic trough solar power and desalination plant in port Safaga (Egypt).* Desalination and Water Treatment, 2013. **51**(7-9): p. 1887-1899.

70.   Moser, M., F. Trieb, and T. Fichter, *Potential of concentrating solar power plants for the combined production of water and electricity in MENA countries.* Journal of Sustainable Development of Energy, Water and Environment Systems, 2013. **1**(2): p. 122-140.

71.   Moser, M., et al., *The MED-CSD project: potential for concentrating solar power desalination development in Mediterranean countries.* Journal of Solar Energy Engineering, 2011. **133**(3): p. 031012.

72.   Palenzuela, P., D.-C. Alarcón-Padilla, and G. Zaragoza, *Large-scale solar desalination by combination with CSP: Techno-economic analysis of different options for the Mediterranean Sea and the Arabian Gulf.* Desalination, 2015. **366**: p. 130-138.

73.   Wellmann, J., *Conceptual design of a concentrating solar power plant for a combined electricity and water supply of the city El Gouna*. 2015.

74.   Kalogirou, S.A. *Concentrating solar power plants for electricity and desalinated water production*. in *World Renewable Energy Congress-Sweden; 8-13 May; 2011; LinkÃ¶ping; Sweden*. 2011. Linköping University Electronic Press.

75.   Iaquaniello, G., et al., *Concentrating solar power (CSP) system integrated with MED–RO hybrid desalination.* Desalination, 2014. **336**: p. 121-128.

76.   Trieb, F., et al., *Combined Solar Power and Desalination Plants: Techno-Economic Potential in Mediterranean Partner Countries.* German Aerospace Center (DLR), 2009.

77.   Ali, M.T., H.E. Fath, and P.R. Armstrong, *A comprehensive techno-economical review of indirect solar desalination.* Renewable and Sustainable Energy Reviews, 2011. **15**(8): p. 4187-4199.

78.   Bataineh, K.M., *Multi-effect desalination plant combined with thermal compressor driven by steam generated by solar energy.* Desalination, 2016. **385**: p. 39-52.

79.   Palenzuela, P., D.-C. Alarcón-Padilla, and G. Zaragoza, *Concentrating Solar Power and Desalination Plants*. 2015, Springer.

80.   Wu, L., Y. Hu, and C. Gao, *Optimum design of cogeneration for power and desalination to satisfy the demand of water and power.* Desalination, 2013. **324**: p. 111-117.

81.   Antipova, E., et al., *Multi-objective design of reverse osmosis plants integrated with solar Rankine cycles and thermal energy storage.* Applied energy, 2013. **102**: p. 1137-1147.

82.   Chen, H. and K.E. Carter, *Water usage for natural gas production through hydraulic fracturing in the United States from 2008 to 2014.* Journal of environmental management, 2016. **170**: p. 152-159.

83.   Kondash, A. and A. Vengosh, *Water footprint of hydraulic fracturing.* Environmental Science & Technology Letters, 2015. **2**(10): p. 276-280.

84. Vengosh, A., et al., *The effects of shale gas exploration and hydraulic fracturing on the quality of water resources in the United States.* Procedia Earth and Planetary Science, 2013. **7**: p. 863-866.

85. Kondash, A.J., E. Albright, and A. Vengosh, *Quantity of flowback and produced waters from unconventional oil and gas exploration.* Science of the Total Environment, 2017. **574**: p. 314-321.

86. Rahm, D., *Regulating hydraulic fracturing in shale gas plays: The case of Texas.* Energy Policy, 2011. **39**(5): p. 2974-2981.

87. Clark, C.E., R.M. Horner, and C.B. Harto, *Life cycle water consumption for shale gas and conventional natural gas.* Environmental science & technology, 2013. **47**(20): p. 11829-11836.

88. Scanlon, B.R., R.C. Reedy, and J.-P. Nicot, *Comparison of water use for hydraulic fracturing for unconventional oil and gas versus conventional oil.* Environmental science & technology, 2014. **48**(20): p. 12386-12393.

89. Carrero-Parreño, A., et al., *Optimal Pretreatment System of Flowback Water from Shale Gas Production.* Industrial & Engineering Chemistry Research, 2017. **56**(15): p. 4386-4398.

90. Butkovskyi, A., et al., *Organic Pollutants in Shale Gas Flowback and Produced Waters: Identification, Potential Ecological Impact, and Implications for Treatment Strategies.* Environmental Science & Technology, 2017. **51**(9): p. 4740-4754.

91.   Estrada, J.M. and R. Bhamidimarri, *A review of the issues and treatment options for wastewater from shale gas extraction by hydraulic fracturing.* Fuel, 2016. **182**: p. 292-303.

92.   Shaffer, D.L., et al., *Desalination and reuse of high-salinity shale gas produced water: drivers, technologies, and future directions.* Environmental science & technology, 2013. **47**(17): p. 9569-9583.

93.   Lira-Barragán, L.F., et al., *Optimal water management under uncertainty for shale gas production.* Industrial & Engineering Chemistry Research, 2016. **55**(5): p. 1322-1335.

94.   Yang, L., I.E. Grossmann, and J. Manno, *Optimization models for shale gas water management.* AIChE Journal, 2014. **60**(10): p. 3490-3501.

95.   Dong, X., J. Trembly, and D. Bayless, *Techno-economic analysis of hydraulic fracking flowback and produced water treatment in supercritical water reactor.* Energy, 2017. **133**: p. 777-783.

96.   El-Halwagi, M.M., *Sustainable design through process integration: fundamentals and applications to industrial pollution prevention, resource conservation, and profitability enhancement.* 2017: Butterworth-Heinemann.

97.   Grossmann, I.E., *Mixed-integer programming approach for the synthesis of integrated process flowsheets.* Computers & chemical engineering, 1985. **9**(5): p. 463-482.

98.   Xianli, W., et al., *Model and Design of Cogeneration System for Different Demands of Desalination Water, Heat and Power Production.* Chinese Journal of Chemical Engineering, 2014. **22**(3): p. 330-338.

99.   Lee, S., et al., *Thermo-environ-economic modeling and optimization of an integrated wastewater treatment plant with a combined heat and power generation system.* Energy Conversion and Management, 2017. **142**: p. 385-401.

100.   Manesh, M.K., et al., *Optimal coupling of site utility steam network with MED-RO desalination through total site analysis and exergoeconomic optimization.* Desalination, 2013. **316**: p. 42-52.

101.   Ferreira, E.M., J.A.P. Balestieri, and M.A. Zanardi, *Optimization analysis of dual-purpose systems.* Desalination, 2010. **250**(3): p. 936-944.

102.   Mussati, S.F., P.A. Aguirre, and N.J. Scenna, *A rigorous, mixed-integer, nonlineal programming model (MINLP) for synthesis and optimal operation of cogeneration seawater desalination plants.* Desalination, 2004. **166**: p. 339-345.

103.   Mussati, S., P. Aguirre, and N. Scenna, *Dual-purpose desalination plants. Part I. Optimal design.* Desalination, 2003. **153**(1-3): p. 179-184.

104.   Uche, J., L. Serra, and A. Valero, *Thermoeconomic optimization of a dual-purpose power and desalination plant.* Desalination, 2001. **136**(1-3): p. 147-158.

105.   Shakib, S.E., et al., *Multi-objective optimization of a cogeneration plant for supplying given amount of power and fresh water.* Desalination, 2012. **286**: p. 225-234.

106.   Mussati, S., P. Aguirre, and N. Scenna, *Optimization of alternative structures of integrated power and desalination plants.* Desalination, 2005. **182**(1-3): p. 123-129.

107.   Gabriel, K.J., M.M. El-Halwagi, and P. Linke, *Optimization across the water–energy nexus for integrating heat, power, and water for industrial processes, coupled with hybrid thermal-membrane desalination.* Industrial & Engineering Chemistry Research, 2016. **55**(12): p. 3442-3466.

108.   El-Nashar, A.M., *Optimal design of a cogeneration plant for power and desalination taking equipment reliability into consideration.* Desalination, 2008. **229**(1-3): p. 21-32.

109.   Al-Azri, N., M. Al-Thubaiti, and M. El-Halwagi, *An algorithmic approach to the optimization of process cogeneration.* Clean Technologies and Environmental Policy, 2009. **11**(3): p. 329-338.

110.   Abdelhady, F., et al., *Optimal design and integration of solar thermal collection, storage, and dispatch with process cogeneration systems.* Chemical Engineering Science, 2015. **136**: p. 158-167.

111.   Tora, E.A. and M.M. El-Halwagi, *Optimal design and integration of solar systems and fossil fuels for sustainable and stable power outlet.* Clean Technologies and Environmental Policy, 2009. **11**(4): p. 401.

112.   Bamufleh, H.S., J.M. Ponce-Ortega, and M.M. El-Halwagi, *Multi-objective optimization of process cogeneration systems with economic, environmental, and*

social tradeoffs. Clean Technologies and Environmental Policy, 2013. **15**(1): p. 185-197.

113. Tora, E.A. and M.M. El-Halwagi, *Integrated conceptual design of solar-assisted trigeneration systems.* Computers & Chemical Engineering, 2011. **35**(9): p. 1807-1814.

114. Lira-Barragán, L.F., et al., *Optimum heat storage design for solar-driven absorption refrigerators integrated with heat exchanger networks.* AIChE Journal, 2014. **60**(3): p. 909-930.

115. Kemp, I.C., *Pinch analysis and process integration: a user guide on process integration for the efficient use of energy.* 2011: Butterworth-Heinemann.

116. Klemeš, J.J., *Handbook of process integration (PI): minimisation of energy and water use, waste and emissions.* 2013: Elsevier.

117. Smith, R., *Chemical Process Design and Integration.* 2016: Wiley.

118. Zhang, C. and M.M. El-Halwagi, *Estimate the Capital Cost of Shale-Gas Monetization Projects.* Chemical Engineering Progress, 2017. **113**(12): p. 28-32.

119. Ortiz-Espinoza, A.P., et al., *Design, simulation and techno-economic analysis of two processes for the conversion of shale gas to ethylene.* Computers & Chemical Engineering, 2017. **107**: p. 237-246.

120. Pérez-Uresti, S.I., et al., *Techno-Economic Assessment of Benzene Production from Shale Gas.* Processes, 2017. **5**(3): p. 33.

121. Jasper, S. and M.M. El-Halwagi, *A techno-economic comparison between two methanol-to-propylene processes.* Processes, 2015. **3**(3): p. 684-698.

122. Julián-Durán, L.M., et al., *Techno-economic assessment and environmental impact of shale gas alternatives to methanol.* ACS Sustainable Chemistry & Engineering, 2014. **2**(10): p. 2338-2344.

123. Salkuyeh, Y.K. and T.A. Adams II, *A novel polygeneration process to co-produce ethylene and electricity from shale gas with zero CO2 emissions via methane oxidative coupling.* Energy Conversion and Management, 2015. **92**: p. 406-420.

124. Ehlinger, V.M., et al., *Process design and integration of shale gas to methanol.* ACS Sustainable Chemistry & Engineering, 2013. **2**(1): p. 30-37.

125. Salkuyeh, Y.K. and T.A. Adams II, *Shale gas for the petrochemical industry: Incorporation of novel technologies*, in *Computer Aided Chemical Engineering*. 2014, Elsevier. p. 603-608.

126. Hasaneen, R. and M.M. El-Halwagi, *Using integrated process and microeconomic analyses to enable effective environmental policy for shale gas in the USA.* Clean Technologies and Environmental Policy, 2017. **19**(6): p. 1775-1789.

127. Arredondo-Ramírez, K., J.M. Ponce-Ortega, and M.M. El-Halwagi, *Optimal planning and infrastructure development for shale gas production.* Energy Conversion and Management, 2016. **119**: p. 91-100.

128. Elsayed, N.A., et al., *Optimal design of thermal membrane distillation systems for the treatment of shale gas flowback water.* Int J Membr Sci Technol, 2015. **2**: p. 1-9.

129.   Lokare, O.R., et al., *Integrating membrane distillation with waste heat from natural gas compressor stations for produced water treatment in Pennsylvania.* Desalination, 2017. **413**: p. 144-153.

130.   Tavakkoli, S., et al., *A techno-economic assessment of membrane distillation for treatment of Marcellus shale produced water.* Desalination, 2017. **416**: p. 24-34.

131.   Bamufleh, H., et al., *Optimization of multi-effect distillation with brine treatment via membrane distillation and process heat integration.* Desalination, 2017. **408**: p. 110-118.

132.   Elsayed, N.A., M.A. Barrufet, and M.M. El-Halwagi, *Integration of thermal membrane distillation networks with processing facilities.* Industrial & Engineering Chemistry Research, 2013. **53**(13): p. 5284-5298.

133.   Pham, V., C. Laird, and M. El-Halwagi, *Convex hull discretization approach to the global optimization of pooling problems.* Industrial & Engineering Chemistry Research, 2009. **48**(4): p. 1973-1979.

134.   Gabriel, F.B. and M.M. El-Halwagi, *Simultaneous synthesis of waste interception and material reuse networks: problem reformulation for global optimization.* Environmental progress, 2005. **24**(2): p. 171-180.

135.   Khor, C.S., et al., *A superstructure optimization approach for membrane separation-based water regeneration network synthesis with detailed nonlinear mechanistic reverse osmosis model.* Industrial & Engineering Chemistry Research, 2011. **50**(23): p. 13444-13456.

136.   Alnouri, S.Y., P. Linke, and M.M. El-Halwagi, *Synthesis of industrial park water reuse networks considering treatment systems and merged connectivity options.* Computers & Chemical Engineering, 2016. **91**: p. 289-306.

137.   El-Halwagi, A.M., V. Manousiouthakis, and M.M. El-Halwagi, *Analysis and simulation of hollow-fiber reverse-osmosis modules.* Separation science and technology, 1996. **31**(18): p. 2505-2529.

138.   El-Halwagi, M.M., *Synthesis of reverse-osmosis networks for waste reduction.* AIChE Journal, 1992. **38**(8): p. 1185-1198.

139.   Mavromatis, S. and A. Kokossis, *Conceptual optimisation of utility networks for operational variations—I. Targets and level optimisation.* Chemical Engineering Science, 1998. **53**(8): p. 1585-1608.

140.   El-Halwagi, M.M., *A return on investment metric for incorporating sustainability in process integration and improvement projects.* Clean Technologies and Environmental Policy, 2017. **19**(2): p. 611-617.

141.   Guillen-Cuevas, K., et al., *Incorporation of safety and sustainability in conceptual design via a return on investment metric.* ACS Sustainable Chemistry & Engineering, 2017. **6**(1): p. 1411-1416.

142.   Atilhan, S., *A systems-integration approach to the optimal design and operation of macroscopic water desalination and supply networks*. 2011: Texas A&M University.

143.   Ghaffour, N., T.M. Missimer, and G.L. Amy, *Technical review and evaluation of the economics of water desalination: current and future challenges for better water supply sustainability.* Desalination, 2013. **309**: p. 197-207.

144.   Mezher, T., et al., *Techno-economic assessment and environmental impacts of desalination technologies.* Desalination, 2011. **266**(1-3): p. 263-273.

145.   Atilhan, S., et al., *A systems integration approach to the design of regional water desalination and supply networks.* International Journal of Process Systems Engineering, 2011. **1**(2): p. 125-135.

146.   Horwitt, D. and L. Sumi, *Up in Flames: US Shale Oil boom comes at Expense of Wasted Natural Gas, Increased CO2.* Earthworks, Washington, DC, USA, 2014.

147.   RPSEA, *Advanced Treatment of Shale Gas Fracturing Water to Produce Re-Use or Discharge Quality Water.* 2015.

148.   Giuliano, S., R. Buck, and S. Eguiguren, *Analysis of solar-thermal power plants with thermal energy storage and solar-hybrid operation strategy.* Journal of Solar Energy Engineering, 2011. **133**(3): p. 031007.

149.   Siirola, J.J., *The impact of shale gas in the chemical industry.* AIChE Journal, 2014. **60**(3): p. 810-819.

150.   Guerra, O.J., et al., *An optimization framework for the integration of water management and shale gas supply chain design.* Computers & Chemical Engineering, 2016. **92**: p. 230-255.

151. Jiang, M., C.T. Hendrickson, and J.M. VanBriesen, *Life cycle water consumption and wastewater generation impacts of a Marcellus shale gas well.* Environmental science & technology, 2014. **48**(3): p. 1911-1920.

152. Gao, J. and F. You, *Design and optimization of shale gas energy systems: Overview, research challenges, and future directions.* Computers & Chemical Engineering, 2017. **106**: p. 699-718.

153. He, L., et al., *Game-based analysis of energy-water nexus for identifying environmental impacts during Shale gas operations under stochastic input.* Science of The Total Environment, 2018. **627**: p. 1585-1601.

154. Kong, L., et al., *A superstructure-based framework for simultaneous process synthesis, heat integration, and utility plant design.* Computers & Chemical Engineering, 2016. **91**: p. 68-84.

155. El-Halwagi, M.M., *Pollution prevention through process integration: systematic design tools.* 1997: Elsevier.

156. Al-Aboosi, F.Y. and M.M. El-Halwagi, *An Integrated Approach to Water-Energy Nexus in Shale-Gas Production.* Processes, 2018. **6**(5): p. 52.

157. Cafaro, D.C. and I.E.J.A.J. Grossmann, *Strategic planning, design, and development of the shale gas supply chain network.* 2014. **60**(6): p. 2122-2142.

158. Su, W., J. Wang, and J. Roh, *Stochastic energy scheduling in microgrids with intermittent renewable energy resources.* IEEE Transactions on Smart Grid, 2014. **5**(4): p. 1876-1883.

159. Charitopoulos, V.M., L.G. Papageorgiou, and V. Dua, *Nonlinear Model-Based Process Operation under Uncertainty Using Exact Parametric Programming.* Engineering, 2017. **3**(2): p. 202-213.

160. Karuppiah, R. and I.E. Grossmann, *Global optimization of multiscenario mixed integer nonlinear programming models arising in the synthesis of integrated water networks under uncertainty.* Computers & Chemical Engineering, 2008. **32**(1-2): p. 145-160.

161. Babazadeh, R., F. Jolai, and J. Razmi, *Developing scenario–based robust optimisation approaches for the reverse logistics network design problem under uncertain environments.* International Journal of Services and Operations Management, 2015. **20**(4): p. 418-440.

162. Shakya, A., *Implementation of Solar Irradiance Forecasting Using Markov Switching Model and Energy Management System.* 2016.

163. Shabani, N., et al., *Tactical supply chain planning for a forest biomass power plant under supply uncertainty.* Energy, 2014. **78**: p. 346-355.

164. Zhou, Z., et al., *A two-stage stochastic programming model for the optimal design of distributed energy systems.* Applied Energy, 2013. **103**: p. 135-144.

165. Chebeir, J., A. Geraili, and J. Romagnoli, *Development of Shale Gas Supply Chain Network under Market Uncertainties.* Energies, 2017. **10**(2): p. 246.

166. You, F., J.M. Wassick, and I.E. Grossmann, *Risk management for a global supply chain planning under uncertainty: models and algorithms.* AIChE Journal, 2009. **55**(4): p. 931-946.

167.   Mavromatidis, G., K. Orehounig, and J. Carmeliet, *Design of distributed energy systems under uncertainty: A two-stage stochastic programming approach.* Applied energy, 2018. **222**: p. 932-950.

168.   Montoya-Bueno, S., J.I. Muoz, and J. Contreras, *A stochastic investment model for renewable generation in distribution systems.* IEEE Transactions on Sustainable Energy, 2015. **6**(4): p. 1466-1474.

169.   Pistikopoulos, E. and M. Ierapetritou, *Novel approach for optimal process design under uncertainty.* Computers & Chemical Engineering, 1995. **19**(10): p. 1089-1110.

170.   Acevedo, J. and E.N. Pistikopoulos, *Stochastic optimization based algorithms for process synthesis under uncertainty.* Computers & Chemical Engineering, 1998. **22**(4-5): p. 647-671.

171.   Paules IV, G. and C. Floudas, *Stochastic programming in process synthesis: a two-stage model with MINLP recourse for multiperiod heat-integrated distillation sequences.* Computers & chemical engineering, 1992. **16**(3): p. 189-210.

172.   Ierapetritou, M.G., J. Acevedo, and E. Pistikopoulos, *An optimization approach for process engineering problems under uncertainty.* Computers & Chemical Engineering, 1996. **20**(6-7): p. 703-709.

173.   Steimel, J. and S. Engell, *Conceptual design and optimization of chemical processes under uncertainty by two-stage programming.* Computers & Chemical Engineering, 2015. **81**: p. 200-217.

174. Shafiee, S. and E. Topal, *A long-term view of worldwide fossil fuel prices.* Applied energy, 2010. **87**(3): p. 988-1000.

175. Mirkhani, S. and Y. Saboohi, *Stochastic modeling of the energy supply system with uncertain fuel price–A case of emerging technologies for distributed power generation.* Applied energy, 2012. **93**: p. 668-674.

176. Rogers, J., *Strategy, value and risk: the real options approach*. 2009: Springer.

177. Geiger, A., *Strategic Power Plant Investment Planning under Fuel and Carbon Price Uncertainty*. 2011: KIT Scientific Publishing.

178. Ross, S.M., *An elementary introduction to mathematical finance*. 2011: Cambridge University Press.

179. Iyer, R. and I.E. Grossmann, *Synthesis and operational planning of utility systems for multiperiod operation.* Computers & Chemical Engineering, 1998. **22**(7-8): p. 979-993.

180. Carpaneto, E., et al., *Cogeneration planning under uncertainty: Part I: Multiple time frame approach.* Applied Energy, 2011. **88**(4): p. 1059-1067.

181. Carpaneto, E., et al., *Cogeneration planning under uncertainty. Part II: Decision theory-based assessment of planning alternatives.* Applied Energy, 2011. **88**(4): p. 1075-1083.

182. Sun, L., L. Gai, and R. Smith, *Site utility system optimization with operation adjustment under uncertainty.* Applied Energy, 2017. **186**: p. 450-456.

183. Goellner, J.F., *Expanding the shale gas infrastructure.* Gas, 2012. **2**(C3): p. C4.

184. Freeman, C., et al. *Measurement, modeling, and diagnostics of flowing gas composition changes in shale gas wells*. in *SPE Latin America and Caribbean Petroleum Engineering Conference*. 2012. Society of Petroleum Engineers.

185. Gong, J., M. Yang, and F. You, *A systematic simulation-based process intensification method for shale gas processing and NGLs recovery process systems under uncertain feedstock compositions.* Computers & Chemical Engineering, 2017. **105**: p. 259-275.

186. Gong, J. and F. You, *Sustainable design and synthesis of energy systems.* Current Opinion in Chemical Engineering, 2015. **10**: p. 77-86.

187. Gueymard, C.A., *Direct and indirect uncertainties in the prediction of tilted irradiance for solar engineering applications.* Solar Energy, 2009. **83**(3): p. 432-444.

188. Al-Aboosi, F. and M. El-Halwagi, *An Integrated Approach to Water-Energy Nexus in Shale-Gas Production.* Processes, 2018. **6**(5): p. 52.

189. Ioannou, A., et al., *Multi-stage stochastic optimization framework for power generation system planning integrating hybrid uncertainty modelling.* Energy Economics, 2019.

190. Brown, S.P. and M.K. Yucel, *What drives natural gas prices?* Energy Journal, 2008. **29**(2): p. 45.

191. Pfeifer, P.E., S.E. Bodily, and S.C. Frey Jr, *Pearson-Tukey Three-Point Approximations Versus Monte Carlo Simulation.* Decision Sciences, 1991. **22**(1): p. 74-90.

192.   Miller III, A.C. and T.R. Rice, *Discrete approximations of probability distributions.* Management science, 1983. **29**(3): p. 352-362.

193.   Keefer, D.L. and S.E. Bodily, *Three-point approximations for continuous random variables.* Management Science, 1983. **29**(5): p. 595-609.

194.   Hammond, R.K. and J.E. Bickel, *Reexamining discrete approximations to continuous distributions.* Decision Analysis, 2013. **10**(1): p. 6-25.

195.   Woodruff, J. and N.B. Dimitrov, *Optimal discretization for decision analysis.* Operations Research Perspectives, 2018. **5**: p. 288-305.

196.   DeCoursey, W., *Statistics and probability for engineering applications*. 2003: Elsevier.

197.   Dupačová, J. and V. Kozmík, *SDDP for multistage stochastic programs: preprocessing via scenario reduction.* Computational Management Science, 2017. **14**(1): p. 67-80.

198.   Pranevicius, H. and K. Sutiene. *Scenario tree generation by clustering the simulated data paths*. in *Proceedings 21st European conference on modelling and simulation*. 2007.

199.   Khatami, M., M. Mahootchi, and R.Z. Farahani, *Benders' decomposition for concurrent redesign of forward and closed-loop supply chain network with demand and return uncertainties.* Transportation Research Part E: Logistics and Transportation Review, 2015. **79**: p. 1-21.

200. Mavromatidis, G., K. Orehounig, and J. Carmeliet, *Trade-offs between risk-neutral and risk-averse decision making for the design of distributed energy systems under uncertainty.* Proceedings of ECOS 2017, 2017.

201. Gülpınar, N., B. Rustem, and R. Settergren, *Simulation and optimization approaches to scenario tree generation.* Journal of economic dynamics and control, 2004. **28**(7): p. 1291-1315.

202. Hasani, A., *Two-stage Stochastic Programing Based on the Accelerated Benders Decomposition for Designing Power Network Design under Uncertainty.* International Journal of Industrial Engineering & Production Research, 2017. **28**(2): p. 163-174.

203. Birge, J.R. and F. Louveaux, *Introduction to stochastic programming.* 2011: Springer Science & Business Media.

204. Clay, R. and I. Grossmann, *A disaggregation algorithm for the optimization of stochastic planning models.* Computers & Chemical Engineering, 1997. **21**(7): p. 751-774.

205. Branan, C., *Rules of Thumb for Chemical Engineers: A Manual of Quick.* Accurate Solutions to Everyday Process Engineering Problems, 3rd ed., Gulf Professional Pub., Amsterdam, 2002.

206. Kumana, J., *How to calculate the true cost of steam.* 2003, DOE/GO-102003-1736. US Department of Energy, Washington.

207. Philibert, C., *Technology roadmap: concentrating solar power.* 2010: OECD/IEA.

208. Dale, M., *A comparative analysis of energy costs of photovoltaic, solar thermal, and wind electricity generation technologies.* Applied Sciences, 2013. **3**(2): p. 325-337.

209. Alnouri, S.Y. and P. Linke, *Optimal SWRO desalination network synthesis using multiple water quality parameters.* Journal of membrane science, 2013. **444**: p. 493-512.

210. Gabriel, K.J., P. Linke, and M.M. El-Halwagi, *Optimization of multi-effect distillation process using a linear enthalpy model.* Desalination, 2015. **365**: p. 261-276.

211. Recovery, L., et al., *TKP4170 PROCESS DESIGN. PROJECT.* 2010.

212. Kaplan, R., et al., *Assessment of desalination technologies for treatment of a highly saline brine from a potential CO 2 storage site.* Desalination, 2017. **404**: p. 87-101.

213. Schrage, L., *Optimization Modeling with LINGO. 2006.* LINDO Systems Inc., Chicago, Illinois, 2006.

214. Arthur, J.D., B. Langhus, and D. Alleman, *An overview of modern shale gas development in the United States.* All Consulting, 2008. **3**: p. 14-17.

215. Mohtar, R.H., et al., *Economic, social, and environmental evaluation of energy development in the Eagle Ford shale play.* Science of the Total Environment, 2019. **646**: p. 1601-1614.

216. Eldar, K., F. Feby, and S. Juejing, *Process Design and Economic Investigation of LPG Production from Natural Gas Liquids (NGL).* TKP4170 Process design, Norway, 2010.

217. Koudouris, G., et al., *A stochastic model for the hourly solar radiation process for application in renewable resources management.* 2018. **45**: p. 139-145.

218. Pavanello, D., et al., *Statistical functions and relevant correlation coefficients of clearness index.* 2015. **130**: p. 142-150.

219. Knapp, C.L., T.L. Stoffel, and S.S. Whitaker, *Insolation data manual.* 1980: US Government Printing Office.

220. Singh, B.R. and O. Singh, *Global trends of fossil fuel reserves and climate change in the 21st century*, in *Fossil Fuel and the Environment*. 2012, InTech.

221. Pepe, D., G. Bianchini, and A.J.S.E. Vicino, *Model estimation for solar generation forecasting using cloud cover data.* 2017. **157**: p. 1032-1046.

222. Law, E.W., et al., *Direct normal irradiance forecasting and its application to concentrated solar thermal output forecasting–a review.* 2014. **108**: p. 287-307.

223. Ferretti, F., et al. *Addressing forecast uncertainty impact on CSP annual performance*. in *AIP Conference Proceedings*. 2017. AIP Publishing.

224. Gueymard, C.A., *A review of validation methodologies and statistical performance indicators for modeled solar radiation data: Towards a better bankability of solar projects.* Renewable and Sustainable Energy Reviews, 2014. **39**: p. 1024-1034.

225.   Kalogirou, S.A., *Solar energy engineering: processes and systems*. 2013: Academic Press.

226.   Wong, L. and W. Chow, *Solar radiation model.* Applied Energy, 2001. **69**(3): p. 191-224.

227.   Gueymard, C.A., *Direct solar transmittance and irradiance predictions with broadband models. Part I: detailed theoretical performance assessment.* Solar Energy, 2003. **74**(5): p. 355-379.

228.   Iqbal, M., *An introduction to solar radiation*. 2012: Elsevier.

229.   Atwater, M.A. and J. Ball, *A numerical solar radiation model based on standard meteorological observations.* Solar Energy, 1978. **21**(3): p. 163-170.

230.   Bird, R.E. and R.L. Hulstrom, *Simplified clear sky model for direct and diffuse insolation on horizontal surfaces*. 1981, Solar Energy Research Inst., Golden, CO (USA).

231.   Hottel, H.C.J.S.e., *A simple model for estimating the transmittance of direct solar radiation through clear atmospheres.* 1976. **18**(2): p. 129-134.

232.   Bird, R.E. and R.L.J.J.o.S.E.E. Hulstrom, *Review, evaluation, and improvement of direct irradiance models.* 1981. **103**(3): p. 182-192.

233.   Batlles, F., et al., *Comparison of cloudless sky parameterizations of solar irradianceat various Spanish midlatitude locations.* 2000. **66**(1-2): p. 81-93.

234.   Ineichen, P.J.S.E., *Comparison of eight clear sky broadband models against 16 independent data banks.* 2006. **80**(4): p. 468-478.

235. Badescu, V.J.S.E., *Verification of some very simple clear and cloudy sky models to evaluate global solar irradiance.* 1997. **61**(4): p. 251-264.

236. Gueymard, C.J.S.E., *Critical analysis and performance assessment of clear sky solar irradiance models using theoretical and measured data.* 1993. **51**(2): p. 121-138.

237. Gueymard, C.A.J.S.E., *Direct solar transmittance and irradiance predictions with broadband models. Part II: validation with high-quality measurements.* 2003. **74**(5): p. 381-395.

238. Badescu, V., et al., *Computing global and diffuse solar hourly irradiation on clear sky. Review and testing of 54 models.* 2012. **16**(3): p. 1636-1656.

239. Gueymard, C.A.J.S.E., *Clear-sky irradiance predictions for solar resource mapping and large-scale applications: Improved validation methodology and detailed performance analysis of 18 broadband radiative models.* 2012. **86**(8): p. 2145-2169.

240. Behar, O., et al., *Comparison of solar radiation models and their validation under Algerian climate–The case of direct irradiance.* 2015. **98**: p. 236-251.

241. Scarpa, F., et al., *Splitting the solar radiation in direct and diffuse components; insights and constrains on the clearness-diffuse fraction representation.* 2017. **35**(2): p. 325-329.

242. Valko, P.J.D.E.-. *An Introduction to Meteorological Measurements and Data Handling for Solar Energy Applications.* 1980.

243. Brinsfield, R., M. Yaramanoglu, and F.J.S.e. Wheaton, *Ground level solar radiation prediction model including cloud cover effects.* 1984. **33**(6): p. 493-499.

244. Tapakis, R. and A.J.S.E. Charalambides, *Equipment and methodologies for cloud detection and classification: A review.* 2013. **95**: p. 392-430.

245. Smith, C.J., J.M. Bright, and R.J.S.E. Crook, *Cloud cover effect of clear-sky index distributions and differences between human and automatic cloud observations.* 2017. **144**: p. 10-21.

246. Bone, V., et al., *Intra-hour direct normal irradiance forecasting through adaptive clear-sky modelling and cloud tracking.* 2018. **159**: p. 852-867.

247. Ahamed, M.S., H. Guo, and K.J.I.J.o.S.E. Tanino, *Evaluation of a cloud cover based model for estimation of hourly global solar radiation in Western Canada.* 2019. **38**(1): p. 64-73.

248. Muneer, T., M.J.E.C. Gul, and Management, *Evaluation of sunshine and cloud cover based models for generating solar radiation data.* 2000. **41**(5): p. 461-482.

249. Yang, D., P. Jirutitijaroen, and W.M.J.S.E. Walsh, *Hourly solar irradiance time series forecasting using cloud cover index.* 2012. **86**(12): p. 3531-3543.

250. Kasten, F. and G.J.S.e. Czeplak, *Solar and terrestrial radiation dependent on the amount and type of cloud.* 1980. **24**(2): p. 177-189.

251. Park, S.-W., et al., *An Irradiation Prediction Model for Photovoltaic Power Generations Under Limited Weather Information.* 2014. **47**(3): p. 3670-3675.

252. Kim, K.H., J.-C. Baltazar, and J.S.J.E.P. Haberl, *Evaluation of meteorological base models for estimating hourly global solar radiation in Texas.* 2014. **57**: p. 1189-1198.

253. Badescu, V. and A.J.R.e. Dumitrescu, *Simple models to compute solar global irradiance from the CMSAF product Cloud Fractional Coverage.* 2014. **66**: p. 118-131.

254. Didari, S., S.J.T. Zand-Parsa, and a. climatology, *Estimation of daily global solar irradiation under different sky conditions in central and southern Iran.* 2017. **127**(3-4): p. 587-596.

255. Yao, W., et al., *New decomposition models to estimate hourly global solar radiation from the daily value.* 2015. **120**: p. 87-99.

256. Whillier, A.J.A.f.M., Geophysik und Bioklimatologie, Serie B, *The determination of hourly values of total solar radiation from daily summations.* 1956. **7**(2): p. 197-204.

257. Liu, B.Y. and R.C.J.S.e. Jordan, *The interrelationship and characteristic distribution of direct, diffuse and total solar radiation.* 1960. **4**(3): p. 1-19.

258. Collares-Pereira, M. and A.J.S.e. Rabl, *The average distribution of solar radiation-correlations between diffuse and hemispherical and between daily and hourly insolation values.* 1979. **22**(2): p. 155-164.

259. Gueymard, C.J.S.E., *Mean daily averages of beam radiation received by tilted surfaces as affected by the atmosphere.* 1986. **37**(4): p. 261-267.

260.   Jain, P.J.S. and W. Technology, *Comparison of techniques for the estimation of daily global irradiation and a new technique for the estimation of hourly global irradiation.* 1984. **1**(2): p. 123-134.

261.   Jain, P.J.S. and w. technology, *Estimation of monthly average hourly global and diffuse irradiation.* 1988. **5**(1): p. 7-14.

262.   shazly, S.E.J.A.i.a.S., *Estimation of hourly and daily global solar radiation at clear days using an approach based on modified version of Gaussian distribution.* 1996. **13**: p. 349-358.

263.   Baig, A., P. Akhter, and A.J.R.E. Mufti, *A novel approach to estimate the clear day global radiation.* 1991. **1**(1): p. 119-123.

264.   Newell, T.J.S.E., *Simple models for hourly to daily radiation ratio correlations.* 1983. **31**(3): p. 339-342.

265.   Ahmad, M.J. and G.J.I.J.o.E.R. Tiwari, *Solar radiation models—A review.* 2011. **35**(4): p. 271-290.

266.   Mousavi Maleki, S., H. Hizam, and C.J.E. Gomes, *Estimation of hourly, daily and monthly global solar radiation on inclined surfaces: Models re-visited.* 2017. **10**(1): p. 134.

267.   Hollands, K.G.T. and R.J.S.E. Huget, *A probability density function for the clearness index, with applications.* 1983. **30**(3): p. 195-209.

268.   Ayodele, T. and A.J.E. Ogunjuyigbe, *Prediction of monthly average global solar radiation based on statistical distribution of clearness index.* 2015. **90**: p. 1733-1742.

211

269. Okogbue, E., J. Adedokun, and B.J.I.J.o.C. Holmgren, *Hourly and daily clearness index and diffuse fraction at a tropical station, Ile-Ife, Nigeria.* 2009. **29**(8): p. 1035-1047.

270. Chang, T.P.J.I.J.o.A.S. and Engineering, *Investigation on frequency distribution of global radiation using different probability density functions.* 2010. **8**(2): p. 99-107.

271. Khorasanizadeh, H., et al., *Attaining optimum tilts of flat solar surfaces utilizing measured solar data: case study for Ilam, Iran.* 2014. **5**(3).

272. Kómar, L., M.J.J.o.A. Kocifaj, and S.-T. Physics, *Statistical cloud coverage as determined from sunshine duration: a model applicable in daylighting and solar energy forecasting.* 2016. **150**: p. 1-8.

273. Sarkar, M.N.I.J.R.W., Water, and Solar, *Estimation of solar radiation from cloud cover data of Bangladesh.* 2016. **3**(1): p. 11.

274. Angstrom, A.J.Q.J.o.t.R.M.S., *Solar and terrestrial radiation. Report to the international commission for solar research on actinometric investigations of solar and atmospheric radiation.* 1924. **50**(210): p. 121-126.

275. Prescott, J.J.T.R.S.S.A., *Evaporation from a water surface in relation to solar radiation.* 1940. **46**: p. 114-118.

276. Paulescu, M., et al., *Ångström–Prescott equation: Physical basis, empirical models and sensitivity analysis.* 2016. **62**: p. 495-506.

277. Bennett, I.J.S.E., *Correlation of daily insolation with daily total sky cover, opaque sky cover and percentage of possible sunshine.* 1969. **12**(3): p. 391-393.

278.   Badescu, V.J.E., *Correlations to estimate monthly mean daily solar global irradiation: application to Romania.* 1999. **24**(10): p. 883-893.

279.   Das, A., et al., *Estimation of available global solar radiation using sunshine duration over south Korea.* 2015. **134**: p. 22-29.

280.   Poudyal, K., et al., *Estimation of global solar radiation using sunshine duration in Himalaya Region.* 2012. **2**(11): p. 20-25.

281.   Okonkwo, G.N., A.O.C.J.I.J.o.R. Nwokoye, and S. Energy, *Relationship between global solar radiation and sunshine hour duration for Bida in Nigeria.* 2014. **3**(2): p. 43-46.

282.   Abdalla, Y.A.J.I.J.o.S.E., *New correlations of global solar radiation with meteorological parameters for Bahrain.* 1994. **16**(2): p. 111-120.

283.   Jahani, B., et al., *Evaluation and development of empirical models for estimating daily solar radiation.* 2017. **73**: p. 878-891.

284.   Jemaa, A.B., et al., *Estimation of global solar radiation using three simple methods.* 2013. **42**: p. 406-415.

285.   Soufi, A., et al., *Investigating the Performance of Chosen Models for the Estimation of Global Solar Radiation on Horizontal Surface-A Case Study in Terny Hdiel, Tlemcen of Algeria.* 2014. **7**(3): p. 45-49.

286.   Jong, R.D. and D.J.C.J.o.P.S. Stewart, *Estimating global solar radiation from common meteorological observations in western Canada.* 1993. **73**(2): p. 509-518.

287.   Hargreaves, G.H., Z.A.J.J.o.t.i. Samani, and D. Division, *Estimating potential evapotranspiration.* 1982. **108**(3): p. 225-230.

213

288. Elagib, N.A., et al., *New empirical models for global solar radiation over Bahrain.* 1998. **39**(8): p. 827-835.

289. Black, J.J.A.f.M., Geophysik und Bioklimatologie, Serie B, *The distribution of solar radiation over the earth's surface.* 1956. **7**(2): p. 165-189.

290. Gopinathan, K.J.S. and w. technology, *A new model for estimating total solar radiation.* 1988. **5**(1): p. 107-109.

291. Orgill, J. and K.J.S.e. Hollands, *Correlation equation for hourly diffuse radiation on a horizontal surface.* 1977. **19**(4): p. 357-359.

292. Erbs, D., S. Klein, and J.J.S.e. Duffie, *Estimation of the diffuse radiation fraction for hourly, daily and monthly-average global radiation.* 1982. **28**(4): p. 293-302.

293. Spencer, J.J.S.E., *A comparison of methods for estimating hourly diffuse solar radiation from global solar radiation.* 1982. **29**(1): p. 19-32.

294. Reindl, D.T., W.A. Beckman, and J.A.J.S.e. Duffie, *Diffuse fraction correlations.* 1990. **45**(1): p. 1-7.

295. Lam, J.C., D.H.J.B. Li, and environment, *Correlation between global solar radiation and its direct and diffuse components.* 1996. **31**(6): p. 527-535.

296. Gopinathan, K.J.S.E., *Empirical correlations for diffuse solar radiation.* 1988. **40**(4): p. 369-370.

297. Oliveira, A.P., et al., *Correlation models of diffuse solar-radiation applied to the city of Sao Paulo, Brazil.* 2002. **71**(1): p. 59-73.

298. Jamil, B., A.T.J.J.o.A. Siddiqui, and S.-T. Physics, *Generalized models for estimation of diffuse solar radiation based on clearness index and sunshine*

214

duration in India: Applicability under different climatic zones. 2017. **157**: p. 16-34.

299. Li, H., et al., *Further investigation of empirically derived models with multiple predictors in estimating monthly average daily diffuse solar radiation over China.* 2012. **44**: p. 469-473.

300. Mefti, A., et al., *Generation of hourly solar radiation for inclined surfaces using monthly mean sunshine duration in Algeria.* 2003. **44**(19): p. 3125-3141.

301. Noorian, A.M., I. Moradi, and G.A.J.R.e. Kamali, *Evaluation of 12 models to estimate hourly diffuse irradiation on inclined surfaces.* 2008. **33**(6): p. 1406-1412.

302. Gueymard, C.A.J.S.E., *Direct solar transmittance and irradiance predictions with broadband models. Part I: detailed theoretical performance assessment.* 2003. **74**(5): p. 355-379.

303. Soulayman, S., *Economical and Technical Considerations for Solar Tracking: Methodologies and Opportunities for Energy Management: Methodologies and Opportunities for Energy Management.* 2017: IGI Global.

304. Solar Energy Laboratory, T.U.o.T.a.A., *National Solar Radiation Data Base Sites for Texas.* Retrieved April, 2019. Available online: http://www.me.utexas.edu (accessed on 20 April 2019).

305. Local, S.E. *Solar Energy Local, Solar Data, Statistics & Information*, Retrieved April, 2019. Available online: https://www.solarenergylocal.com/ (accessed on 20 April 2019).

APPENDIX A

Solar data for case study:

The solar data for Eagle Ford Shale Play as extracted from National Solar Radiation

Data Base (NSRDB) are shown in Tables A1–A4 to represent:

- Average hourly dry bulb temperature (^{o}C)

- Average hourly wet bulb temperature (^{o}C)

- Average hourly direct solar irradiance (W/m^2)

- Average hourly solar incidence angle (degree).

The solar beam radiation is 500 (W/m^2) at the design point.

Table A1: Average hourly dry bulb temperature ($°C$)

Hour \ Month	January	February	March	April	May	June	July	August	September	October	November	December
0.5	7.1	8.1	13.4	17.3	20.9	23.6	13.4	25.1	24.1	18.9	13.1	8.2
1.5	6.6	7.71	13.0	16.9	20.4	23.3	13.0	24.5	23.6	18.2	12.6	7.7
2.5	6.1	7.24	12.6	16.4	19.9	23.1	12.6	24.0	23.2	17.4	12.3	7.36
3.5	6.0	6.98	12.3	16.2	19.6	23.0	12.3	23.6	22.9	17.1	11.6	7.11
4.5	5.9	6.74	12.0	16.0	19.3	22.8	12.0	23.2	22.6	16.8	11.4	7.13
5.5	5.9	6.49	11.7	15.8	19.0	22.8	11.7	22.8	22.4	16.5	11.3	6.96
6.5	5.5	7.37	12.6	16.8	20.1	23.3	12.6	24.2	22.4	17.9	10.9	7.03
7.5	5.4	8.28	13.5	17.8	21.2	24.6	13.5	25.6	23.7	19.3	11.8	7.21
8.5	7.7	9.20	14.5	18.8	22.3	26.0	14.5	27.0	25.6	20.6	14.0	9.10
9.5	10	11.1	16.2	20.1	23.4	27.3	16.2	28.5	27.0	22.1	16.3	11.0
10.5	12	13.0	17.9	21.4	24.5	28.4	17.9	30.1	28.2	23.6	18.0	12.8
11.5	13	14.9	19.6	22.7	25.6	29.4	19.6	31.6	29.4	25.2	19.3	14.1
12.5	14	15.7	20.5	23.5	26.2	30.4	20.5	32.4	30.3	25.8	20.3	15.1
13.5	15	16.6	21.4	24.4	26.8	31.3	21.4	33.3	30.7	26.5	21.1	16.0
14.5	15	17.5	22.3	25.2	27.5	31.4	22.3	34.1	31.0	27.2	21.3	16.4
15.5	16	17.0	21.7	24.8	27.4	31.7	21.7	33.5	31.2	26.5	21.2	16.5
16.5	15	16.5	21.2	24.4	27.4	31.2	21.2	32.9	31.0	25.8	20.5	16.0
17.5	13	16.1	20.7	23.9	27.3	30.4	20.7	32.3	30.2	25.1	19.0	14.4
18.5	12	14.6	19.1	22.5	26.1	29.0	19.1	30.9	28.8	24.0	17.3	12.7
19.5	10.9	13.21	17.5	21.2	24.95	27.64	17.5	29.53	27.76	22.88	15.84	11.2
20.5	9.73	11.77	16.0	19.8	23.7	26.47	16.0	28.10	26.68	21.75	14.63	10.3
21.5	8.63	10.79	15.3	19.2	23.0	25.44	15.3	27.30	25.93	21.00	13.95	9.77
22.5	7.91	9.825	14.5	18.5	22.3	24.75	14.5	26.46	25.36	20.25	13.45	9.55
	7.56	8.846	13.8	17.7	21.5	24.0	13.8	25.6	24.7	19.6	13.30	9.31

Table A2: Average hourly wet bulb temperature (°C)

Hour \ Month	January	February	March	April	May	June	July	August	September	October	November	December
0.5	5.7	6.3	9.85	15.3	18.5	21.6	22.9	22.0	21.5	16.3	11.4	6.41
1.5	5.4	6.0	9.69	15.1	18.3	21.5	22.8	22.0	21.3	15.9	11.1	6.03
2.5	4.9	5.7	9.52	14.9	18.0	21.4	22.7	21.9	21.2	15.4	10.8	5.75
3.5	4.9	5.5	9.43	14.7	17.8	21.4	22.7	21.8	21.0	15.1	10.2	5.55
4.5	4.8	5.3	9.35	14.6	17.6	21.4	22.6	21.6	20.9	14.9	10.1	5.56
5.5	4.8	5.0	9.21	14.5	17.4	21.4	22.6	21.4	20.8	14.6	10.0	5.40
6.5	4.5	5.7	9.64	15.1	18.1	21.7	22.9	22.0	20.8	15.6	9.78	5.44
7.5	4.3	6.3	10.0	15.7	18.8	22.2	23.3	22.6	21.4	16.4	10.3	5.60
8.5	6.1	7.0	10.4	16.3	19.4	22.6	23.4	23.1	22.0	17.2	11.6	6.99
9.5	7.5	8.0	11.3	17.0	19.8	22.7	23.6	23.4	22.2	17.8	12.7	8.08
10.5	8.4	8.9	12.0	17.6	20.1	22.8	23.6	23.4	22.2	18.3	13.3	8.90
11.5	9.1	9.6	12.5	18.1	20.4	23.0	23.5	23.3	22.1	18.7	13.8	9.42
12.5	9.5	10	12.7	18.4	20.7	23.0	23.5	23.3	22.3	18.8	14.0	9.82
13.5	10	10	12.9	18.6	21.0	23.2	23.5	23.2	22.2	18.9	14.2	10.1
14.5	10	10	13.0	18.8	21.2	22.9	23.5	23.0	22.1	19.0	14.1	10.3
15.5	10	10	12.8	18.5	21.1	22.9	23.4	22.8	22.0	18.7	14.1	10.2
16.5	9.8	10	12.5	18.3	20.9	22.8	23.3	22.6	22.0	18.5	13.8	10.0
17.5	9.2	9.8	12.2	18.1	20.7	22.7	23.3	22.3	22.0	18.2	13.3	9.39
18.5	8.6	9.4	11.9	17.6	20.5	22.4	23.4	22.4	21.8	18.0	12.7	8.72
19.5	8.0	8.9	11.4	17.1	20.2	22.3	23.4	22.4	21.8	17.7	12.2	8.13
20.5	7.4	8.3	10.8	16.5	19.8	22.1	23.2	22.1	21.6	17.3	11.7	7.78
21.5	6.9	7.9	10.6	16.3	19.5	22.0	23.2	22.2	21.6	17.1	11.4	7.50
22.5	6.4	7.4	10.3	16.0	19.2	21.9	23.1	22.1	21.6	16.9	11.3	7.37
23.5	6.1	6.8	9.91	15.5	18.7	21.7	22.9	21.9	21.6	16.7	11.4	7.30

218

Table A3: Average hourly direct solar irradiance (w/m^2)

Month Hour	January	February	March	April	May	June	July	August	September	October	November	December
0.5	0	0	0	0	0	0	0	0	0	0	0	0
1.5	0	0	0	0	0	0	0	0	0	0	0	0
2.5	0	0	0	0	0	0	0	0	0	0	0	0
3.5	0	0	0	0	0	0	0	0	0	0	0	0
4.5	0	0	0	0	0	0	0	0	0	0	0	0
5.5	0	0	0	0	5.1	3.8	1	0.0	0	0	0	0
6.5	0	0	9.6	26	109	86	65	57	34	26	1.8	0
7.5	48	95	140	145	216	164	236	229	184	221	171	49
8.5	240	244	287	228	258	319	350	347	315	337	328	199
9.5	339	346	365	281	318	377	467	463	450	460	388	272
10.5	396	413	413	352	362	470	550	524	516	497	462	359
11.5	415	487	478	394	383	496	630	573	557	553	545	389
12.5	473	468	498	439	462	526	621	599	569	566	544	459
13.5	457	474	481	461	460	545	603	600	521	542	504	489
14.5	415	440	417	467	445	520	576	540	540	544	481	499
15.5	397	433	380	473	503	489	529	539	493	498	437	440
16.5	283	365	323	414	434	475	536	417	422	401	361	323
17.5	128	246	234	338	356	389	427	323	311	181	93	80
18.5	0.4	32	54	119	166	217	234	140	53	3.6	0	0
19.5	0	0	0	0.1	7.2	21	24	4.3	0	0	0	0
20.5	0	0	0	0	0	0	0	0	0	0	0	0
21.5	0	0	0	0	0	0	0	0	0	0	0	0
22.5	0	0	0	0	0	0	0	0	0	0	0	0
23.5	0	0	0	0	0	0	0	0	0	0	0	0

Table A4: Average hourly solar incidence angle (degree)

Hour \ Month	January	February	March	April	May	June	July	August	September	October	November	December
0.5	0	0	0	0	0	0	0	0	0	0	0	0
1.5	0	0	0	0	0	0	0	0	0	0	0	0
2.5	0	0	0	0	0	0	0	0	0	0	0	0
3.5	0	0	0	0	0	0	0	0	0	0	0	0
4.5	0	0	0	0	0	0	0	0	0	0	0	0
5.5	0	0	0	0	0	0	0	0	0	0	0	0
6.5	0	0	0	6.04	16.1	20.2	19.2	11.1	0	0	0	0
7.5	0	4.33	7.10	2.51	9.26	13.4	12.3	5.49	4.95	16.1	23.4	0
8.5	30.6	23.6	14.3	4.99	2.85	6.99	5.77	2.49	11.8	23.4	31.8	34.4
9.5	37.8	30.5	20.7	10.9	2.76	1.52	1.14	7.13	18.0	29.8	38.5	41.4
10.5	43.8	36.3	26.1	15.6	7.01	2.69	4.28	11.8	22.9	35.0	44.0	47.1
11.5	48.2	40.6	30.0	18.7	9.73	5.40	7.20	14.9	26.3	38.4	47.6	51.1
12.5	50.2	42.7	31.8	20.0	10.7	6.44	8.40	16.2	27.5	39.3	48.5	52.6
13.5	49.5	42.1	31.0	19.0	9.79	5.70	7.78	15.3	26.2	37.5	46.5	51.1
14.5	46.1	39.0	27.8	16.0	7.06	3.20	5.40	12.7	22.8	33.4	42.2	47.2
15.5	40.7	34.0	22.9	11.5	2.79	0.83	1.58	8.49	17.8	27.8	36.2	41.4
16.5	34.0	27.7	16.9	5.74	2.83	6.15	3.82	3.07	11.7	21.1	29.2	34.4
17.5	21.1	20.4	9.96	2.65	9.23	12.4	10.1	3.61	4.78	11.5	0	0
18.5	0	0	0.17	8.06	16.1	19.2	16.9	10.5	0.99	0	0	0
19.5	0	0	0	0	0	0	0	0	0	0	0	0
20.5	0	0	0	0	0	0	0	0	0	0	0	0
21.5	0	0	0	0	0	0	0	0	0	0	0	0
22.5	0	0	0	0	0	0	0	0	0	0	0	0
23.5	0	0	0	0	0	0	0	0	0	0	0	0

Table B: Extracted stream data for the fractionation process from simulated flowsheet

Stream Name	First Feed (from well)	Second Stream (from dehydration unit)	3	4	5	6	7	8	9	10	11	12	13	14	15
Pressure (bar)	30	30	30	26	18	19.8	17	16	17.8	10	9	10.8	5	4	6.9
Temperature (ºC)	25	25	24.8	25.0	41.8	246.6	241.0	61.4	244.2	56.4	27.7	77.6	46.1	29.1	62.2
Mass Flow Rate (kg/hr)	25000	8000	33000	33000	1490	31510	31510	519.	30990	519	299	220	220	100	120
Mole Fraction (Methane)	0.097	0.13	0.108	0.108	0.609	0	0	0	0	0	0	0	0	0	0
Mole Fraction (Ethane)	0.029	0.08	0.046	0.046	0.263	0	0	0.00	0	0.00	0.00	0	0	0	0
Mole Fraction (Propane)	0.035	0.1	0.057	0.057	0.091	0.050	0.050	0.64	0.027	0.64	0.99	0.00	0.00	0.01	0
Mole Fraction (i-Butane)	0.018	0.055	0.030	0.030	0.009	0.035	0.035	0.16	0.030	0.16	0.00	0.46	0.46	0.96	0.04
Mole Fraction (n-Butane)	0.028	0.113	0.057	0.058	0.013	0.067	0.067	0.16	0.063	0.16	0	0.47	0.47	0.02	0.86
Mole Fraction (i-Pentane)	0.026	0.104	0.053	0.053	0.005	0.063	0.063	0.01	0.065	0.01	0	0.03	0.03	0	0.07
Mole Fraction (n-Pentane)	0.025	0.091	0.048	0.048	0.003	0.057	0.057	0.00	0.059	0.00	0	0.01	0.01	0	0.02
Mole Fraction (n-Hexane)	0.064	0.122	0.084	0.084	0.002	0.102	0.102	0	0.106	0	0	0.00	0.00	0	0.00
Mole Fraction (n-Heptane)	0.09	0.11	0.097	0.097	0.000	0.117	0.117	0	0.122	0	0	0	0	0	0
Mole Fraction (n-Octane)	0.15	0.072	0.122	0.122	0.000	0.149	0.149	0	0.154	0	0	0	0	0	0
Mole Fraction (n-Nonane)	0.11	0.02	0.078	0.078	0.000	0.095	0.095	0	0.099	0	0	0	0	0	0
Mole Fraction (n-Decane)	0.09	0.003	0.059	0.059	0	0.072	0.072	0	0.075	0	0	0	0	0	0
Mole Fraction (n-C11)	0.079	0	0.051	0.051	0	0.062	0.062	0	0.064	0	0	0	0	0	0
Mole Fraction (n-C12)	0.071	0	0.046	0.046	0	0.056	0.056	0	0.058	0	0	0	0	0	0
Mole Fraction (n-C13)	0.031	0	0.020	0.020	0	0.024	0.024	0	0.025	0	0	0	0	0	0

Stream Name	First Feed (from well)	Second Stream (from dehydration unit)	3	4	5	6	7	8	9	10	11	12	13	14	15
Mole Fraction (n-C14)	0.023	0	0.014	0.014	0	0.018	0.018	0	0.018	0	0	0	0	0	0
Mole Fraction (n-C15)	0.018	0	0.011	0.011	0	0.014	0.014	0	0.014	0	0	0	0	0	0
Mole Fraction (n-C16)	0.014	0	0.009	0.009	0	0.011	0.011	0	0.011	0	0	0	0	0	0
H_2O	0.002	0	0.001	0.001	0	0.001	0.001	0	0.001	0	0	0	0	0	0

APPENDIX C

Table C1:January

Model	MBE	RMSE	MAPE	R^2	t-statistics
Fu & Rich	-223.1	344.7	-29.5	0.61	4.0
DPP	-13.7	44.3	-2.2	0.99	1.5
Meinel	-57.1	93.2	-7.8	0.97	3.7
Laue	-47.4	80.7	-6.5	0.97	3.4
Haurwitz	-162.1	252.2	-21.8	0.79	4.0
Berger &Duffie	-166.2	258.6	-22.1	0.78	4.0
ABCG	-180.8	280.6	-24.0	0.74	4.0
Kasten & Czeplak	-183.4	283.1	-24.3	0.73	4.1
Robledo & Sole	-162.3	253.2	-21.8	0.79	4.0
ASHRAE	8.8	53.1	0.56	0.99	0.8
Kumer	-23.9	59.0	-3.6	0.98	2.12
HLJ	23.8	73.2	2.4	0.98	1.65
Bird	-13.9	55.0	-2.2	0.99	1.2
Iqbal Model C	-11.0	52.9	-1.8	0.99	1.0
METSTAT	0.98	49.5	-0.26	0.99	0.09
Modified Iqbal Model C	15.6	57.0	1.7	0.98	1.3
CSR	21.3	55.0	2.3	0.99	2.0
Atwater and Ball	-104.0	192.6	-15.6	0.87	3.07
ESRA	-13.8	49.6	-2.2	0.90	1.3
Hoyt (Iqbal model B)	-52.0	89.1	-7.4	0.97	3.4
Heliosat-1	-14.7	50.0	-2.3	0.99	1.4
Davies and Hay (Iqbal model A)	-71.9	137.9	-11.3	0.93	2.9

Table C2: February

Model	MBE	RMSE	MAPE	R^2	t-statistics
Fu & Rich	-176.4	267.2	-24.2	0.51	4.2
DPP	39.5	69.5	4.9	0.96	3.3
Meinel	-2.6	35.6	-0.14	0.99	0.36
Laue	7.34	40.4	0.95	0.98	0.88
Haurwitz	-101.3	157.5	-14.2	0.83	4.0
Berger &Duffie	-110.2	172.1	-15.4	0.79	3.9
ABCG	-124.8	192.9	-17.3	0.74	4.0
Kasten & Czeplak	-130.6	199.5	-17.8	0.72	4.15
Robledo & Sole	-102.2	160.2	-14.5	0.82	3.9
ASHRAE	59.1	93.1	8.6	0.94	3.9
Kumer	36.4	59.2	4.1	0.97	3.7
HLJ	83.7	138.3	8.8	0.86	3.6
Bird	44.2	87.3	4.7	0.94	2.8
Iqbal Model C	47.5	89.9	5.2	0.94	2.9
METSTAT	60.5	140.7	6.8	0.92	3.3
Modified Iqbal Model C	74.7	126.0	8.5	0.89	3.5
CSR	83.9	129.5	9.8	0.88	4.0
Atwater and Ball	-35.5	99.2	-6.4	0.93	1.8
ESRA	50.8	86.2	5.8	0.94	3.5
Hoyt (Iqbal model B)	11.5	30.2	1.7	0.99	1.9
Heliosat-1	45.2	79.4	5.1	0.95	3.3
Davies and Hay (Iqbal model A)	-4.8	57.3	-0.9	0.97	0.4

Table C3: March

Model	MBE	RMSE	MAPE	R^2	t-statistics
Fu & Rich	193.2	281.5	-21.6	0.53	4.5
DPP	18.2	41.6	1.3	0.98	2.3
Meinel	-8.6	22.8	-0.9	0.99	0.9
Laue	2.5	24.0	-0.1	0.99	0.5
Haurwitz	-111.7	172.0	-12.5	0.82	4.0
Berger &Duffie	-115.3	175.0	-13.2	0.81	4.2
ABCG	-138.6	207.7	-15.7	0.74	4.2
Kasten & Czeplak	-147.2	216.9	-16.5	0.72	4.4
Robledo & Sole	-113.5	174.6	-12.9	0.82	4.1
ASHRAE	21.2	36.8	2.7	0.99	3.3
Kumer	37.4	55.9	3.4	0.89	4.3
HLJ	9.3	141.7	6.6	0.88	3.9
Bird	41.8	83.0	2.3	0.95	2.8
Iqbal Model C	45.6	85.5	2.8	0.95	3.0
METSTAT	59.9	101.2	4.1	0.93	3.5
Modified Iqbal Model C	75.8	123.5	5.4	0.91	3.7
CSR	86.4	127.6	6.9	0.90	4.4
Atwater and Ball	-37.3	107.0	-3.1	0.93	1.7
ESRA	93.2	61.4	3.2	0.97	3.9
Hoyt (Iqbal model B)	-13.4	21.9	-1.2	0.99	3.7
Heliosat-1	37.0	58.9	3.1	0.97	3.8
Davies and Hay (Iqbal model A)	-28.3	81.6	-1.5	0.96	1.7

Table C4:April

Model	MBE	RMSE	MAPE	R^2	t-statistics
Fu & Rich	-91.8	155.5	-13.4	0.82	3.5
Meinel	95.8	172.0	9.0	0.78	3.2
Laue	108.3	183.8	9.9	0.75	3.4
Haurwitz	20.3	81.9	0.3	0.95	1.2
Berger &Duffie	1.7	81.6	-2.4	0.95	0.1
ABCG	-12.0	83.5	-4.0	0.95	0.6
Kasten & Czeplak	-28.3	91.9	-5.6	0.93	1.5
Robledo & Sole	15.2	79.6	-0.4	0.95	0.9
ASHRAE	103.8	181.1	10.6	0.76	3.3
Kumer	154.5	226.5	15.5	0.63	4.4
HLJ	178.5	270.5	15.0	0.47	4.6
Bird	143.1	227.0	10.4	0.63	3.8
Iqbal Model C	147.3	230.6	10.9	0.62	3.9
METSTAT	126.9	248.3	12.3	0.56	4.1
Modified Iqbal Model C	181.1	271.5	13.9	0.47	4.2
CSR	188.5	272.8	15.2	0.47	4.5
Atwater and Ball	60.5	114.5	7.0	0.90	2.9
ESRA	-46.8	155.6	-9.8	0.82	1.5
Hoyt (Iqbal model B)	65.9	135.0	6.1	0.87	2.6
Heliosat-1	123.4	202.9	11.7	0.70	3.6
Davies and Hay (Iqbal model A)	62.8	128.3	7.5	0.88	2.6
DDP	128.7	215.6	12.5	0.66	3.5

226

Table C5: May

Model	MBE	RMSE	MAPE	R^2	t-statistics
Fu & Rich	-76.1	137.2	-7.1	0.82	3.1
DPP	158.7	233.3	22.1	0.49	4.4
Meinel	113.9	182.2	17.2	0.96	3.8
Laue	125.6	193.0	18.2	0.65	4.1
Haurwitz	48.9	135.5	10.1	0.82	1.8
Berger &Duffie	22.5	103.3	5.5	0.9	1.1
ABCG	15.4	108.9	4.8	0.88	0.6
Kasten & Czeplak	-1.5	97.9	2.6	0.91	0.1
Robledo & Sole	43.1	125.5	9.0	0.85	1.7
ASHRAE	106.1	177.2	17.1	0.70	3.5
Kumer	174.1	246.5	24.9	0.43	4.7
HLJ	198.0	271.6	23.8	0.31	5.1
Bird	145.6	212.7	18.3	0.57	4.5
Iqbal Model C	149.7	217.1	18.8	0.56	4.5
METSTAT	163.9	133.5	20.4	0.49	4.7
Modified Iqbal Model C	182.8	256.7	22.1	0.38	4.8
CSR	192.1	256.1	24.2	0.34	5.0
Atwater and Ball	72.3	171.9	16.4	0.72	2.2
ESRA	-69.1	143.7	-6.8	0.80	2.6
Hoyt (Iqbal model B)	87.2	156.1	15.2	0.77	3.2
Heliosat-1	144.4	210.5	20.0	0.58	4.5
Davies and Hay (Iqbal model A)	83.6	174.2	17.4	0.71	2.6

Table C6: June

Model	MBE	RMSE	MAPE	R^2	t-statistics
Fu & Rich	-116.1	170.8	-11.7	0.77	4.4
DPP	115.9	162.6	9.3	0.79	4.8
Meinel	85.0	126.5	7.4	0.87	4.3
Laue	96.7	138.8	8.2	0.84	4.6
Haurwitz	5.8	115.6	2.0	0.89	0.2
Berger &Duffie	-10.7	96.9	-0.6	0.92	0.5
ABCG	-28.6	111.4	-2.2	0.90	1.2
Kasten & Czeplak	-46.0	108.4	-4.3	0.90	2.2
Robledo & Sole	-0.79	107.4	1.0	0.90	0.1
ASHRAE	48.8	89.6	4.3	0.93	3.1
Kumer	147.7	199.1	13.9	0.69	5.3
HLJ	166.9	223.3	12.6	0.61	5.3
Bird	110.6	157.5	7.7	0.80	4.7
Iqbal Model C	114.9	162.0	8.1	0.79	4.8
METSTAT	129.4	179.1	9.3	0.74	5.1
Modified Iqbal Model C	149.8	205.4	10.8	0.67	5.1
CSR	158.5	212.8	12.4	0.64	5.4
Atwater and Ball	33.7	131.8	7.1	0.86	1.2
ESRA	-182.9	225.9	20.3	0.48	4.9
Hoyt (Iqbal model B)	35.1	75.6	3.7	0.95	2.5
Heliosat-1	112.2	154.3	9.3	0.81	5.1
Davies and Hay (Iqbal model A)	38.2	92.4	5.7	0.93	2.1

Table C7: July

Model	MBE	RMSE	MAPE	R^2	t-statistics
Fu & Rich	-91.5	146.1	0	0.81	3.8
DPP	136.7	184.4	13.0	0.70	5.2
Meinel	108.3	151.2	11.2	0.80	4.9
Laue	120.2	164.2	12.0	0.76	5.1
Haurwitz	27.4	125.7	4.9	0.86	1.1
Berger &Duffie	12.7	102.2	2.2	0.90	0.6
ABCG	6.6	111.0	0.3	0.98	0.2
Kasten & Czeplak	-23.9	100.0	-1.8	0.91	1.2
Robledo & Sole	21.1	115.5	3.8	0.88	0.8
ASHRAE	86.3	102.9	7.4	0.90	4.2
Kumer	170.4	227.5	18.1	0.55	5.4
HLJ	192.6	251.9	16.8	0.45	5.6
Bird	136.9	184.4	11.6	0.70	5.3
Iqbal Model C	141.2	189.3	12.1	0.69	5.3
METSTAT	155.9	207.2	13.4	0.62	5.4
Modified Iqbal Model C	176.2	233.7	15.0	0.52	5.5
CSR	184.6	240.8	16.7	0.49	5.7
Atwater and Ball	59.8	141.9	-1.4	0.82	2.2
ESRA	-137	201.3	-16.1	0.64	4.4
Hoyt (Iqbal model B)	85.6	93.7	7.1	0.92	3.8
Heliosat-1	143.7	181.1	13.4	0.71	5.3
Davies and Hay (Iqbal model A)	59.6	111.3	9.3	0.89	3.1

Table C8: August

Model	MBE	RMSE	MAPE	R^2	t-statistics
Fu & Rich	-70.6	173.1	16.1	0.74	2.1
DPP	156.4	264.4	93.0	0.41	3.5
Meinel	114.6	219.4	78.9	0.59	2.9
Laue	125.1	228.6	81.4	0.56	3.1
Haurwitz	47.6	169.7	46.5	0.75	1.4
Berger &Duffie	22.5	149.6	40.6	0.81	0.7
ABCG	15.0	151.3	36.6	0.80	0.4
Kasten & Czeplak	0.3	146.0	34.5	0.82	0
Robledo & Sole	42.4	163.3	45.1	0.77	1.3
ASHRAE	104.0	212.6	87.0	0.62	2.6
Kumer	170.4	273.3	92.3	0.37	3.8
HLJ	187.5	291.3	95.2	0.28	4.0
Bird	139.1	242.5	83.1	0.50	3.3
Iqbal Model C	143.0	246.2	84.3	0.49	3.4
METSTAT	156.4	260.3	88.1	0.43	3.6
Modified Iqbal Model C	174.5	281.0	93.1	0.33	3.8
CSR	182.1	286.1	95.7	0.30	3.9
Atwater and Ball	73.9	198.0	66.6	0.67	1.9
ESRA	-106.7	216.2	8.8	0.60	2.7
Hoyt (Iqbal model B)	82.6	194.0	70.4	0.68	2.2
Heliosat-1	137.6	239.8	84.0	0.51	3.3
Davies and Hay (Iqbal model A)	82.6	202.8	72.9	0.65	2.1

Table C9: September

Model	MBE	RMSE	MAPE	R^2	t-statistics
Fu & Rich	-130.9	191.6	-16.4	0.71	4.5
DPP	81.4	114.6	9.2	0.89	4.8
Meinel	58.6	82.9	7.1	0.94	4.8
Laue	69.3	96.4	8.1	0.92	4.9
Haurwitz	-42.3	96.6	-5.3	0.92	2.3
Berger &Duffie	-45.8	90.3	-6.1	0.93	2.8
ABCG	-71.1	120.4	-9.2	0.88	3.5
Kasten & Czeplak	-81.8	127.2	-10.4	0.87	4.3
Robledo & Sole	-44.9	96.6	-5.8	0.92	2.5
ASHRAE	59.1	89.4	7.8	0.93	4.2
Kumer	111.9	155.7	13.0	0.81	4.9
HLJ	130.7	182.5	13.4	0.73	4.9
Bird	86.7	123.1	8.9	0.88	4.7
Iqbal Model C	90.5	127.7	9.4	0.87	4.8
METSTAT	103.8	145.6	10.9	0.83	4.8
Modified Iqbal Model C	181.8	171.1	12.7	0.77	4.8
CSR	128.3	176.7	13.9	0.75	5.0
Atwater and Ball	12.5	112.2	2.3	0.90	0.5
ESRA	-89.3	143.4	-11.6	0.85	4.2
Hoyt (Iqbal model B)	10.8	38.6	2.1	0.98	1.4
Heliosat-1	88.4	121.7	9.8	0.88	5.0
Davies and Hay (Iqbal model A)	12.8	66.8	2.5	0.96	0.94

Table C10: October

Model	MBE	RMSE	MAPE	R^2	t-statistics
Fu & Rich	-207.1	301.3	-22.9	0.45	4.5
DPP	13.7	26.8	0.8	0.99	2.8
Meinel	-31.4	46.1	-3.5	0.98	4.4
Laue	-20.7	35.3	-2.6	0.99	3.4
Haurwitz	-117.5	184.1	-13.0	0.79	3.9
Berger &Duffie	-132.9	200.3	14.9	0.76	4.2
ABCG	-144.1	217.4	-16.1	0.71	4.2
Kasten & Czeplak	-152.9	225.6	-16.9	0.69	4.4
Robledo & Sole	-119.1	186.2	-13.3	0.79	3.9
ASHRAE	17.7	35.0	2.2	0.99	2.8
Kumer	17.3	38.0	1.2	0.99	2.4
HLJ	63.4	112.5	3.9	0.92	3.2
Bird	4.7	58.4	-1.2	0.97	0.4
Iqbal Model C	8.2	57.7	-0.8	0.98	0.7
METSTAT	121.1	36.5	0.4	0.97	1.6
Modified Iqbal Model C	37.5	80.0	1.9	0.69	2.5
CSR	43.4	75.9	2.7	0.96	3.3
Atwater and Ball	-74.8	153.5	-7.8	0.85	2.6
ESRA	-95.1	144.4	-11.0	0.87	0.1
Hoyt (Iqbal model B)	-47.4	71.0	-4.9	0.96	4.3
Heliosat-1	2.8	31.4	-0.6	0.99	0.4
Davies and Hay (Iqbal model A)	-54.6	112.9	-6.0	0.92	2.6

Table C11: November

Model	MBE	RMSE	MAPE	R^2	t-statistics
Fu & Rich	179.1	286.9	-27.2	0.43	3.8
DPP	24.4	66.7	4.0	0.96	1.8
Meinel	-1.7	50.7	-1.5	0.98	0.1
Laue	9.2	55.1	0.6	0.97	0.8
Haurwitz	-122.2	201.4	-19.4	0.72	3.6
Berger &Duffie	-116.9	196.2	-17.8	0.73	3.5
ABCG	-142.1	233.1	-21.6	0.62	3.6
Kasten & Czeplak	-145.1	236.1	-22.3	0.61	3.7
Robledo & Sole	-122.7	203.7	-19.1	0.71	3.6
ASHRAE	39.4	71.2	2.8	0.96	3.1
Kumer	43.9	75.2	5.0	0.96	2.5
HLJ	82.2	142.7	17.8	0.86	3.3
Bird	39.2	91.2	8.5	0.94	2.2
Iqbal Model C	42.3	93.4	8.9	0.94	2.4
METSTAT	55.0	106.8	11.2	0.92	2.8
Modified Iqbal Model C	71.0	129.1	14.5	0.88	3.1
CSR	94.2	126.6	14.1	0.89	3.4
Atwater and Ball	-50.3	122.2	-11.3	0.89	2.1
ESRA	28.0	80.4	5.4	0.95	1.7
Hoyt (Iqbal model B)	-20.1	57.4	-5.7	0.97	1.8
Heliosat-1	39.1	48.5	7.2	0.95	2.5
Davies and Hay (Iqbal model A)	-37.3	87.5	-9.0	0.95	2.5

<p align="center">***Table C12***: December</p>

Model	MBE	RMSE	MAPE	R^2	t-statistics
Fu & Rich	-167.9	277.9	-27.6	0.34	3.9
DPP	26.6	59.1	3.5	0.97	2.4
Meinel	-0.7	49.1	-1.2	0.97	0.1
Laue	9.6	48.6	0.6	0.98	0.9
Haurwitz	-123.5	198.3	-19.8	0.66	3.8
Berger &Duffie	-116.9	188.6	-18.4	0.70	3.7
ABCG	-141.4	224.1	-22.1	0.57	3.8
Kasten & Czeplak	-134.7	225.8	-22.5	0.57	3.9
Robledo & Sole	-123.5	198.8	-19.6	0.67	3.8
ASHRAE	48.4	98.8	5.6	0.91	2.7
Kumer	32.8	57.7	4.2	0.95	2.3
HLJ	86.3	138.6	14.0	0.83	3.8
Bird	43.3	76.9	6.8	0.95	3.2
Iqbal Model C	46.3	80.6	7.3	0.94	3.4
METSTAT	59.1	96.6	9.3	0.92	3.7
Modified Iqbal Model C	75.7	118.8	12.2	0.88	3.9
CSR	77.1	121.3	12.0	0.87	3.9
Atwater and Ball	-58.0	165.3	-11.7	0.77	1.8
ESRA	36.4	69.7	5.6	0.95	2.9
Hoyt (Iqbal model B)	-17.8	61.4	-4.1	0.96	1.4
Heliosat-1	41.6	76.0	6.2	0.95	3.1
Davies and Hay (Iqbal model A)	-37.6	112.7	-8.3	0.89	1.7

APPENDIX D

VITA

Fadhil Al-Aboosi holds a bachelor's degree and master's degree in Nuclear Engineering from Baghdad University. His undergraduate studies involved three years of Chemical Engineering which gave him a great deal of appreciation for this exciting engineering discipline and how it relates to other engineering fields. Later, he majored in Nuclear Engineering because the College of Engineering invited the top ten students in Chemical, Electrical, and Mechanical Engineering to spend more two more years of studies and earn a B.S. in Nuclear Engineering. Upon graduation, he was outstanding for the College of Engineering.

His undergraduate studies involved various aspects of engineering with numerous courses, lectures from Chemical, Electrical, Mechanical, as well as Nuclear engineering. He has received a scholarship to obtain a master's degree and the thesis was under "Hydrodynamic and Heat Transfer Over Two Spheres." The research of the thesis involved several engineering concepts and areas including fluid mechanic, heat transfer, and thermodynamics.

After he got his master's degree he worked at the Department of Nuclear Engineering as a lecturer for three years. Then, he started a new position in the same department as a faculty member. In addition, he was fortunate to receive a scholarship from Baghdad University to get his Ph.D. in Process System Engineering (focusing on Renewable Energy System).

He has joined the Process Integration and Systems Optimization Group in the Artie McFerrin Chemical Engineering Department at Texas A & M University to work under the supervision of Prof. Mahmoud El-Halwagi who is an expert in the field of process design, integration, and optimization.

Al-Aboosi may be reached by his email:alaboosi@tamu.edu